Black Holes Beyond General Relativity: Scalar Hair and Dynamical Evolution

Farid Thaalba

University of Nottingham

School of Mathematical Sciences

A thesis submitted to the University of Nottingham
for the degree of
Doctor of Philosophy

September 2025

To my parents,
Abir and Saba, who value education above all else.

Acknowledgements

Over the past four years, I have learned an incredible amount of physics and very much enjoyed the journey. Thomas, our many conversations about physics and beyond, were a highlight. Thank you for your time, patience, and the ideas we explored together. I had the great fortune of working with Miguel and Nicola, who somehow found the patience to put up with my endless questions. Whenever I hit a roadblock, they were always there to talk things through and help me find a way forward. They guided me through more trials and tribulations than I can count, and I could not have made this progress without them. Thank you, Thomas, Miguel, and Nicola, for everything.

I am also grateful to all my collaborators, who shaped much of what I have learned, and to the group at Nottingham for the engaging meetings, seminars, workshops, and discussions.

I am thankful to the University of Nottingham and the UKRI for funding my PhD and to the School of Mathematical Sciences for supporting my attendance at conferences and research travel abroad.

Outside of physics, I am grateful for the time spent with Miguel, his constant support, and for opening his home for me. My thanks also go to the group in Nottingham for the many social events we shared.

A special thank you goes to Ian, who has supported my education since school and has always been there for me and my family. You are a true gentleman and a remarkable friend.

Finally, to my parents, I am at a loss for words to express my gratitude fully. You have supported me, Lourdes, and Sami with a love and dedication that often came at your own expense. I cannot fathom the depth of your love. Thank you.

Abstract

We discuss extensions of general relativity, focusing on theories that incorporate an additional scalar degree of freedom. We mainly discuss theories that break no-hair theorems and endow black holes with a non-trivial scalar profile. In this context, we investigate several aspects of scalar Gauss-Bonnet gravity. In the shift-symmetric case, we examine the effect of additional interactions on black holes with scalar hair and how these operators affect their properties. We also discuss the possibility of supermassive black hole scalarization from the perspective of effective field theories. Next, we switch our focus to the initial value problem in these theories and address the lack of a well-posed Cauchy problem by including additional interactions that prove crucial in this regard. With this at hand, we study the dynamics of spherical black holes using excision and discuss the effect of the gauge choice and field redefinitions on this issue.

Collaborations

This thesis is based on the following research papers:

- F. Thaalba, G. Antoniou, and T. P. Sotiriou, *Black hole minimum size and scalar charge in shift-symmetric theories*. Class. Quantum Grav. 40 155002.
- F. Thaalba, M. Bezares, N. Franchini, and T. P. Sotiriou, *Spherical collapse in scalar-Gauss-Bonnet gravity: Taming ill-posedness with a Ricci coupling*. PhysRevD.109.L041503.
- F. Thaalba, N. Franchini, M. Bezares and T. P. Sotiriou, *Dynamics of spherically symmetric black holes in scalar-Gauss-Bonnet gravity with a Ricci coupling*. PhysRevD.111.064054.
- F. Thaalba, N. Franchini, M. Bezares and T. P. Sotiriou, *Hyperbolicity in scalar-Gauss-Bonnet gravity: A gauge invariant study for spherical evolution*. PhysRevD.111.024053.
- F. Thaalba, P. G. S. Fernandes and T. P. Sotiriou, *Supermassive black hole scalarization and effective field theory*. arXiv:2506.21434.

Additional work not included in this thesis:

- F. Thaalba, G. Ventagli, and T. P. Sotiriou, *Exotic compact objects and light bosonic fields*. PhysRevD.110.024034.

Notation

The metric signature is $(-,+,+,+)$. Greek letters denote spacetime indices. We primarily work in units of $c = 1 = G$, unless otherwise stated.

c:	Speed of light.
G:	Newton's constant.
$\hbar$:	Planck's constant.
$M_\odot$:	Solar mass.
M_{Pl}:	Reduced Planck mass; $M_{\text{Pl}} = \sqrt{\frac{\hbar c}{8\pi G}}$.
$g_{\mu\nu}$:	Spacetime metric.
$g^{\mu\nu}$:	Inverse metric.
g:	Metric determinant.
$\eta_{\mu\nu}$:	Flat spacetime metric.
∇_μ:	Covariant derivative.
$\Gamma^\alpha_{\beta\gamma}$:	Christoffel symbol.
$\mathfrak{L}_v$:	Lie derivative with respect to the vector v.
$\partial\mathcal{M}$:	Boundary of a region $\mathcal{M}$.
$(\mu\nu)$:	Symmetrization.
$R_{\mu\nu\alpha\beta}$:	Riemann tensor.
$R_{\mu\nu}$:	Ricci tensor.

R:	Ricci scalar.
$G_{\mu\nu}$:	Einstein tensor.
$\mathcal{G}$:	Gauss-Bonnet invariant.
ϵ:	Levi-Civita antisymmetric tensor density.
$\delta^{\alpha\beta\gamma\delta}_{\mu\nu\rho\sigma}$:	Generalized Kronecker delta.
$S_{\rm M}$:	Matter action.
$T_{\mu\nu}$:	Energy-momentum tensor.
$\boldsymbol{\Psi}$:	Matter fields.
ϕ:	Scalar field.
X:	Kinetic term; $X = -\frac{1}{2}\partial_\mu\phi\partial^\mu\phi \equiv -\frac{1}{2}\left(\partial\phi\right)^2$.
$V\left(\phi\right)$:	Scalar potential.
NEP:	Newton's equivalence principle.
WEP:	Weak equivalence principle.
EEP:	Einstein's equivalence principle.
BH:	Black hole.
sBH:	Scalarized black hole.
LoH:	Loss of hyperbolicity.
ID:	Initial data.
ADM:	Arnowitt–Deser–Misner.
NER:	Naked elliptic region.

Preface

The general theory of relativity arguably stands as the crown jewel of modern theoretical physics. It reenvisioned the most intuitive interaction in nature as the manifestation of spacetime curvature. Practically, it has achieved remarkable successes, from resolving Mercury's anomalous precession to predicting gravitational waves.

Gravitational waves, as novel channels of discovery, now offer unprecedented opportunities to probe the gravitational interaction and test general relativity. The emergence of gravitational-wave astronomy has ushered in an era of precision tests, with detections from binary black hole and neutron star mergers granting direct access to the high-curvature, relativistic, and non-perturbative regime of gravitational dynamics. Questioning the completeness of general relativity may seem audacious, yet compelling observational and theoretical motivations demand such inquiry.

Observationally, the accelerated expansion of the universe remains unexplained beyond the placeholder of dark energy, whose nature is unknown. Likewise, the concept of dark matter was introduced to account for phenomena such as flat galactic rotation curves and other gravitational anomalies, yet its composition remains elusive. These two mysteries rank among the most pressing challenges in modern physics. Theoretically, general relativity predicts singularities inside black holes and at the Big Bang, signalling a breakdown of its predictive power. Moreover, efforts to reconcile general relativity with quantum mechanics have so far failed, in stark contrast to the successful quantisation of the other fundamental interactions. Although numerous proposals for quantum gravity exist, none has emerged as a clear successor, and direct experimental access to this regime appears unlikely. Given these challenges, we regard general relativity as an effective field theory with lim-

ited validity and investigate possible extensions.

A common route to extending general relativity is to introduce additional degrees of freedom that may encode physics beyond general relativity or the Standard Model of particle physics. This thesis focuses on scalar fields. In general relativity, the Kerr metric uniquely describes quiescent, isolated astrophysical black holes due to the uniqueness and no-hair theorems. Extensions predicting deviations from this picture would provide compelling evidence for departures from general relativity. Since black hole binaries dominate gravitational wave detections, understanding black holes in extensions of general relativity is essential. Gravitational-wave observations offer powerful probes of phenomena such as black hole scalar hair. Scalar Gauss-Bonnet gravity has emerged as a leading framework for studying these effects.

The Introduction I expands on the triumphs and limitations of general relativity, highlighting predictions such as black holes and gravitational waves, as well as the problems that motivate its extensions. Chapter II examines the foundations of gravity, focusing on conceptual aspects that must underpin extended theories. Chapter III introduces scalar fields as new degrees of freedom, starting with the Brans-Dicke model, in which a scalar field couples non-minimally to the Ricci scalar, and extending to general scalar-tensor theories. We discuss Horndeski gravity, the most general non-degenerate scalar-tensor theory with second-order equations of motion, and identify scalar Gauss-Bonnet gravity as a Horndeski example that evades no-hair theorems. We also review spontaneous scalarization, which yields hairy black holes. Chapter IV investigates black holes in shift-symmetric scalar Gauss-Bonnet gravity and how additional interactions modify their properties. Chapter V explores scalarization of supermassive black holes in a two-scalar-field framework. Chapters VI – VIII turn to the dynamical evolution of black holes in scalar Gauss-Bonnet gravity, analysing the effect of additional interactions on the hyperbolicity of the equations. We demonstrate that such interactions can enhance the character of the equations, and we conduct numerical simulations using excision to investigate the dynamics of spherical black holes. We also assess the impact of gauge choices and field redefinitions on hyperbolicity. Chapter IX concludes the thesis.

Contents

Chapter I

Introduction

Contents

1.1 The road to general relativity and beyond

Gravity, a fundamental interaction in both everyday life and scientific exploration, remains one of the most mysterious. Its study spans human history. Though early scientific inquiries were often intertwined with philosophy and theology, they underscore humanity's long-standing desire to understand the world and its workings. Galileo Galilei's 16th-century experiments with pendulums and inclined planes marked the beginning of systematic experimental investigations into gravity, establishing him as a key figure in the foundation of modern science. Isaac Newton's 1665 theory unified terrestrial and celestial phenomena through the inverse-square law, based on the concept of absolute space (later overturned by Einstein's theory) and the equivalence of inertial and gravitational mass (later incorporated and revolutionised in Einstein's theory). The famous story of Newton's epiphany—spurred by the fall of an apple—allegedly led him to wonder whether the same force that caused the apple to fall also kept the moon in orbit. While this narrative is iconic, it is often clouded by myth. Though such stories suggest that scientific breakthroughs occur in a tidy and immediate fashion, in reality, shifts in scientific understanding are usually slow, driven by both a natural attachment to established ideas and the inherent complexity of the issues at hand.

Newton's theory was successful in predicting planetary motion and terrestrial phenomena, yet it faced significant challenges and struggled to account for the anomalous precession of Mercury's orbit. Le Verrier, building on his success in predicting Neptune's existence through perturbations in Uranus's orbit, proposed the existence of a "missing" planet to account for Mercury's anomalous motion. This hypothesis, though ultimately disproven, parallels modern attempts to explain cosmological discrepancies by introducing dark matter.

In 1915, Einstein's General Relativity resolved these issues, marking one of the most significant milestones in physics [1]. Similar to Newton's apple story, Einstein's insight was prompted by a thought experiment involving a falling elevator, though the development of general relativity was far from

straightforward.

Unlike Newtonian physics, which assumes fixed space and absolute time, general relativity replaces these with dynamic spacetime and conceptualises gravity as its curvature, influenced by the presence of mass and energy. Einstein's equation is

$$R_{\mu\nu} - \frac{1}{2} R g_{\mu\nu} = \frac{8\pi G}{c^4} T_{\mu\nu} \,, \tag{1.1.1}$$

where $g_{\mu\nu}$ is the metric tensor, $R_{\mu\nu}$, R are the Ricci tensor and scalar respectively, and $T_{\mu\nu}$ is the energy-momentum tensor of matter. The constants G and c are Newton's constant and the speed of light, respectively. The theory has passed numerous empirical tests, explaining Mercury's precession and successfully predicting gravitational light deflection, black holes, and gravitational waves.

However, like Newtonian gravity before it, general relativity faces significant challenges. These include the unresolved nature of singularities within black holes and early cosmology, the conundrums of dark matter and dark energy, the cosmological constant problem, and its incompatibility with Quantum Field Theory.

Recognising these difficulties, some approaches treat general relativity as an incomplete theory—just as Newtonian gravity is—and explore possible extensions that may provide a deeper understanding of gravity at both cosmic and quantum scales.

1.2 Milestones of general relativity

General relativity has long been regarded as one of the cornerstones of modern theoretical physics. Its elegant description of gravity as the curvature of spacetime, shaped by the presence of mass and energy, has passed a multitude of empirical tests with flying colours [2–4]. General relativity has provided profound insights into the universe's nature, confirming predictions in the strong-field regime and at cosmological scales. The theory's success in explaining the perihelion precession of Mercury, light deflection, predicting the existence of black holes, and gravitational waves has led to its widespread

acceptance as the most accurate description of gravity to date.

1.2.1 The Standard Model of Cosmology

In this thesis, we do not delve into cosmology in depth. This section's purpose is to provide clarity for the discussion in subsequent sections. We follow the discussion of [5]. For a more thorough treatment of cosmology, we refer the reader to [6, 7].

On large scales, the universe is approximately spatially isotropic and homogeneous, as indicated by various observations, most notably the cosmic microwave background [8]. These two conditions are sufficient to fix the structure of the metric tensor as

$$\mathrm{d}s^2 = -\mathrm{d}t^2 + a^2(t)\left(\frac{\mathrm{d}r^2}{1-kr^2} + r^2\mathrm{d}\Omega^2\right), \qquad \mathrm{d}\Omega^2 = \mathrm{d}\theta^2 + \sin^2\theta\mathrm{d}\phi^2, \tag{1.2.1}$$

where t is the cosmological time, $a(t)$ is the scale factor, and $k = 0$, $k > 0$, and $k < 0$ represent flat, positive, and negative curvature, respectively. This metric is known as the Robertson-Walker metric [9–12]. Given the assumptions of homogeneity and isotropy, the universe's only evolving characteristic is its size, as described by the scale factor, which measures the evolution of length scales. We assume matter and energy are described by a perfect fluid with an energy-momentum tensor

$$T_{\mu\nu} = (\rho + p)u_\mu u_\nu + p g_{\mu\nu}, \tag{1.2.2}$$

where ρ is the energy density, p is the pressure, and u_μ is the fluid velocity. An equation of state relates pressure and density, and we assume $p/\rho = w =$ constant. The two most commonly studied examples of cosmological fluids are matter and radiation. Matter is characterized by zero pressure, $p_\mathrm{M} = 0$, while radiation satisfies $p_\mathrm{R} = \frac{1}{3}\rho_\mathrm{R}$. Einstein's equations yield two key relations, known as the Friedmann equations [13–16]

$$H^2 = \frac{8\pi G}{3}\rho - \frac{k}{a^2}, \qquad H \equiv \frac{\dot{a}}{a}, \tag{1.2.3}$$

and

$$\frac{\ddot{a}}{a} = -\frac{4\pi G}{3}(\rho + 3p)\,. \tag{1.2.4}$$

Here, H represents the Hubble parameter, and the dot denotes a derivative with respect to cosmological time t. Equation (1.2.3) represents the rate of expansion (or contraction) of the universe, while equation (1.2.4) describes the acceleration of this expansion. A useful quantity to introduce in this context is the density parameter, given by

$$\Omega_i \equiv \frac{8\pi G}{3H^2}\rho_i = \frac{\rho_i}{\rho_{\text{crit}}}\,, \qquad \rho_{\text{crit}} \equiv \frac{3H^2}{8\pi G}\,, \qquad \Omega = \sum_i \Omega_i\,. \tag{1.2.5}$$

For the curvature term, we introduce $\Omega_{\text{curv}} = -k/(H^2a^2)$. This is not an energy density, but is used for notational convenience. With these definitions, the Friedmann equation (1.2.3) can be rewritten as

$$\Omega_{\text{curv}} = 1 - \Omega\,, \tag{1.2.6}$$

thus, for $\Omega < 1$, we have $k < 0$; for $\Omega = 1$, $k = 0$; and for $\Omega > 1$, $k > 0$. If the perfect fluid satisfies the condition $\rho + 3p > 0$, then $\ddot{a} < 0$, indicating that the expansion will always decelerate, as is expected in the Big Bang scenario. However, this is *not* consistent with current observations [17–20].

The simplest explanation for the accelerated expansion of the universe is the introduction of a cosmological constant, with an equation of state $p_\Lambda = -\rho_\Lambda$. However, this solution introduces the infamous cosmological constant problem, which we discuss in Section 1.3.3.

Observational data indicate that the density of visible matter is $\Omega_{\text{m}} = 0.046 \pm 0.002$, while the dark matter density is $\Omega_{\text{DM}} = 0.23 \pm 0.01$. Additionally, the observed expansion of the universe requires a cosmological constant with density $\Omega_\Lambda = 0.73 \pm 0.02$ [17–23]. These contributions sum to $\Omega \sim 1$, indicating that the universe is flat.

Assuming the presence of dark matter and a cosmological constant as the "solutions" to the "missing mass" and accelerated expansion problems (see Section 1.3.3) gives rise to the Lambda Cold Dark Matter (ΛCDM) Standard

Model of Cosmology.

1.2.2 Black holes

Black holes are a stark prediction of general relativity. Schwarzschild, in 1916, wrote down the first exact solution to Einstein's equations [24]. It describes a static spherically symmetric point mass in an otherwise empty space. In the appropriately named Schwarzschild coordinates $\{t, r, \theta, \phi\}$, it takes the form

$$\mathrm{d}s^2 = -\left(1 - \frac{2M}{r}\right)\mathrm{d}t^2 + \left(1 - \frac{2M}{r}\right)^{-1}\mathrm{d}r^2 + r^2\left(\mathrm{d}\theta^2 + \sin^2\theta\mathrm{d}\phi^2\right) . \tag{1.2.7}$$

This solution forms a one-parameter family in terms of the mass M. The solution is singular at $r = 0$ and $r = 2M$, which will be discussed in Section 1.3.2. The defining property of a black hole is the existence of a boundary surface, the *event horizon*, such that two events separated by this boundary cannot be causally connected. In the Schwarzschild case, this boundary occurs at $r = 2M$ [5, 25]. It took several decades after Schwarzschild's solution to appreciate its implications. However, some aspects of the black hole nature of the Schwarzschild solution were discussed as early as 1921 [26].

Chandrasekhar's crucial result—that a cold, massive body with a mass exceeding $\sim 1.44M_\odot$ will inevitably collapse—was deeply unsettling to the community [27]. Eddington famously commented that a fundamental law of nature must prevent such an event [28, 29]. By the late 1930s, strong evidence for the existence of black holes had emerged, including the Chandrasekhar limit, the Oppenheimer-Volkoff limit for neutron star mass [30], and the possibility of collapse as demonstrated in the Oppenheimer-Snyder model for pressureless, homogeneous dust [31]. Additionally, Kerr's discovery of the rotating solution [32] and the subsequent uniqueness theorems [33, 34] were key breakthroughs. Notably, the singularity theorems of Penrose and Hawking [35, 36] demonstrated that singularity formation is a generic feature of gravitational collapse (see Section 1.3.2).

The existence of black holes has since been confirmed by several observations, including the supermassive black hole at the centre of the Milky Way,

Sgr$A*$ [37, 38], and the images of $M87*$ and Sgr$A*$ obtained by the Event Horizon Telescope [39, 40]. Moreover, gravitational wave observations by the LIGO-Virgo-KAGRA collaboration are fully consistent with the description of black hole binaries [41].

1.2.3 Gravitational waves

Einstein predicted gravitational waves in 1916 [42], and later argued with Rosen that such waves do not exist. Einstein revised his view in 1937 [43] on the advice of Robertson [44]. Nonetheless, the status of gravitational waves remained uncertain until the Chapel Hill conference in 1957 [45]. At that meeting, Feynman introduced the "sticky-beads" thought experiment, arguing that gravitational waves must carry energy—a point still under debate at the time. Bondi later established that gravitational waves indeed carry energy [46]. Wheeler and Weber also suggested that gravitational waves might be detectable [47]. In 1960, Weber proposed a method for detecting gravitational waves [48] and built the first detector [49], claiming a detection [50, 51]. However, subsequent attempts by other groups failed to detect gravitational waves [52].

The first indirect evidence of gravitational waves came with the discovery of the binary pulsar by Taylor and Hulse [53], which earned them the Nobel Prize in 1993. According to general relativity, gravitational waves extract energy from a binary system, causing the separation between the objects to decrease and the orbital period to decay. In 1981, measurements of the orbital-period decay in this system were obtained, and the observed rate closely matched Einstein's predictions, with only a small observational uncertainty [54]. However, direct detection of gravitational waves remained elusive. In 1972, Weiss laid the groundwork for the implementation of a laser interferometer to detect gravitational waves [55].

Gravitational waves were first directly detected in 2015 [56], marking a monumental breakthrough after decades of efforts. The detection resulted from the coalescence of two black holes, with masses approximately $29M_\odot$ and $36M_\odot$, merging to form a black hole of around $62M_\odot$. The event, dubbed GW150914, released $3M_\odot$ of energy into gravitational waves within a fraction of a second. This detection provided the first direct evidence of

black hole binaries. Subsequent detections by the LIGO-Virgo-KAGRA collaboration of black holes with masses in the range $\mathcal{O}(1)M_\odot - \mathcal{O}(100)M_\odot$ further confirmed the presence of gravitational waves. Figure 1.1 shows the first gravitational wave signal observed [56], along with subsequent detections of black holes and neutron star binaries.

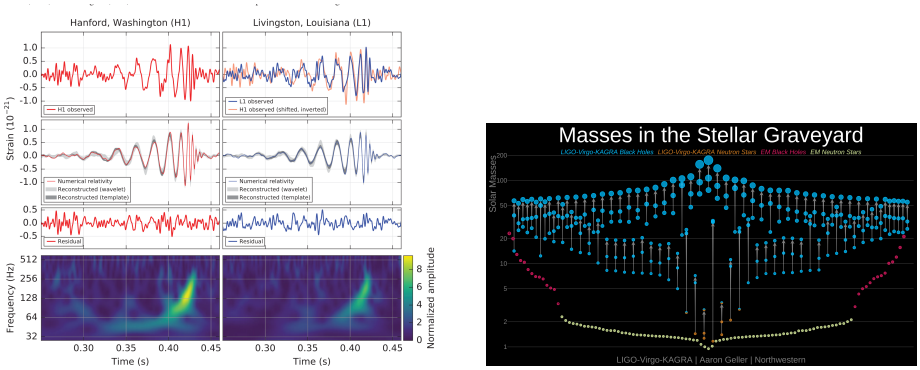

Figure 1.1: On the left is the GW150914 event observed by the LIGO Hanford and Livingston detectors [56]. On the right are the black holes and neutron stars observed so far by the LIGO-VIRGO-KAGRA collaboration. Illustration by Aaron Geller.

The advent of gravitational wave astronomy has opened new possibilities for studying compact objects in unprecedented detail. It offers a unique opportunity to test the nature of gravity and explore fundamental physics in extreme environments, which cannot be replicated on Earth or within the solar system. Interest in testing general relativity is at an all-time high [57–63], fuelled by the landmark detection of gravitational waves [41, 64–66]. Third-generation detectors, such as the Einstein Telescope [67, 68], and space-borne detectors like LISA [60, 69, 70], will enable the search for potential anomalies in our understanding of the gravitational interaction in unexplored regions of extreme dynamical gravity.

1.3 When general relativity fails

Despite its many triumphs, general relativity is not without its limitations. It is fundamentally incompatible with quantum mechanics, the other pillar

of modern physics, and fails to provide a framework for understanding the quantum nature of spacetime. Moreover, its classical treatment of gravity breaks down in extreme conditions, such as at the centre of black holes or in the early universe, where spacetime curvature becomes "infinite". The theory also encounters difficulty in explaining the observed phenomena of dark matter and dark energy, whose presence is inferred from gravitational effects, yet their exact nature remains elusive.

1.3.1 Relativity meets Quantum?

Efforts to quantise gravity date back almost a century [71]. Heisenberg [72] first noted that the dimensionality of Newton's constant could pose issues in quantising general relativity. Later, it was understood that canonical quantisation of general relativity leads to perturbative non-renormalizability [73–75], which can be attributed to the negative mass dimension (-2) of Newton's constant.

Stelle demonstrated that including higher-order curvature terms renders the theory renormalizable [76]. However, Ostrogradsky [77, 78] showed that higher-derivative theories possess an unbounded Hamiltonian from below, leading to ghost degrees of freedom and loss of unitarity when quantised [79]. Yet, numerical simulations suggest that stationary and dynamical spacetime solutions do not exhibit runaway behaviour associated with ghost excitations [80–82]. Modern perspectives view non-renormalizability less negatively, indicating that the theory is sensitive to the integrated-out high-energy physics, and general relativity is considered an effective field theory [83–86] (see Section 3.4), providing answers up to a specific energy scale and necessitating an ultraviolet completion.

Nevertheless, numerous technical and conceptual challenges remain in formulating a quantum theory of gravity [87–90]. General relativity is *background independent* (see Section 2.2.1), whereas quantum field theory assumes a fixed, flat background, with quantum fields propagating on it. In contrast, quantising general relativity involves (potentially) quantising spacetime itself [1], which presents a significant challenge. A formidable open prob-

[1] Whatever that means.

lem remains in reconciling these fundamental differences. Furthermore, the "problem of time" [87, 91] and the issue of defining observables in quantum gravity remain unresolved, as diffeomorphism invariance implies non-local observables [90, 92].

Several approaches to quantum gravity exist. Superstring theory [93–95] seeks to unify all known interactions through postulating vibrating strings as the fundamental building blocks of nature. In its original formulation, string theory abandons background independence and employs perturbative techniques around a fixed background. Nonetheless, it is argued that the anti-de Sitter/conformal field theory (AdS/CFT) correspondence [96] provides a non-perturbative definition of string theory on the AdS side. For more details and various views, see [97, 98]. Loop quantum gravity [99–102] posits a granular structure of spacetime, providing a non-perturbative approach while preserving background independence. Asymptotic safe gravity [103–107] aims for non-perturbative quantisation via the renormalisation group, seeking a non-trivial fixed point in the renormalisation flow. If such a fixed point exists, a well-defined quantum gravity theory would emerge, free from divergences at arbitrarily high energies [108, 109]. Other approaches, such as causal dynamical triangulation, based on the path integral formulation of quantum gravity, use simplicial complexes to regularise the path integral [110–112].

Many of these approaches introduce deviations from general relativity, either through additional degrees of freedom or higher-order curvature corrections, or both. However, no consensus has been reached on the quantum nature of gravity.

1.3.2 Singularities

In general relativity "singularities" appear in the early universe and black hole spacetimes. It is quite a non-trivial task to define exactly what we mean by a "singularity" [25]. Notwithstanding, we can broadly identify two types of singularities: (i) a "naive" singularity due to the failure of the coordinate system to cover a portion of the spacetime; or (ii) a "true" or a physical singularity where a physical trajectory abruptly ends. More precisely, (an inextendible) spacetime must contain one or more incomplete time-like or null geodesics.

These singularities need not be curvature singularities, *i.e.*, curvature invariants need not blow up. See [25, 113] for an extended discussion and technical details.

In the context of black holes, let us consider for simplicity the Schwarzschild solution

$$\mathrm{d}s^2 = -\left(1-\frac{2M}{r}\right)\mathrm{d}t^2 + \left(1-\frac{2M}{r}\right)^{-1}\mathrm{d}r^2 + r^2\left(\mathrm{d}\theta^2+\sin^2\theta\mathrm{d}\phi^2\right)\,. \tag{1.3.1}$$

The Schwarzschild metric is singular at $r = 0$ and $r = 2M$. The apparent singular behaviour of the metric at $r = 2M$ is nothing worrisome as it is merely of the first type, *i.e.*, due to an ill-chosen coordinate system [25]. However, the singularity at $r = 0$ is a curvature singularity. We can observe this, for example, in the Kretschmann scalar

$$R_{\mu\nu\alpha\beta}R^{\mu\nu\alpha\beta} = \frac{48M^2}{r^6}\,, \tag{1.3.2}$$

which blows up as $r \to 0$. This indicates that general relativity is no longer valid and predicts its demise.

It is tempting to think that the singularity at $r = 0$ is due to spherical symmetry, and in realistic gravitational collapse, this would not occur. However, Penrose and Hawking *singularity theorems* [35, 36] (see [114] for a review) provide evidence to the contrary. The essence of these theorems is that, under appropriate causality and energy conditions, black holes must contain a singularity [2] (see [25, 113] for technical details). As the singularity is hidden behind the event horizon, an outside observer can never deduce its presence or effects. Therefore, Penrose has conjectured that all singularities must be veiled by an event horizon [115]—the so-called weak cosmic censorship conjecture—and that is how general relativity or Nature protects itself from these nonsensical conclusions. There is also the strong cosmic censorship conjecture; colloquially, it asserts that, *generically*, initial data determines the future [116, 117] [3]. Weak and strong cosmic censorship conjectures are math-

[2] Interestingly, these theorems do not say anything about the nature of the singularity, and virtually nothing is known beyond that they must form.

[3] The difference between global uniqueness results in general relativity [117, 118]

ematically independent. The conjectures and reformulations thereof remain one of the main open questions in mathematical general relativity. For comprehensive reviews, see [116, 119–121].

1.3.3 The dark sector

A limitation of general relativity arises when attempting to explain certain large-scale cosmological phenomena, such as the universe's accelerated expansion. The discovery that the universe's expansion is speeding up, rather than slowing down as previously expected, led to the introduction of dark energy—an enigmatic substance with negative pressure. While the ΛCDM model, which incorporates a cosmological constant, can explain these observations phenomenologically (this has been questioned recently by the DESI collaboration [122, 123]), the underlying origin of dark energy remains unclear, with its tiny value viewed as a fine-tuning problem. General relativity cannot adequately explain why dark energy is so small and why it has the precise properties needed to drive cosmic acceleration.

Assuming dark matter, an invisible substance inferred from its gravitational effects on galaxies and clusters of galaxies. General relativity can describe the universe's large-scale structure. Notwithstanding, it does not offer a compelling explanation for the nature of dark matter. The inability of general relativity to account for dark matter and dark energy within a unified framework suggests that extensions of the theory, or an entirely new theoretical framework, may be required.

Dark matter

Dark matter is a hypothesised form of matter introduced to explain the "missing" mass in galaxy clusters and account for the observed flat rotation curves [22, 23]. It is crucial to the ΛCDM model, which is central to contemporary cosmology and explains the observed structure of the universe. In 1933, Zwicky (see [23] for a historical review) studied the redshift of several galaxy clusters and found that the Coma cluster exhibited large velocity

and strong cosmic censorship conjecture is the restriction, in the former, to globally hyperbolic developments of initial data.

dispersion. While this phenomenon had been noted earlier by Hubble and Humason [124], Zwicky applied the virial theorem to estimate the cluster's mass based on observed velocities. He found that the virial mass was approximately 400 times greater than the mass inferred from galaxy counts.

Further evidence for dark matter comes from galaxy rotation curves, particularly the circular velocities of stars as a function of their distance from the galactic centre. These curves remained "flat" at large distances, contrary to the expected fall-off under Keplerian dynamics. Since most visible matter is concentrated near the galactic centre, the flatness of the curves suggests the presence of additional unseen mass [125, 126].

Several hypotheses have been proposed regarding the nature of dark matter. Observational evidence indicates that baryonic dark matter accounts for only a small fraction of the total dark matter [20, 22, 23, 127, 128]. Numerous dark matter candidates are present in the literature [22, 23, 129–133]. Here, we briefly mention a few possibilities.

One option is primordial black holes [129, 134–140]. These black holes may have formed in the early universe due to gravitational collapse in densely populated regions [141–145]. Various constraints on this hypothesis have been discussed, see, for example, [129, 146, 147].

Additionally, any viable particle dark matter candidate must be stable, interact via gravity, and not through electromagnetism or the strong force. Within the standard model, the neutrino stands out. Early studies of neutrinos in cosmology did not focus on the "missing mass" problem but instead sought to place upper bounds on their mass [148–155]. Over time, the connection between missing mass and neutrinos began to emerge [156–159].

However, numerical simulations indicated that relativistic (hot) dark matter, such as neutrinos [160, 161], cannot account for the majority of the dark matter in the universe [162]. In contrast, cold dark matter is more effective, as it tends to form larger halos through the merger of smaller ones, while hot dark matter initially forms large structures that later fragment into smaller ones [23].

Dodelson and Widrow [163] proposed the possibility of producing other types of neutrinos in the early universe that do not participate in electroweak interactions, unlike standard model neutrinos, and could account for dark

matter. These so-called sterile neutrinos interact primarily through gravity but also mix with standard model neutrinos, albeit weakly [163]. While the original model has been ruled out, alternative models remain under investigation [131, 164]. Furthermore, the consideration of neutrinos as potential dark matter candidates led to the exploration of weakly interacting massive particles (WIMPs) as a possible dark matter hypothesis [165–170].

In addition to sterile neutrinos, many attempts to explain these phenomena involve new physics beyond the standard model. Supersymmetry, for example, predicts a partner fermion for each boson and vice versa, potentially offering dark matter candidates [151, 171–177]. Another proposal is the axion, a pseudo-scalar, which arises as a solution to the strong-CP problem [178, 179]. This solution involves a spontaneously broken $U(1)$ global symmetry, which resolves the fine-tuning problem by dynamically driving the fine-tuned parameter to zero. Wilczek [180] and Weinberg [181] independently pointed out that this process leads to a new light boson, the axion, which was later considered a potential candidate for dark matter. For axions to be viable dark matter candidates, however, they must be much lighter and interact more weakly than initially thought [182–184]. For further details, we refer the reader to [133].

Alternatively, the need for dark matter may be circumvented by modifying gravitational dynamics at galactic scales. Modified Newtonian Dynamics (MOND), originally proposed by Milgrom [185, 186], attempts to explain the observed motions of galaxies without invoking unseen mass. The theory modifies Newton's law of gravitation, yielding the relation $F = ma^2/a_0$ for accelerations $a \ll a_0 \sim 1.2 \times 10^{-2}$ m/s^2. In this framework, dark matter is not needed, and the dynamics of stars in galaxy clusters can be explained without requiring dark matter. This idea was later extended to a relativistic context, resulting in Tensor-Vector-Scalar (TeVeS) gravity, formulated by Bekenstein [187]. MOND has been successful in accounting for various observations related to the rotation curves of hundreds of spiral galaxies [188–191]. Nonetheless, it fails to explain several key observations, particularly on the scale of galaxy clusters, including those from the Bullet Cluster and other high-precision cosmological measurements. As a result, it remains an open question whether TeVeS can fully address these discrepancies [192–196].

Dark energy

The inordinate amount of observational evidence in support of the universe undergoing an accelerated expansion, coming from type Ia supernovae [17, 197–206], the Cosmic Microwave Background measurements [127, 207–215], and large-scale structure studies [216–223], is far from being satisfactory explained. Several ideas have been proposed to explain this phenomenon. The simplest of which is introducing a (bare) cosmological constant Λ_B, for which Einstein's equation reads

$$R_{\mu\nu} - \frac{1}{2}R g_{\mu\nu} + \Lambda g_{\mu\nu} = \kappa T_{\mu\nu} \,, \qquad \kappa = \frac{8\pi G}{c^4} \,. \tag{1.3.3}$$

This, however, comes with a heavy price, known as the cosmological constant problem [224–230].

General relativity teaches us that all forms of matter and energy gravitate, as per the equivalence principle (see Section 2.2.1). But what about the energy of the vacuum? In flat spacetime, the vacuum state must be invariant for all observers, and since the only invariant tensor is $\eta_{\mu\nu}$, we must have $\langle T_{\mu\nu} \rangle \propto \eta_{\mu\nu}$. In curved spacetime, this leads to the expression (by the principle of minimal coupling, see Section 2.2.1)

$$\langle T_{\mu\nu} \rangle = -\rho_{\text{vac}} g_{\mu\nu} \,, \tag{1.3.4}$$

with a constant ρ_{vac} since the energy momentum tensor is conserved [227]. Thus, the Einstein equation with quantum fields seems to take on the form

$$R_{\mu\nu} - \frac{1}{2}R g_{\mu\nu} + \Lambda_B g_{\mu\nu} = \kappa T^{\text{matter}}_{\mu\nu} + \kappa \langle T_{\mu\nu} \rangle \,, \tag{1.3.5}$$

where $T^{\text{matter}}_{\mu\nu}$ is ordinary matter, and $\langle T_{\mu\nu} \rangle$ is the vacuum contribution from all the particles in the universe. Using the form of $\langle T_{\mu\nu} \rangle$ derived earlier we can write the equation as

$$R_{\mu\nu} - \frac{1}{2}R g_{\mu\nu} + \Lambda_{\text{eff}} g_{\mu\nu} = \kappa T^{\text{matter}}_{\mu\nu} \,, \tag{1.3.6}$$

with the effective cosmological constant $\Lambda_{\text{eff}} = \Lambda_B + \kappa \rho_{\text{vac}}$ is the quantity we observe.

In quantum field theory, the vacuum energy can be calculated by computing the vacuum loop diagrams for each particle in the Standard Model. The energy density of the vacuum ρ_{vac} is given by [227, 230]

$$\rho_{\text{vac}} \sim \sum_{\text{particles}} m^4_{\text{particle}} \,. \tag{1.3.7}$$

As the Standard Model is well tested up to the TeV scale, we would estimate the vacuum energy density $\rho_{\text{vac}} \gtrapprox (\text{TeV})^4 \sim \left(10^{-60} M_{\text{Pl}}\right)^4$. However, observational data suggests that $\Lambda_{\text{eff}} \sim \left(10^{-30} M_{\text{Pl}}\right)^4$, implying that Λ_{bar} cancels ρ_{vac} to within approximately 60 decimal places, which appears to be an extremely fine-tuned coincidence. Yet, this is only the beginning of our troubles. The theory proves to be highly sensitive to ultraviolet physics, as fine-tuning must be performed at each order in perturbation theory, a phenomenon known as *radiative instability* [227, 230]. Thus, the central question remains: how can we make the cosmological constant radiatively stable? One possibility is to introduce additional fields in the matter sector that could "absorb" the large vacuum energy. However, this is not feasible (for a translationally invariant vacuum) without invoking fine-tuning, as demonstrated by Weinberg's no-go theorem [224].

It is tempting to consider a scenario in which the cosmological constant is not constant; rather, the potential energy of a field drives the accelerated expansion, which eventually dynamically relaxes to a small value. This is known as the dynamical dark energy proposal, which can be realised through a slowly rolling cosmological scalar field [231–238]. However, fine-tuning remains a challenge for these models.

To illustrate how such a scenario can be achieved, consider a simple example of a scalar field minimally coupled to gravity with potential $V(\phi)$

$$\mathcal{L}_\phi = -\frac{1}{2}\partial_\mu\phi\partial^\mu\phi - V(\phi)\,, \tag{1.3.8}$$

The corresponding energy-momentum tensor is

$$T^\phi_{\mu\nu} = \partial_\mu\phi\partial_\nu\phi - g_{\mu\nu}\left(\frac{1}{2}\partial_\mu\phi\partial^\mu\phi + V(\phi)\right)\,, \tag{1.3.9}$$

For a homogeneous configuration $\phi = \phi(t)$, the scalar field behaves as a perfect fluid with equation of state $w_\phi = p_\phi/\rho_\phi$, given by

$$w_\phi = \frac{\frac{1}{2}\dot{\phi}^2 - V(\phi)}{\frac{1}{2}\dot{\phi}^2 + V(\phi)} \,. \tag{1.3.10}$$

For a very slowly rolling field, *i.e.*, $\dot{\phi}^2 \ll V(\phi)$, we have $w(\phi) \approx -1$. These models are known as quintessence [238–246]. To ensure the scalar is slowly rolling today, we require $\sqrt{V''(\phi_0)} \sim H_0$. For the simple potential $V(\phi) = \frac{1}{2}m^2\phi^2$, this implies $m \sim H_0 \sim 10^{-33}$ eV. This fine-tuning remains a challenge for such models; further discussion can be found in [224, 229]. Additionally, considering derivative couplings as a generalisation of quintessence has been applied to cosmic acceleration, leading to the K-essence theories [247, 248].

Finally, extensions of general relativity that avoid Weinberg's no-go theorem show promise in addressing the cosmological constant problem [249–252]. However, general relativity has been rigorously tested in the solar system [2, 3], presenting additional challenges in this context. If such scalars exist, a mechanism must shield them from detection in the solar system. Various "screening" mechanisms have been proposed in the literature. For further details, see [253, 254] and references therein. Currently, no universally accepted solution exists for explaining the universe's accelerated expansion.

Chapter II

Foundations of Gravity

Contents

2.1 Geometric foundations

We take gravity as best described by the curvature of spacetime, a perspective further developed in the next Section 2.2. For now, we focus on the geometric framework of general relativity and introduce the essential concepts and tools of differential geometry required for the treatment of general relativity. We are not aiming for an exhaustive or rigorous presentation but rather a collection of definitions to establish notation and conventions.

Spacetime, denoted $(\mathcal{M}, \boldsymbol{g})$, is a four-dimensional differentiable manifold $\mathcal{M}$ equipped with a Lorentzian metric $\boldsymbol{g}$. Roughly speaking, an n-dimensional differentiable manifold is composed of smoothly stitched-together regions that locally resemble $\mathbb{R}^n$. A *diffeomorphism* $\Phi : \mathcal{M} \to \mathcal{N}$ between manifolds $\mathcal{M}$ and $\mathcal{N}$ is a bijective map such that both Φ and its inverse are smooth; in this case, the manifolds are said to be *diffeomorphic*.

In a coordinate chart, the tangent space at a point p is spanned by the basis $(\partial/\partial x^\mu)_p$ or, for short, ∂_μ, and the corresponding basis of the cotangent space is denoted as $(\mathrm{d}x^\mu)_p$, such that

$$(\mathrm{d}x^\mu)_p \left((\partial/\partial x^\nu)_p \right) = \delta^\mu_\nu \,, \tag{2.1.1}$$

where δ^μ_ν is the Kronecker delta symbol. Under a coordinate change $x^\mu \to \tilde{x}^\mu$ a rank (k, l) tensor transforms as

$$\tilde{T}^{\mu_1 \dots \mu_k}{}_{\nu_1 \dots \nu_k}(\tilde{x}) = \frac{\partial \tilde{x}^{\mu_1}}{\partial x^{\alpha_1}} \cdots \frac{\partial \tilde{x}^{\mu_k}}{\partial x^{\alpha_k}} \frac{\partial x^{\beta_1}}{\partial \tilde{x}^{\nu_1}} \cdots \frac{\partial x^{\beta_l}}{\partial \tilde{x}^{\nu_l}} T^{\alpha_1 \dots \alpha_k}{}_{\beta_1 \dots \beta_k}(x) \,. \tag{2.1.2}$$

The metric is a smooth, symmetric, non-degenerate $(0, 2)$ tensor field, which maps two tangent vectors to a real number, thus defining a notion of distance on the manifold. The components of the metric are $g_{\mu\nu} = \boldsymbol{g}(\partial_\mu, \partial_\nu)$, and the *spacetime interval* is commonly denoted as,

$$\mathrm{d}s^2 = g_{\mu\nu} \mathrm{d}x^\mu \mathrm{d}x^\nu \,. \tag{2.1.3}$$

Since the metric is non-degenerate, it has an inverse, denoted by $g^{\mu\nu} \coloneqq (\boldsymbol{g}^{-1})_{\mu\nu}$, satisfying $g^{\mu\nu} g_{\mu\alpha} = \delta^\nu_\alpha$. Using the metric and its in-

verse, we can raise and lower indices. The determinant of $g_{\mu\nu}$ is denoted as $g = \det g_{\mu\nu}$. The metric has a Lorentzian signature of $(1, n-1)$, meaning one negative eigenvalue and $n-1$ positive eigenvalues.

A vector v_p at a point p in the tangent space is called

- *Time-like* if $g_{\mu\nu}v^\mu v^\nu < 0$,
- *Space-like* if $g_{\mu\nu}v^\mu v^\nu > 0$,
- *Light-like* or *Null* if $g_{\mu\nu}v^\mu v^\nu = 0$.

A vector field is time-like, space-like, or null if its vectors have these properties at each point. Similarly, a curve $c : \mathbb{R} \supseteq I \to \mathcal{M}$, where I is an interval, is time-like, space-like, or null if its tangent vector field satisfies the respective conditions. Every smooth Lorentzian manifold admits a unique, torsion-free, metric-compatible connection, known as the *Levi-Civita* connection. The covariant derivative along a vector field X is denoted ∇_X, and for coordinate basis vector fields, we abbreviate it as ∇_μ. The *Riemann curvature tensor* $R_{\alpha\beta\delta}{}^\gamma$ measures the failure of the covariant derivative to commute, such that for a vector field v^α,

$$\left(\nabla_\alpha\nabla_\beta - \nabla_\beta\nabla_\alpha\right) v^\gamma = -R_{\alpha\beta\delta}{}^\gamma v^\delta \,. \tag{2.1.4}$$

The *Ricci tensor* is defined as $R_{\alpha\gamma} = R_{\alpha\beta\gamma}{}^\beta$, and the *Ricci scalar* is $R = R_\alpha{}^\alpha$.

In addition to the covariant derivative, we can define the *Lie derivative* along a vector field v, denoted $\mathfrak{L}_v$. For details on the general construction of the Lie derivative, see [25]. Its action on a scalar function f, vector field w^μ, and the metric $g_{\mu\nu}$ is

$$\mathfrak{L}_v f = v(f) = v^\mu \partial_\mu f \,, \tag{2.1.5}$$

$$\mathfrak{L}_v w^\mu = [v, w]^\mu \,, \qquad [\cdot,\cdot] \equiv \text{Commutator}, \tag{2.1.6}$$

$$\mathfrak{L}_v g_{\mu\nu} = \nabla_\mu v_\nu + \nabla_\nu v_\mu \,. \tag{2.1.7}$$

If $\mathfrak{L}_v g_{\mu\nu} = 0$, the vector field v is a *Killing vector field*, and the Killing equation is $\nabla_\mu v_\nu + \nabla_\nu v_\mu = 0$.

Lastly, we define a *geodesic* as a curve whose tangent vector is parallel trans-

ported along itself. Specifically, a curve with tangent T^μ satisfies the equation

$$T^\mu \nabla_\mu T^\nu = f T^\nu \,, \tag{2.1.8}$$

where f is an arbitrary function along the curve. It is always possible to find a parametrisation such that [25]

$$T^\mu \nabla_\mu T^\nu = 0 \,, \tag{2.1.9}$$

in which case, the curve is said to be *affinely parametrised*. In coordinates, the geodesic equation is

$$\frac{\mathrm{d}^2 x^\mu}{\mathrm{d}\lambda^2} + \Gamma^\mu{}_{\alpha\beta} \frac{\mathrm{d}x^\alpha}{\mathrm{d}\lambda} \frac{\mathrm{d}x^\beta}{\mathrm{d}\lambda} = 0 \,, \tag{2.1.10}$$

where the $\Gamma^\mu{}_{\alpha\beta}$ are the *Christoffel symbols*, defined by $\nabla_\mu \partial_\nu = \Gamma^\alpha{}_{\mu\nu} \partial_\alpha$.

2.2 Conceptual foundations

For Einstein, the central tenets of the general theory of relativity are the *Equivalence Principle* and *General Covariance* [255]. In 1915, he finalised and published his theory, marking a monumental achievement in theoretical physics. Despite the groundbreaking nature of this work, the "principles" initially faced significant criticism, with many arguing that Einstein's principles were flawed.

While this discussion will not focus extensively on these criticisms, it is valuable to explore what these principles reveal about the nature of gravity, especially in the context of extensions of general relativity.

2.2.1 The principle(s) of equivalence

The weak equivalence principle

The first principle traces back to Newton, who in *Principia* distinguished between two quantities: "mass," which governs an object's response to force, and "weight," which governs its response to gravity. In [256], Bondi intro-

duced the terms "inertial mass" m_{I} and "passive gravitational mass" m_{P}. Accordingly, Newton's second law of gravitation takes the form

$$\boldsymbol{F} = m_{\mathrm{I}}\boldsymbol{a}\,, \qquad \boldsymbol{F} = m_{\mathrm{P}}\mathbf{g}\,, \tag{2.2.1}$$

where $\boldsymbol{F}$ is the force vector, $\boldsymbol{a}$ is the acceleration vector, and $\mathbf{g}$ is the gravitational acceleration vector. Thus, Newton's equivalence principle (in modern terms) can be stated as

Newton's Equivalence Principle (NEP): *The inertial mass of a body is equal to its passive gravitational mass,* $m_I = m_P$.

Einstein, through thought experiments such as the famous falling elevator, became convinced that the key to generalising the principle of relativity to accelerated motion and gravity lies in the equality of inertial and gravitational masses [257]. To avoid the term "mass," the principle was reformulated in terms of *free fall*. The statement: "Free fall is universal" [1] captures the essence of the principle.

Given NEP, the motion of a particle in a gravitational field $\mathbf{g}(\boldsymbol{x}(t), t)$ is given by

$$\ddot{\boldsymbol{x}} = \mathbf{g}(\boldsymbol{x}(t), t)\,, \tag{2.2.2}$$

where a dot denotes a time derivative, $\boldsymbol{x}$ is the trajectory of a particle in the gravitational field. This equation is solved uniquely by specifying the particle's initial position and velocity. Particles with the same initial data will follow the same trajectory. NEP implies the Weak Equivalence Principle as stated by Will [3, 4, 258]

Weak Equivalence Principle (WEP): *If an uncharged test body is placed at an initial event in spacetime with an initial velocity, its subsequent trajectory will be independent of its internal structure and composition.*

Will further elaborates: "By uncharged test body, we mean a body that is electrically neutral, has negligible self-gravitational energy (as estimated by Newtonian theory) and is small enough so that its interaction with external field inhomogeneities can be ignored." [2]

[1] This idea originates with Galileo's inclined plane experiments, or perhaps the Leaning Tower of Pisa.

[2] Ohanian [259] defines a test particle by a limiting procedure: as its size $R \to 0$

Newton, in *Principia* (Book III, Proposition VI, Theorem VI), tested the equality of inertial and passive gravitational masses to within one part in a thousand using pendulums. Newton's work was refined by Bessel in 1832, achieving an accuracy of about one part in a hundred thousand, and by Potter in 1923, who improved this to one part in a million [3, 4]. Eötvös [261] proposed an alternative method to test the universality of free fall by studying the acceleration of two bodies of different composition in an external gravitational field. If the WEP was violated, the inertial and gravitational masses would differ. The relation between them would then take the form

$$m_{\mathrm{P}} = m_{\mathrm{I}} + \sum_i \eta^i E^i / c^2 \,, \tag{2.2.3}$$

where E^i represents the internal energy of the body due to interaction i, η^i is a dimensionless parameter quantifying the strength of the WEP violation, and c is the speed of light. The Eötvös ratio is defined as

$$\eta \equiv 2\frac{|a_1 - a_2|}{|a_1 + a_2|} \,, \tag{2.2.4}$$

where a_1 and a_2 are the accelerations of the two bodies. The Eötvös experiment uses a torsion balance to determine the ratio η for two different materials. Classical experiments by Eötvös [261], Dicke [262], and Braginsky [263] yielded limits on η around $10^{-11} - 10^{-12}$. More recent experiments, such as the "Eot-Wash" experiments, have advanced torsion balance setups to achieve limits of approximately 2×10^{-13} [264–266]. The MICROSCOPE mission has tested the WEP with an accuracy of 10^{-15} [267]. For further details on WEP tests, see [3, 4, 268].

Einstein's equivalence principles

Einstein presented various formulations of the Equivalence Principle throughout the development of general relativity. The earliest criticisms of the equivalence between gravity and acceleration were raised by Kottler [269], with similar remarks later made by Max von Laue [258]. Synge,

and mass $m \to 0$, its gravitational potential vanishes, as well as its spin and higher-order moments. See also [260].

in his book on general relativity, expressed the following scepticism [270]

> "I have never been able to understand this Principle [of Equivalence]. […] Does it mean that the effects of a gravitational field are indistinguishable from the effects of an observer's acceleration? If so, it is false. In Einstein's theory, either there is a gravitational field or there is none, according as the Riemann tensor does not or does vanish. This is an absolute property; it has nothing to do with any observer's world-line. Space-time is either flat or curved, and in several places in the book I have been at considerable pains to separate truly gravitational effects due to curvature of space-time from those due to curvature of the observer's world-line. […] The Principle of Equivalence performed the essential office of midwife at the birth of general relativity, but, as Einstein remarked, the infant would never have got beyond its long-clothes had it not been for Minkowski's concept. I suggest that the midwife be now buried with appropriate honours and the facts of absolute space-time faced."

In response to Kottler's critique, Einstein refined his explanation, clarifying that his principle pertains specifically to homogeneous gravitational fields. Crucially, it does not allow for the "removal" of gravity but rather proposes that homogeneous gravitational fields can be replaced by acceleration in a local frame. Although the "Einstein Equivalence Principle" as understood today is not identical to Einstein's original formulation, it is defined as follows, according to Will [3, 4]

Einstein's Equivalence Principle (EEP): *(i) The WEP holds, (ii) The outcome of any local non-gravitational test experiment is independent of the velocity of the freely falling apparatus (Local Lorentz Invariance, LLI), and (iii) The outcome of any local non-gravitational test experiment is independent of the location and time at which it is performed (Local Position Invariance, LPI).*

A "local non-gravitational test experiment" is conducted in a sufficiently small, shielded, freely falling frame where external gravitational inhomogeneities and self-gravitational effects are negligible. For instance, measuring the fine-structure constant qualifies as such an experiment.

The EEP implies that gravity is a manifestation of spacetime curvature [3, 4]. Consider a collection of test particles coupled to a second-rank tensor $g_{\mu\nu}$.

The Lagrangian density for the point particles is given by

$$\mathcal{L} = \sum_I \int m_I \sqrt{-g_{\mu\nu} u^\mu u^\nu} \mathrm{d}\lambda \,, \tag{2.2.5}$$

where m_I is the mass of the particle and $u^\mu = \mathrm{d}x^\mu/\mathrm{d}\lambda$ is the four-velocity with respect to some parameter λ. The resulting equation shows that particles follow geodesics of $g_{\mu\nu}$, and, by the postulates of Riemannian geometry, there exist coordinates in which $g_{\mu\nu}$ locally reduces to $\eta_{\mu\nu}$, thereby satisfying the EEP. If the matter fields couple to two distinct second-rank tensors, the Lagrangian takes the form

$$\mathcal{L} = \sum_I \int \left[m_I \sqrt{-g_{\mu\nu} u^\mu u^\nu} + n_I \sqrt{-h_{\mu\nu} u^\mu u^\nu} \right] \mathrm{d}\lambda \,, \tag{2.2.6}$$

where $h_{\mu\nu}$ is another second-rank tensor distinct from $g_{\mu\nu}$, and n_I is the coupling constant for each particle to $h_{\mu\nu}$. The resulting equation cannot be reduced to a geodesic equation unless $g_{\mu\nu}$ and $h_{\mu\nu}$ are conformally related. Hence, without this relationship, a local coordinate system in which special relativity holds cannot be established, violating the EEP [271, 272].

Assuming the WEP holds to current experimental accuracy, testing the EEP reduces to examining local Lorentz invariance and local position invariance in non-gravitational experiments; for experimental tests of the EEP, see [3, 4]. Additionally, Schiff's conjecture suggests: *any complete and self-consistent gravitational theory that obeys the WEP must also satisfy the EEP* [3]. This conjecture is supported by the fact that violations of the WEP lead to preferred frames and locations [272]. Although no proof exists, heuristic arguments in support of the conjecture are found in [3, 4, 273].

Finally, we must mention the minimal-coupling principle. Given a physical law valid in Minkowski spacetime in an inertial frame, its generalisation to curved spacetime is expressed as

$$\eta_{\mu\nu} \to g_{\mu\nu} \,, \qquad \partial_\mu \to \nabla_\mu \,. \tag{2.2.7}$$

Consider, as a simple example, the motion of a freely falling, unaccelerated

[3] In Section 2.3, we give the definitions of complete, and self-consistent theories.

particle. The particle's motion is described by

$$\frac{\mathrm{d}^2 x^\mu}{\mathrm{d}\lambda^2} = 0\,, \tag{2.2.8}$$

where $x^\mu(\lambda)$ represents the particle's parametrized path. We can rewrite this as

$$\frac{\mathrm{d}^2 x^\mu}{\mathrm{d}\lambda^2} = \frac{\mathrm{d}x^\nu}{\mathrm{d}\lambda}\partial_\nu \frac{\mathrm{d}x^\mu}{\mathrm{d}\lambda}\,. \tag{2.2.9}$$

To generalise this to curved spacetime, we replace the partial derivative with a covariant derivative, yielding

$$\frac{\mathrm{d}x^\nu}{\mathrm{d}\lambda}\partial_\nu \frac{\mathrm{d}x^\mu}{\mathrm{d}\lambda} \to \frac{\mathrm{d}x^\nu}{\mathrm{d}\lambda}\nabla_\nu \frac{\mathrm{d}x^\mu}{\mathrm{d}\lambda} = \frac{\mathrm{d}^2 x^\mu}{\mathrm{d}\lambda^2} + \Gamma^\mu_{\alpha\beta}\frac{\mathrm{d}x^\alpha}{\mathrm{d}\lambda}\frac{\mathrm{d}x^\beta}{\mathrm{d}\lambda}\,. \tag{2.2.10}$$

This procedure was straightforward in this example with no ambiguities. However, in the presence of higher-order partial derivatives, it may lead to ambiguous results due to the non-commutativity of the covariant derivative. Loosely speaking, non-minimal coupling typically refers to coupling between fields and curvature invariants.

2.2.2 General covariance

The principle of general covariance played a central role in the development of general relativity. In his 1916 paper [255], Einstein stated:

> "The general laws of nature are to be expressed by equations which hold good for all systems of coordinates, that is, are covariant with respect to any substitutions whatever (generally covariant)."

Einstein emphasised that this principle was not merely a generalisation of the relativity principle from special relativity. A direct generalisation would extend Lorentz covariance to include transformations between frames under arbitrary motion. General covariance, however, goes further: it encompasses all spacetime transformations, including those unrelated to motion, such as transformations between Cartesian and spherical coordinates. Einstein justified this broader generalisation by noting the absence of any natural restriction on the coordinate systems used to describe spacetime [274].

At first glance, general covariance may appear trivial—coordinates should not influence the predictions of a physical theory, a principle already established in Newtonian mechanics and special relativity. This was the basis of Kretschmann's objection [275], where he argued that any theory could be cast in a generally covariant form, rendering general covariance physically vacuous. For instance, Newtonian gravitation can be expressed in a generally covariant form, as shown by Cartan and Friedrichs (see [276], section 12.4), albeit by introducing *non-dynamical* fields, often referred to as absolute objects.

What distinguishes general relativity is its lack of non-dynamical quantities; in general relativity, the metric is not given *a priori*, but is instead determined dynamically by solving the field equations. This dynamical nature of the metric ensures that its interpretation and the coordinate system acquire meaning only after the solution is obtained. Bergmann captured this idea succinctly [277]

> "It is one's task to calculate the metric […] as a dynamical variable. We can take one coordinate system or another for this job, but all that we can know is the relation of one frame to the other: we do not know the relation of either to the world. 'Strong Covariance', therefore, contains not only a reference to the structural similarity of an equation and its transform: it implies as well that one frame is as good a starting point as another—that we do not need prior knowledge of its physical meaning […] which is generated at the end."

This perspective is often referred to as *background independence*. The distinction between *dynamical* and *absolute* objects introduces physical content to general covariance. Anderson [278, 279] formalised this notion, in an attempt to strengthen the principle of general covariance (see [280] for a modern discussion). However, distinguishing between dynamical and non-dynamical objects can be subtle, and rigorously identifying them might require a Hamiltonian analysis.

2.3 Dicke framework

As noted, various experiments test the principles of general relativity. The distinction between experiments that test principles rather than specific field

equations was first emphasised by Schiff [281] and Dicke [282]. Dicke introduced a framework for categorising experimental tests of gravity and initially identified two fundamental requirements for the mathematical structure of any gravitational theory:

1. Spacetime is a four-dimensional manifold, where each point represents an event.

2. The equations must be expressed in covariant form.

However, the manifold is not assumed to possess a metric or an affine connection *a priori*; rather, it is treated as a "bare" manifold. The second requirement pertains to general covariance. As previously discussed, a theory that appears non-covariant can be reformulated covariantly by introducing absolute structures. Dicke adopts a broader notion of covariance, requiring that the equations be written in tensorial form. After establishing the mathematical structure of gravitational theories, Dicke introduces two additional constraints

1. Gravity must be described by tensorial fields, such as scalars, vectors, and tensors of any rank.

2. The equations must be derivable from an invariant action.

The first condition follows naturally from the two fundamental requirements. The second condition, while more restrictive and classically less fundamental, can be relaxed. However, the most successful theories of gravity satisfy both conditions [3, 4].

Dicke's criteria may be regarded as the minimal set of conditions any gravitational theory must satisfy. We impose additional viability requirements based on theoretical and experimental considerations [3, 4, 273, 276]

- **Completeness**: The theory must account for the results of all known gravitational and non-gravitational experiments. Consequently, it must incorporate established non-gravitational physics. It should recover the correct Newtonian limit, and in the absence of gravity, it should reduce to special relativity. Since no gravitational theory is universally compatible with quantum mechanics, we do not impose such compatibility as a requirement.

- **Self-consistency**: The theory must yield unique predictions, independent of the computational approach.

These requirements arise from the well-tested nature of special relativity and Newtonian gravity within their respective domains. Any viable gravitational theory must reproduce their predictions in the appropriate limits.

2.3.1 Metric theories

Based on the previous discussion and assuming the EEP holds with high precision, we consider gravitation as a phenomenon of curved spacetime described by a Lorentzian metric $g_{\mu\nu}$. Additionally, any gravitational theory must incorporate the standard model of particle physics. No alternative formulation of the non-gravitational sectors of physics has been proposed that avoids a metric without undermining the self-consistency, completeness, or experimental validity of the theory [3, 4, 273, 276].

In [283], Thorne and Will propose a set of postulates to incorporate the requirement that spacetime must possess a metric that satisfies the EEP [276]. They state that any viable theory must allow for a mathematical formulation where

1. Spacetime is endowed with a metric.
2. The world lines of test bodies follow the geodesics of the metric.
3. The EEP is satisfied, and gravitational laws reduce to special relativity in the absence of gravity.

Note that geodesic motion follows from energy-momentum conservation, $\nabla_\mu T^{\mu\nu} = 0$, a result of the diffeomorphism invariance of the action. To illustrate, consider a gravitational theory of the form

$$S = S_{\mathrm{G}}[\boldsymbol{g}, \boldsymbol{\Phi}] + S_{\mathrm{M}}[\boldsymbol{g}, \boldsymbol{\Psi}] \,, \tag{2.3.1}$$

where $S_{\mathrm{G}}[\boldsymbol{g}, \boldsymbol{\Phi}]$ is the gravitational action, depending on the metric $\boldsymbol{g}$ and possibly other tensor fields (scalars, vectors, *etc.*) denoted as $\boldsymbol{\Phi}$, and $S_{\mathrm{M}}[\boldsymbol{g}, \boldsymbol{\Psi}]$ is the matter action, which reduces to the standard model in flat spacetime,

with $\boldsymbol{\Psi}$ representing the matter fields. We assume that matter fields couple universally only to the metric, and not to any other fields in S_{G}.

For the theory's action S to be diffeomorphism invariant, the matter action must also be invariant. Consider the variation of the matter action under a diffeomorphism generated by a compactly supported infinitesimal vector field χ

$$\delta S_{\mathrm{M}} = \int \mathrm{d}^4x \left[\frac{\delta S_{\mathrm{M}}}{\delta g^{\mu\nu}} \mathfrak{L}_\chi g^{\mu\nu} + \frac{\delta S_{\mathrm{M}}}{\delta \boldsymbol{\Psi}} \mathfrak{L}_\chi \boldsymbol{\Psi} \right] = 0 \,, \tag{2.3.2}$$

where $\delta S_{\mathrm{M}}/\delta \boldsymbol{\Psi} = 0$ represents the equation of motion for the matter fields and evaluates to zero on-shell. This follows from the assumption that no gravitational fields other than the metric appear in S_{M}, as dictated by the EEP. Thus, we obtain

$$0 = 2 \int \mathrm{d}^4x \frac{\delta S_{\mathrm{M}}}{\delta g_{\mu\nu}} \nabla_\mu \chi_\nu = - \int \mathrm{d}^4x \sqrt{-g} \chi_\nu \nabla_\mu \left(\frac{2}{\sqrt{-g}} \frac{\delta S_{\mathrm{M}}}{\delta g_{\mu\nu}} \right) , \tag{2.3.3}$$

where we applied integration by parts and discarded boundary terms due to the compact support of χ. From this, and using the definition of the energy-momentum tensor, we conclude

$$\nabla_\mu T^{\mu\nu} = 0 \,. \tag{2.3.4}$$

This shows that diffeomorphism invariance implies energy-momentum conservation. However, this is only valid when the matter action S_{M} depends solely on the metric as the gravitational field. If, for example, a scalar field ϕ is present in both actions, then $\delta S_{\mathrm{M}}/\delta\phi$ would not vanish, and energy-momentum conservation would not hold as described.

To see how the geodesic equation follows from energy-momentum conservation, consider non-interacting dust particles with proper mass density ρ and common four-velocity u^μ, so that $T^{\mu\nu} = \rho u^\mu u^\nu$. Then

$$\nabla_\mu T^{\mu\nu} = \rho u^\mu \nabla_\mu u^\nu + u^\nu \nabla_\mu (\rho u^\mu) \,. \tag{2.3.5}$$

The second term vanishes due to particle conservation, and the first term gives the geodesic equation.

These postulates have been particularly useful in the context of the parametrised post-Newtonian framework [283–286]. The post-Newtonian formalism is an approximation of general relativity and other metric theories of gravity, valid in the weak-field limit where gravitational sources are approximated by Newtonian theory and velocities are small (non-relativistic). The parameters in the post-Newtonian framework vary by theory and can be experimentally constrained, providing a method to compare these theories.

The postulates discussed provide a foundational framework for constructing and analysing viable metric theories of gravity. They serve as guiding principles for ensuring consistency with the equivalence principle and experimental constraints. However, for instance, Brans-Dicke theory, in its original formulation [287], satisfies the EEP, whereas in the representation given in [288], it does not. This example illustrates that the theory's formulation can influence whether it satisfies these principles or not. Moreover, open questions remain regarding the precise classification of gravitational and non-gravitational fields [289].

2.4 General relativity

After addressing geometric concepts and conceptual issues to establish gravity as the curvature of spacetime, we must specify how matter and geometry interact; Einstein's field equations precisely encapsulate this idea. Multiple derivations exist; for example, see section 17.5 of [276]. The most convenient approach is through the principle of least action. We impose the following conditions on the action

1. It must be a scalar constructed solely from the metric.

2. It must be at most second-order in derivatives of the metric.

The first condition is trivial, as covariant equations of motion must be expressed in terms of tensors. The second condition is less intuitive. In physics, second-order equations of motion are typically preferred; they are less prone to instabilities and easier to solve. Hence, the action should be at most first-order in derivatives to yield second-order equations upon variation. However, two considerations complicate this: first, the metric and its derivatives

can be set to zero at any point; second, no covariant quantity can be constructed from the first derivative of the metric. As a result, we are left with the Ricci scalar, the simplest non-trivial scalar constructed from the metric and its derivatives. Hilbert defined the gravitational action for general relativity as

$$S_{\mathrm{EH}} = \frac{1}{2\kappa}\int \mathrm{d}^4x\sqrt{-g}R\,. \tag{2.4.1}$$

The variation of this action is detailed in any standard textbook on general relativity (*e.g.*, [5, 25, 290]). It turns out that the equations derived from extremizing this action are second-order in derivatives, as the Einstein-Hilbert action is degenerate. However, to ensure a well-defined variational principle, we must supplement the Einstein-Hilbert action (2.4.1) with a boundary term known as the Gibbons-Hawking-York boundary term [291, 292], which is constructed from the trace of the intrinsic curvature

$$K = \gamma^{\mu\nu}K_{\mu\nu} = \gamma^{\mu}{}_{\nu}\nabla_{\mu}n^{\nu}\,, \tag{2.4.2}$$

where $\gamma_{\mu\nu}$ is the induced metric on the boundary and n_{μ} is the normal. The boundary term is

$$S_{\mathrm{GHY}} = \frac{1}{\kappa}\int_{\partial\mathcal{M}} \mathrm{d}^3x\sqrt{|\gamma|}K\,. \tag{2.4.3}$$

For a more detailed discussion of these issues, see [293]. The total action is then

$$S = S_{\mathrm{EH}} + S_{\mathrm{GHY}} + S_{\mathrm{M}}\,, \tag{2.4.4}$$

which yields Einstein's equation upon variation

$$G_{\mu\nu} = \kappa T_{\mu\nu}\,, \tag{2.4.5}$$

with the energy-momentum tensor given by

$$T_{\mu\nu} \equiv -\frac{2}{\sqrt{-g}}\frac{\delta S_{\mathrm{M}}}{\delta g^{\mu\nu}}\,, \tag{2.4.6}$$

and the Einstein tensor $G_{\mu\nu}$

$$G_{\mu\nu} \equiv R_{\mu\nu} - \frac{1}{2} g_{\mu\nu} R \,. \tag{2.4.7}$$

Einstein's theory of gravity, based on the conceptual foundations outlined in Section 2.2, assumes a four-dimensional spacetime $(\mathcal{M}, \boldsymbol{g})$, with gravity dynamics governed by the Einstein field equations. The sole degree of freedom mediating gravity is the metric governed by second-order (quasi-linear) partial differential equations.

Chapter III

Gravity and scalar fields

Contents

After examining the conceptual foundations and mathematical structure underlying general relativity, a natural question arises: Are the Einstein field equations *unique*? Lovelock addressed this question affirmatively.

Theorem 3.0.1 *(Lovelock [294, 295]) In four spacetime dimensions, the only diffeomorphism invariant, divergence-free, symmetric rank-*2 *tensor constructed only from the metric and its first and second derivatives is the Einstein tensor and the metric tensor itself.*

To develop a theory of gravity different from Einstein's, we must relax some of these assumptions. Focusing on theories with second-order equations of motion, three possibilities arise:

1. More space dimensions.

2. Breaking diffeomorphism invariance.

3. Including additional degrees of freedom besides the metric.

The first option, which retains the metric as the sole degree of freedom, leads to Lovelock theories of gravity [294], which generalise general relativity to higher-dimensional spacetimes. The third option allows for the inclusion of scalar, vector, and tensor fields alongside the metric. These two options are not mutually exclusive, as higher-dimensional theories can be mapped onto lower-dimensional ones with extra degrees of freedom, such as in Kaluza-Klein theory [296]. Additionally, broken gauge symmetries can be restored by introducing further fields, as demonstrated by the Stueckelberg mechanism [297].

We maintain the requirement for second-order equations, as higher-derivative theories are often plagued by Ostrogradsky instabilities [77, 78]. Nonetheless, higher-derivative terms naturally arise within the effective field theory approach (see Section 3.4), and the differential order of the equations can be reduced by introducing additional degrees of freedom. Other approaches extend general relativity by considering non-local theories, non-Riemannian geometries, or by breaking local Lorentz invariance. For reviews, see [58, 63, 272, 298]. Therefore, in general, relaxing any of the assumptions in Lovelock's theorem results in extra degrees of freedom.

As discussed in Section 1.3, general relativity faces certain challenges, and various approaches aim to address them. In this context, scalar fields are particularly prominent. They appear in numerous extensions of the Standard Model to address issues such as the hierarchy problem [1] [128], the Strong-CP problem, dark matter, and the universe's accelerated expansion, as well as in many approaches to quantum gravity. In this work, we primarily focus on light scalar fields as additional degrees of freedom. If such scalar fields couple to curvature, they can significantly influence extreme gravitational dynamics.

3.1 Brans-Dicke theory

Dicke, through his pioneering work on the foundations of gravity, along with Brans, introduced one of the earliest theories challenging general relativity [287]. This theory includes, in addition to the metric, a scalar degree of freedom described by the following action

$$S_{\rm BD} = \frac{1}{16\pi G}\int \mathrm{d}^4x\sqrt{-g}\left[\varphi R - \frac{\omega_{\rm BD}}{\varphi}\nabla_\mu\varphi\nabla^\mu\varphi\right] + S_{\rm M}[g_{\mu\nu}, \boldsymbol{\Psi}]\,, \tag{3.1.1}$$

where φ is the scalar field, $\boldsymbol{\Psi}$ collectively represents matter fields, and $\omega_{\rm BD}$ is the Brans-Dicke parameter. In this formulation, the scalar field couples non-minimally to the Ricci scalar R, but does not couple to matter.

This formulation shows that the theory satisfies Einstein's equivalence principles (see Section 2.2.1). The theory also predicts a varying effective gravitational "constant" given by $G_{\rm eff} = G/\varphi$, where G is Newton's constant. A variable gravitational coupling embodies Mach's principle as formulated by Dicke: "the gravitational constant should be a function of the mass distribution of the universe," which was a key motivation for this theory.

The extra free parameter $\omega_{\rm BD}$ can be constrained by solar system tests to the bound:

$$|\omega_{\rm BD}| > 4\times 10^4\,. \tag{3.1.2}$$

[1] The hierarchy problem concerns the large difference between the electroweak and Planck energy scales.

While dimensionless parameters are typically expected to be of order unity, the large value of the Brans-Dicke parameter renders the theory an unlikely competitor to general relativity. However, it serves as a special case of more general theories that include a scalar field, and can be generalised to the broader class of scalar-tensor theories of gravity.

3.2 Scalar-tensor theories

Scalar-tensor theories are a generalisation of Brans-Dicke theory. They are described by the following action [299]

$$S_{\mathrm{ST}} = \frac{1}{2\kappa}\int \mathrm{d}^4x\sqrt{-g}\left[A\left(\varphi\right)R - \frac{1}{2}B\left(\varphi\right)\nabla_\mu\varphi\nabla^\mu\varphi - V\left(\varphi\right)\right] + S_{\mathrm{M}}\left[e^{2C\left(\varphi\right)}g_{\mu\nu}, \boldsymbol{\Psi}\right] . \tag{3.2.1}$$

In this form, scalar-tensor theories have four free functions: $A\left(\varphi\right)$, $B\left(\varphi\right)$, $C\left(\varphi\right)$, and the potential $V\left(\varphi\right)$. However, action (3.2.1) is formally invariant under a scalar field redefinition and a conformal transformation [299], leaving only two functional degrees of freedom. Thus, we can freely fix any two of the four functions without selecting a specific theory. Further choices specify a particular scalar-tensor theory.

This freedom allows different representations in which various functions are fixed. These are called "conformal frames" and, with reasonable transformations [289, 300], are physically equivalent. They reflect our choice of rods and clocks [288, 289, 300]. Choosing one frame over another can simplify the problem, much like using a convenient coordinate system. Thus, care is required when interpreting non-conformally invariant quantities, as different frames may present different features.

Alternatively, the more commonly used practice is to fix two functions, while still allowing for field redefinitions of the metric and the scalar field. In this way, although the theory itself is specified, the freedom to choose different representations via field redefinitions remains entirely unrestricted [289, 300].

In the literature, there are two commonly used representations or choices

of conformal frames:

- The **Jordan frame**—In this case, we fully fix the representation by choosing $A(\varphi) = \phi$ and $C(\varphi) = 0$. The free functions are $B(\varphi)$ and $V(\varphi)$. In the Jordan frame, the energy-momentum tensor is covariantly conserved with respect to the metric $g_{\mu\nu}$ (see Section 2.3.1); thus, the metric postulates are satisfied.

- The **Einstein frame**—In this case, we have $A(\varphi) = 1$ and $B(\varphi) = 1$. The free functions are $C(\varphi)$ and $V(\varphi)$. Due to the conformal factor, $e^{2C(\varphi)}$, present when coupling the metric to matter fields, the energy-momentum tensor is *not* covariantly conserved [289, 300]. This is simple to see in light of the discussion in Section 2.3.1. Put differently, under a conformal transformation $g_{\mu\nu} \to \hat{g}_{\mu\nu} = \Omega^2 g_{\mu\nu}$, the relation $\nabla_\mu T^{\mu\nu} = 0$ in the Jordan frame translates to [25]

$$\hat{\nabla}_\alpha \hat{T}^{\alpha\beta} = -\hat{T}\frac{\hat{g}^{\alpha\beta}\hat{\nabla}_\alpha \Omega}{\Omega}\,, \tag{3.2.2}$$

  in the Einstein frame. Hence, the metric postulates are not satisfied.

If we are only presented with the theory in the Einstein frame, we could, for example, naively conclude that it is not a metric theory. Notwithstanding, such conclusions are representation-dependent, and it suffices to have at least one representation in which the theory is a metric theory to treat it as such. In scalar-tensor theories, identifying and constructing frame-independent quantities is not a trivial task, and as already emphasised, general statements must be deduced prudently.

Now, let us consider the following generalisations of Brans-Dicke theory (3.1.1)

$$S_{\text{gBD}} = \frac{1}{2\kappa}\int \mathrm{d}^4x\sqrt{-g}\left[\varphi R - \frac{\omega(\varphi)}{\varphi}\nabla_\mu\varphi\nabla^\mu\varphi - V(\varphi)\right] + S_{\text{M}}[g_{\mu\nu}, \boldsymbol{\Psi}]\,. \tag{3.2.3}$$

We arrive at such a theory by promoting the coupling constant ω_{BD} to a function of the scalar field and including a potential $V(\varphi)$. This is precisely scalar-tensor theory (3.2.1) in the Jordan frame with the more familiar convention

for the function $B\left(\varphi\right) = 2\omega\left(\varphi\right)/\varphi$.

As mentioned, the theory (3.2.3) is a metric theory of gravity in which the scalar field does not couple to matter. Instead, the scalar field influences the metric and, consequently, the curvature of spacetime [2, 4]. Additionally, the constraint on $\omega_{\rm BD}$ still applies to $\omega(\varphi_{\rm present})$, where $\varphi_{\rm present}$ is the current value of the scalar field. The constraint no longer holds if the scalar field has a large mass, and the scalar becomes short-ranged [2].

To explicitly rewrite $S_{\rm gBD}$ in the Einstein frame we perform the scalar field redefinition as $2\varphi {\rm d}\phi = \sqrt{2\omega(\phi)+3}{\rm d}\varphi$ and the conformal transformation $\hat{g}_{\mu\nu} = \varphi\, g_{\mu\nu}$. The action then becomes

$$S_{\rm gBD} = \frac{1}{2\kappa}\int {\rm d}^4x\sqrt{-\hat{g}}\left[\hat{R} - 2\hat{g}^{\mu\nu}\partial_\mu\phi\partial_\nu\phi - U(\phi)\right] + S_{\rm M}[g_{\mu\nu}, \boldsymbol{\Psi}]\,, \tag{3.2.4}$$

where $U(\phi) = V(\varphi)/\varphi^2$.

As already discussed, and to sum up, the variables $(\hat{g}_{\mu\nu}, \phi)$ define the *Einstein frame*, while $(g_{\mu\nu}, \varphi)$ are the *Jordan frame* variables. In the Einstein frame, the gravitational action of scalar-tensor theories is reduced to general relativity minimally coupled to a scalar field. However, matter fields couple *non-minimally* to the scalar field, as evidenced when $S_{\rm M}[g_{\mu\nu}, \boldsymbol{\Psi}]$ is expressed in terms of $\hat{g}_{\mu\nu}$, ϕ, and $\boldsymbol{\Psi}$. Hence, in the Einstein frame, matter does not follow geodesics of $\hat{g}_{\mu\nu}$, since the energy-momentum tensor is not conserved. Conversely, in the Jordan frame, matter follows geodesics of $g_{\mu\nu}$. Although the two frames are equivalent, and will lead to the same results for physical observables, they do provide distinct interpretations of the variables (see, *e.g.*, [289, 299]).

3.3 Horndeski theory

The action for scalar-tensor theories can be further generalised by allowing higher-order derivatives of the scalar field in the action, while ensuring that the equations of motion remain second-order in both the scalar field and the

[2] A short-ranged scalar field typically implies a rapidly decaying force with distance, effectively limiting the influence of the field to small scales.

metric derivatives. This generalisation was first proposed by Horndeski [301]. The action of the theory can be written as

$$S_{\rm H} = \sum_{i=2}^{5} \int \mathrm{d}^4x \sqrt{-g}\mathcal{L}_i + S_{\rm M}[g_{\mu\nu}, \boldsymbol{\Psi}] \,, \tag{3.3.1}$$

where

$$\mathcal{L}_2 = G_2(\phi, X) \,, \tag{3.3.2}$$
$$\mathcal{L}_3 = -G_3(\phi, X)\Box\phi \,, \tag{3.3.3}$$
$$\mathcal{L}_4 = G_4(\phi, X)R + G_{4X}[(\Box\phi)^2 - (\nabla_\mu\nabla_\nu\phi)^2] \,, \tag{3.3.4}$$
$$\mathcal{L}_5 = G_5(\phi, X)G_{\mu\nu}\nabla^\mu\nabla^\nu\phi \tag{3.3.5}$$
$$- \frac{G_{5X}}{6}\left[(\Box\phi)^3 - 3\Box\phi(\nabla_\mu\nabla_\nu\phi)^2 + 2(\nabla_\mu\nabla_\nu\phi)^3\right] \,, \tag{3.3.6}$$

and the G_i's are functions of the scalar field and its kinetic term $X = -\nabla_\mu\phi\nabla^\mu\phi/2$. We define $G_{iX} \equiv \partial G_i/\partial X$, $\Box \equiv g^{\mu\nu}\nabla_\mu\nabla_\nu$, $(\nabla_\mu\nabla_\nu\phi)^2 \equiv \nabla_\mu\nabla_\nu\phi\nabla^\mu\nabla^\nu\phi$, and $(\nabla_\mu\nabla_\nu\phi)^3 \equiv \nabla_\mu\nabla_\nu\phi\nabla^\nu\nabla^\lambda\phi\nabla_\lambda\nabla^\mu\phi$.

Scalar fields that satisfy local Galilean symmetry, *i.e.*, $\phi \to \phi + c_\mu x^\mu + c$ for constants c_μ and c, are known as Galileons. Only a subclass of the Horndeski action reduces to that of Galileons in flat spacetime. Hence, scalar fields satisfying (3.3.1) are sometimes referred to as generalised Galileons [302].

3.3.1 Scalar Gauss-Bonnet gravity

A notable model within the Horndeski family is scalar Gauss-Bonnet gravity, characterised by a non-minimal coupling between a scalar field ϕ and the Gauss-Bonnet invariant $\mathcal{G}$

$$S_{\rm GB} = \frac{1}{2\kappa}\int \mathrm{d}^4x\sqrt{-g}\left[R - \frac{1}{2}\nabla_\mu\phi\nabla^\mu\phi + f(\phi)\mathcal{G}\right] \,, \tag{3.3.7}$$

where $f(\phi)$ is a coupling function. From an effective field theory perspective (see Section 3.4), the leading order corrections to general relativity minimally coupled to a scalar field are the $f(\phi)\mathcal{G}$ and X^2 interactions [303]. In this thesis, however, our analysis is restricted to the Gauss-Bonnet coupling. The motivation for focusing on this specific interaction, particularly in the con-

text of black holes, is discussed in detail below. The choices of G_i's that lead to the Gauss-Bonnet term are given by [304]

$$G_2^{\rm GB} = 8\frac{\partial^4 f}{\partial\phi^4}X^2\,(3-\ln X)\ , \tag{3.3.8}$$

$$G_3^{\rm GB} = 4\frac{\partial^3 f}{\partial\phi^3}X\,(7-3\ln X)\ , \tag{3.3.9}$$

$$G_4^{\rm GB} = 4\frac{\partial^2 f}{\partial\phi^2}X\,(2-\ln X)\ , \tag{3.3.10}$$

$$G_5^{\rm GB} = -4\frac{\partial f}{\partial\phi}\ln X\ . \tag{3.3.11}$$

These choices are not smooth at $X = 0$. However, the combinations that appear in action (3.3.7) and its equations of motion are. Moreover, when the theory is expressed in terms of the various G functions, the limit $X \to 0$ can be analysed with care, leading to no singular behaviour. For the technical details see [305].

The equations of motion are

$$G_{\mu\nu} = T^{\phi}_{\mu\nu}\,, \tag{3.3.12}$$

$$\Box\phi = -f'(\phi)\mathcal{G}\,, \tag{3.3.13}$$

where the energy-momentum tensor $T^{\phi}_{\mu\nu}$ is

$$\begin{aligned} T^{\phi}_{\mu\nu} = &-\frac{1}{4}g_{\mu\nu}(\nabla\phi)^2 + \frac{1}{2}\nabla_\mu\phi\nabla_\nu\phi \\ &-\frac{\alpha}{g}g_{\mu(\rho}g_{\sigma)\nu}\epsilon^{\kappa\rho\alpha\beta}\epsilon^{\sigma\gamma\lambda\tau}R_{\lambda\tau\alpha\beta}\nabla_\gamma\nabla_\kappa f(\phi)\,, \end{aligned} \tag{3.3.14}$$

and $\epsilon^{\sigma\gamma\lambda\tau}$ is the Levi-Civita totally antisymmetric tensor density.

If the coupling between the scalar and the Gauss-Bonnet invariant is linear, *i.e.*, $f(\phi) = \alpha\phi$, then the scalar field equation takes the form

$$\Box\phi = -\alpha\mathcal{G}\,, \tag{3.3.15}$$

demonstrating that the geometry sources the scalar field. The scalar field cannot remain trivial because the Gauss-Bonnet term is generally non-vanishing

in black hole spacetimes (see Section 4.2) [306–308]. Consequently, *all* black hole solutions in this theory necessarily differ from those in general relativity. This provides a clear example of a violation of the no-hair theorems when a scalar field couples non-minimally to gravity.

This raises a natural question: Can a single theory admit both general relativity and non-general relativity black hole solutions? The answer is affirmative. This can occur when the scalar field couples to the Gauss-Bonnet invariant through higher-order interactions, such as a quadratic coupling $\alpha\phi^2\mathcal{G}$.

This can be understood qualitatively by considering linear perturbations of the scalar on a fixed general relativity background. The scalar perturbations will acquire a spacetime-dependent effective squared mass. If the effective squared mass becomes sufficiently negative, a tachyonic instability will develop. If non-linear effects suppress this instability, the system can settle into a new equilibrium state involving both a non-trivial scalar field and a modified geometry—a *scalarized* configuration. We discuss this phenomenon in more detail in the next section.

3.3.2 Scalarization mechanism

Scalarization, first introduced in [309] in the context of neutron stars, is a mechanism by which compact objects can be dressed up with a non-trivial scalar configuration. At the perturbative level, spontaneous scalarization manifests as a tachyonic instability that drives an exponential growth of the scalar field. For this instability to appear, scalar perturbations have to acquire a negative effective squared mass on a fixed background that is a solution of general relativity. This only happens if the mass or spin of the general relativity solution is within some range. As the scalar field grows due to this instability, perturbative analysis will eventually cease to be valid, and non-linear effects will take control. If they drive the configuration to a new stable equilibrium, then this will be a "scalarized" compact object. See [310] for a more comprehensive introduction.

Consider, for example, a theory in which the scalar field couples to the Ricci scalar as $\phi^2 R$. The effective mass of the scalar field will be proportional to the Ricci scalar, so if the Ricci scalar acquires the right sign and size in a region of spacetime, the scalar field will become tachyonically unstable. Such

an effect was first illustrated in the case of neutron stars [309] in a model that is equivalent to having $\phi^2 R$ interaction at the linear level [311]. Since vacuum black hole spacetimes in general relativity have zero Ricci scalar, scalar perturbations around them are massless in this model, and black hole scalarization does not occur. Indeed, this class of theories is covered by no-hair theorems [312, 313].

Black hole scalarization can be implemented in the framework of Horndeski gravity through a coupling between the scalar and the Gauss-Bonnet invariant [314, 315]

$$S = \int \mathrm{d}^4x\sqrt{-g}\left(R + 2X + f(\phi)\mathcal{G}\right) . \tag{3.3.16}$$

The function $f(\phi)$ is a general function of the scalar field, and the scalar equation is

$$\Box\phi + \frac{1}{2}f'(\phi)\mathcal{G} = 0\,, \qquad \Box \coloneqq \nabla_\mu\nabla^\mu\,. \tag{3.3.17}$$

If f is taken to be linear in ϕ, the only allowed solutions are those with non-trivial scalar profile [306, 307] (see Section 4.2), with the linear coupling not contributing to the effective mass. If instead $f'(\phi_0) = 0$ and $f''(\phi_0)\mathcal{G} < 0$ for some ϕ_0, it was shown in [314] that stationary and asymptotically flat general relativity black holes are unique. The first condition specifies that general relativity black holes are allowable, whereas the subsequent condition pertains to the mass of the scalar perturbation near ϕ_0. Consider a perturbation $\delta\phi$ of the scalar around ϕ_0 *i.e.*, take $\phi = \phi_0 + \delta\phi$ on a fixed background, then equation (3.3.17) yields,

$$(\Box - \mu_{\rm eff}^2)\delta\phi = 0\,, \qquad \mu_{\rm eff}^2 = -\frac{1}{2}f''(\phi_0)\mathcal{G}\,, \tag{3.3.18}$$

therefore, the term $-f''(\phi_0)\mathcal{G}$ acts as an effective mass for the perturbations. Now, assuming that $f'(\phi_0) = 0$ holds, if $f''(\phi_0)\mathcal{G} > 0$ and sufficiently large, the scalar will develop the tachyonic instability associated with scalarization. The endpoint of this instability will vary depending on which other non-linear interactions one might choose to include in the action [316–320], which can lead to scalarized black holes with different properties. For a study

of the most general interactions that contribute to the onset of scalarization, see [311].

It is important to note that, for a Schwarzschild black hole, the Gauss-Bonnet invariant is $\mathcal{G} = 48M^2/r^6$, where M is the mass of the black hole, and r is the areal radius coordinate. Hence, $\mathcal{G}$ is positive definite and monotonic in r. This implies that less massive black holes are more prone to suffer from a tachyonic instability and that above a mass threshold, scalarization will not occur because the effective mass is not sufficiently negative. For the Kerr geometry, the situation is more subtle since the Gauss-Bonnet invariant is not monotonic and can even become negative close to the horizon. In this case, scalarization can occur for rapidly rotating black holes with $a/M \gtrsim 0.5$, where a is the spin parameter [321–323]. This is referred to as spin-induced scalarization.

3.3.3 Scalar Gauss-Bonnet with a Ricci coupling

In the previous section, we examined how compact objects such as neutron stars and black holes can acquire a non-trivial scalar profile through spontaneous scalarization. In the neutron star case, the scalar field couples quadratically to the Ricci scalar, while for black holes the leading-order contribution to the tachyonic instability arises from a quadratic coupling to the Gauss–Bonnet invariant. These two terms are the only interactions capable of triggering a tachyonic instability around a general relativity background [310], motivating the following model

$$S = \frac{1}{16\pi}\int \mathrm{d}^4x\sqrt{-g}\left[R + X + f(\phi)\mathcal{G} + h(\phi)R\right], \qquad (3.3.19)$$

where $g = \det(g_{\mu\nu})$, $X = -\nabla_\mu\phi\nabla^\mu\phi/2$. We use units of $G = 1 = c$. The function $h(\phi)$ is a dimensionless coupling function while $f(\phi)$ is of dimension length squared. Here, we are using the coupling functions f, g for generality's sake. The coupling $h(\phi)R$ can be removed by a conformal transformation and a field redefinition of the scalar. However, for a non-perturbative transformation, the Gauss-Bonnet term will generate itself under a confor-

mal transformation. It also produces various derivative self-interactions of the scalar and a non-minimal coupling to gravity (See, *e.g.*, [324, 325]). Even if we put aside the simplicity of having only the coupling $h(\phi)R$, it is not obvious that the conclusions reached in the following chapters—regarding well-posedness (see Section 6.1)—will still hold. Well-posedness is ultimately a statement about a specific formulation of the theory. See also the discussion in Section 8.6.

The equations of motion read

$$\begin{aligned} E^{\mu}{}_{\nu} \equiv & -T^{(\phi)\mu}{}_{\nu} + \delta^{\mu\gamma\kappa\lambda}_{\nu\alpha\rho\sigma} R^{\rho\sigma}{}_{\kappa\lambda} \nabla_{\gamma}\nabla^{\alpha} f \\ & + (1+h) G^{\mu}{}_{\nu} + \delta^{\mu}{}_{\nu}\Box h - \nabla^{\mu}\nabla_{\nu} h = 0\,, \end{aligned} \tag{3.3.20}$$

$$E \equiv -\Box\phi - h'(\phi)R - f'(\phi)\mathcal{G} = 0\,, \tag{3.3.21}$$

with

$$T^{(\phi)}_{\mu\nu} = \frac{1}{2}\nabla^{\mu}\phi\nabla_{\nu}\phi - \frac{1}{4}(\nabla\phi)^2 g_{\mu\nu}\,, \tag{3.3.22}$$

where, $\delta^{\mu\gamma\kappa\lambda}_{\nu\alpha\rho\sigma}$ is the generalized Kronecker delta. As we have discussed, we will mainly focus on the class of theories specified by

$$f(\phi) = \frac{\alpha}{2}\phi^2\,, \qquad h(\phi) = -\frac{\beta}{4}\phi^2\,. \tag{3.3.23}$$

Scalarization occurs for strongly gravitating compact objects. In weak gravitational fields, the geometry follows general relativity without deviations. For scalarization, we assumed a constant scalar field and considered perturbations of the form $\phi = \phi_0 + \delta\phi$ around a general relativity background. However, it was shown in [326] that cosmic evolution can drive the scalar field away from ϕ_0. In such cases, and without fine-tuning of the initial conditions, even weakly gravitating objects can scalarize, ruling out both the original scalarization model and the Gauss-Bonnet model through weak-field and cosmological tests [327–329].

The Ricci-Gauss-Bonnet model, first studied in late-time cosmology, avoids these constraints. In the theory (3.3.19) with the coupling (3.3.23) and $\beta > 0$, general relativity emerges as a late-time cosmic attractor [330], leading to a constant scalar field asymptotically. Binary pulsars provide

the most stringent constraints, motivating scenarios where black holes scalarize but neutron stars do not. Indeed, the work in [331] showed that for $\beta > 0$, this occurs when α lies in a specific range. Moreover, in [332] it was demonstrated that $\beta > 0$ yields radially stable black holes, unlike the $\beta = 0$ case.

3.4 Effective field theories

Effective field theories are essential tools in theoretical physics. They rest on the principle that, in practice, not all degrees of freedom influence one another at all scales, and that meaningful physical phenomena emerge at distinct energy scales. An effective theory enables predictive power using a finite number of input parameters, making it particularly valuable for systems characterised by widely separated energy scales [84, 85, 333–335].

To illustrate this, consider a theory defined by an ultraviolet cut-off Λ, containing light degrees of freedom l with masses $m_l \ll \Lambda$ and energies $E_l \ll \Lambda$, and heavy degrees of freedom H with masses $m_H \sim \Lambda$. When probing energies $E \ll \Lambda$, the influence of the heavy fields on low-energy physics simplifies, allowing for a systematic expansion in the small parameter E/Λ. A low-energy theory can then be derived by integrating out the heavy fields from the full theory. Assuming the complete action is $S[l, H]$, the effective field theory at low energies is given by

$$e^{iS_{\text{eff}}[l]} = \int \mathcal{D}H(x) e^{iS[l,H]} \,. \tag{3.4.1}$$

It follows that $S_{\text{eff}}[l]$ is a local action for the light fields, expressed as

$$S_{\text{eff}}[l] = \sum_i c_i \int \mathrm{d}^4x \, \mathcal{O}_i(x) \,, \tag{3.4.2}$$

where the sum runs over an infinite set of local operators $\mathcal{O}_i$. The coefficients c_i, known as Wilson coefficients, encode the effects of high-energy physics. If the operator $\mathcal{O}_i$ has mass dimension Δ_i (in $\hbar = 1 = c$ units), then the

corresponding Wilson coefficient scales as

$$c_i = \frac{\tilde{c}_i}{\Lambda^{\Delta_i - 4}}\,, \tag{3.4.3}$$

where $\tilde{c}_i$ is a dimensionless constant typically of order unity. In practice, the series is truncated at a finite order, determined by the desired level of accuracy.

Thus, the ultraviolet physics is effectively captured by the Wilson coefficients in the low-energy theory, up to a specified precision. A straightforward power-counting argument reveals how each operator O_i depends on the high-energy scale Λ. In general, the effective theory admits two primary applications:

- **Top-down approach**—The ultraviolet theory is known. Effective field theories are employed to simplify calculations. When probing energy scales well below the cut-off Λ, integrating out heavy modes yields a systematic and simplified description of the impact of high-energy physics on low-energy observables.

- **Bottom-up approach**—The ultraviolet theory is unknown. Regardless of the specific high-energy dynamics at scale Λ, the low-energy theory is described by (3.4.2). If the low-energy symmetries are known or assumed, the operators O_i must respect them. The ultraviolet physics is then encoded by constructing the most general effective action consistent with these symmetries.

The bottom-up approach is helpful when the ultraviolet theory is unknown, as is the case for the gravitational interaction. In this context, the Ricci scalar in the Einstein-Hilbert action appears as the leading non-trivial operator in the gravitational effective action at low energies. Assuming the metric is the sole low-energy degree of freedom and imposing diffeomorphism invariance, the effective action for gravity can be written as [84, 85]

$$\mathcal{L}_{\text{eff}} = c_0\Lambda^4 + \frac{M_{\text{Pl}}^2}{2}R + c_1 R_{\mu\nu}R^{\mu\nu} + c_2 R^2 + c_3 R_{\mu\nu\alpha\beta}R^{\mu\nu\alpha\beta} + \frac{c_4}{\Lambda^2}R^3 + \dots\,. \tag{3.4.4}$$

The coefficients c_i are all dimensionless, with Λ being an energy scale. Assume, in general, that the high-energy completion has many scales. The first

term, corresponding to the cosmological constant, does not fit within the traditional framework of effective field theory. To elaborate, the first term in action (3.4.4) is the zero-derivative term. By effective field theory logic, one would naively expect that the largest scale contributing to Λ, such as $M_{\rm Pl}$, would dominate. That is, $c_0\Lambda^4 = c_0 M_{\rm Pl}^4 + c_0 M^4$, where M is a lower mass/energy scale(s) than $M_{\rm Pl}$. So the cosmological constant should be the largest contribution in theory (3.4.4). After all, this is exactly the case for the two-derivative term, $M_{\rm Pl}^2 R$. The largest scale $M_{\rm Pl}$ dominates the contribution to the Ricci term. Therefore, *puzzlingly*, the tiny value of the cosmological constant does not conform to effective field theory arguments.

On the other hand, the coefficients of the quadratic curvature terms are dimensionless of order unity. Moreover, for higher than quadratic curvature terms, the energy scale Λ should be set by the lowest energy scale that has been integrated out. It need not coincide with the Planck scale [84, 85].

Finally, a similar interpretation holds for other extensions of general relativity. For example, Horndeski gravity introduces an additional low-energy scalar degree of freedom alongside the metric.

Chapter IV

Black holes in extensions of general relativity

Contents

4.1 No-hair theorems

Uniqueness theorems for black holes [33, 34] assert that all vacuum, asymptotically-flat, and stationary black holes in general relativity are described by a two-parameter family of solutions characterised by their mass and spin, known as the Kerr metric [32]. Wheeler coined the expression "a black hole has no hair" based on these assertions. Many no-hair theorems (or conjectures) attempt to generalise the uniqueness theorems in the presence of additional forms of matter [312, 313, 336–343]. The advent of gravitational wave astronomy, together with very-long-baseline-interferometry observations, presents a great opportunity to test whether astrophysical black holes are indeed described by the Kerr metric and potentially challenge the principles of general relativity [57–63, 69, 70]. In this context, deviations from the Kerr metric would indicate a breakdown in our understanding of gravity, which together with the many shortcomings of general relativity, and puzzles in the standard model of particle physics [63, 181, 234, 344–347] motivate the study of theories beyond general relativity and their black hole solutions (see Section 1.3).

Scalar fields are ubiquitous in extensions of general relativity and of the standard model. When non-minimally coupled to gravity, scalar fields can endow a theory with non-Kerr black holes as solutions. A prominent example is scalar-Gauss-Bonnet theories [306, 307, 310, 314, 315, 321–323, 348–350] where a scalar field is coupled to the Gauss-Bonnet invariant (see Section 3.3.1).

Initially, we will study, in Section 4.2, and Chapter V, static black holes. After which, in Chapters VI – VIII, we will turn our attention to the initial value problem and dynamical black holes.

4.1.1 Scalar no-hair theorems

We begin by considering the simple case of a massless scalar field minimally coupled to gravity

$$S = \frac{1}{2\kappa}\int \mathrm{d}^4x\sqrt{-g}\left[R - \frac{1}{2}\nabla_\mu\phi\nabla^\mu\phi\right] . \tag{4.1.1}$$

This theory is subject to a no-hair theorem. Several proofs exist, with the most concise presented by Hawking [312], which we outline here.

Consider an isolated, stationary, axisymmetric black hole as the end state of gravitational collapse. Hence, there are two Killing vector fields, ξ, ζ, one of which is time-like and the other is space-like at infinity. The scalar field is taken to respect the symmetries of the spacetime, *i.e.*, $\mathfrak{L}_\xi \phi = \mathfrak{L}_\zeta \phi = 0$. The scalar equation is given by $\Box\phi = 0$. Multiplying this equation by ϕ and integrating over a region of spacetime, $\mathcal{V}$, we obtain

$$0 = \int_{\mathcal{V}} \mathrm{d}^4x\sqrt{-g}\phi\Box\phi = \int_{\partial\mathcal{V}} \mathrm{d}^3x\sqrt{|h|}\phi n^\mu \nabla_\mu\phi - \int_{\mathcal{V}} \mathrm{d}^4x\sqrt{-g}\nabla_\mu\phi\nabla^\mu\phi\,, \tag{4.1.2}$$

where $\partial\mathcal{V}$ is the boundary of the region $\mathcal{V}$, $h_{\mu\nu}$ is the induced metric, and h is its determinant. Assume that $\mathcal{V}$ is bounded by the Killing horizon and a time-like surface at spatial infinity. The integral over the horizon vanishes because the normal n_μ to the horizon is a linear combination of the Killing vector fields, and $n^\mu\partial_\mu\phi = \mathfrak{L}_n\phi = 0$, by assumption. Moreover, the integral at spatial infinity vanishes under the assumptions of asymptotic flatness and sufficient fall-off of the scalar field. Additionally, $\partial_\mu\phi$ cannot be time-like anywhere or null everywhere since it is orthogonal to both Killing vector fields (due to the scalar's symmetries). Therefore, the integral $\int_{\mathcal{V}} \nabla_\mu\phi\nabla^\mu\phi$ can only vanish if $\partial_\mu\phi = 0$, implying $\phi =$ constant everywhere, *i.e.*, a trivial scalar field configuration.

This theorem can be extended to include a potential for the scalar field, assuming linear stability of the scalar [313]. The results imply that black hole solutions in Brans-Dicke theory are identical to those in general relativity.

In the context of Horndeski theory, assuming shift-symmetry, the only interaction that can yield a non-trivial scalar configuration is the coupling between the scalar field and the Gauss-Bonnet invariant $\mathcal{G}$ [306, 307, 351]:

$$\mathcal{G} = R_{\mu\nu\alpha\beta}R^{\mu\nu\alpha\beta} - 4R_{\mu\nu}R^{\mu\nu} + R^2\,, \tag{4.1.3}$$

which we will discuss next.

4.1.2 Linear scalar Gauss-Bonnet gravity

The case of shift-symmetric scalars is of particular interest in the context of black hole hair, both observationally and theoretically—strong gravity observations probe length (or curvature) scales on the order of kilometres. Massive scalar profiles around compact objects are expected to decay exponentially, with the characteristic decay scale set by the inverse of the scalar mass. Therefore, these observations primarily probe ultralight or massless scalars. Shift-symmetry, *i.e.*, invariance under $\phi \to \phi +$ constant, prevents scalars from acquiring a mass. As a result, strong gravity observations effectively probe scalars exhibiting either this symmetry or small violations thereof.

Interestingly, shift-symmetry implies that the equation of motion for the scalar can be written as a conservation law for a current. This property was used in [351] to establish a powerful no-hair theorem. However, it was later shown in [306] that a linear coupling between the scalar ϕ and the Gauss-Bonnet invariant $\mathcal{G}$ evades this theorem, with this coupling term being unique in this regard. Notably, the linear coupling $\phi\mathcal{G}$ arises from a small coupling or small ϕ expansion of the exponential coupling $e^{\phi}\mathcal{G}$, which has been known to introduce black hole hair [348, 349, 352].

Indeed, hairy black hole solutions in both the $\phi\mathcal{G}$ and $e^{\phi}\mathcal{G}$ models share two key properties [307]. First, the scalar charge [1] is not an independent parameter but is fixed in relation to the black hole mass and spin by a regularity condition on the horizon. Second, for any fixed value of the coupling constant governing these terms (*i.e.*, for any given theory within the class), black holes have a minimum mass, determined by the coupling constant. In Section 4.2, we focus on the linear coupling case and examine how these two properties are influenced by the presence of additional shift-symmetric (derivative) interactions in the action.

It is worth emphasising that the existence of a minimum mass for black holes in the $\phi\mathcal{G}$ model places a strong constraint on the coupling constant, derived from the lightest observed black hole [353]. Most other observations are sensitive to the scalar charge; however, this sensitivity translates into a constraint on the same coupling constant using the relation that fixes the scalar

[1] The scalar charge Q is the $1/r$ coefficient in the asymptotic expansion of the scalar field at infinity, *i.e.*, $\phi(r \to \infty) = \phi_\infty + Q/r + O(1/r^2)$.

charge in terms of the black hole mass (and spin) [354–357]. In the case of extreme mass ratio inspirals, a scaling of the scalar charge with respect to the black hole mass, inspired by the $\phi\mathcal{G}$ theory, proved to be a crucial ingredient for simplifying the modelling of a broader class of non-minimally coupled scalars [356]. Although there are strong reasons to believe that such terms remain subdominant in modelling binary dynamics and gravitational wave radiation [356, 358], they could still significantly affect the properties of the sources, including their quasi-normal ringing [359], and their dependence on the theory's coupling constants [305]. This can influence how observations are used to derive bounds on these coupling constants.

Given that effective field theory suggests the presence of additional terms, it is crucial to understand their contributions to relations between mass and charge and investigate whether they influence the minimum size of black holes.

The first step in this direction was made in [305], where it was shown that for the most general shift-symmetric action leading to second-order equations upon variation (shift-symmetric Horndeski theory), while respecting local Lorentz symmetry, the scalar charge Q for black holes is given by

$$4\pi Q = \alpha \int_{\mathcal{H}} n_\mu \mathcal{G}^\mu \,, \tag{4.1.4}$$

where $\mathcal{H}$ denotes the Killing horizon, n^μ is its normal, $\mathcal{G}^\mu$ is implicitly defined by $\mathcal{G} = \nabla_\mu \mathcal{G}^\mu$, and α is the coupling constant associated with the $\phi\mathcal{G}$ term. The scalar charge Q is not a Noether charge; it is merely the monopole of the scalar field, and characterises its $1/r$ fall-off. Consequently, it is not expected to alter the first law of black hole thermodynamics [360]. As expected, the charge vanishes if the $\phi\mathcal{G}$ term is absent. However, the value of $\mathcal{G}^\mu$ depends on any additional couplings, with corrections relative to the general relativity value of $\mathcal{G}^\mu$ suppressed by mass scales associated with these couplings. Assuming continuity as these couplings are driven to zero and similar characteristic energy scales for these couplings and α (*i.e.*, no hierarchy of scales), corrections to the charge and its scaling with the black hole mass are expected to be subdominant, though this requires further investigation. Additionally, this expression for the charge does not provide information about the mini-

mum size of black holes.

In Section 4.2, we review the necessary theoretical background, and in Section 4.2.1, we present the class of theories we consider. In Section 4.2.2, we formulate the problem in a static, spherically symmetric setup and study the behaviour of a scalar field in a Schwarzschild background (decoupling) as a warm-up. In Section 4.2.3, we derive hairy black hole solutions perturbatively in the coupling constant α and analyse their properties. In contrast, in Section 4.2.4, we present numerical results and compare them with the perturbative results. Finally, in Section 4.2.5, we summarise our conclusions.

4.2 Black holes in shift-symmetric Horndeski

Shift-symmetry implies that the field equation for the scalar can be written as a conservation of a current,

$$\nabla_\mu J^\mu = 0\,, \tag{4.2.1}$$

where

$$\begin{aligned}
J^\mu = &-\partial^\mu\phi\Big(G_{2X} - G_{3X}\Box\phi + G_{4X}R + G_{4XX}\left[(\Box\phi)^2 - (\nabla_\rho\nabla_\sigma\phi)^2\right] \\
&+ G_{5X}G^{\rho\sigma}\nabla_\rho\nabla_\sigma\phi - \frac{G_{5XX}}{6}\left[(\Box\phi)^3 - 3\Box\phi(\nabla_\rho\nabla_\sigma\phi)^2 + 2(\nabla_\rho\nabla_\sigma\phi)^3\right]\Big) \\
&- \partial^\nu X\Big(-\delta^\mu_\nu G_{3X} + 2G_{4XX}(\Box\phi\delta^\mu_\nu - \nabla^\mu\nabla_\nu\phi) + G_{5X}G^\mu{}_\nu \\
&- \frac{1}{2}G_{5XX}\left[\delta^\mu_\nu(\Box\phi)^2 - \delta^\mu_\nu(\nabla_\rho\nabla_\sigma\phi)^2 - 2\Box\phi\nabla^\mu\nabla_\nu\phi + 2\nabla^\mu\nabla_\rho\phi\nabla^\rho\nabla_\nu\phi\right]\Big) \\
&+ 2G_{4X}R^\mu{}_\rho\nabla^\rho\phi + G_{5X}\Big(-\Box\phi R^\mu{}_\rho\nabla^\rho\phi + R_{\rho\nu}{}^{\sigma\mu}\nabla^\rho\nabla_\sigma\phi\nabla^\nu\phi \\
&+ R_\rho{}^\sigma\nabla^\rho\phi\nabla^\mu\nabla_\sigma\phi\Big)\,.
\end{aligned} \tag{4.2.2}$$

As already mentioned, the conservation equation was used to prove a no-hair theorem in [351]. It was first shown that, for vacuum, static, spherically-

symmetric, asymptotically flat black holes, the only non-vanishing component of the current is the radial one J^r. It was then argued that J^r must vanish at the horizon, otherwise $(J^r)^2/g^{rr}$ would diverge there. Current conservation then implied that J^r must be zero everywhere. Finally, it was argued that $J^r = 0$ everywhere implies that the scalar field must be constant everywhere. This no-hair theorem generalised to slowly rotating black holes straightforwardly [307].

It was however shown in [306] that a linear coupling between ϕ and the Gauss-Bonnet invariant, $\mathcal{G} = R^{\mu\nu\rho\sigma}R_{\mu\nu\rho\sigma} - 4R^{\mu\nu}R_{\mu\nu} + R^2$, circumvents this no-hair theorem. Indeed, $\mathcal{G}$ is a total divergence, and so $\phi\mathcal{G}$ respects shift-symmetry. However, consider the action

$$S = \frac{1}{2k}\int \mathrm{d}^4x\sqrt{-g}\left[\frac{R}{2} + X + \alpha\phi\mathcal{G}\right]. \tag{4.2.3}$$

The corresponding scalar equation is

$$\Box\phi = -\alpha\mathcal{G}\,. \tag{4.2.4}$$

It can be written as a conservation of a current in the form $\nabla_\mu(\nabla^\mu\phi + \alpha\mathcal{G}^\mu) = 0$, exploiting the fact that $\mathcal{G}$ is a total divergence. However, it does not admit any constant ϕ solutions unless $\mathcal{G} = 0$, which is not the case for black holes; hence, they will have to have hair. The apparent contradiction with the no-hair theorem of [351] is resolved by the final argument of [351]—that vanishing current implies constant ϕ—relies on the assumption that every single term in the current depends on the gradient of ϕ. The contribution of the linear coupling to $\mathcal{G}$ clearly violates this assumption and is indeed unique in this respect [306]. Interestingly, hairy black hole solutions in this theory violate another assumption of the theory of [351]: $(J^r)^2/g^{rr}$ diverges on the horizon [361]. It was subsequently shown in [362] that this quantity is not an invariant when it receives a contribution from a linear coupling with $\mathcal{G}$ and hence there is no reason to impose that it is finite in this case.

In [305] theories described by action (3.3.1) where classified as follows:

$$\textbf{Class-1: } \mathcal{E}_\phi[\phi = 0,\ g] = 0\,, \qquad \forall g\,, \tag{4.2.5}$$

$$\textbf{Class-2: } \lim_{g\to\eta} \mathcal{E}_\phi[\phi = 0,\ g] = 0\,. \tag{4.2.6}$$

$$\textbf{Class-3: } \text{All the rest.} \tag{4.2.7}$$

where $\mathcal{E}_\phi$ denotes the scalar equation.

Class-1 theories are defined by having $\phi = 0$ as a solution for any general background; hence, they admit all possible general relativity solutions. Class-2 theories allow for $\phi = 0$ to be realised only for flat spacetimes. The third class is defined as the complement of the other two. Therefore, class-3 theories admit a non-trivial scalar configuration in flat spacetime as a solution, or flat spacetime is not a solution, and hence they violate Local Lorentz symmetry.

At first sight, it appears that classes 1 and 2 are unrelated. On the contrary, it was shown in [305] that a class-2 Lagrangian can always be expressed as a class-1 Lagrangian plus a contribution from the Gauss-Bonnet invariant, namely:

$$\mathcal{L}_{(2)} = \mathcal{L}_{(1)} + \alpha\phi\mathcal{G}\,. \tag{4.2.8}$$

Consequently, all shift-symmetric non-Lorentz-violating Horndeski theories admit all general relativity solutions, provided that a linear coupling between the scalar and the Gauss-Bonnet invariant is not present.

4.2.1 The model

The hairy black holes of the theory in action (4.2.3) have two key properties: their scalar charge Q is not an independent parameter, but it is instead determined by their mass (and spin), by equation (4.1.4), and they have a minimum mass. In the next section, we will see in detail how these properties relate to regularity conditions for static, spherically symmetric black holes. Our broader goal is to understand how adding additional shift symmetric terms to action (4.2.3) would affect these properties.

To make the calculations more tractable, we will not consider ac-

tion (3.3.1). We will instead restrict ourselves to the following theory

$$S = \frac{1}{2k}\int \mathrm{d}^4x\sqrt{-g}\left[\frac{R}{2} + X + \alpha\phi\mathcal{G} + \gamma G_{\mu\nu}\nabla^\mu\phi\nabla^\nu\phi + \sigma X\Box\phi + \kappa X^2\right]. \tag{4.2.9}$$

This action can be obtained from action (3.3.1) by selecting [2]

$$\begin{aligned} G_2(X) &:= X + \kappa X^2\,, \\ G_3(X) &:= -\sigma X\,, \\ G_4(X) &:= 1/2 + \gamma X\,, \\ G_5(X) &:= -4\alpha\ln|X|\,. \end{aligned} \tag{4.2.10}$$

In units where $G = 1 = c$, the scalar field is dimensionless, while $\alpha,\ \gamma,\ \sigma,\ \kappa$ have dimensions of length squared.

4.2.2 Spherically symmetric setup

In this section, we consider a static and spherically symmetric background, described by the following metric

$$\mathrm{d}s^2 = -A(r)\mathrm{d}t^2 + \frac{1}{B(r)}\mathrm{d}r^2 + r^2\mathrm{d}\Omega^2\,, \tag{4.2.11}$$

while the scalar field depends only on the radial coordinate, $\phi = \phi(r)$.

Shift-symmetric current

The only non-vanishing component of the current J^μ is J^r, given by

$$\begin{aligned} J^r = &-B\phi'(1-\kappa B\phi'^2) - \sigma\phi'^2\frac{rA' + 4A}{2rA}B^2 + \gamma\phi'\frac{2AB - 2A + 2rA'B}{r^2A}B \\ &+ \alpha\frac{4(1-B)BA'}{r^2A}\,, \end{aligned} \tag{4.2.12}$$

[2] Up to a total derivative the term $XR + (\Box\phi)^2 - (\nabla_\mu\nabla_\nu\phi)^2$ is equivalent to $G_{\mu\nu}\nabla^\mu\phi\nabla^\nu\phi$. Since, $\int \mathrm{d}^4x\sqrt{-g}(\Box\phi)^2 = \int \mathrm{d}^4x\sqrt{-g}\left[(\nabla_\mu\nabla_\nu\phi)^2 + R_{\mu\nu}\nabla^\mu\phi\nabla^\nu\phi\right] + \int$ total derivative .

where a prime denotes a derivative with respect to the radial coordinate r. As discussed earlier, and according to the classification of [305], the current can be separated into a part for which every term contains ϕ' and a contribution by the coupling with $\mathcal{G}$, as follows

$$J^r = \tilde{J}^r - \alpha \mathcal{G}^r \,, \qquad \mathcal{G}^r = \frac{4(B-1)BA'}{r^2 A} \,, \tag{4.2.13}$$

The conservation of the current can be straightforwardly integrated

$$\nabla_\mu J^\mu = 0 \;\Rightarrow J^r = \frac{c}{r^2}\sqrt{\frac{B}{A}} \,. \tag{4.2.14}$$

Using (4.2.12), one can then determine ϕ' and then integrate once more to obtain $\phi(r)$. Due to shift-symmetry, the constant c in (4.2.14) is the only meaningful integration constant. Hence, considering also the mass parameter of the black hole, one would have a two-parameter family of solutions described by the mass and the scalar charge.

However, ϕ' evaluated on the horizon of a black hole, $r = r_h$, denoted as ϕ'_h, generically diverges. If we assume that the scalar is regular on the horizon, and hence ϕ'_h is finite, and we take into account that at $r = r_h$ we have $A(r_h), B(r_h) \to 0$, then (4.2.12) implies that $\tilde{J}^r(r_h) = 0$. Evaluating (4.2.13) on the horizon then fixes the value of c. As a consequence, the scalar charge ceases to be an independent parameter.

Decoupling limit

As a warm-up, we consider the scalar in a fixed Schwarzschild background. We look for solutions that are regular on the horizon and approach a constant value asymptotically. For simplicity, we choose that value to be zero, as the value of the constant is irrelevant due to shift-symmetry. The γ term is not expected to contribute anything to the decoupled equations since it multiplies the Einstein tensor, which vanishes at decoupling. The scalar equation on a Schwarzschild background is

$$mr^3\kappa(2m-r)\phi'^3 + mr^2\sigma(2r-3m)\phi'^2 + mr^4\phi' + 2\alpha\left(4m^2 + 2mr + r^2\right) = 0 \,. \tag{4.2.15}$$

First, let us note that if only the α-term is present, one can find an analytic solution for the scalar field [306]

$$\phi_\alpha = \frac{2\alpha\left(4m^2+3mr+3r^2\right)}{3mr^3}\,. \tag{4.2.16}$$

We note that, in this case, no specific restriction on the choices of α is suggested. We then consider the σ-term in addition to the α one, and we solve for the derivative of the scalar field

$$\phi'_{\alpha\sigma} = \frac{1}{6mr\sigma-4r^2\sigma}\left[r^3-\sqrt{r^6+8\alpha\sigma\left(12m^2-2mr-r^2-\frac{2r^3}{m}\right)}\right]. \tag{4.2.17}$$

It is straightforward to see that

$$\lim_{\sigma\to 0}\phi'_{\alpha\sigma}=\phi'_\alpha\,,\qquad \phi'_{\alpha\sigma}(r\gg r_h)=\phi'_\alpha(r\gg r_h)\approx-\frac{2\alpha}{mr^2}\,. \tag{4.2.18}$$

Moreover, we employ a near-horizon expansion, *i.e.*, $r=r_h+\epsilon$, for the two cases discussed above. This yields

$$\phi'_\alpha = -\frac{3\alpha}{2m^3}+O(r-2m)\,, \tag{4.2.19}$$

$$\phi'_{\alpha\sigma} = -\frac{2m^2-\sqrt{4m^4-6\alpha\sigma}}{m\sigma}+O(r-2m)\,, \tag{4.2.20}$$

The quantity under the square root in (4.2.20) needs to be positive; therefore, an existence condition emerges,

$$\alpha\sigma\leq\frac{2m^4}{3}\,. \tag{4.2.21}$$

The inequality condition appearing in (4.2.21) imposes an upper bound on the product $\alpha\sigma$. This, in turn, yields an upper bound on α when $\sigma>0$, and a lower bound when $\sigma<0$.

When α is positive, from the near-horizon expressions we can deduce that for $\sigma>0$ ($\sigma<0$) the scalar field fall-off is larger (smaller) than in the $\sigma=0,\ \alpha\neq 0$ case. In the limit $\sigma\to-\infty$ we retrieve the trivial solution $\phi_{\alpha\sigma}=0$

for the near-horizon expansion. When α is negative, we have the opposite behaviour.

The case where $\kappa \neq 0$ is more subtle. By examining the ϕ'^3 coefficient in (4.2.15), we see that when the κ-term is present, the derivative of the scalar at the horizon does not depend on κ; therefore, we deduce that κ does not enter an existence condition analogous to (4.2.21). If one attempts to solve the equation in the region $[r_h + \epsilon, \infty)$, for $\epsilon \ll 1$, it turns out that a regular solution can be found $\forall \kappa \in \mathbb{R}$. However, not all of those solutions possess the desired asymptotic behaviour, and for large positive values of κ, $\phi'_{\alpha\kappa}(\infty) \neq 0$.

Existence conditions

In the previous subsection, we saw how the existence conditions for the scalar equation are affected by the extra terms in the decoupling limit. Here, we derive the existence conditions for black holes beyond decoupling for the full system of equations. To do so, we assume the existence of a horizon located at $r = r_h$, so that $A_{h^\pm} \to 0^\pm$, where the plus sign corresponds to approaching the horizon from the outside, while the minus sign from the inside. By employing near-horizon expansions, we obtain the following expression for the second derivative of the scalar at the horizon

$$\phi'' = -\frac{(4\alpha\phi' + r)\left\{24\alpha + \phi'^2\left[24\alpha\gamma + r^2(8\alpha+\sigma)\right] + 2r^3\phi'\right\}}{2\left\{r^4 - 96\alpha^2 + \phi'\left[r^3(4\alpha+\sigma) + 24\alpha\gamma r\right]\right\}}\left(\frac{A'}{A}\right) + O(1)\,. \tag{4.2.22}$$

We note that to get a black hole solution with a non-trivial scalar field, it is required that $(4\alpha\phi' + r) \neq 0$ [307, 348, 363]. Since $(A'/A)_h$ diverges, for ϕ to be regular at the horizon, it is required that

$$\left[24\alpha + \phi'^2\left[24\alpha\gamma + r^2(8\alpha+\sigma)\right] + 2r^3\phi'\right]_{r_h} = 0\,, \tag{4.2.23}$$

therefore,

$$\phi'_h = \frac{\sqrt{r_h^6 - 576\alpha^2\gamma - 24\alpha r_h^2(8\alpha+\sigma)} - r_h^3}{24\alpha\gamma + r_h^2(8\alpha+\sigma)}\,. \tag{4.2.24}$$

It is possible to derive from equations (4.2.22), and (4.2.24) two conditions:

$$\textbf{I:} \quad r_h^6 - 576\alpha^2\gamma - 24\alpha r_h^2(8\alpha+\sigma) \geq 0\,, \tag{4.2.25}$$

$$\begin{aligned}\textbf{II:} \quad & \left[24\alpha\gamma r_h + (4\alpha+\sigma)r_h^3\right]\sqrt{r_h^6 - 576\alpha^2\gamma - 24\alpha(8\alpha+\sigma)r_h^2} \\ & + 4\alpha\left[r_h^6 - 576\alpha^2\gamma - 24\alpha(8\alpha+\sigma)r_h^2\right] \neq 0\,.\end{aligned} \tag{4.2.26}$$

Condition **I** comes from the requirement that the quantity under the square root in equation (4.2.24) needs to be positive. Condition **II** comes from requiring that the denominator of the fraction in the right-hand side of equation (4.2.22) does not vanish on the horizon (where ϕ' is given by equation (4.2.24)). Although not obvious, these two conditions also guarantee that the denominator of the fraction on the right-hand side of equation (4.2.24) does not vanish.

It is worth pointing out that when we consider only the Gauss-Bonnet term, conditions I and II reduce to the existence condition appearing in [307]. Thus, we see that in the non-perturbative approach, σ but also γ enter the existence conditions. In particular, in the case $\gamma = 0$, the parameter α has both an upper and a lower bound for either sign of σ. This will become clearer in Section 4.2.4 where particular choices of the couplings are examined.

4.2.3 Perturbative treatment

First, we employ a perturbative approach with respect to the coupling constant α, which is associated with the term that sources the hair. To do that, we define the dimensionless parameter $\tilde{\alpha} \equiv \alpha/r_h^2 \ll 1$, where the horizon radius r_h is the length scale we associate with our solution. In a similar manner we can define $\tilde{\gamma} \equiv \gamma/r_h^2$, $\tilde{\sigma} \equiv \sigma/r_h^2$ and $\tilde{\kappa} \equiv \kappa/r_h^2$. For non-zero, small values of $\tilde{\alpha}$, we expect to acquire perturbative deformations to the Schwarzschild solution. Those are expressed through the following expansions for the metric

elements [3]

$$A(r) = \left(1 - \frac{2M}{r}\right)\left(1 + \sum_{n=1}^{\infty} A_n(r)\tilde{\alpha}^n\right)^2 , \tag{4.2.27}$$

$$B(r) = \left(1 - \frac{2M}{r}\right)\left(1 + \sum_{n=1}^{\infty} B_n(r)\tilde{\alpha}^n\right)^{-2} , \tag{4.2.28}$$

$$\phi(r) = \phi_0 + \sum_{n=1}^{\infty} \phi_n \tilde{\alpha}^n . \tag{4.2.29}$$

For $\tilde{\alpha} = 0$, we retrieve general relativity minimally coupled to a scalar field, which for the spherically symmetric static configurations yields the Schwarzschild solution. These expansions are substituted in the equations of motion, which are then solved order by order for the unknown coefficients $\{A_n,\ B_n,\ \phi_n\}$. We work out the calculations up to the fifth order in the perturbative parameter $O(\tilde{\alpha}^5)$. The solutions become very lengthy beyond 2^{nd}-order and, therefore, are omitted. However, the expressions for the scalar charge and the mass of the black hole can be written in the following compact form

$$Q = Q_1\tilde{\alpha} + Q_3\tilde{\alpha}^3 + Q_4(\sigma)\tilde{\alpha}^4 + Q_5(\gamma,\sigma,\kappa)\tilde{\alpha}^5 , \tag{4.2.30}$$

$$M = m + M_2\tilde{\alpha}^2 + M_3(\sigma)\tilde{\alpha}^3 + M_4(\gamma,\sigma,\kappa)\tilde{\alpha}^4 + M_5(\gamma,\sigma,\kappa)\tilde{\alpha}^5 , \tag{4.2.31}$$

where the coefficients Q_n and M_n can be found in Appendix A. Notice that we have to expand to 5^{th} order in $\tilde{\alpha}$ before we see κ contributing to the scalar charge.

The perturbative treatment will break down at some radius. To trace

[3] The expansion is only performed in $\tilde{\alpha}$, since the Gauss-Bonnet term is the only interaction that introduces the hair.

when that happens, we simultaneously scan the following expressions

$$A(r) = \bar{A}_0(r) + \bar{A}_2(r)\tilde{\alpha}^2 + \bar{A}_3(r,\sigma)\,\tilde{\alpha}^3\,, \tag{4.2.32}$$

$$B(r) = \bar{B}_0(r) + \bar{B}_2(r,\gamma)\tilde{\alpha}^2 + \bar{B}_3(r,\gamma,\sigma)\tilde{\alpha}^3\,, \tag{4.2.33}$$

$$\phi(r) = \phi_0 + \phi_1(r)\tilde{\alpha} + \phi_2(r,\sigma)\tilde{\alpha}^2 + \phi_3(r,\gamma,\sigma,\kappa)\tilde{\alpha}^3\,, \tag{4.2.34}$$

$$\mathcal{G}(r) = \mathcal{G}_0(r) + \mathcal{G}_2(r,\gamma)\tilde{\alpha}^2 + \mathcal{G}_3(r,\gamma,\sigma)\tilde{\alpha}^3\,, \tag{4.2.35}$$

for perturbative inconsistencies. Note that the quantities $\bar{A}_n$, $\bar{B}_n$ appearing in equations (4.2.32) and (4.2.33) differ from A_n, B_n appearing in equations (4.2.27) and (4.2.28). If at some radius $r_{\rm np}$ terms of different orders of $\tilde{\alpha}$ become comparable in size, the perturbative treatment can no longer be trusted. The coefficients ϕ_n, $\mathcal{G}_n$ are given in Appendix A. From equations (4.2.32) – (4.2.35) we see that even at second-order in $\tilde{\alpha}$, terms involving γ appear. We note that in the case where $\tilde{\gamma} = \tilde{\sigma} = \tilde{\kappa} = 0$, it was shown in [307] that loss of perturbativity occurred at roughly the same radius at which the non-perturbative solutions exhibited a finite area singularity. We will return to this issue in the next section.

In the top panel of Figure 4.1 we present the normalised charge $\hat{Q} \equiv Q/\sqrt{\alpha}$, as a function of the normalised mass $\hat{M} \equiv M/\sqrt{\alpha}$, for $\tilde{\gamma} = 0,\ \pm 0.5,\ \pm 1,\ \pm 5$ and $\tilde{\sigma} = 0$. In the bottom panel of Figure 4.1, we present the radius $r_{\rm np}$ denoting the point where the perturbative analysis breaks down, for the same choices of $\tilde{\gamma}$. In Figure 4.2, we present the analogous results for the case $\tilde{\sigma} = 0,\ \pm 0.5,\ \pm 1,\ \pm 5$ and $\tilde{\gamma} = 0$.

When $r_{\rm np}$ exceeds r_h, part of the exterior cannot be described by the perturbative solution. One can read the corresponding mass from Figure 4.1, and notice a mass increase/decrease for positive/negative values of $\tilde{\gamma}$. We also see that for $\hat{M} \gtrapprox 2.5$ all curves start merging, as the γ-term becomes significantly subdominant compared to the Gauss-Bonnet term. Another interesting property we notice occurs for the value of $\tilde{\gamma} = -0.5$ for which more than one solution exists for the same mass, as seen in the top panel of Figure 4.1. The radius of the singularity does not display similar behaviour, and different mass black holes have different singularity radii, which is shown in the bottom panel of Figure 4.1. These solutions differ from one another as they describe black holes with different scalar charges.

From Figure 4.2, we notice a similar trend regarding the effects of $\tilde{\sigma}$ and the mass for which perturbativity is lost already at the exterior. For $\hat{M} \gtrapprox 3.5$, all solutions in the $\hat{M}$-$\hat{Q}$ plots begin to merge as the σ-term becomes subdominant. One of the main differences concerning Figure 4.1, however, has to do with the maximum scalar charge. In the $\tilde{\sigma} = 0, \tilde{\gamma} \neq 0$ scenario, we manage to get solutions with larger scalar charges in comparison to the $\tilde{\sigma} = \tilde{\gamma} = 0$ (blue line). In the $\tilde{\gamma} = 0, \tilde{\sigma} \neq 0$ case this does not happen. Let us also point out that the values for $r_{\rm np}$ depicted in the bottom panel of Figure 4.2 are the same for positive and negative values of σ. To understand why this occurs, it is helpful to see the way σ enters the perturbative expansions, which are presented in Appendix A. Specifically, σ appears at second order in the expansion of the scalar field as a multiplicative constant, which explains why changing its sign yields the same solution for $r_{\rm np}$.

It should be noted, however, that these conclusions have to be drawn with care, as they correspond to a region of the parameter space where $\hat{M} < 5$, or $\tilde{\alpha} > 0.01$. This is a region where the perturbative approach might be problematic, and perturbativity might be lost. In general, only a proper numerical analysis can either confirm or disprove the previous discussion.

4.2.4 Numerical results

We now move to solve the full system of equations numerically. This is a system of ordinary partial differential equations of the form $\{\phi'', A', B'\} = f(r, \phi', \phi, A, B)$. We separate the analysis into two regions: the black hole exterior and the black hole interior. In both cases, the integration starts at the horizon. The theoretical parameter space consists of $\{\gamma,\ \sigma,\ \kappa,\ r_h\}$, where r_h is the black hole horizon radius. Since r_h appears in the existence condition (4.2.24), the allowed values for the coupling parameters are expected to be affected if we vary r_h. We can straightforwardly reduce the dimension of the parameter space by one if we normalise the coupling parameters with the horizon radius, as we did in the previous section.

For a given theory defined by $\{\tilde{\gamma},\ \tilde{\sigma},\ \tilde{\kappa}\}$ we allow the values of $\tilde{\alpha}$ to scan the parameter space starting from small $\tilde{\alpha}$ and gradually increasing until the existence conditions are saturated, therefore, we need the set of values $\{\phi',\ \phi,\ A,\ B\}_{r_h}$. Despite appearing to constitute "initial data," this set

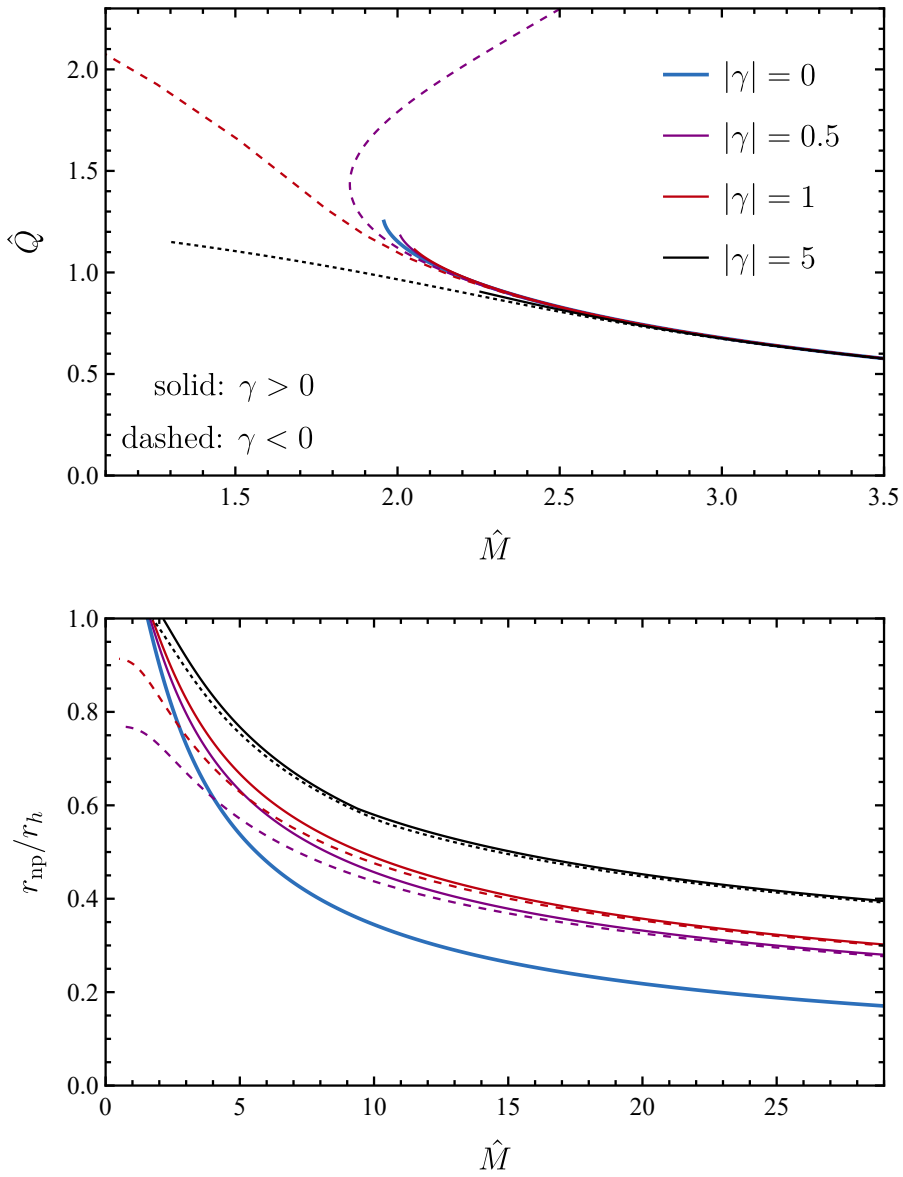

Figure 4.1: In the top panel, we show the normalised scalar charge and mass derived from the perturbative analysis. In the bottom panel, we have the singular radius derived from the perturbative analysis, for $\tilde{\sigma} = \tilde{\kappa} = 0$ and $\tilde{\gamma} = 0,\ \pm 0.5,\ \pm 1,\ \pm 5$.

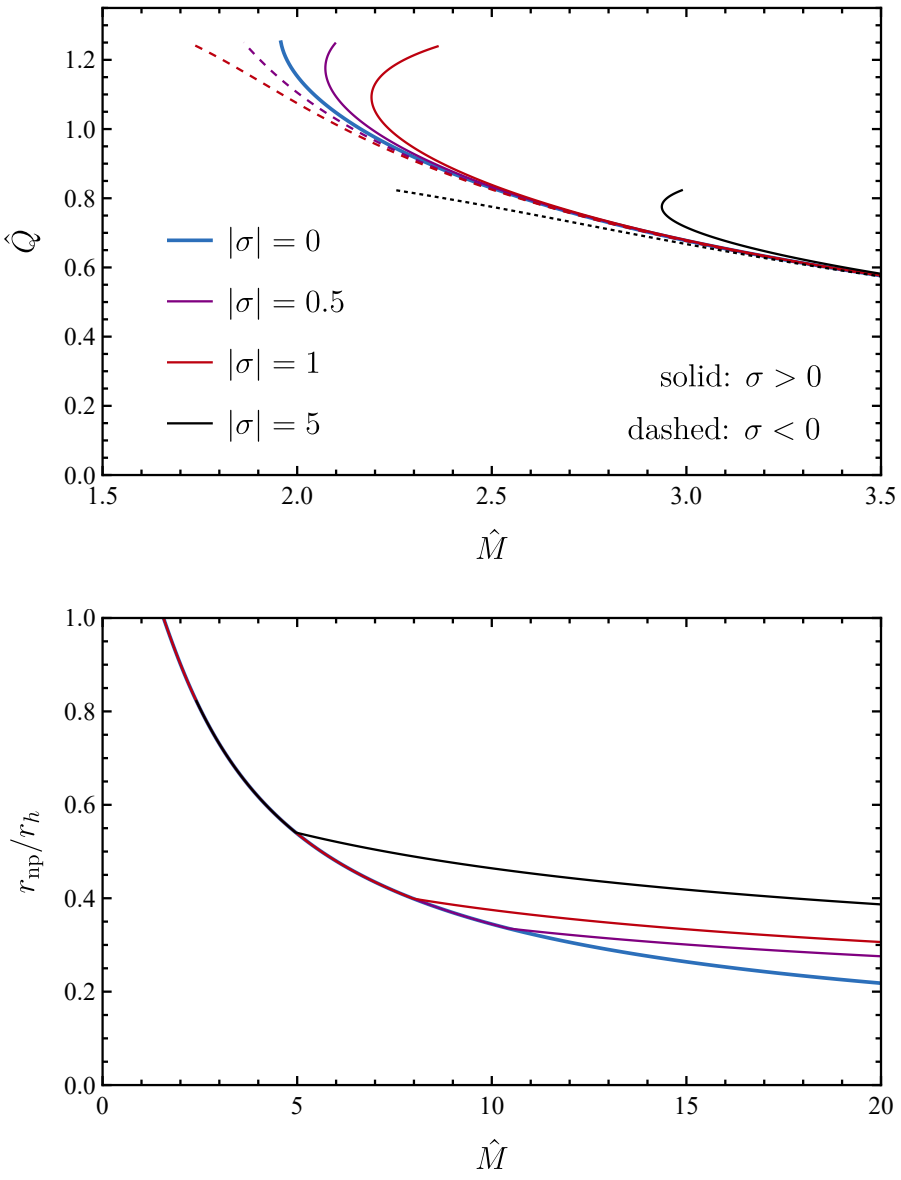

Figure 4.2: Same as Figure 4.1, but for $\tilde{\gamma} = \tilde{\kappa} = 0$ and $\tilde{\sigma} = 0, \pm 0.5, \pm 1, \pm 5$.

of values is not entirely free to choose. In practice, to apply the existence conditions (4.2.25) – (4.2.26) with reasonable numerical accuracy, we use a perturbative expansion near the horizon and numerically solve the system of algebraic equations for the first few coefficients appearing in the expansions (up to order $O(r - r_h)^2$). This process reduces the number of free initial conditions to two, namely the value of the scalar field at the horizon and that of the first-order coefficient of A. The latter one, however, is fixed by asymptotic flatness, leaving ϕ_h as the only free-to-choose initial condition. The asymptotic value of the scalar field should be constant but otherwise unconstrained since our model is shift-symmetric. For simplicity, we choose ϕ_h so that $\phi_\infty = 0$. For that, we integrate outwards using a shooting method to demand ϕ vanishing to a part in 10^4. The remaining free parameter is the horizon radius r_h. We then start the numerical integration outwards (inwards) from $r = r_h \pm O(10^{-5})$. In the exterior, we typically integrate up to $r/r_h \approx 10^5$.

In the following subsections, we present plots corresponding to the different couplings. In each case, we numerically calculate the scalar charge and the Arnowitt-Deser-Misner (ADM) mass of the black hole using the following expressions

$$Q = -\lim_{r\to\infty}\left(r^2\phi'\right), \qquad M = \lim_{r\to\infty}\left[\frac{r\left(2 - 2B + r^2\phi'^2\right)}{r^2\phi'^2 - 4}\right]. \quad (4.2.36)$$

We were also able to verify the emergence of a finite-radius singularity, consistent with the existence conditions. While integrating from the horizon and inwards, we noticed the following general trend: Starting from general relativity ($\alpha \to 0$) and gradually increasing the couplings, the geometric invariants diverge and the solutions become singular at some radius r_s. The larger the general relativity deviations become, the more r_s approaches r_h. When one of the existence conditions is saturated, the singularity radius approaches the horizon radius, *i.e.*, $r_s \to r_h$.

Charge, mass and scalar profile

In these subsections, we attempt to present the overall generic trend that the black hole properties follow, if one considers action (4.2.9). We discuss the charge, mass and scalar profile for a few examples corresponding to different scenarios, which motivate the more thorough analysis that follows in the next subsections.

The top panel of Figure 4.3, shows the $\hat{M}$-$\hat{Q}$ plot for different negative values of the coupling constants $\tilde{\gamma}$ and $\tilde{\sigma}$. The corresponding plots for positive couplings are not presented here, since—at these scales—they are overshadowed by the $\tilde{\gamma} = \tilde{\sigma} = 0$ curve, as explained later in more detail. In all positive-coupling cases, the minimum black hole mass is larger than the one corresponding to $\tilde{\gamma} = \tilde{\sigma} = 0$. Furthermore, non-zero $\tilde{\kappa}$ curves are almost indistinguishable from the $\tilde{\gamma} = \tilde{\sigma} = 0$ case, since, as we saw, $\tilde{\kappa}$ does not enter the existence conditions. Consequently, the corresponding $\tilde{\kappa}$-plots are not presented here. We see that for large $\hat{M}$, which corresponds to small Gauss-Bonnet couplings, the charge in all cases drops off to zero and general relativity is retrieved. This is, of course, associated with the fact that the Gauss-Bonnet term is the one sourcing the hair. In the small $\hat{M}$ regime, significant deviations are observed, which are explained in the following coupling-specific subsections. On the bottom panel of Figure 4.3, we show the profile of the scalar field, properly normalised with the distance and the scalar charge. All curves exhibit a $1/r$ fall-off and asymptotically approach 1. For large radii, the scalar field profiles are indiscernible for different couplings. In the near-horizon regime, however, there are apparent deviations as shown in the top panel.

To make things easier for the reader, in what follows, we consider the Gauss-Bonnet coupling $\tilde{\alpha}$ in combination with $\tilde{\gamma}$, $\tilde{\sigma}$ and $\tilde{\kappa}$ separately. In this work, we consider $\alpha > 0$ as this is consistent with most of the literature. However, it is worth pointing out, that action (4.2.9) is invariant under the simultaneous transformation $\alpha \to -\alpha$, $\phi \to -\phi$ and $\sigma \to -\sigma$ and that in the case of $\sigma = \gamma = \kappa = 0$, the sign of ϕ is determined by the sign of α for solutions that are continuously connected to Schwarzschild as $\alpha \to 0$. In what follows, we consider both positive and negative values for σ, γ, and κ, and our analysis should effectively cover the $\alpha < 0$ case as well, at least for

Minimum mass for $\tilde{\sigma} = \tilde{\kappa} = 0,\ \tilde{\gamma} \neq 0,\ \tilde{\alpha} > 0$

$\tilde{\gamma}$	-5.0	-1.0	-0.5	0.0	$+0.5$	$+1.0$	$+5.0$
$\hat{M}$	1.45	1.77	1.87	2.08	2.45	2.71	3.75

configurations that are continuously connected to Schwarzschild.

The $\tilde{\gamma}$ term

First we consider the case $\tilde{\sigma} = \tilde{\kappa} = 0$. From (4.2.25) and (4.2.26) we find the conditions on $\tilde{\gamma}$ necessary for regularity at the horizon. The existence conditions I-II are, in general, non-trivial, and the easiest way to track them is to examine the corresponding region plot in the top panel of Figure 4.4. The first obvious observation relates to the apparent asymmetry about the vertical axis. Therefore, we expect the sign of $\tilde{\gamma}$ to influence the black hole solutions and properties. In particular, for negative values of $\tilde{\gamma}$, the parameter space of allowed values for $\tilde{\alpha}$ increases, and so we expect negative values of $\tilde{\gamma}$ to allow for hairy solutions with smaller masses. On the other hand, when $\tilde{\gamma} > 0$, the parameter space of $\tilde{\alpha}$ shrinks, and we expect the black hole mass range to decrease. Regarding the Gauss-Bonnet coupling $\tilde{\alpha}$, extending the plot to negative values of $\tilde{\alpha}$ is trivial as, for $\tilde{\sigma} = 0$, the action (4.2.9) is invariant under the simultaneous transformation $\tilde{\alpha} \to -\tilde{\alpha}$ and $\phi \to -\phi$.

These are indeed verified in Figure 4.5, where the emergence of a finite-radius singularity is demonstrated in the interior of the black hole. The top panel shows the singularity radius as a function of the normalised black hole mass for $\tilde{\gamma} = \{0,\ 0.5,\ 1,\ 5\}$ while the bottom panel shows the corresponding results for $\tilde{\gamma} = \{0,\ -0.5,\ -1,\ -5\}$. The values are chosen to be of order $\sim 1 - 10$ with respect to $\tilde{\alpha}_{\rm max}$, where $\tilde{\alpha}_{\rm max}$ corresponds to the largest allowed value for α satisfying the existence conditions. For the choices of $\tilde{\gamma}$ made, we present the results for the minimum hairy black hole mass in the following table For a negative $\tilde{\gamma}$, we notice another interesting property of the solutions: at small masses, the apparent change in monotonicity in the $\hat{M}$-$\hat{Q}$ and $\hat{M}$-r_s (see the inset) plots indicates that black holes with the same mass can correspond to different scalar charges and singularity radii. Therefore, one would expect that the black hole with the larger scalar charge would shed some of it to reach a more favourable scalar configuration with a smaller charge. Fi-

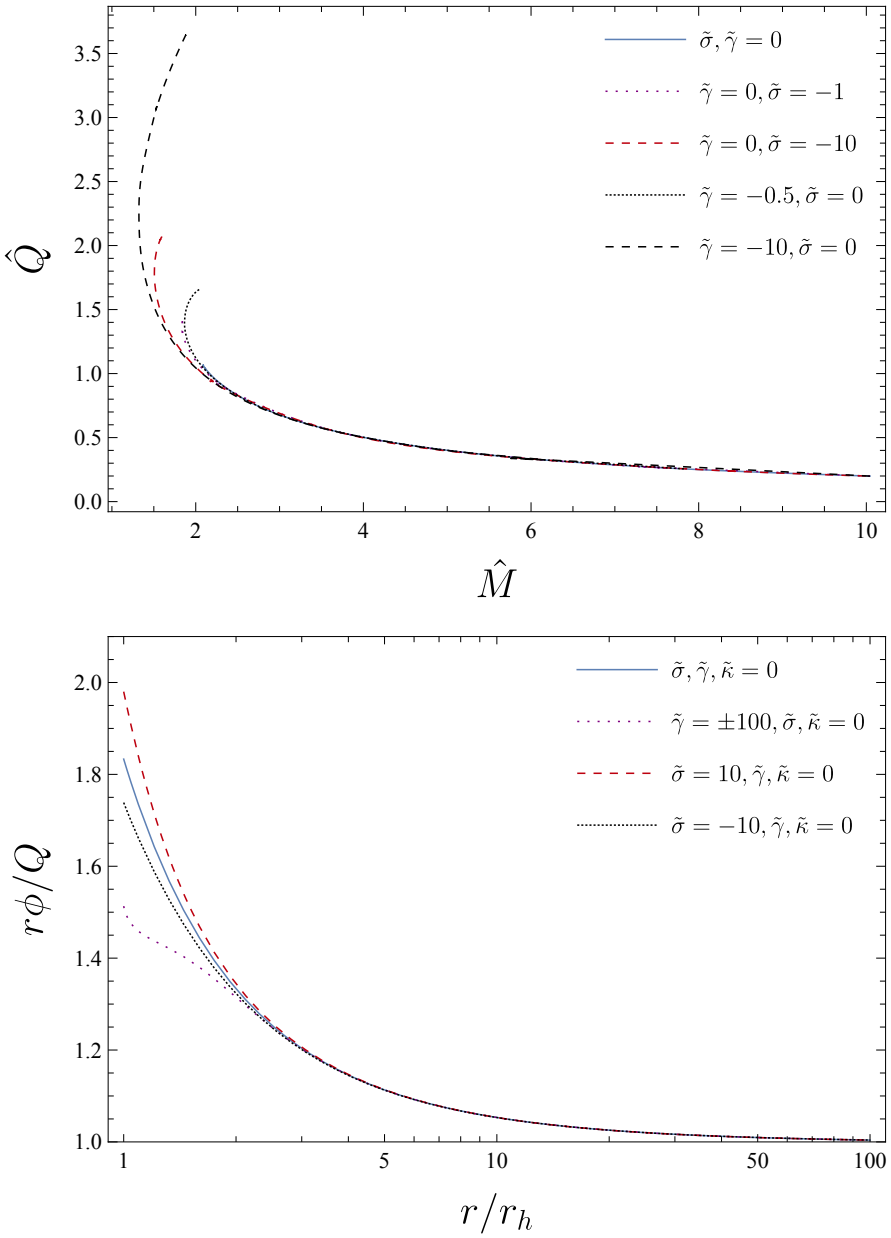

Figure 4.3: In the top panel, we have the relation between the normalised mass and charge. In the bottom panel, we show the scalar field profile for black holes with $\hat{M} \sim 10$.

Minimum mass for $\tilde{\gamma} = \tilde{\kappa} = 0,\ \tilde{\sigma} \neq 0\,, \tilde{\alpha} > 0$

$\tilde{\sigma}$	-5.0	-1.0	-0.5	0.0	$+0.5$	$+1.0$	$+5.0$
$\hat{M}$	1.61	1.84	1.91	2.08	2.47	2.83	5.55

nally, from Figure 4.5 we point out that in the larger mass regime, the sign of $\tilde{\gamma}$ becomes unimportant and the cases with opposite signs merge.

The $\tilde{\sigma}$ term

In the top panel of Figure 4.6, we present the allowed and excluded regions of the parameter space according to the existence conditions in the case of $\tilde{\gamma} = 0$, with $\tilde{\sigma}$ being on the horizontal and $\tilde{\alpha}$ on the vertical axis. For negative values of $\tilde{\alpha}$ the region plot we retrieve demonstrates an origin symmetry which was anticipated since the action (4.2.9) is invariant under the simultaneous transformation $\tilde{\alpha} \longrightarrow -\tilde{\alpha}$, $\tilde{\sigma} \longrightarrow -\tilde{\sigma}$, and $\phi \longrightarrow -\phi$. For $\tilde{\alpha} > 0$, $\tilde{\sigma} < 0$, the allowed values for $\tilde{\alpha}$ increase and therefore the mass range also increases, and hairy black holes with smaller masses are found. At the same time, for $\tilde{\alpha} > 0$, $\tilde{\sigma} > 0$, the parameter space of $\tilde{\alpha}$ shrinks, and the black hole mass range should also decrease. If we considered $\tilde{\alpha} < 0$, the above conclusions would be reversed.

In Figure 4.7, we display the singularity radius in this scenario and its dependence on the value of $\tilde{\sigma}$. Verifying the above, positive (negative) $\tilde{\sigma}$ leads to a larger(smaller) minimum black hole mass. In the $\tilde{\sigma} \neq 0$ scenario, the relation between the finite singularity radius and the normalised mass exhibits discontinuous behaviour, as shown in Figure 4.7. As already explained, we identify the singularity radius as the one for which a geometric invariant (*e.g.*, the Gauss-Bonnet or, equivalently, the Kretschmann invariant) diverges. To explain the discontinuity, let us imagine that we start from some large $\hat{M}$ moving inwards towards smaller masses. At $r = r_s$, the Gauss-Bonnet invariant diverges, and we identify r_s as the singularity radius. There exists a second special point at $r = r_s' > r_s$ where the metric functions and the scalar field appear to lose differentiability because they develop a kink. This is because the second derivative becomes discontinuous. The differential equations, however, can still be integrated for $r_s' > r > r_s$. If we plotted r_s' instead of r_s, then the vertical jump would no longer be present and the lines would be contin-

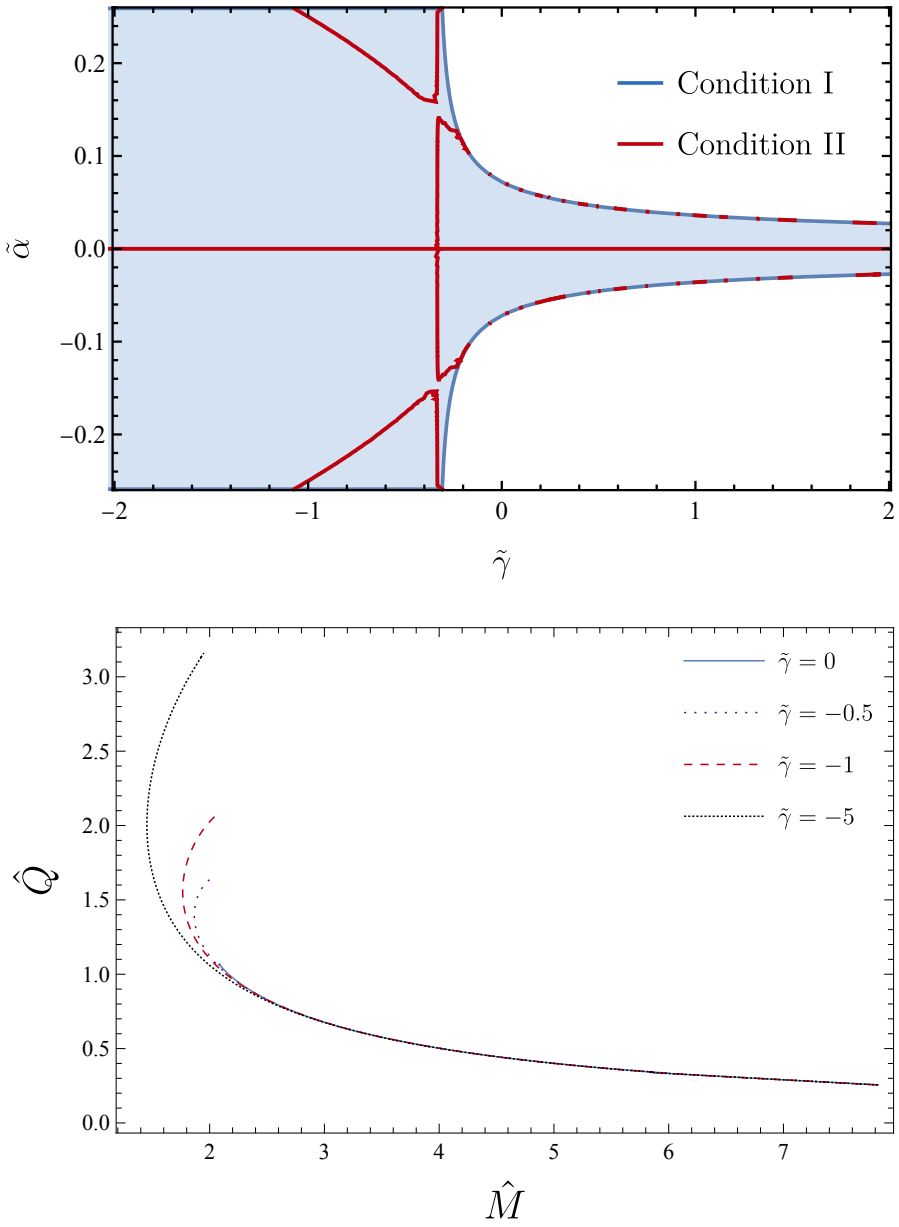

Figure 4.4: In the top panel, we illustrate the existence conditions in the case of $\tilde{\sigma} = \tilde{\kappa} = 0$. The blue shaded region corresponds to the area of the parameter space allowed by condition I (4.2.25). The red line corresponds to the values within the allowed blue region that are excluded by condition II (4.2.26). In the bottom panel we show the Mass-Charge plots for $\tilde{\sigma} = \tilde{\kappa} = 0$ and $\tilde{\gamma} = \{-5, -1, -0.5, 0\}$.

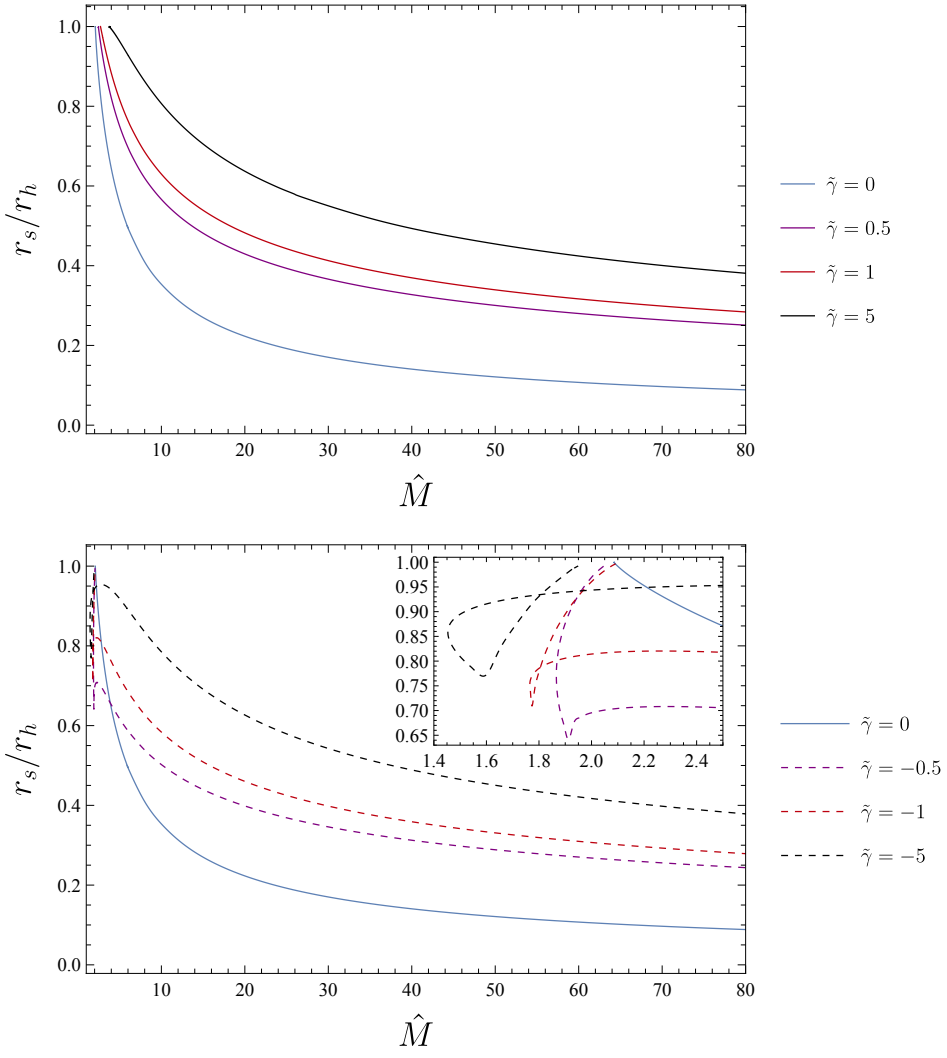

Figure 4.5: The finite singularity radius r_s as a function of the normalized mass $\hat{M}$ for $\tilde{\sigma} = \tilde{\kappa} = 0$ and $\tilde{\gamma} = \{-5,\ -1,\ -0.5,\ 0,\ 0.5,\ 1,\ 5\}$.

uous. In all cases, however, we chose to plot the singularity corresponding to the divergence of the geometric invariants. On the other hand, for positive $\tilde{\sigma}$, we do not encounter any other "singularities" than the ones we plot, which correspond once again to the geometric invariants diverging.

Similar discontinuities have also been encountered in [353] assuming quadratic and exponential couplings. In the zoomed-in part of the bottom panel of Figure 4.7, similar behaviour to the negative $\tilde{\gamma}$ case is exhibited, where the same-mass black holes have different singularity radii. This can also be understood from the $\hat{M}$-$\hat{Q}$ plot, in the bottom panel of Figure 4.6, where a turning point appears at small masses.

The $\tilde{\kappa}$ term

It is evident from equations (4.2.25) and (4.2.26) that κ does not enter the existence conditions. As a result, one might naively conclude that black hole solutions exist irrespective of the value that κ takes, given that the remaining parameters satisfy the existence conditions. Contrarily, that is not the observed behaviour. If κ is positive, then we cannot find solutions for all values of α that are allowed by the existence conditions; however, if κ is negative, then solutions could be found for all values of α allowed by the conditions. This behaviour is illustrated in Figure 4.8, where for negative values of κ it is possible to saturate the existence condition and have solutions with a naked singularity, but for $\kappa > 0$, in general, that cannot be achieved. To better understand this trend, it is useful to rewrite the scalar equation for $\gamma = \sigma = 0$ as

$$h^{\mu\nu}\nabla_\mu\nabla_\nu\phi \equiv \left[g^{\mu\nu}\left(1-\kappa(\nabla\phi)^2\right) - 2\kappa\nabla^\mu\phi\nabla^\nu\phi\right]\nabla_\mu\nabla_\nu\phi = -\alpha\mathcal{G}\,. \tag{4.2.37}$$

In practice, we see that when $\tilde{\kappa} > 1$, not all values of $\tilde{\alpha}$ allowed by the existence conditions yield black hole solutions. To explain this issue, we numerically examine the value of the quantity inside the square brackets in equation (4.2.37), namely $h^{\mu\nu}$. Due to the symmetry of our problem, we will only examine the quantity h^{rr}. In Figure 4.9, we plot h^{rr} (and $h^r{}_r$) for values of $\tilde{\kappa}$ spanning a few orders of magnitude, *i.e.*, $O(1) - O(10^2)$. We see

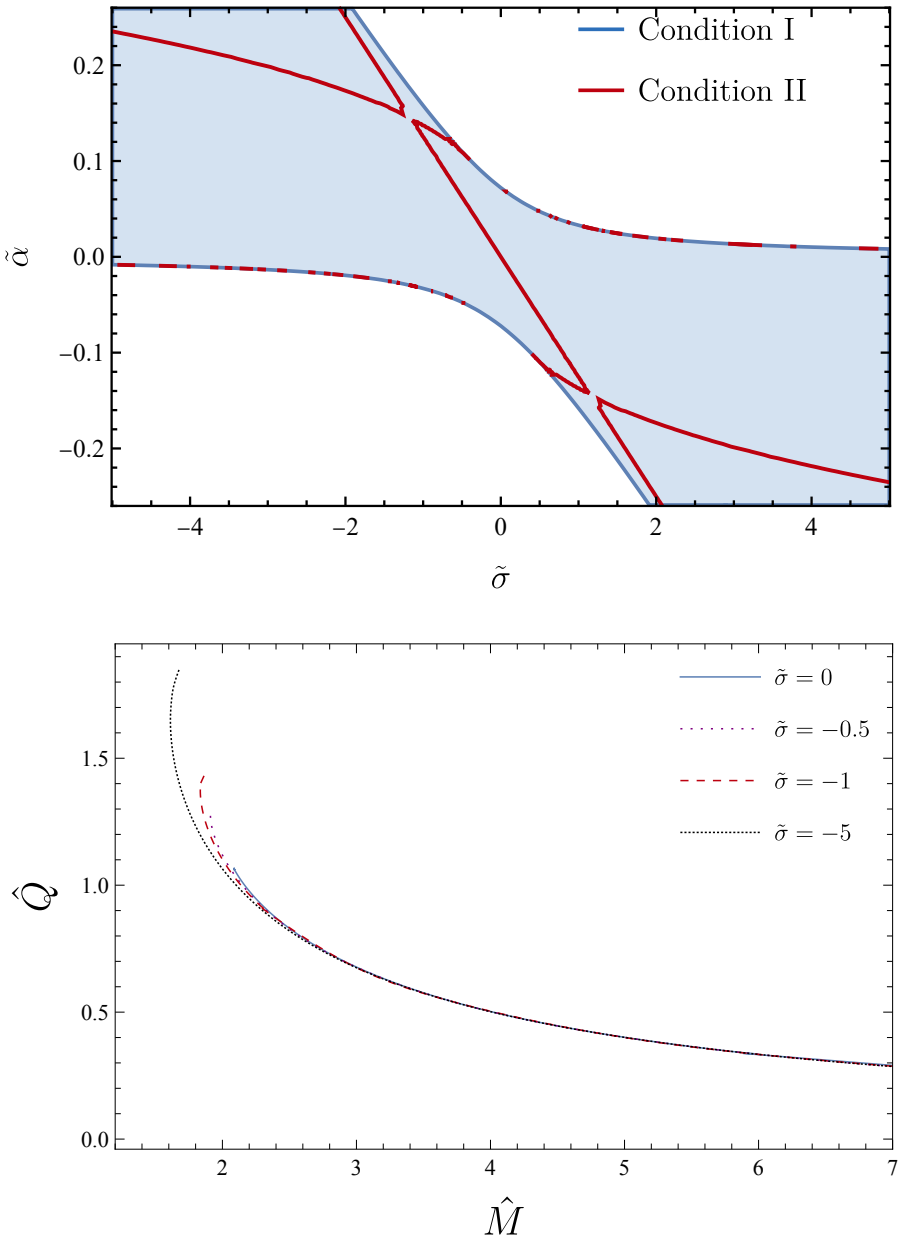

Figure 4.6: In the top panel, we display the existence conditions in the case of $\tilde{\gamma} = \tilde{\kappa} = 0$. The blue shaded region corresponds to the inequality of condition I (4.2.25), while the red line corresponds to the inequality of condition II (4.2.26). In the bottom panel we have the Mass-Charge plots for $\tilde{\gamma} = \tilde{\kappa} = 0$ and $\tilde{\sigma} = \{-5, -1, -0.5, 0\}$.

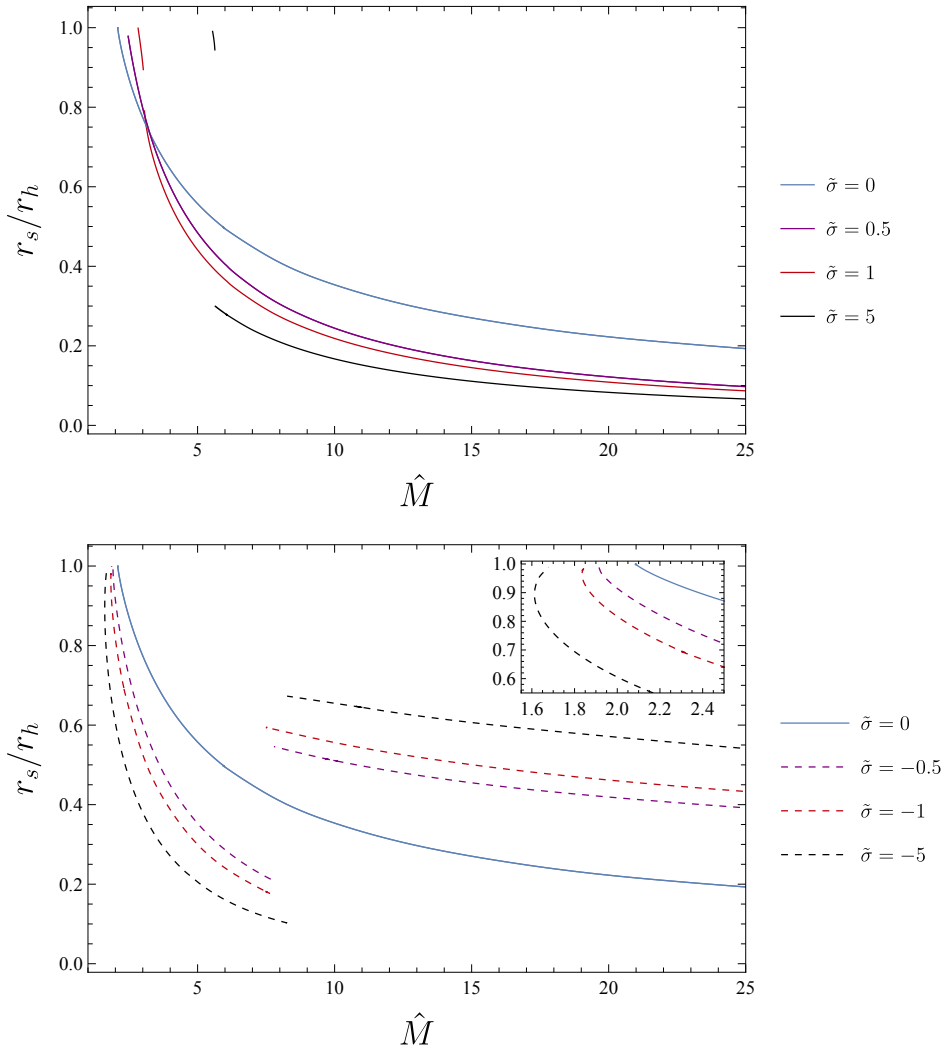

Figure 4.7: The finite singularity radius r_s as a function of the normalized mass $\hat{M}$, for $\tilde{\gamma} = \tilde{\kappa} = 0$. The horizon radius $r_h = 1$.

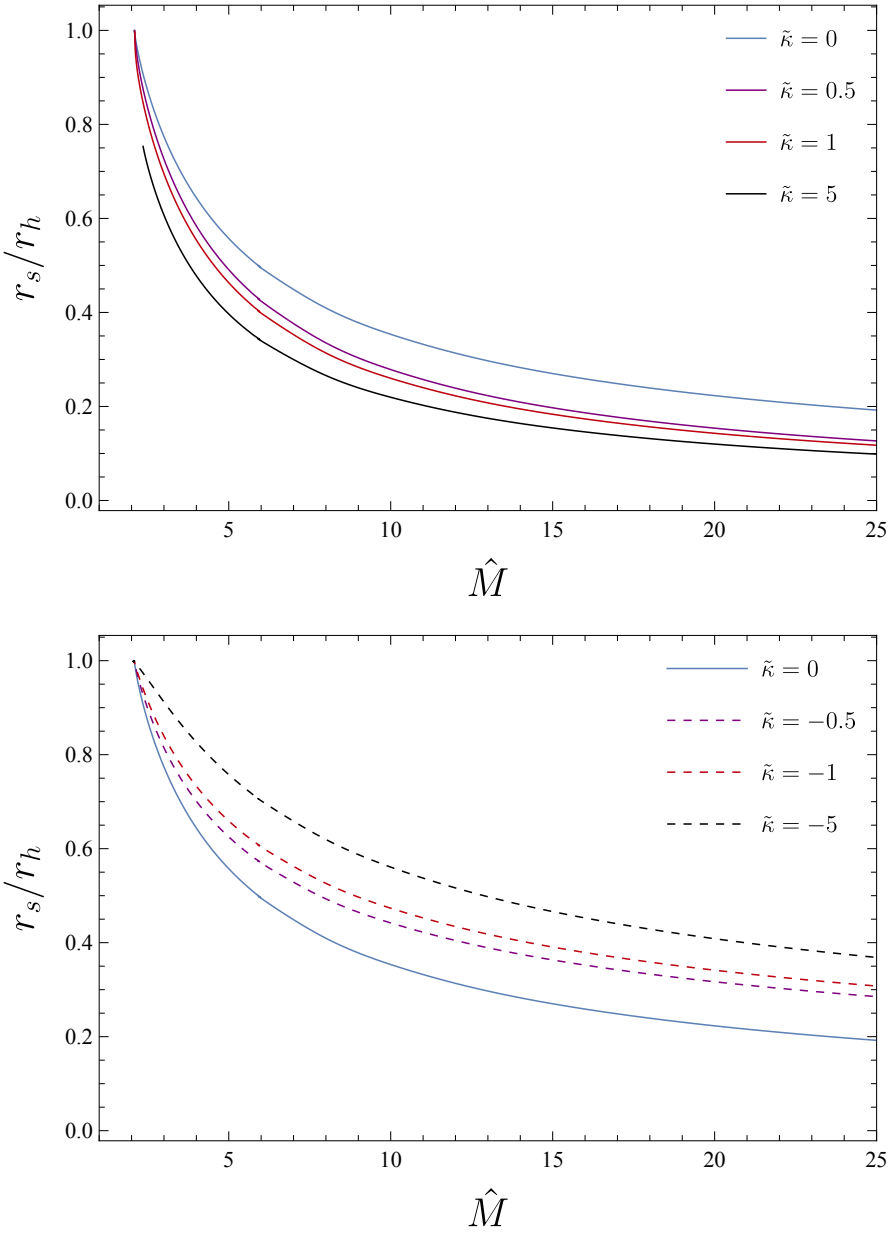

Figure 4.8: The finite singularity radius r_s as a function of the normalized mass $\hat{M}$, with $\tilde{\sigma} = \tilde{\gamma} = 0$. The horizon radius $r_h = 1$.

that for $O(\tilde{\kappa}) > O(1)$, the quantity h^{rr} approaches zero at some intermediate radius, which seems to increase as we increase the value of κ. Beyond that point, the system of equations can not be integrated. This bears similarities with the behaviour of ϕ'' at the horizon, the regularisation of which yielded the existence conditions. Thus, it appears that imposing regularity for the scalar field at the horizon results in divergences appearing elsewhere for large positive values of $\tilde{\kappa}$.

Numerical solutions vs perturbative solutions

As mentioned earlier, it has already been demonstrated that in the case $\gamma = \sigma = 0$, loss of perturbativity is associated with the appearance of a finite-radius singularity in the black hole interior. Here we discuss the relation between the perturbative treatment breakdown radius $r_{\rm np}$ and the finite-radius singularity r_s in the general case where $\tilde{\gamma}$, $\tilde{\sigma}$ are non-zero.

We present the comparative plots in Figure 4.10. Verifying the results of [307], we see that the radius of the singularity in the black hole interior in the case $\tilde{\gamma} = \tilde{\sigma} = 0$ is traced almost perfectly by the perturbative analysis. However, this is not the case, at least to the same level of success, when one considers the γ and σ contributions. From the top panel of Figure 4.10, we see that when $\tilde{\gamma} \neq 0$ the $r_{\rm np}$ curve sits below the singularity radius r_s. From the bottom panel, $\tilde{\sigma} \neq 0$, the $r_{\rm np}$ curve sits between the disconnected branches of the numerical solutions.

We can also compare the results regarding the scalar charge and the mass of the black holes by inspecting Figures 4.1, 4.2, 4.4, and 4.6. Specifically, for the $\tilde{\gamma} \neq 0$ case, by comparing Figures 4.1, 4.2 and 4.4 we deduce that the perturbative approach captures at least qualitatively the two main conclusions drawn by the numerical analysis: (i) For $\tilde{\gamma} > 0$ the minimum black hole mass for each $\tilde{\gamma}$ increases and the mass-parameter space of solutions shrink. (ii) For $\tilde{\gamma} < 0$, the minimum black hole mass for each $\tilde{\gamma}$ decreases, and for small masses it is possible to retrieve black holes of the same mass with different scalar charges. Similar conclusions hold in the $\tilde{\sigma} \neq 0$ scenario (with the addition of the discontinuities), where the perturbative analysis captured the qualitative trends observed in the numerical solution.

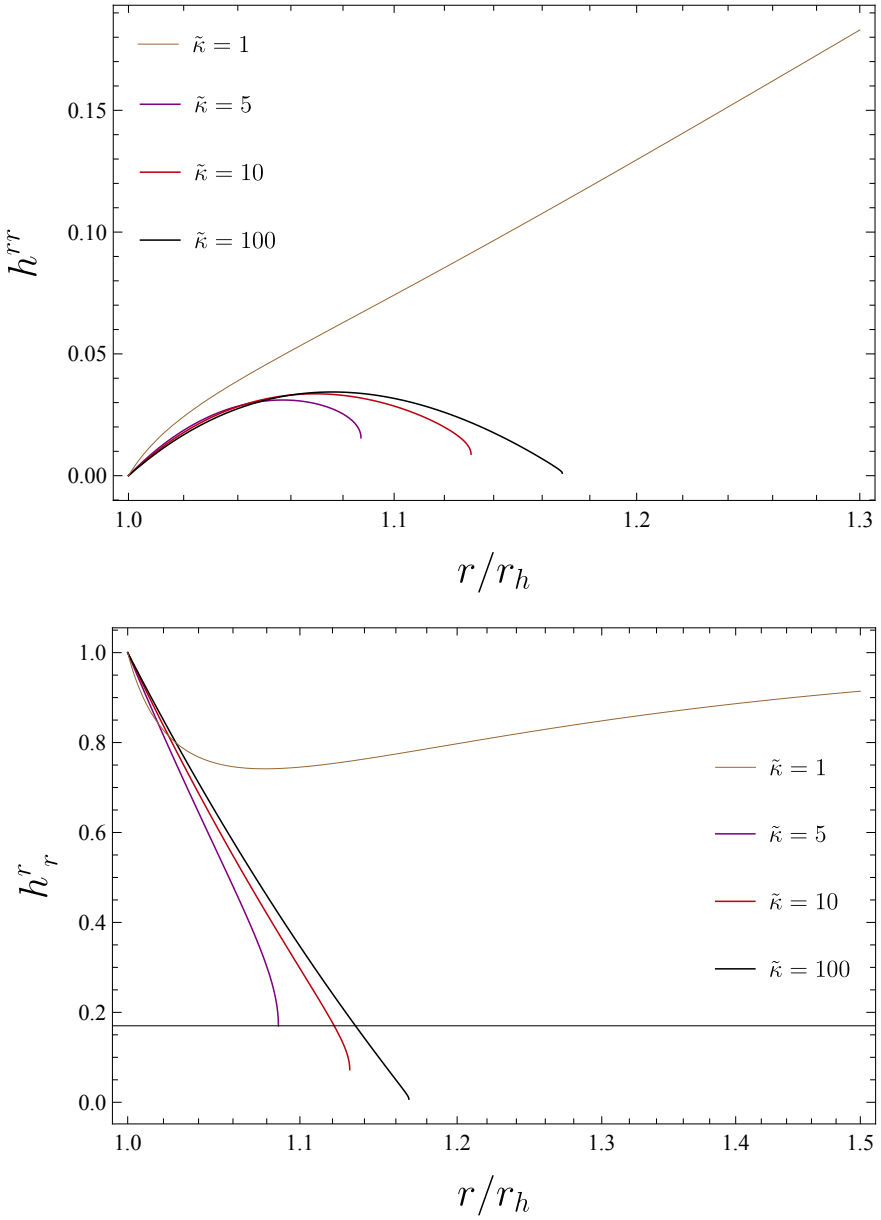

Figure 4.9: The behaviour of $h_{\mu\nu}$, as defined in equation (4.2.37), near the horizon. In the top we have $h^{rr} = B(1 - 3\kappa B\phi'^2)$, and in the bottom we have $h^r{}_r = 1 - 3\kappa B\phi'^2$.

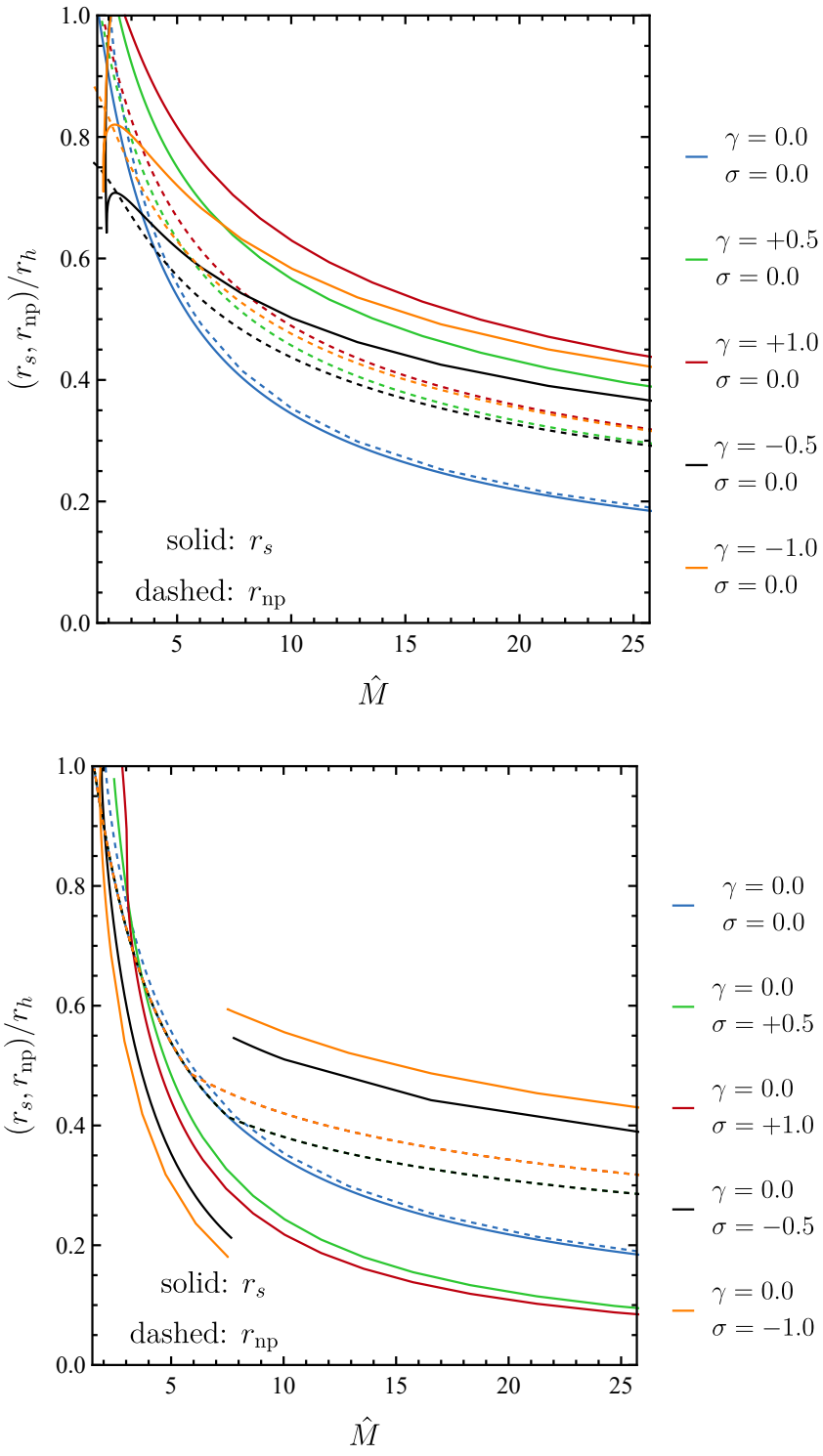

Figure 4.10: We show the radii $r_{\rm np}$ and r_s for different values of γ, and σ. In the top panel, we have $\sigma = 0$, while the bottom panel is for $\gamma = 0$.

4.2.5 Discussion

We have studied hairy black holes in generalised scalar-tensor theories that exhibit a range of shift-symmetric derivative interactions, in addition to the linear coupling to the Gauss-Bonnet invariant that is known to introduce black hole hair. We found that, although these additional interactions cannot introduce hair themselves, they can significantly influence the behaviour of the scalar fields near the horizon of the black hole and hence affect the configuration in general, including the value of a scalar charge for a given mass.

Interestingly $G_{\mu\nu}\nabla^{\mu}\phi\nabla^{\nu}\phi$ and $X\Box\phi$ modify the regularity condition on the horizon that determines the scalar charge of the black hole with respect to its mass and affects the regularity condition that determines the minimum black hole mass, whereas X^2 leaves both conditions unaffected. All terms affect the scalar configuration; however, a large positive coupling for X^2 can compromise the existence of black holes altogether.

Our two key findings are the following: (i) additional shift-symmetric interactions affect the minimum size of hairy black holes, hence the constraints one can derive from that, but their effect is rather moderate for dimensionless couplings (with respect to the scale of the black hole in geometric units) of order 1 or less. (ii) Additional shift-symmetric interactions affect the scaling of the charge per unit mass versus the mass of the black hole only for masses that are fairly close to the minimum mass. Hence, sufficiently large black holes in shift-symmetric theories will not carry a significant charge per unit mass, irrespective of the presence of additional shift-symmetric interactions (see, *e.g.*, [305, 356, 357]).

Chapter V

Supermassive black hole scalarization and effective field theory

Contents

In Section 4.2, we examined static black holes and their properties in linear scalar Gauss-Bonnet gravity. We have seen that the scalar charge of a hairy black hole is fixed by its mass, spin, and the coupling constant(s) of the theory [305–308, 348, 349]. This has been used in the literature to argue that the scalar charge will become entirely negligible for black holes that are much larger than the characteristic scale of the coupling constant(s) that control the deviations from general relativity or the Standard model [356]. Constraints coming from solar mass black hole observations by the LIGO-Virgo-KAGRA collaboration [56, 64, 65, 364], and binary pulsars [365–367] generically impose, on the new couplings, a maximum length scale of the order of kilometres. This, combined with the charge-mass scaling, has been used to drastically simplify the modelling of very asymmetric binaries [357, 368, 369] and of black hole ringdowns for massive black holes [370]. This same fact, however, rules out the possibility that supermassive black holes could have hair in any known model, if their solar-mass counterparts do not.

Recently, the work in [371] proposed a model that circumvents this argument. In this model, solar-mass compact objects are well-described by general relativity solutions, while black hole uniqueness is broken at supermassive scales. This is achieved in the context of spontaneous scalarization (see Section 3.3.2 for details). The crux of this proposal is to have scalar perturbations satisfy an equation of the form

$$(\Box - \mu_{\rm eff}^2)\delta\phi = 0\,, \tag{5.0.1}$$

where $\mu_{\rm eff}^2$ is only sufficiently negative as to lead to scalarization at supermassive scales, whereas at other mass/curvature scales it is positive or not negative enough to cause an instability. The proposed model does require an auxiliary scalar field, whose dynamics are not completely clear. We will elaborate on the details in Section 5.1.

Our main goal here is to examine whether we can recover the theory of [371] from an effective field theory perspective in the limit where the second scalar is heavy. We start in Section 5.1 by presenting the model of [371] and discussing how the scalarization of supermassive black holes can be achieved without conflicting with current observations. In Section 5.2,

we consider two interacting scalars that couple to the Gauss-Bonnet term, where one of the scalars is massive, and try to derive the model of [371] by integrating out the heavy scalar. We find two main drawbacks to this approach. First, integrating out the heavy field reproduces the interactions of [371] but with a sign difference that prevents scalarization of supermassive black holes. Secondly, the scale of the heavy field highly suppresses the novel contribution to the effective mass of scalar perturbations. In Section 5.2.2, we drop the assumption that the second scalar is heavy and study scalarization in the bi-scalar Gauss-Bonnet model in full generality. In Section 5.3, we show that we can obtain a coupling with the correct sign for supermassive black hole scalarization if we use a Higgs-like heavy field. However, in this case, general relativity vacuum geometries are no longer solutions to the theory. We end with a discussion in Section 5.4.

5.1 Supermassive black holes scalarization: Theoretical background

The key idea of the model proposed in [371] is to ensure that the effective mass of scalar perturbations is composed of various terms that compete depending on the considered curvature scale. The model, in geometric units, is

$$S = \int \mathrm{d}^4x\sqrt{-g}\Big[R - (\partial\phi)^2 + \alpha_1 F(\phi)\,\mathcal{G} - 2\alpha_2^3 F(\phi)\left(\psi\mathcal{G} - \frac{\psi^2}{2}\right)\Big], \tag{5.1.1}$$

here, ϕ and ψ are real scalar fields. The scalar field ϕ is dimensionless while ψ is of inverse length to the fourth. Hence, the coupling constants α_1 and α_2 have dimensions length squared. Note that the scalar ψ is auxiliary, which does not, however, mean it is not dynamical. The field equations for the scalar fields are

$$\psi - \mathcal{G} = 0\,, \tag{5.1.2}$$

and

$$\Box\phi = \left[-\alpha_1\mathcal{G} + 2\alpha_2^3\left(\psi\mathcal{G} - \frac{\psi^2}{2}\right)\right]\frac{F'(\phi)}{2}\,. \tag{5.1.3}$$

Combining the two, the purpose of the field ψ becomes manifest as the equation for ϕ becomes

$$\Box\phi = \frac{1}{2}F'(\phi)\left(-\alpha_1\mathcal{G} + \alpha_2^3\mathcal{G}^2\right)\,. \tag{5.1.4}$$

A basic feature of scalarization is that only some black holes have hair, while others are described by general relativity. To have general relativity solutions for $\phi = \phi_0 = 0$, we take the coupling function $F(\phi)$ to satisfy

$$F'(0) = 0\,, \qquad F(0) = 0\,. \tag{5.1.5}$$

The first condition ensures that the scalar field equation is compatible with a constant scalar field Kerr metric, while the second ensures compatibility with the field equations for the metric. Therefore, we can consider a scalar perturbation around $\phi = 0$ of the form $\phi = 0 + \delta\phi$. Using equation (5.1.4) we obtain the perturbation equation (5.0.1) with an effective mass given by

$$\mu_{\rm eff}^2 = -\alpha_1\mathcal{G} + \alpha_2^3\mathcal{G}^2\,, \tag{5.1.6}$$

where we assumed, without loss of generality, that $F''(0) = 2$. The key feature of this model becomes manifest, at least for spherically symmetric black holes: two competing terms control the effective mass of scalar perturbations. For sufficiently low curvatures, the $\mathcal{G}$ term dominates and the theory reduces to the usual scalar-Gauss-Bonnet models [314, 315] discussed in previous sections. The value of α_1 will then control what the threshold mass below which scalarization can occur, and this can be tuned to be high enough to allow supermassive black holes to scalarize. On the other hand, if the curvature is high enough for the $\mathcal{G}^2$ term to dominate, the effective mass will be positive. This suppresses scalarization for black holes with lower masses, and tuning the value of α_2 sets the minimum threshold mass. Therefore, in this model, black hole uniqueness can be broken solely on supermassive black hole scales, while all other regimes agree with general relativity. This motivates and makes

a case for experiments whose goal is to observe supermassive black holes, such as the Event Horizon Telescope [39, 40], because deviations from general relativity might manifest solely in this regime. This model is also free from the early universe instability discussed in [328, 372].

For a discussion of the rotating black hole solutions in this model, see [373]. For an analysis of how supermassive black hole scalarization affects the gravitational wave background observed by pulsar timing arrays, refer to [374].

In what follows, we address whether such a model can be derived from a canonical scalar field theory.

5.2 Two dynamical scalar fields and effective field theory

5.2.1 Integrating out a heavy field

The dynamics of ψ in the theory (5.1.1) are unclear as there is no standard kinetic term. Indeed, the ψ part of theory (5.1.1) is an $f(\mathcal{G})$ theory [371, 375], which is known to potentially suffer from instabilities [376, 377]. Here, we explore if such an action can arise from a theory with a light and a heavy scalar, ϕ and ψ respectively, after "integrating out" the heavy field. These fields have no relation to those in equation (5.1.1), even though we use the same symbols. We start from the following Lagrangian

$$\frac{2\mathcal{L}}{M_{\rm Pl}^2} = R - (\partial\phi)^2 - (\partial\psi)^2 - M_\psi^2\psi^2 + \alpha\phi^2\mathcal{G} + 2\beta\phi\psi\mathcal{G}\,, \qquad (5.2.1)$$

with units $c = 1 = \hbar$. The reduced Planck mass is $M_{\rm Pl}^{-2} = 8\pi G$, and we have canonically normalised the scalar fields. We further choose $\beta > 0$, which is always possible by changing the sign of one of the scalars.

In this model, both scalar fields have a canonical kinetic term and are dimensionless. The coupling constants α and β have dimensions of inverse mass squared (length squared).

Action (5.2.1) is not the most general theory that is quadratic in the two

scalars. However, we assume the ϕ field is light enough to ignore its mass term. A term of the form $\sim \phi\psi$ can be diagonalised away. An interaction between ψ and $\mathcal{G}$ of the form $\psi^2\mathcal{G}$ is allowed, but its contributions would show up at higher order when integrating out the ψ field. Linear interactions between the scalar fields and the Gauss-Bonnet term could be present, but they would introduce permanent hair [307, 308]. Symmetry under $\phi \to -\phi$ and $\psi \to -\psi$ can justify excluding these terms. Finally, self-interactions of the scalar or couplings to R could be present, but they do not affect our conclusions.

We take the scalar field ψ to be "heavy," that is, its Compton wavelength is much smaller than that of ϕ, and of the gravitational radius of the black hole. With this in mind, we can (formally) solve for ψ using its equation of motion, and substitute it back into the Lagrangian (*i.e.*, we are integrating out the heavy field at tree level). The equation of motion for ψ is

$$\Box\psi - M_\psi^2\psi + \beta\phi\mathcal{G} = 0\,, \tag{5.2.2}$$

which we can solve to leading order in $1/M_\psi^2$ as

$$\psi = \frac{\beta}{M_\psi^2}\phi\mathcal{G} + O\left(1/M_\psi^4\right)\,, \tag{5.2.3}$$

and the Lagrangian (5.2.1) reduces to

$$\frac{2\mathcal{L}}{M_{\rm Pl}^2} \approx R - (\partial\phi)^2 + \alpha\phi^2\mathcal{G} + \frac{\beta^2}{M_\psi^2}\phi^2\mathcal{G}^2\,. \tag{5.2.4}$$

The resulting theory has the $\mathcal{G}^2$ term observed in [371]. However, it suffers from two shortcomings. Firstly, and most obviously, the $\mathcal{G}^2$ term has the "wrong" sign compared to theory (5.1.1) [1]. Secondly, the $\mathcal{G}^2$ term is suppressed by the mass scale M_ψ. To see this, consider a Schwarzschild background

$$\mathrm{d}s^2 = -\left(1 - \frac{r_s}{r}\right)\mathrm{d}t^2 + \left(1 - \frac{r_s}{r}\right)^{-1}\mathrm{d}r^2 + r^2\mathrm{d}\Omega^2\,, \tag{5.2.5}$$

[1] The "correct" sign can be obtained if ψ is a tachyon.

where r_s is the Schwarzschild radius of the black hole, and let us define dimensionless coupling constants as

$$\tilde{\alpha} \equiv \frac{\alpha}{r_s^2}\,, \qquad \tilde{\beta} \equiv \frac{\beta}{r_s^2}\,. \tag{5.2.6}$$

Then, the terms $\alpha\phi^2\mathcal{G}$, and $\beta^2\phi^2\mathcal{G}^2/2M_\psi^2$ are comparable near the horizon $r \sim r_s$ if

$$\tilde{\alpha} \sim \tilde{\beta}^2 \frac{1}{M_\psi^2 r_s^2}\,, \tag{5.2.7}$$

since $1 \ll M_\psi r_s$, the relation (5.2.7) does not hold for $\sim O(1)$ dimensionless couplings $\tilde{\alpha}$, $\tilde{\beta}$, as required to have significant $\mathcal{G}^2$-related effects.

5.2.2 Bi-Scalar Gauss-Bonnet scalarization

In the last section, we demonstrated that the model of [371] does not come from a simple effective field theory by integrating out a massive scalar.

In this section, we will not integrate out the heavy field ψ. We will explore if the theory in equation (5.2.1) allows for supermassive black hole scalarization if both ϕ and ψ are considered dynamical. Most of this section is dedicated to studying the tachyonic instability on a fixed Schwarzschild background and exploring the parameter space of the theory (5.2.1) for which scalarized black holes are present. The equations governing the perturbations $\delta\phi$, and $\delta\psi$ read

$$\Box\delta\phi = -\alpha\mathcal{G}\delta\phi - \beta\mathcal{G}\delta\psi\,, \tag{5.2.8}$$

$$\Box\delta\psi = M_\psi^2\delta\psi - \beta\mathcal{G}\delta\phi\,. \tag{5.2.9}$$

In a static, spherically symmetric background, we can perform the following decomposition of the perturbations

$$\delta\Phi_i = u_i(r)\exp(-\mathrm{i}\omega t)Y_{\ell m}(\theta,\varphi)/r\,, \qquad i \in \{1,2\}\,, \tag{5.2.10}$$

where $\Phi_i = \{\phi,\ \psi\}$, and $Y_{\ell m}$ are the spherical harmonics. We solve these equations for static ($\omega = 0$) monopolar ($\ell = 0$) excitations in a Schwarzschild

background. Note that these equations cannot, generally, be decoupled except in special cases. First, it is instructive to consider two limiting cases: (i) the large mass ("frozen" ψ) case, *i.e.*, we take $\Box\delta\psi = 0$, and (ii) the zero mass case $M_\psi = 0$. Finally, we solve the system in full generality and compare it with the limiting cases.

We solve the equations in isotropic coordinates ρ such that $r = \rho(1 + M/2\rho)^2$. Near the horizon $\rho_h = M/2$, we use a series expansion in $(\rho - \rho_h)$ up to second-order precision for the functions u_i in equation (5.2.10) as

$$u_i = u_i^{(0)} + u_i^{(2)} \left(\rho - \frac{M}{2}\right)^2 . \tag{5.2.11}$$

We can fix $u_1^{(0)} = 1$ by an appropriate rescaling of the equations, and solve algebraically for $u_i^{(2)}$ in terms of $u_2^{(0)}$ and the various coupling constants, thereby establishing the boundary conditions close to the horizon. Subsequently, for a fixed value of the coupling constant β a shooting method is utilized to determine the values of $u_2^{(0)}$ and α admitting a non-trivial solution where $u_i(r)$ asymptotically approach a constant (zero) value for large ρ (for asymptotic flatness). We typically integrate to a large ρ value, $\rho = 100M$, and fix $M = 1$.

In the first limiting case, where ψ is heavy, it decouples from the spectrum of the theory, and we have only one scalar perturbation equation for $\delta\phi$ to solve for with an effective mass given by

$$\mu_{\text{eff}}^2 = -\alpha\mathcal{G} - \kappa^3\mathcal{G}^2 , \qquad \kappa^3 \equiv \frac{\beta^2}{M_\psi^2} . \tag{5.2.12}$$

In the other limiting case, where we consider ψ to be massless ($M_\psi = 0$), the system of equations can be diagonalised. To appreciate this fact, let us rewrite the Lagrangian (5.2.1) in a matrix form as [2]

$$\mathcal{L} = R - (\partial\Phi)^2 - \Phi \cdot \mathcal{M} \cdot \Phi , \tag{5.2.13}$$

[2] Here, we have dropped overall factors of the Lagrangian.

where,

$$\Phi = \begin{pmatrix} \phi \\ \psi \end{pmatrix}, \qquad \mathcal{M} = \begin{pmatrix} -\alpha\mathcal{G} & -\beta\mathcal{G} \\ -\beta\mathcal{G} & M_\psi^2 \end{pmatrix}. \tag{5.2.14}$$

If ψ is massless, then the matrix $\mathcal{M}$ can be diagonalised, with eigenvectors that are spacetime independent, and the following eigenvalues

$$\lambda_\pm = \frac{-\alpha \pm \sqrt{\alpha^2 + 4\beta^2}}{2}\mathcal{G}\,, \tag{5.2.15}$$

Consequently, there must exist a unitary transformation such that the Lagrangian can be written as

$$\mathcal{L} = R - (\partial\phi_+)^2 - (\partial\phi_-)^2 + \alpha_+\phi_+^2\mathcal{G} + \alpha_-\phi_-^2\mathcal{G}\,, \tag{5.2.16}$$

for two scalar fields ϕ_+, ϕ_-, and with $\alpha_{+,-}$ given by

$$\alpha_+ = \frac{\alpha + \sqrt{\alpha^2 + 4\beta^2}}{2}, \qquad \alpha_- = \frac{\alpha - \sqrt{\alpha^2 + 4\beta^2}}{2}. \tag{5.2.17}$$

It is important to note that α_+ is always positive, and α_- is always negative, regardless of the non-vanishing values of α and β. This implies that in this model, both types of scalarization curvature- and spin-induced, must occur. Of course, it is trivial to write a theory with two scalar fields that allows both, but one has to force the couplings to be of a fixed sign in an *ad-hoc* manner. However, in this model, the sign of the couplings is not free; instead, it is fixed by the diagonalisation process. As a consequence, as long as there is an interaction term of the form $\phi\psi\mathcal{G}$ in the theory, then both types of scalarization are inevitable.

In Figures 5.1 and 5.2, we present the bulk of our numerical results. The results obtained for the effective mass in equation (5.2.12), and finite M_ψ are shown in Figure 5.1. We observe that for a fixed black hole mass M and coupling α, larger values of κ are needed for scalarization to occur, when a smaller M_ψ is considered. In some cases, we observe scalarization even for negative values of α, which does not happen when the coupling between ϕ and ψ is absent. For a fixed value of β, we would need a smaller M_ψ to acquire

a negative effective mass and trigger the instability.

In Figure 5.2, we compare the massless limit $M_\psi = 0$ with the massive scalar cases. We find that, for fixed coupling β, larger values of M_ψ demand larger values of α to scalarize a black hole as the mass of the scalar field will contribute positively to the effective mass of the perturbations.

We also observe that for $\beta = 0$, we have $\alpha/M^2 \sim 0.726$ as the threshold for scalarization, consistent with the results of [314, 315]. This is true because for $\beta = 0$ we have two decoupled scalar fields with ϕ coupled to gravity as in the usual scalar Gauss-Bonnet theories, while ψ is just a free massive scalar field which is covered by a no-hair theorem. On the other hand, when $\alpha = 0$, the bifurcation point changes depending on the value of M_ψ as expected.

We do not find evidence for a scenario similar to that of [371], where supermassive black holes can scalarize, while solar-mass compact objects remain stable and well-described by general relativity.

Finally, as a remark, we note that the curves in Figures 5.1 and 5.2 for finite values of the scalar field mass M_ψ stop at some finite value of α. This is merely an artefact of the numerical stiffness of the perturbation equations when a finite mass M_ψ is considered, because of the exponential decay of ψ. We expect the curves to continue their trend towards larger negative values of α as suggested by the large mass limit, where the system is no longer stiff. The curves shown in Figures 5.1 and 5.2 belong to the portion of the parameter space where we were able to accurately solve the stiff system of differential equations numerically.

5.3 The correct coupling sign from a Higgs-like mechanism

We now consider if a low-energy effective field theory that includes a mass term given by equation (5.1.6), and hence can have supermassive black hole scalarization, could arise from a Higgs-like interaction. To this effect, we start

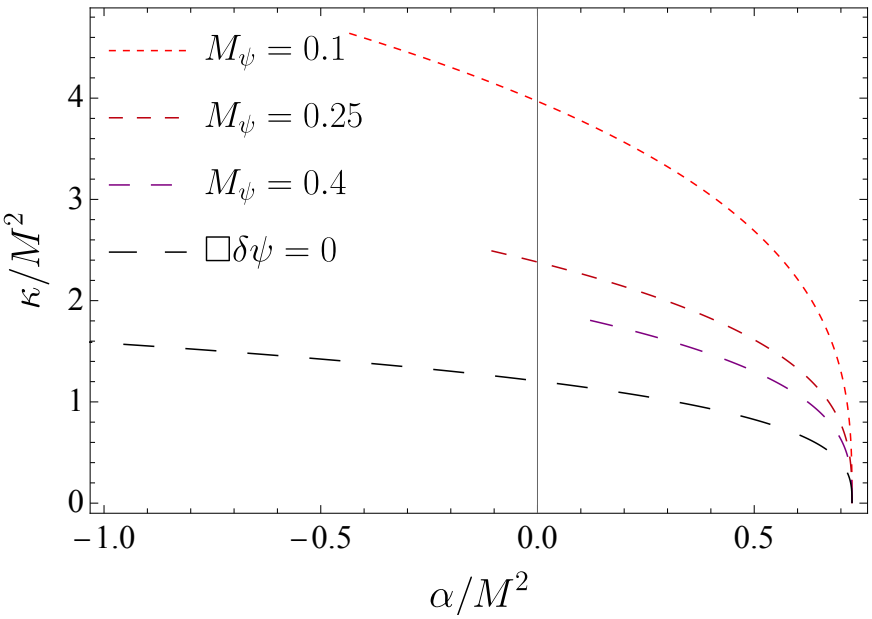

Figure 5.1: Parameter space of scalarized solutions for different values of M_ψ. We compare the behaviour of the large mass case ($\Box\delta\psi = 0$) with the general case of finite non-zero M_ψ. Black holes are tachyonically unstable above and to the right of the curves. We observe that for fixed M_ψ smaller values of α/M^2 require larger κ (where $\kappa^3 = \beta^2/M_\psi^2$), thus larger β, to exhibit a tachyonic instability.

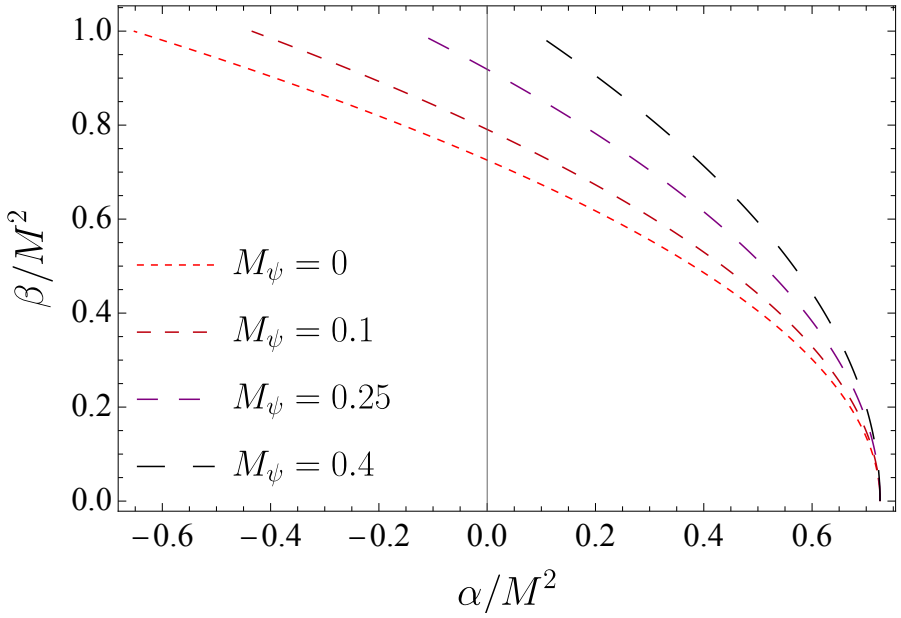

Figure 5.2: Parameter space of scalarized solutions for different values of M_ψ. We compare the massless scenario with the more general case where M_ψ is non-zero. As M_ψ increases, for fixed α, higher values of β are required to allow scalarization.

from the action

$$\begin{aligned}\mathcal{L} =&\frac{M_{\rm Pl}^2}{2}R - \frac{1}{2}(\partial\phi)^2 - \frac{1}{2}(\partial H)^2 - \frac{\lambda}{4}(H^2 - v^2)^2 \\ &- \frac{1}{2}\alpha F\left(\phi/\Lambda\right) H^2\mathcal{G}\,,\end{aligned} \tag{5.3.1}$$

where H is a Higgs-type scalar field with vacuum expectation value (VEV) at infinity $H = v$, and Λ is an energy scale. The main difference of this model in comparison with the one in equation (5.2.1) is precisely that the massive field has a non-zero VEV. We consider perturbations of H around the VEV, $H = v + h$, for which we obtain the following Lagrangian

$$\begin{aligned}\mathcal{L} =& \frac{M_{\rm Pl}^2}{2}R - \frac{1}{2}(\partial\phi)^2 - \frac{1}{2}(\partial h)^2 \\ &- \frac{\lambda}{4}(h + 2v)^2h^2 - \frac{1}{2}\alpha F\left(\phi/\Lambda\right)(h + v)^2\mathcal{G}\,.\end{aligned} \tag{5.3.2}$$

The equation of motion for h is

$$\begin{aligned}\Box h =&\left(\alpha F\left(\phi/\Lambda\right)\mathcal{G} + 2\lambda v^2\right)h + \alpha v F\left(\phi/\Lambda\right)\mathcal{G} \\ &+ 3\lambda v h^2 + \lambda h^3\,,\end{aligned} \tag{5.3.3}$$

where we observe that the Higgs field acquires a bare mass $m_h^2 = 2\lambda v^2$. Assuming the Higgs to be heavy ($m_h r_s \gg 1$), we can freeze it, $\Box h \approx 0$, and solve for h,

$$h \approx v\left(\sqrt{1 - \frac{2\alpha}{m_h^2}F\left(\phi/\Lambda\right)\mathcal{G}} - 1\right)\,, \tag{5.3.4}$$

and we obtain the low-energy effective field theory,

$$\mathcal{L} = \frac{M_{\rm Pl}^2}{2}R - \frac{1}{2}(\partial\phi)^2 - \frac{\alpha v^2}{2}F\left(\phi/\Lambda\right)\mathcal{G} + \frac{v^2\alpha^2}{2m_h^2}F\left(\phi/\Lambda\right)^2\mathcal{G}^2\,. \tag{5.3.5}$$

The equation of motion for ϕ obtained from the effective field theory is given by

$$\Box\phi = \frac{\alpha v^2}{2\Lambda} F'(\phi/\Lambda)\mathcal{G} - \frac{\alpha^2 v^2}{m_b^2 \Lambda} F(\phi/\Lambda) F'(\phi/\Lambda)\mathcal{G}^2 \,, \tag{5.3.6}$$

which allows for constant scalar configurations $\phi = 0$ as long as $F'(0) = 0$. The scalar perturbations around the background are described by a Klein-Gordon equation with a squared effective mass given by

$$\mu_{\text{eff}}^2 = \frac{\alpha v^2}{2\Lambda^2} F''(0)\mathcal{G} - \frac{\alpha^2 v^2}{m_b^2 \Lambda^2} F(0) F''(0)\mathcal{G}^2 \,. \tag{5.3.7}$$

Using the symmetry $\alpha \to -\alpha$, together with $F \to -F$, we can fix the coupling function so that $F(0) \geq 0$, ensuring the two contributions to the effective mass have opposite signs. For $F''(0) < 0$ and $\alpha > 0$ it is possible to reproduce the perturbation equation from [371], given in equation (5.1.6).

Under these circumstances ($F(0) \geq 0$, $F''(0) < 0$, and $\alpha > 0$), there are two possible cases to consider, depending on whether $F(0)$ is vanishing or not.

1. $F(0) = 0$: In this case, the Kerr metric together with $\phi = 0$ solves all field equations. However, the perturbation equation reduces to the usual one of standard scalarization because the contribution containing the $\mathcal{G}^2$ term vanishes.

2. $F(0) > 0$: In this case, the Kerr metric together with $\phi = 0$ no longer solves the field equations of the theory. Instead, a solution with $\phi = 0$ is allowed if the metric is a solution of the theory

$$\mathcal{L} = \frac{M_{\text{Pl}}^2}{2} R + \frac{k}{2}\mathcal{G}^2 \,, \qquad k = \frac{\alpha^2 v^2}{m_b^2} F(0)^2 \,. \tag{5.3.8}$$

   Then, scalar perturbations governed by equation (5.3.7) are realised in this non-general relativity vacuum.

Consequently, in this setting, the effective mass of scalar perturbations necessary for supermassive black hole scalarization (5.1.6) can be reproduced, but not in a theory allowing general relativity vacuum solutions.

Although the results in this section suggest that an action of the type considered in [371] is unlikely to arise from a Higgs-like interaction in a natural way, they also suggest another way in which hair could arise for supermassive black holes only. Corrections to general relativity in the form of higher-curvature corrections are expected on general grounds. Assuming, for instance, a coupling function which can be expanded as $F(\phi/\Lambda) = 1 - (\phi/\Lambda)^2 + O\left((\phi/\Lambda)^3\right)$, the effective mass (5.3.7) becomes

$$\mu_{\rm eff}^2 = \frac{v^2}{\Lambda^2}\left(-\alpha\mathcal{G} + \frac{2\alpha^2}{m_h^2}\mathcal{G}^2\right), \tag{5.3.9}$$

which can be brought to the form of equation (5.1.6), with $\alpha_1 = \alpha v^2/\Lambda^2$ and $\alpha_2^3 = 2v^2\alpha^2/(\Lambda^2 m_h^2)$. From the results of [371], we expect scalarization of supermassive black holes to be possible if $\alpha_1 \sim \alpha_2$, which translates to $\Lambda^2/v^2 \sim m_h\sqrt{\alpha}$. Moreover, a positive contribution to the effective mass that can prevent the theory from exhibiting catastrophic instabilities in the early universe [328, 372], as discussed in [371], is produced. Finally, as the model (5.3.8) introduces higher curvature corrections, which are expected from an effective field theory perspective, we still need to choose k small enough to pass current tests. However, as k also controls the effect of the $\mathcal{G}^2$ term on the effective mass in (5.3.7), a small k might not lead to supermassive black hole scalarization. Therefore, we require a more thorough analysis to assess whether the Higgs model is phenomenologically viable.

5.4 Discussion

One of the central observational and theoretical questions in modern physics is whether all astrophysical dark compact objects are accurately described by the Kerr metric, and if not, in what regimes the predictions of general relativity break down. In most models where deviations from the Kerr metric arise, these deviations typically occur for smaller black holes, making solar-mass black holes promising candidates for testing the gravitational interaction. However, recently [371] proposed a model where the opposite occurs: black hole uniqueness is violated at supermassive scales, while solar-mass ob-

jects remain well-described by general relativity. This finding emphasises the importance of experiments targeting different mass ranges of astrophysical compact objects, such as the Event Horizon Telescope or LISA.

The model proposed in [371] features two scalar fields, one of which is auxiliary but dynamically active, and might lead to instabilities. This auxiliary field mediates a coupling between the other scalar field and a higher-order curvature term. As a result, the effective mass of scalar perturbations is determined by two competing terms proportional to $\mathcal{G}$ and $\mathcal{G}^2$, with opposite signs. This competition enables scalarization within a specific mass range, which can encompass supermassive black holes, providing a novel mechanism for breaking the uniqueness of black holes at these scales. Our goal here was to investigate whether such a model can naturally arise in the context of effective field theory.

We have first investigated whether we can recover the model from a theory with two canonical scalar fields by assuming that one scalar is heavy and remains unexcited in a black hole background. Integrating out this heavy field yields an effective field theory description of the system, resulting in an emergent coupling between the light scalar and $\mathcal{G}^2$. However, our analysis uncovered two key limitations: first, the generated term acquires the "wrong" sign upon integrating out the heavy field, preventing it from contributing to the effective mass of perturbations in a manner that would enable scalarization of supermassive black holes; second, dimensional analysis reveals that this interaction is significantly suppressed compared to the $\mathcal{G}$ interaction.

Then, we relaxed the assumption that the second scalar field is heavy enough to be integrated out and analysed scalar perturbations on a fixed Schwarzschild background of a theory with two dynamical scalars described by equation (5.2.1). In the limit in which both scalars are massless, we were able to diagonalise and obtain two decoupled scalar fields, each coupling quadratically to $\mathcal{G}$ with coupling constants of opposite signs. Interestingly, this ensures that both curvature- and spin-induced scalarization *must* occur within the same theory. In the more general case, we solved the full system and explored the parameter space. Our analysis revealed no evidence of a scalarization mechanism capable of breaking the uniqueness of black holes at supermassive scales.

Next, we examined a similar model in which the heavy scalar is a Higgs-like field. Upon integrating out the Higgs field, we derived an effective field theory where the squared effective mass of the scalarization scalar matches that of [371]. However, in this scenario, vacuum general relativity solutions, such as the Kerr metric, no longer satisfy the equations of motion. Instead, scalarization would occur around stationary black hole solutions of a modified theory of the form $\mathcal{L} = R + k\mathcal{G}^2$. For this model to be phenomenologically interesting, the constant k must be small enough to pass current observational constraints. This might be possible to achieve; however, it could lead to further suppressing the effect of $\mathcal{G}^2$ on the effective mass, making it less relevant for supermassive black holes.

Future work could extend our analysis to the dynamical evolution of scalar perturbations around rotating Kerr black hole backgrounds, as well as to the study of spin-induced scalarization. Rotating solutions could be investigated using, for example, the numerical framework developed in [378]. Additionally, it would be valuable to explore in greater detail whether vacuum solutions of the theory with the Higgs field are susceptible to scalarization and, if so, at which mass scales this occurs. A natural first step in this direction would involve studying static and spherically symmetric black holes within the effective field theory described by equation (5.3.8), by employing both perturbation theory in the small-coupling limit and numerical techniques.

Chapter VI

Non-linear phenomena and dynamical evolution

Contents

The Einstein field equations are notoriously difficult to solve analytically. A common approach involves perturbative techniques, which treat small deviations from exact solutions. While effective in certain regimes, this method fails to capture the full complexity of non-linear phenomena inherent to general relativity. To explore such dynamics, one must resort to numerical relativity—the only available framework capable of fully capturing the non-linear nature of gravity.

Numerical relativity is invaluable in enabling precise simulations of scenarios that are otherwise intractable, such as black hole mergers and gravitational collapse. Central to this progress is the formulation of a well-posed initial value problem and the development of robust numerical methods. These advancements have allowed for the generation of gravitational waveforms that can be directly compared with observational data.

An essential property of any meaningful theory describing a physical system is its predictivity. From the perspective of Newtonian physics, if we know the initial position and velocity of a collection of particles with the forces acting on them, we can predict the future and retrodict the past. Mathematically, Newton's second law provides a second-order system of ordinary differential equations

$$\frac{\mathrm{d}^2 q_i}{\mathrm{d}t^2} = F_i\left(t; q_1, \ldots, q_n; \frac{\mathrm{d}q_1}{\mathrm{d}t}, \ldots, \frac{\mathrm{d}q_n}{\mathrm{d}t}\right), \tag{6.0.1}$$

where $i = 1, \ldots, n$, and n is the number of degrees of freedom, corresponding to the positions $q_i(t)$ of the particles. Given initial conditions for the positions $q_i(t = t_0)$ and velocities $\dot{q}_i(t = t_0)$, equation (6.0.1) uniquely determines the motion of the particles at any time t, as guaranteed by the theory of ordinary differential equations.

In classical field theory, consider the simple example of a free massless scalar field $\phi(x)$ governed by the Klein-Gordon equation

$$\Box\phi = 0\,. \tag{6.0.2}$$

This second-order partial differential equation allows us to specify ϕ and $\partial\phi/\partial t$ on a spatial hypersurface Σ_{t_0} at constant time $t = t_0$. The evolution of the scalar field is uniquely determined by equation (6.0.2).

However, uniqueness alone is insufficient. Since infinite accuracy in specifying initial conditions is unattainable and measurement errors are inevitable, we must require that "small" changes in initial conditions lead to only "small" changes in the solution. This establishes naturally the notion of well-posedness for partial differential equations.

Definition 6.0.1 *Hadamard [379] A partial differential equation system is well-posed if:*

1. *A solution exists for each choice of data within a certain class.*
2. *The solution is unique for each choice of data in some space.*
3. *The map from data to solutions is continuous in some topology.*

The first two conditions are straightforward to interpret. If we impose too many restrictions on the solution, it might not exist; conversely, if we impose too few, the solution might not be unique. In the coming sections, we will elaborate on the third condition, which is less trivial.

An initial value problem is called *locally well-posed* if the above conditions hold for some time interval $[t_0,\ T]$, and *globally well-posed* if the conditions hold for all $T > 0$. Here, we focus on local well-posedness and will omit the distinction.

In the next section, we review key aspects of well-posedness and its connection to the concept of hyperbolicity.

6.1 Hyperbolicity

To establish the connection between the concept of hyperbolicity and the well-posedness of an initial value problem, we need to translate the conditions of uniqueness and continuous dependence on the initial data to algebraic conditions on the principal symbol of the system (*i.e.*, the highest derivative terms). We will use this approach to demonstrate and examine the well-posedness of an initial value problem. We will focus on first- and second-order partial differential equations that describe initial value problems. We

will define the concepts of weak and strong hyperbolicity, as well as the necessary algebraic conditions that lead to a well-posed initial value problem. We will base our discussion on [380–382].

6.1.1 First order system

Consider an initial value problem in $d+1$ spacetime dimensions of the following form

$$\begin{aligned} P^\mu \partial_\mu u(t,x) + Qu(t,x) &= 0\,, \qquad (t,x) \in \mathbb{R}^{d+1}\,, \\ u(0,x) &= f(x)\,, \qquad x \in \mathbb{R}^d\,, \end{aligned} \tag{6.1.1}$$

where u is an n-dimensional column vector of all the variables in the system. P^μ and Q are real constant $n \times n$ matrices. A formal solution of the system (6.1.1) can be obtained by performing a Fourier transform in space

$$\hat{u}(t,\xi) = \frac{1}{(2\pi)^{d/2}} \int_{\mathbb{R}^d} e^{-i\xi\cdot x} u(x,t) \mathrm{d}x\,, \qquad \omega \in \mathbb{R}^d\,, \tag{6.1.2}$$

then, the initial value problem (6.1.1) becomes

$$\begin{aligned} \partial_t \hat{u} - iA(\xi_i)\hat{u} &= 0\,, \\ \hat{u}(0,\xi) &= \hat{f}(0,\xi)\,, \end{aligned} \tag{6.1.3}$$

where $A(\xi_i) = (P^0)^{-1}(-P^i\xi_i + iQ)$, and we have assumed that P^0 is invertible. This initial value problem has a solution of the form

$$\hat{u}(t,\xi_i) = e^{iA(\xi_i)t}\hat{f}(\xi_i)\,, \tag{6.1.4}$$

which we can inverse Fourier transform to obtain a solution of the original problem (6.1.1) as

$$u(t,x) = \frac{1}{(2\pi)^{d/2}} \int_{\mathbb{R}^d} e^{i\xi\cdot x} e^{iA(\xi_i)t} \hat{f}(\xi_i) \mathrm{d}\xi\,. \tag{6.1.5}$$

This solution is formal in that we can not guarantee its convergence. Even if the initial data f is chosen such that $\hat{f}$ is smooth and decays to zero as $|\xi| := \sqrt{\xi^i\xi_i} \to \infty$, the term $|e^{iA(\xi_i)t}|$ might diverge in the limit $|\xi| \to \infty$. On the

other hand, if we require that $|e^{iA(\xi_i)t}|$ is bounded by an exponential in time that is independent of ξ_i as

$$|e^{iA(\xi_i)t}| \leq ce^{\kappa t}\,, \qquad \forall \xi_i,\ \forall t \geq 0, \tag{6.1.6}$$

for some constants $c \geq 1$, and $\kappa \in \mathbb{R}$, the integral will converge. If the initial data is L^2 [1]. The bound (6.1.6) will imply, by Parseval's identity, the following

$$\|u\|_{L^2} = \|\hat{u}\|_{L^2} = \left\|e^{iA(\xi_i)t}\hat{f}(\xi_i)\right\|_{L^2} \leq ce^{\kappa t}\left\|f\right\|_{L^2}\,. \tag{6.1.7}$$

Hence, the norm of the initial data controls that of the solution, precisely the condition for well-posedness.

To arrive at the algebraic conditions for well-posedness, let us consider the behaviour of the solution at high frequencies, *i.e.*, in the limit $|\xi| \to \infty$, and let $t = \tilde{t}/|\xi|$, then equation (6.1.6) becomes

$$|e^{iB(\tilde{\xi}_i)\tilde{t}}| \leq c\,, \qquad \tilde{\xi}_i = \frac{\xi_i}{|\xi|}\,, \tag{6.1.8}$$

where

$$B(\xi_i) = -(P^0)^{-1}P^i\xi_i\,, \tag{6.1.9}$$

corresponds to the highest derivative terms. Now, let b be an eigenvector of the matrix $B(\xi_i)$ with eigenvalue λ, then

$$e^{iB(\tilde{\xi}_i)\tilde{t}}b = e^{i\lambda\tilde{t}}b\,, \tag{6.1.10}$$

since the B matrix is real then λ^* is an eigenvalue as well with the eigenvector b^*, therefore we also have

$$e^{iB(\tilde{\xi}_i)\tilde{t}}b^* = e^{i\lambda^*\tilde{t}}b^*\,, \tag{6.1.11}$$

and to prevent exponential growth we must have $\mathrm{Im}(\lambda) = 0$. The concept of weak hyperbolicity is based on this condition, that is to say, the initial value

[1] A function f is an L^2 function if $x \to |f(x)|^2$ is Lebesgue-integrable over $\mathbb{R}^d$.

problem (6.1.1) is weakly hyperbolic if, and only if, the matrix B has only real eigenvalues for all unit-norm ξ_i. Nonetheless, this requirement is generally insufficient for well-posedness. For assume that the matrix B is not diagonalizable, *i.e.*, there exists an $m \times m$ (for some $2 \leq m \leq n$) Jordan block in its Jordan normal form, then $|e^{iB(\bar{\xi}_i)\bar{t}}|$ may exhibit polynomial growth of the form $|\xi|^m$, see [380]. Therefore, to establish well-posedness, the matrix B needs to be diagonalizable with real eigenvalues [380]. Consequently, we will state that a partial differential equation system is said to be strongly hyperbolic if, and only if, its matrix B is diagonalizable with real eigenvalues.

Hyperbolicity is related to the existence of characteristics. Let ξ_0 be an eigenvalue of $B(\xi_i)$ with an eigenvector ω. Then this is equivalent to having

$$\mathcal{P}(\xi)\omega \equiv P^{\mu}\xi_{\mu}\omega = 0\,, \tag{6.1.12}$$

and this equation has a non-trivial solution if, and only if, $\det\mathcal{P}(\xi) = 0$. That is, a non-trivial solution exists if, and only if, ξ is a characteristic covector.

6.1.2 Second order system

We consider a linear second-order system in $d+1$ spacetime dimensions of the form

$$P^{\mu\nu}\partial_{\mu}\partial_{\nu}u + Q^{\mu}\partial_{\mu}u + Ru = 0\,, \tag{6.1.13}$$

as in the first-order system case, u is an n-dimensional vector, with $P^{\mu\nu}$, Q^{μ}, and R are $n \times n$ real constant matrices. The principal symbol is defined as

$$\mathcal{P}(\xi) \equiv P^{\mu\nu}\xi_{\mu}\xi_{\nu}\,. \tag{6.1.14}$$

We will only outline the analysis for this case (for more details, see [380–382]). We initially proceed as in the first-order case by performing a spatial Fourier transform and then writing the resultant equation in a first-order form as [382]

$$\hat{w} = iA(\xi_i)\hat{w}\,, \qquad \hat{w}^T = \left(\sqrt{1+|\xi|^2}\hat{u}, -i\hat{u}_t\right)\,, \tag{6.1.15}$$

for some $2n \times 2n$ matrix $A(\xi_i)$. Therefore, we can now establish a formal solution. After which, we can study the behaviour of high-frequency solutions to identify the dominant part of $A(\xi)$ in the $|\xi| \to \infty$ limit, which yields

$$B(\xi_i) = \begin{pmatrix} 0 & I \\ -(P^{00})^{-1} P^{ij} \xi_i \xi_j & -2(P^{00})^{-1} P^{0i} \xi_i \end{pmatrix} . \tag{6.1.16}$$

The same definitions for weak and strong hyperbolicity carry over. To connect our hyperbolicity discussion of second-order systems to the characteristics of such partial differential equations, we take ξ_0 to be an eigenvalue of B with an eigenvector $v = (\omega, \omega')$. The eigenvalue equation will then yield,

$$P^{\mu\nu} \xi_\mu \xi_\nu \omega = 0 \,, \qquad \omega' = \xi_0 \omega \,, \tag{6.1.17}$$

which has a non-trivial solution if, and only if, ξ_μ is characteristic. So, we can demonstrate strong hyperbolicity by finding the characteristic covectors and their "polarisation" ω.

6.1.3 Variable coefficients and non-linear partial differential equations

Up to this point, we have only discussed linear partial differential equation systems with constant coefficients. An obvious question is how to generalise the previous discussion to non-linear systems with variable coefficients. The "localisation principle" addresses partial differential equation systems with variable coefficients. The principle of localisation is based on well-posedness being a high-frequency question, *i.e.*, on the premise that we should only worry about the high-frequency (very short wavelength) solutions. If we assume that the coefficients are smooth, then in this regime (of high frequencies), we can "localise" the coefficients of the partial differential equation at a point p, and consider them "frozen" to their value at p. Then the localisation principle states that "A necessary condition for local well-posedness of the varying coefficient equations near p is that the frozen coefficient equation should be locally well-posed for all points p (with additional smoothness requirements on the eigenvalues and vectors)." [380, 381].

On the other hand, non-linear problems generally introduce many complications. For instance, non-linearities may cause the solution to blow up in finite time or lead to the crossing of the characteristics producing shocks [380, 381]. Consequently, it is almost always only possible to establish the existence of a solution for some time interval. If a non-linear system is well-posed, then a small perturbation u_1 of the solution u_0 as $u = u_0 + \epsilon u_1$ will produce a well-posed linear system for u_1. Hence, a necessary condition for the well-posedness of the non-linear system is that when linearising around any solution, the consequent linear problem is well-posed. More importantly, the converse is true [380, 381] for a quasilinear problem. This is known as the linearization principle: "The quasilinear problem is well-posed in the neighbourhood of a solution if all the linearised problems around that solution are well-posed." As we are interested in completely non-linear partial differential equations, it is worth noting that such systems are more complex to analyse and require more advanced tools to tackle. The treatment of such problems is available in [383] (see *e.g.*, chapter 5). The main difference between quasilinear and completely non-linear systems lies in the required order of regularity imposed on the initial data. That subtlety aside, strong hyperbolicity as defined above still guarantees (local) well-posedness.

6.2 Initial value formulation in general relativity and beyond

Astrophysical phenomena involving strong gravitational fields, such as the collapse of compact objects or the merger of coalescing binaries, cannot be adequately described using perturbative techniques. Instead, these phenomena require the formulation of Einstein's equations as an initial value problem, which must then be solved numerically. To test gravity in its non-linear regime and search for new physics beyond general relativity or the standard model of particle physics, it is essential to formulate a well-posed initial value problem and conduct numerical simulations in extensions of general relativity. The ability to make predictions depends on the existence of a well-posed

initial value problem formulation.

We first discuss the initial value problem in general relativity, and in the following section, we address the status of this problem in extensions of the theory.

6.2.1 General relativity is strongly hyperbolic

A drawback of the covariant nature of Einstein's equations is the ambiguity in their character as a system of partial differential equations. The coordinate system chosen to study the system's character is crucial for setting up a well-posed initial value problem. For instance, the Arnowitt–Deser–Misner (ADM) formalism [384] produces only a weakly hyperbolic system of partial differential equations for general relativity, and leads to an ill-posed system [2].

Choquet-Bruhat was the first to demonstrate that Einstein's equations are locally well-posed in the harmonic gauge [385]. She later extended this work with Geroch [118] to prove global well-posedness. Sbierski [117] further demonstrated that general relativity admits a unique maximal globally hyperbolic development (without resorting to Zorn's lemma).

It took some time after these developments to successfully simulate and study the merger of black holes. The first binary black hole simulations were successfully performed using the generalised harmonic gauge [386–388] or the BSSN formalism [389–391], and the CCZ4 [392] formulation thereafter.

Here, we briefly discuss the strong hyperbolicity of the vacuum Einstein's equation

$$R_{\mu\nu} = 0\,, \tag{6.2.1}$$

where the Ricci tensor is explicitly given by

$$R_{\mu\nu} = -\frac{1}{2} g^{\alpha\beta} \left(\partial_\alpha \partial_\beta g_{\mu\nu} - 2\partial_\beta \partial_{(\mu} g_{\nu)\alpha} + \partial_\mu \partial_\nu g_{\alpha\beta} \right) + \mathcal{F}_{\mu\nu}(g, \partial g)\,. \tag{6.2.2}$$

[2] The ADM equations are weakly hyperbolic for any fixed choice of shift and desensitised lapse. The desensitised lapse is the lapse rescaled by a constant power of $\sqrt{\det \gamma}$, where γ is the induced metric on the Cauchy hypersurfaces of the foliation.

For the hyperbolicity analysis, the $\mathcal{F}_{\mu\nu}$ term is irrelevant, as we focus on the highest derivative terms. The first term contains second-order derivatives, which are relevant for hyperbolicity. The first term in the parentheses has the form of a wave equation, though the remaining terms spoil this property. The harmonic gauge

$$0 = \Box x^{\mu} = \partial_{\alpha} g^{\alpha\mu} + \frac{1}{2} g^{\alpha\mu} g^{\rho\sigma} \partial_{\alpha} g_{\rho\sigma} \equiv H^{\mu} , \tag{6.2.3}$$

provides a way to address this issue. The harmonic gauge allows us to express the problematic second-order derivative terms in the Ricci tensor (6.2.2) in terms of H^{μ} and lower-order terms. Thus, the vacuum Einstein's equation is equivalent to

$$g_{\alpha(\mu}\partial_{\nu)} H^{\alpha} = -\frac{1}{2} g^{\alpha\beta} \partial_{\alpha}\partial_{\beta} g_{\mu\nu} + \tilde{\mathcal{F}}_{\mu\nu}(g, \partial g) . \tag{6.2.4}$$

in the harmonic gauge (6.2.3). This system takes the form of a wave equation.

Additionally, we must ensure that if $H^{\mu} = 0$ is satisfied initially on a Cauchy slice Σ, it is preserved by the evolution equations. Given initial data on Σ that satisfy the constraints, with $H^{\mu} = 0$, and assuming equation (6.2.4) holds, then $\partial H^{\mu}/\partial t = 0$ on Σ, where t is the time coordinate [25]. Furthermore, when equation (6.2.4) holds, the Bianchi identity gives

$$0 = \nabla^{\mu} G_{\mu\nu} = -\frac{1}{2} g_{\alpha\nu} g^{\rho\mu} \partial_{\rho}\partial_{\mu} H^{\alpha} + \mathcal{H}_{\nu}(H, \partial H) , \tag{6.2.5}$$

where $\mathcal{H}_{\nu}(H, \partial H)$ is linear in H^{α}. Thus, H^{α} satisfies a wave equation with a unique solution. Given that $H^{\alpha} = 0 = \partial H^{\alpha}/\partial t$ on the initial slice Σ, it follows that H^{α} will vanish everywhere, and the gauge condition is therefore propagated.

Next, we show that Einstein's equation is strongly hyperbolic in the Harmonic gauge. To do this, we compute the principal symbol of the Einstein equation acting on symmetric second-rank tensors $\omega_{\mu\nu}$

$$\big(P(\xi)\cdot\omega\big)_{\mu\nu} = -\frac{1}{2} g^{\alpha\beta} \xi_{\alpha}\xi_{\beta}\omega_{\mu\nu} , \tag{6.2.6}$$

for some covector ξ_μ. Recall (see Section 6.1) that a covector ξ_μ is characteristic if and only if there exists an $\omega_{\mu\nu}$ such that

$$\big(P(\xi)\cdot\omega\big)_{\mu\nu} = 0\,, \tag{6.2.7}$$

Hence, in general relativity, for any symmetric $\omega_{\mu\nu}$, a hyper-surface is characteristic if and only if it is null, *i.e.*, $\xi^2 = 0$.

Consider a coordinate chart $x^\mu = (t, x^i)$, in which $\xi_\mu = (\xi_0, \xi_i)$ with real ξ_i. The two solutions of $\xi^2 = 0$ are real, implying that characteristics with a real spatial part must also have real temporal parts. Therefore, Einstein's equation is weakly hyperbolic.

To establish strong hyperbolicity, we need to show that the $2n\times 2n$ matrix B discussed in Section 6.1.2 is diagonalizable. Since ξ_μ is characteristic for any symmetric $\omega_{\mu\nu}$ with two real solutions, say $\xi_0^\pm$, then the matrix B has these solutions as real eigenvalues, with eigenvectors $(\omega_{\mu\nu}, \xi_0^\pm\omega_{\mu\nu})$. For each eigenvalue of B, there are n linearly independent eigenvectors, meaning that B has $2n$ linearly independent eigenvectors and is therefore diagonalizable. Thus, Einstein's equation is strongly hyperbolic in the Harmonic gauge.

Finally, if the matter sector does not introduce second- or higher-order derivatives—as in the case of a perfect fluid—the above analysis remains valid. However, the formulation of a well-posed initial value problem becomes non-trivial when additional effects, such as viscosity, are included [393–396].

6.2.2 Extensions of general relativity: The jury is out

The most direct way to test general relativity against binary coalescence data is to use its predictions as a null hypothesis. However, modelling waveforms that include deviations from general relativity offers several advantages. It enables the interpretation of new physics if deviations are detected and provides quantitative bounds, with the tightest constraints arising from theory-specific models. Additionally, these theory-specific waveforms can be used to calibrate more generic parametrisations, thereby enhancing their accuracy.

A major obstacle is that in many extensions of general relativity, it is not

obvious how to obtain a well-posed formulation of the initial value problem because the new physics drastically changes the structure of the field equations as partial differential equations. Scalar fields provide a characteristic example. No-hair theorems [312, 313, 337, 342, 351, 397] (see Section 4.1) dictate that scalars cannot leave an imprint on black holes in most cases. All the known counterexamples (*e.g.*, [306, 307, 314, 315, 348, 398, 399]) require coupling the scalar to the Gauss-Bonnet invariant. Einstein's equations are quasi-linear, *i.e.*, linear in the second derivatives of the metric, and this is a key property concerning their well-posedness as an initial value problem. In contrast, the Gauss-Bonnet invariant is quadratic in the curvature and hence quadratic in the second derivatives of the metric. This places well-posedness in jeopardy.

One can circumvent this problem by working perturbatively in the coupling constants that control the deviations from general relativity. Assuming that the solutions are continuously connected to general relativity as the coupling goes to zero, one can generate solutions order by order [358, 400–406]. One disadvantage of this approach is that secular growth can drive it out of its range of validity [407]. Another is that the perturbative treatment in the coupling is not suitable for capturing effects that involve non-linearities in the new fields.

This last point is demonstrated in the phenomenon of scalarization [310] (see Section 3.3.2). Scalarization can be understood as a linear tachyonic instability of the scalar that is eventually non-linearly quenched. The instability occurs in a general relativity spacetime describing compact objects. It is controlled by interactions that are quadratic in the scalar [311] and, for black holes, it appears below a mass [314, 315] or above a spin [321, 322] threshold. The endpoint is a compact object with a non-trivial scalar configuration, whose properties are determined by non-linear interactions of the scalar [316–318]. Hence, the dynamics of theories exhibiting scalarization cannot be fully captured working perturbatively in the coupling constant [405, 406, 408–410].

Indeed, the study of the initial value problem for scalars non-minimally coupled to gravity, and in particular for the broad class of theories that lead to second-order equations described by the Horndeski action [301], has re-

ceived a lot of attention recently [382, 411–418]. It was established in [419] that an appropriate formulation exists that renders the initial value problem well-posed in these theories in the weakly coupled regime, *i.e.*, when the non-minimal couplings of the scalar remain "small". Numerical studies, restricted so far to theories where the scalar couples only to the Gauss-Bonnet invariant (see [420] for an exception), have verified this result for small values of the coupling constant that controls this coupling [409, 421–423]. For larger values of the coupling constant, however, well-posedness is eventually lost, as the equations tend to change character from hyperbolic to elliptic in a region of spacetime [409, 412–414, 421–424].

Viewing these theories as non-linear effective field theories, and hence as products of some truncation of a more "fundamental" theory, a promising strategy could be to try to employ a method inspired by viscous relativistic hydrodynamics to render them predictive [425]. How to import such a method to gravity theories is currently being explored [425–434]. An interesting alternative would be to study whether additional couplings of the scalar, which one could expect to be there in an effective field theory, could improve the theory's behaviour and lead to well-posed evolution.

In the context of scalarization, the quadratic coupling between the scalar and the Gauss-Bonnet invariant is the leading order contribution to the onset of the tachyonic instability that leads to black hole scalarization [311, 314, 321] (see Section 3.3.2). However, it has been shown in [332] that an additional coupling of the type $\phi^2 R$ leads to an improvement of the hyperbolic nature of the equations for linear perturbations in scalarization theories that contain $\phi^2\mathcal{G}$ couplings. Interestingly, that same curvature interaction, $\phi^2 R$, has been shown to resolve radial stability problems for scalarized black holes [318, 332], to help evade binary pulsar constraints by suppressing neutron star scalarization [331], and to render general relativity a cosmological attractor without the need for the fine-tuning of the initial conditions [330], thereby making scalarization models compatible with late time cosmological dynamics.

Motivated by the above, we study gravitational collapse of scalar clouds in a theory with quadratic scalar couplings to both the Gauss-Bonnet invariant and the Ricci scalar, as we discussed in Section 3.3.3.

For the reader's convenience, we provide again the theory we are considering

$$S = \frac{1}{16\pi}\int \mathrm{d}^4x\sqrt{-g}\left[R + X + f(\phi)\mathcal{G} + h(\phi)R\right] , \tag{6.2.8}$$

and the equations of motion read

$$\begin{aligned} E^{\mu}{}_{\nu} \equiv &- T^{(\phi)\mu}{}_{\nu} + \delta^{\mu\gamma\kappa\lambda}_{\nu\alpha\rho\sigma} R^{\rho\sigma}{}_{\kappa\lambda}\nabla_{\gamma}\nabla^{\alpha}f \\ &+ (1+h)G^{\mu}{}_{\nu} + \delta^{\mu}{}_{\nu}\Box h - \nabla^{\mu}\nabla_{\nu}h = 0 , \end{aligned} \tag{6.2.9}$$

$$E \equiv -\Box\phi - h'(\phi)R - f'(\phi)\mathcal{G} = 0 , \tag{6.2.10}$$

with

$$T^{(\phi)}_{\mu\nu} = \frac{1}{2}\nabla^{\mu}\phi\nabla_{\nu}\phi - \frac{1}{4}(\nabla\phi)^2 g_{\mu\nu} . \tag{6.2.11}$$

We choose,

$$f(\phi) = \frac{\alpha}{2}\phi^2 , \qquad h(\phi) = -\frac{\beta}{4}\phi^2 . \tag{6.2.12}$$

6.3 Spherical collapse and taming ill-posedness

We demonstrate that the Ricci coupling significantly improves the dynamical behaviour of the theory and allows it to be predictive for values of the Gauss-Bonnet coupling that would otherwise yield an ill-posed initial value problem. Our numerical simulations enable us to track the formation of scalarized black holes for suitable initial data. For data that would have led to the formation of a black hole with a mass smaller than the existence threshold of the theory, we instead see the scalar cloud smoothly dispersing.

6.3.1 Evolution in spherical symmetry

Here, we focus on the study of the initial value problem in spherical symmetry. We follow closely the prescription given in [413]. To this end, we

consider a spherically-symmetric background, with the following ansatz in Schwarzschild coordinates (t, r, θ, φ)

$$\mathrm{d}s^2 = -\mathrm{e}^{2A(t,r)}\mathrm{d}t^2 + \mathrm{e}^{2B(t,r)}\mathrm{d}r^2 + r^2\mathrm{d}\Omega^2 \,, \tag{6.3.1}$$

and same symmetries for the scalar field $\phi = \phi(t, r)$. We introduce new variables

$$P(t, r) \coloneqq \mathrm{e}^{-A+B}\,\partial_t\phi \,, \qquad Q(t, r) \coloneqq \partial_r\phi \,. \tag{6.3.2}$$

With this choice of variables and the ansatz of equation (6.3.1), the system (6.2.9) and (6.2.10) reduces to three time-evolution equations for ϕ, P and Q, and two radial constraints for A and B.

This system of equations might not always admit a well-posed initial value problem. Recall, a system of partial differential equations is well-posed if there exists a unique solution that depends continuously on its initial data. This will be the case if the system is strongly hyperbolic, *i.e.*, its principal part (the highest derivative terms) is diagonalizable with real eigenvalues [380] (for more details, see Section 6.1).

In numerical considerations, the characteristic speeds are a useful diagnostic tool as they convey information regarding the character of the evolution equations. In spherical symmetry, they are given by [413]

$$c_\pm = \frac{1}{2}\left(\mathrm{Tr}(C) \pm \sqrt{\mathcal{D}}\right) \,, \tag{6.3.3}$$

where C, and $\mathcal{D}$ depend on the functions A, B, ϕ, P, and Q, and their derivation can be found in Appendix B.1. The system is hyperbolic if the characteristic speeds are real ($\mathcal{D} > 0$), elliptic if they are complex ($\mathcal{D} < 0$), and parabolic if the speeds are degenerate ($\mathcal{D} = 0$).

6.3.2 Initial data

For initial data, we are free to specify the values of ϕ and P at $t = 0$, whereas by definition we must have $Q(0, r) = \partial_r\phi(0, r)$. We use two types of initial

data. Type-I initial data is a static Gaussian pulse

$$\phi(0,r) = a_0 \exp\left[-\left(\frac{r-r_0}{w_0}\right)^2\right], \qquad P(0,r) = 0\,, \tag{6.3.4}$$

while type-II initial data is an approximately ingoing pulse

$$\phi(0,r) = a_0 \left(\frac{r}{w_0}\right)^2 \exp\left[-\left(\frac{r-r_0}{w_0}\right)^2\right], \tag{6.3.5}$$

$$P(0,r) = -\frac{1}{r}\phi(0,r) - Q(0,r)\,, \tag{6.3.6}$$

where a_0, r_0 and w_0 are constants.

6.3.3 Numerical implementation

We employ a fully constrained evolution scheme. The equations are discretized over the domain $[0,\ T] \times [0,\ R]$ for some choice of R, and T. For a given resolution N, the radial step Δr is given by $\Delta r = R/N$, and the time step is defined by setting the Courant parameter to $\lambda = 0.25$, *i.e.*, $\Delta t = \lambda \Delta r$. Most of the simulations presented in this work have been performed with a spatial resolution of $\Delta r = 0.025$ in a domain with the outer boundary located at $r = 200$. We have verified that the results do not vary significantly when the position of the outer boundary is changed.

To impose regularity at the centre, we take a staggered grid and perform the following expansion

$$\phi(t,r) = \phi_0(t) + \phi_2(t) r^2 + \phi_4(t) r^4 + O(r^6)\,, \tag{6.3.7}$$

$$A(t,r) = A_0(t) + A_2(t) r^2 + A_4(t) r^4 + O(r^6)\,, \tag{6.3.8}$$

$$B(t,r) = B_0(t) + B_2(t) r^2 + B_4(t) r^4 + O(r^6)\,, \tag{6.3.9}$$

and solve for $A_0,\ A_2,\ A_4,\ B_2,\ B_4$ by using the initial data. Moreover, the boundary conditions at $r = 0$ require that $\partial_r A = 0$ and $\partial_r B = 0$. One can see from the equations that choosing $B_0 = 0$ satisfies this automatically. Without such treatment at the origin, it was only possible to evolve the system for a small subset of coupling constants. At the outer boundary of the do-

main, we impose approximately outgoing boundary conditions for $\phi,\ Q,\ P$, while the metric functions are completely specified by solving the constraint.

Given the initial data, we solve the constraint equations for the metric functions on the discretised domain $[0,\ R]$ using a fourth-order Runge-Kutta (RK4) scheme. This scheme requires knowledge of the value of $\phi,\ Q$, and P at intermediate virtual points, and we obtain such information by employing a fifth-order Lagrangian interpolator. Once we have the solution, we set $A(t,r) \to A(t,r) - A(t,R)$ by utilising the remaining gauge freedom. This guarantees that at the outer boundary of the domain, the time function t measures the proper time of a static observer. After obtaining the metric functions, we integrate the variables $\phi,\ Q$, and P in time using the method of lines with an RK4 scheme and a sixth-order Kreiss-Olliger dissipation term. We use a fourth-order finite differences operator satisfying summation by parts to discretise radial derivatives [435]. At the initial step we compute the initial Misner-Sharp mass [436] as $M = R\left(1 - \mathrm{e}^{-2B(0,R)}\right)/2$, which we use for the rescaling of the output. We keep track of the formation of an apparent horizon by checking the largest radius for which $\exp(A-B)$ falls below a chosen tolerance, indicating the formation of a black hole.

6.3.4 Results

We first investigate how the inclusion of the Ricci term enhances the hyperbolic nature of the evolution system for a specific value of $\alpha/M^2 = 0.25$. In Figure 6.1, we plot how the maximum of c_- and the minimum of c_+ vary with time for different values of β, type-II initial data with $r_0 = 25, w_0 = 6$ and for two different amplitudes $a_0 = 0.01,\ 0.016$. A vanishing or rather small value of β leads to the formation of a naked elliptic region, *i.e.*, a region of spacetime where the characteristic speeds change sign, signalling that the character of the equations has changed from hyperbolic to elliptic without being shielded by an apparent horizon [437]. On the other hand, for a sufficiently large coupling to the Ricci scalar, the plot suggests that this coupling heals the problem and allows for the evolution to continue for later times. Motivated by these results, we explore the parameter space more thoroughly. We start with fixed $\alpha/M^2 = 0.25$ and type-II initial data with $r_0 = 25,\ w_0 = 6$, and varied the amplitude a_0 in the range $[0.2,\ 2] \times 10^{-2}$ and the Ricci coupling

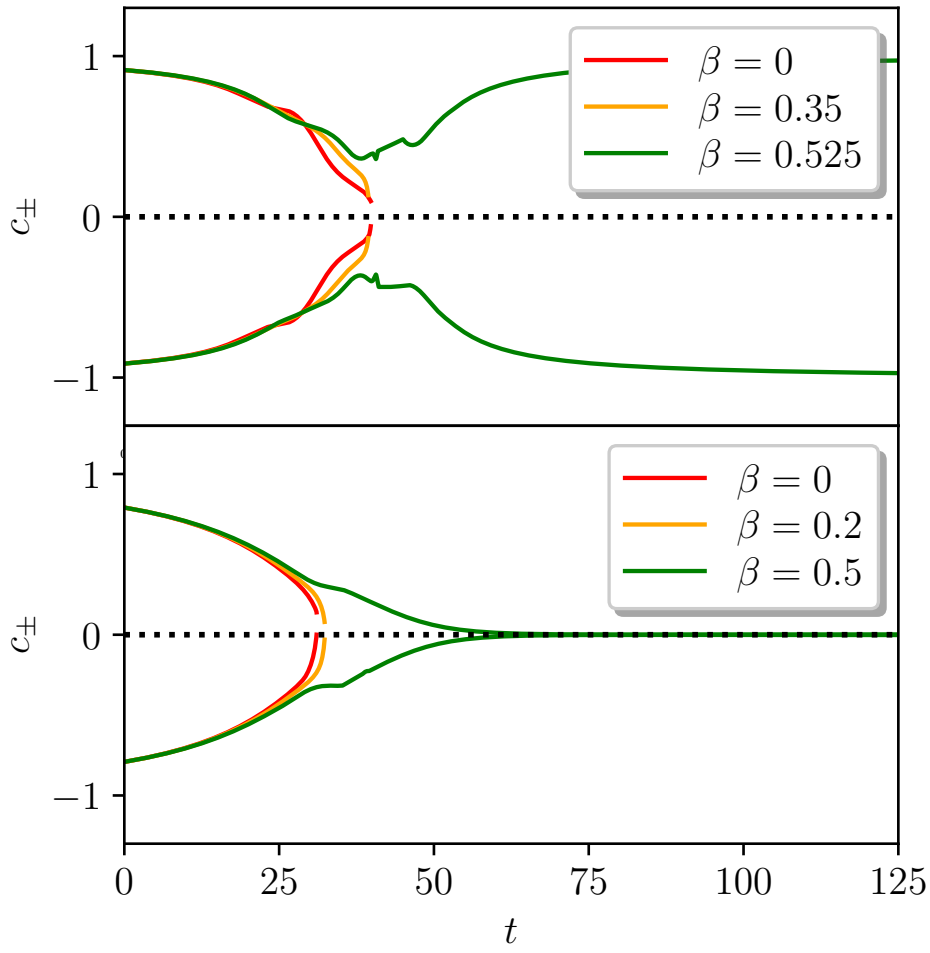

Figure 6.1: Both plots are for $\alpha/M^2 = 0.25$ and type-II initial data with $r_0 = 25$, $w_0 = 6$. The plot on the top is for $a_0 = 0.01$, and the one on the bottom is for $a_0 = 0.016$. We show the maximum of c_- (solid lines) and the minimum of c_+ (dashed lines) in space for different values of β. In the top panel, for $\beta = 0,\ 0.35$, the characteristic speeds approach zero and will eventually change sign. Therefore, the equations change character, and we cannot follow the evolution further. However, for $\beta = 0.525$, the characteristic speeds do not cross zero, and the end state of the evolution is flat geometry. In the bottom panel, we observe the formation of an apparent horizon for $\beta = 0.5$. The curves indeed asymptote to zero, unlike the $\beta = 0,\ 0.2$ cases.

β in the range $[0,\ 1]$. For each of the cases considered, we establish whether the outcome of the evolution is flat space, a naked elliptic region, or the development of an apparent horizon. Outcomes are summarised in Figure 6.2. For $\beta = 0$ and low enough initial amplitudes, the theory is predictive, and the outcome is flat spacetime. For certain larger amplitudes, an apparent horizon forms. However, we encounter a naked elliptic region both in the transition between these two outcomes and when the amplitude is increased further. Remarkably, increasing the value of β eventually removes the naked elliptic region in all cases.

On a few occasions, labelled by an orange star in Figure 6.2, it was not possible to conclude whether the outcome is a formation of an apparent horizon or a naked elliptic region due to the steep gradients in the metric sector. This is because Schwarzschild coordinates are not horizon penetrating, and it does not affect our previous conclusions regarding the effect of the Ricci coupling. We have performed additional simulations with different values of α/M^2 and for the two different types of initial data, which confirm the positive effect this coupling has on hyperbolicity in the case of spherical collapse. A summary of the other simulations performed is found in Table B.1 in Appendix B.3. Since for large enough β we can track the evolution, we delve a bit deeper into the properties of the end state. We present three representative cases in Figure 6.3, where we show an early and a late snapshot of the evolution of the scalar field ϕ and the metric combination $\exp(A - B)$, which vanishes on the apparent horizon, for type-II initial data with fixed $r_0 = 25$, and $w_0 = 6$ for three different cases. (The fact that $\exp(A - B)$ vanishes also at smaller radii, once an apparent horizon forms, is due to the use of coordinates that are not horizon-penetrating). For each of them, the amplitude a_0 is chosen such that it would produce an apparent horizon in general relativity. From the analysis of static solutions in [318] (see also Section 7.1), we know that, for large enough values of β, black holes below some threshold mass and down to some minimum mass will exhibit hair. Black holes above the threshold mass will have no hair. Below that minimum mass, the Schwarzschild metric is unstable, and no hairy black holes appear to exist either. The parameters of the three panels of Figure 6.3, top to bottom, have been chosen such that the mass associated with the initial data corre-

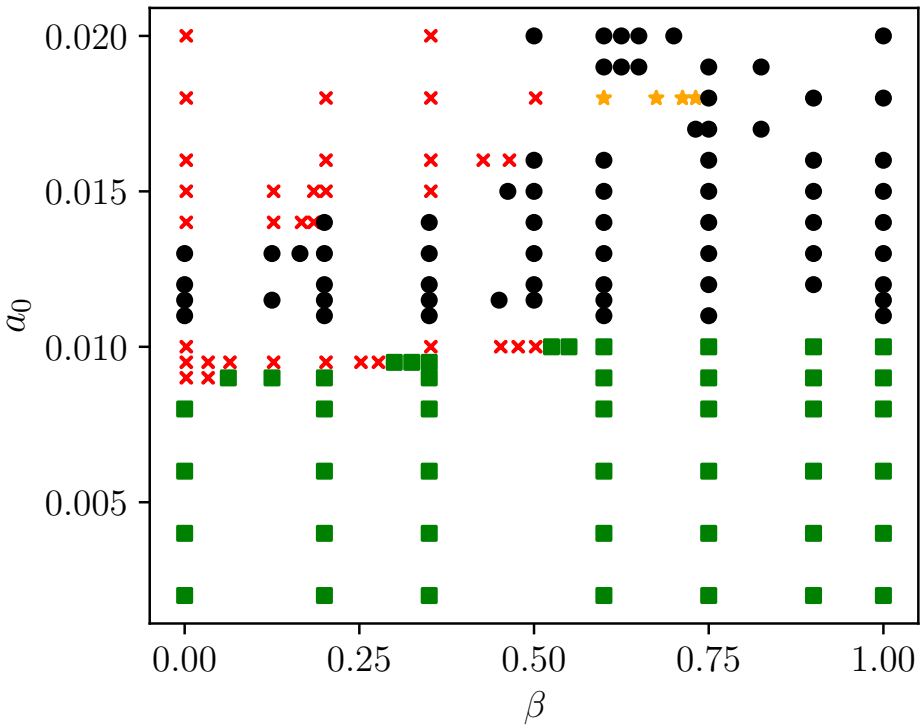

Figure 6.2: Scatter plot for $\alpha/M^2 = 0.25$ and type-II initial data with $r_0 = 25$, $w_0 = 6$, and a varying amplitude a_0. The end state of the evolution is indicated by green squares for flat spacetime, red crosses for naked elliptic regions, and black dots for black holes. Orange stars denote cases for which it is difficult to conclude if the end state is a black hole or a naked elliptic region (in Schwarzschild coordinates). For large enough β, the Ricci coupling "cures" the loss of hyperbolicity for both flat space and black hole end states.

sponds to each of the three cases, respectively. As can be seen from the plots, the end state of evolution is in agreement with the analysis of the static solutions. When applicable, we provide a comparison with a static and spherically symmetric profile, obtained by integrating numerically the equations (6.2.9) and (6.2.10), as described in [318]. Note that the lack of perfect overlap between the scalar profile and the static configuration is in part due to the limitations of using Schwarzschild coordinates. Remarkably, in the case where the static limit predicts that no (stable) black hole can exist (bottom panel), we find no impediment in the time evolution, and the scalar field dissipates to infinity, leaving a flat background.

6.3.5 Discussion

We have investigated the effect of non-minimally coupling the scalar field quadratically to the Ricci scalar on the well-posedness of the initial value problem in scalar Gauss-Bonnet gravity, in the case of spherical collapse. Our results show that this additional coupling, for large enough values of the corresponding coupling constant, which are still within the range for which black holes are radially stable, general relativity is a cosmological attractor and the constraints on neutron stars scalarization are evaded, can mitigate against the formation of a naked elliptic region, which signals a loss of hyperbolicity and plagued earlier numerical simulations. This demonstrates that including specific additional interactions—other than those essential for interesting phenomenology, such as black hole hair—can be a successful strategy for tackling well-posedness problems in effective field theories of gravity with non-minimally coupled scalars.

There are three important limitations to our results, which also highlight interesting future directions to explore. The first one is spherical symmetry. It is likely that the coupling to the Ricci scalar might not be sufficient to cure ill-posedness in a less symmetric setup, and a broader range of couplings would need to be explored. Simulations in 3 + 1 dimensions would also allow us to analyse numerically the non-radial stability of scalarized black holes [438, 439]. The second limitation is that we only considered the collapse of a scalar cloud. The third limitation is that our numerical implementation involved coordinates that are not horizon-penetrating, and hence are

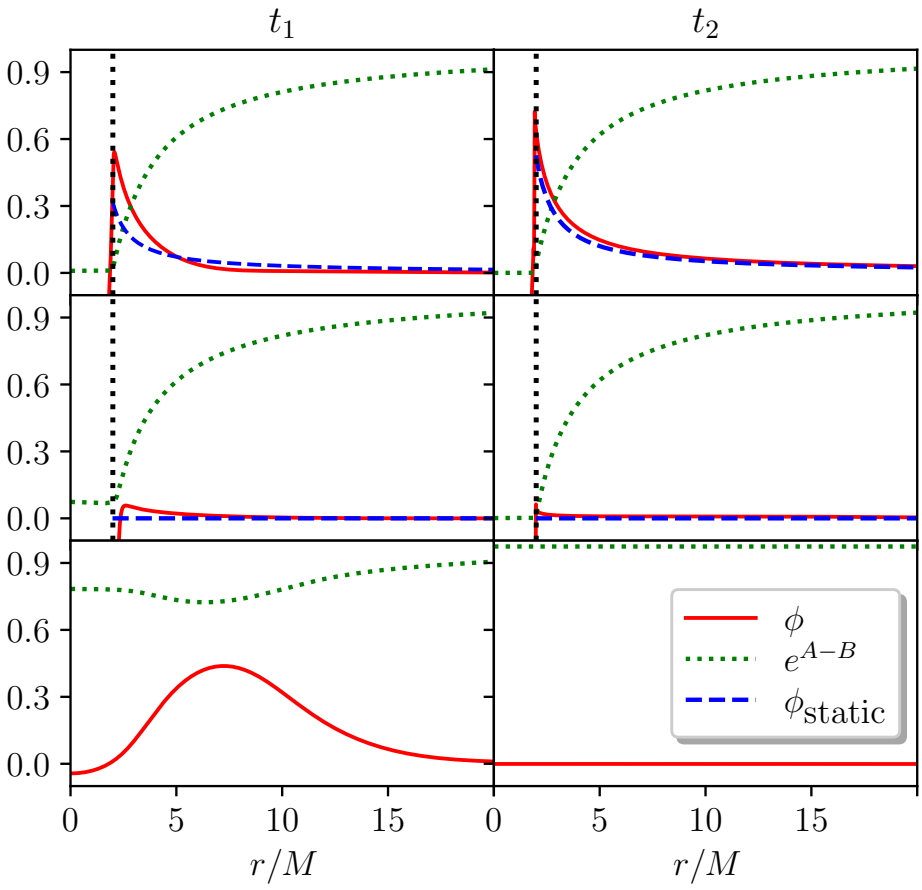

Figure 6.3: Scalar field and e^{A-B}, which vanishes at the apparent horizon, as a function of radius for two different time instances for type-II initial data with fixed $r_0 = 25$, and $w_0 = 6$. The static solution is denoted by ϕ_{static}. The black dotted line in the first two panels is the location of the apparent horizon. Top panel: is for $\alpha/M^2 = 0.75$, $\beta = 1.5$ with $a_0 = 0.015$. Snapshots with $\{t_1,\ t_2\}/M = \{22,\ 88\}$ show the formation of an apparent horizon where the quantity $e^{A-B} \to 0$, with the late time behaviour maintaining a scalar profile with a $1/r$ fall off. Middle panel: is for $\alpha/M^2 = 0.25$, $\beta = 1$ with $a_0 = 0.02$ and $\{t_1,\ t_2\}/M = \{11,\ 28\}$. In this case, an apparent horizon forms, but the late-time behaviour does not support a scalar profile. Bottom panel: is for $\alpha/M^2 = 1.25$, $\beta = 2$ with $a_0 = 0.01$ and $\{t_1,\ t_2\}/M = \{39,\ 97\}$. Here, the end state is flat geometry for which the scalar field dissipates to infinity.

not ideal for probing the properties of the end state when the latter is a black hole.

Interestingly, our simulations did allow us to confirm the expectations arising from combining static results and linear perturbations (*e.g.*, [310, 314, 315, 318, 332]: that spherical collapse will lead to black holes with scalar hair when their mass is below a mass threshold and above a minimum mass bound and that above the mass threshold collapse leads to black holes without hair. Remarkably, in simulations that would form a black hole below the minimum mass bound, where stable black holes are not known to exist, the scalar cloud smoothly dissipated, leaving behind flat space.

In Chapter VII, we will discuss the dynamics of black holes. We explored these cases in more detail by using horizon-penetrating coordinates, which allowed us to trace the evolution of the apparent horizon and probe the end state in more detail.

Chapter VII

Spherical black holes dynamics

Contents

In this chapter, we study the dynamics of spherically symmetric black holes in horizon-penetrating coordinates by employing excision techniques. We briefly revisit the effect of the Ricci coupling on well-posedness, focusing on coupling parameters for which the final black hole is scalarized. We observe that excision leads to well-posed evolution for a larger part of the parameter space, as the ill-posed region was beyond the horizon in certain cases. We study the dynamics of black holes that are near the threshold of scalarization or near the minimum mass threshold, which is a characteristic feature of black holes in this class of theories. We also study initial data for which the initial black hole lies near but below the minimum mass threshold. Moreover, we extract the monopolar quasi-normal modes and estimate the time scale of the tachyonic instability that leads to scalarization. For ease of reference, the Ricci-Gauss-Bonnet model is (for more details, see Section 3.3.3)

$$S = \frac{1}{16\pi}\int \mathrm{d}^4x\sqrt{-g}\left[R + X + f(\phi)\mathcal{G} + h(\phi)R\right] , \tag{7.0.1}$$

and the equations of motion read

$$\begin{aligned} E^{\mu}{}_{\nu} \equiv &- T^{(\phi)\mu}{}_{\nu} + \delta^{\mu\gamma\kappa\lambda}_{\nu\alpha\rho\sigma} R^{\rho\sigma}{}_{\kappa\lambda}\nabla_{\gamma}\nabla^{\alpha} f \\ &+ (1+h)G^{\mu}{}_{\nu} + \delta^{\mu}{}_{\nu}\Box h - \nabla^{\mu}\nabla_{\nu} h = 0 , \end{aligned} \tag{7.0.2}$$

$$E \equiv -\Box\phi - h'(\phi)R - f'(\phi)\mathcal{G} = 0 , \tag{7.0.3}$$

with

$$T^{(\phi)}_{\mu\nu} = \frac{1}{2}\nabla^{\mu}\phi\nabla_{\nu}\phi - \frac{1}{4}(\nabla\phi)^2 g_{\mu\nu} . \tag{7.0.4}$$

We choose,

$$f(\phi) = \frac{\alpha}{2}\phi^2 , \qquad h(\phi) = -\frac{\beta}{4}\phi^2 . \tag{7.0.5}$$

7.1 Static black holes

A characteristic feature of black holes with scalar hair in theories that include an interaction between the Gauss-Bonnet invariant and a scalar field is that their scalar charge is not a free parameter, but instead uniquely determined

by their mass (and spin for rotating black holes) [307, 308, 318, 348]. The regularity condition on the horizon fixes the scalar charge in terms of the mass (see Section 4.2, which discusses the linear coupling case).

Static, spherically symmetric black holes in the theory we consider here were first studied in [318, 332]. Black hole solutions with a non-trivial scalar profile, dubbed scalarized black holes, only exist for a specific range of masses, *i.e.*, only for $M \in [M_{\rm min}, M_{\rm th}]$. Scalarized black holes with mass $M < M_{\rm min}$ do not exist, as for such masses the regularity condition on the horizon is violated and the solution is no longer a black hole but rather a naked singularity.

On the other hand, if $M > M_{\rm th}$, the only stable black holes are those of general relativity. Additionally, as opposed to general relativity, scalarized black holes possess a finite-area singularity. What is known from the static analysis is that as the mass decreases, the singularity moves closer to the horizon; when the minimum mass is reached, the singularity coincides with the horizon. Figure 7.1 shows the relation between the scalar charge and the mass of such scalarized black holes. To find these solutions, we follow a similar procedure as in [318].

In Section 7.3, we analyse the dynamics of such black holes. Before doing so, we introduce a modified numerical scheme to account for the formation of an apparent horizon.

7.2 Setup

In this section, we discuss the numerical implementation and the various techniques employed to evolve black holes with scalar perturbations. We then describe the initial data used. We further elaborate on useful diagnostic tools that keep track of the hyperbolic nature of the equations.

7.2.1 Numerical setup

We choose to work with Painleve-Gullstrand-like coordinates in spherical symmetry [437, 440, 441]. These coordinates are horizon-penetrating, *i.e.*, the metric functions remain regular through the formation of an apparent

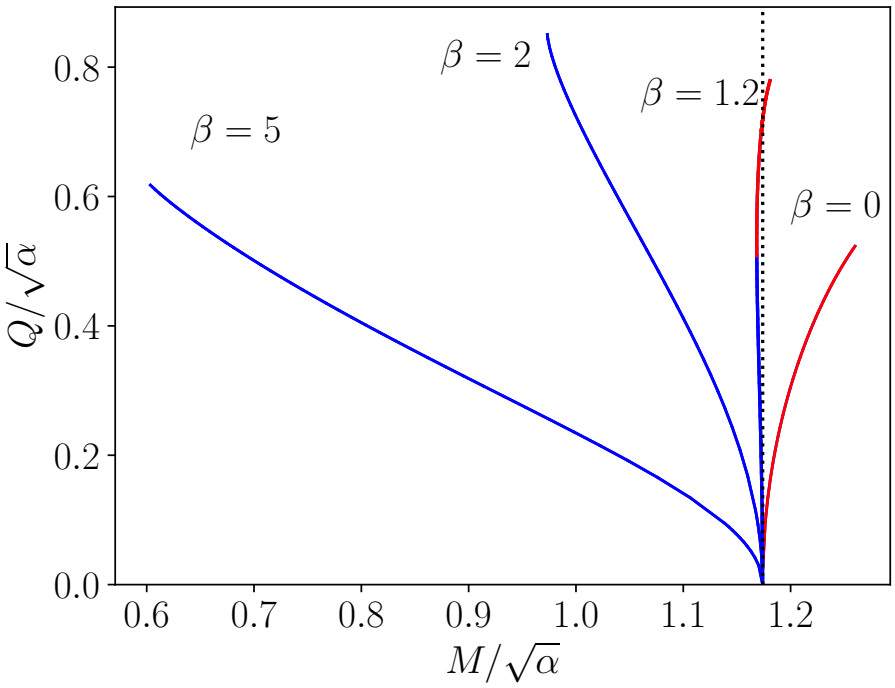

Figure 7.1: Charge-Mass plot for scalarized black holes. The blue curves correspond to stable solutions while the red ones are unstable, as shown in [332]. The threshold mass, marked by the black dotted line, is $M_{\rm th}/\sqrt{\alpha} \approx 1.174$, while the minimum mass varies for different values of β.

horizon. Consequently, the genesis and the horizon dynamics can be followed without encountering the singularity present in Schwarzschild coordinates. The line element is given by

$$\begin{aligned} \mathrm{d}s^2 = &-\alpha(t,r)^2\mathrm{d}t^2 + \left[\mathrm{d}r + \alpha(t,r)\zeta(t,r)\mathrm{d}t\right]^2 \\ &+ r^2\left(\mathrm{d}\theta^2 + \sin^2\theta\mathrm{d}\varphi^2\right) , \end{aligned} \tag{7.2.1}$$

and the scalar field is also spherically symmetric, *i.e.*, $\phi = \phi(t,r)$. To write the equations of motion as a first-order system of partial differential equations, we introduce the following variables

$$Q \equiv \partial_r\phi \,, \tag{7.2.2}$$

$$P \equiv \frac{1}{\alpha}\partial_t\phi - \zeta Q \,. \tag{7.2.3}$$

Then, the evolution equations for ϕ and Q can be obtained from the definitions of P and Q as

$$E_\phi \equiv \partial_t\phi - \alpha(P + \zeta Q) = 0 \,, \tag{7.2.4}$$

$$E_Q \equiv \partial_t Q - \partial_r\left(\alpha(P + \zeta Q)\right) = 0 \,, \tag{7.2.5}$$

and, from the equations of motion, we obtain evolution equations for P and ζ, and constraint equations for ζ and α, which can be written schematically as

$$E_P \equiv E_P(\partial_t P; \alpha, \zeta, \phi, P, \partial_r P, Q, \partial_r Q) = 0 \,, \tag{7.2.6}$$

$$E_\zeta \equiv E_\zeta(\partial_t\zeta; \zeta, \partial_r\zeta, \alpha, \partial_r\alpha, \phi, P, \partial_r P, Q, \partial_r Q) = 0 \,, \tag{7.2.7}$$

$$C_\alpha \equiv C_\alpha(\partial_r\alpha; \zeta, \phi, P, \partial_r P, Q, \partial_r Q) = 0 \,, \tag{7.2.8}$$

$$C_\zeta \equiv C_\zeta(\partial_r\zeta; \phi, P, \partial_r P, Q, \partial_r Q) = 0 \,. \tag{7.2.9}$$

We discretise the numerical domain for a given resolution N non-uniformly. This is done by employing the so-called fish-eye coordinate [442–444]. This allows for more resolution in high curvature regions where the derivatives of the scalar are very steep and changing rapidly. In this setup, we define our

areal radial coordinate r as a function of a uniform grid x as follows

$$r(x) = \eta_2 x + (1-\eta_1)\log\left(\frac{1+e^{x_1-x}}{1+e^{x_1}}\right) - (1-\eta_2)\log\left(\frac{1+e^{x_2-x}}{1+e^{x_2}}\right), \tag{7.2.10}$$

where $\eta_1 \leq 1$, $\eta_2 \geq 1$ and $0 < x_1 < x_2$ are real parameters. By definition, the spatial step of the uniform grid is $\Delta x = X/\mathrm{N}$, where X denotes the outer boundary. The time step is given by $\Delta t = \lambda \Delta x$ where λ is the Courant factor. The uniform spatial derivatives are discretised using a second-order finite differences operator satisfying summation by parts [435]. Since we solve the equations in the areal radius grid, we need to transform the radial derivatives with the Jacobian

$$\frac{\partial f}{\partial r} = \frac{\partial x}{\partial r}\frac{\partial f}{\partial x}\,. \tag{7.2.11}$$

During the evolution, we track the expansion of null congruences, which determine the location of the apparent horizon. In these coordinates, the expansion is proportional to $1-\zeta$; therefore, the horizon is at $\zeta = 1$, and we update its location accordingly. Nevertheless, we only perform this update if the horizon increases in size. After pinpointing the horizon, we place the excision surface $r_{\rm exc}$ inside of it. Furthermore, we chose $\eta_1 = 0.25$, $\eta_2 = 15$, $x_1 = 51$, and $x_2 = 100$. This choice ensures that the sampling of the areal radius r is denser close to the excision surface and sparser towards the last point $R = r(X)$. Given the initial data at $t = 0$, we solve the constraint equations for ζ and α on $[r_{\rm exc},\ R]$ using a second-order Runge Kutta (RK2) scheme.

We employ a one-sided stencil to compute radial derivatives at the excision surface. We solve a time evolution equation for ϕ, P, Q, and ζ, by using the method of lines, for which we discretise radial derivatives using second-order finite differences, and integrate in time using a fourth-order Runge Kutta and a fourth-order Kreiss-Olliger (KO) dissipation term. On the other hand, the metric function α is obtained by solving its constraint equation (7.2.8) by choosing $\alpha(t, r_{\rm exc}) = 1$ and then, using residual gauge freedom, we rescale α such that $\alpha(t, R) = 1$. We have followed a similar procedure to the one discussed in [437].

7.2.2 Initial data

We evolve a scalar field on a black hole background with mass $M_{\rm BH}$. The region inside the apparent horizon, located at $\zeta = 1$, is excised. At the excision radius, the shift ζ and the lapse α are set to their general relativity values, namely

$$\zeta(0, r_{\rm exc}) = \sqrt{\frac{2M_{\rm BH}}{r_{\rm exc}}}\,, \tag{7.2.12}$$

$$\alpha(0, r_{\rm exc}) = 1\,. \tag{7.2.13}$$

The scalar field ϕ and its time derivative are given by equations (6.3.5) and (6.3.6) for studying the quasi-normal modes in Section 7.3, we will use the following initial data field

$$\phi(0, r) = a_0 r \exp\left[-\left(\frac{r - r_0}{w_0}\right)^2\right]\,, \tag{7.2.14}$$

$$P(0, r) = 0\,, \tag{7.2.15}$$

with $a_0 = 0.01$, $r_0 = 10$, and $w_0 = 2$.

7.2.3 Well-posedness and diagnostics

We keep track of the character of the system through the characteristic speeds (6.3.3) where $\mathcal{C}$ and $\mathcal{D}$ depend on the functions α, ζ, ϕ, P, and Q, and their derivation is similar to that in Schwarzschild coordinates (see Appendix B.1) [445]. The surfaces where $\mathcal{D} = 0$, separating the elliptic and hyperbolic regions, are called sonic lines. We keep track of the discriminant $\mathcal{D}$ to ensure that the partial differential equations are hyperbolic during the evolution.

We excise the elliptic region if it is confined to the apparent horizon. If the elliptic region emerges or appears outside the horizon, then we stop the evolution. We also compute the Misner-Sharp mass as $M(t, r) \equiv \frac{r}{2}\left(1 - (\nabla r)^2\right) = \frac{r}{2}\zeta(t, r)^2$ [436]. To capture the spacetime mass denoted as M, we evaluate $M(t, r)$ at the outer boundary of the

numerical domain.

7.3 Results

7.3.1 Well-posedness analysis

First, we briefly examine the effect of the $\phi^2 R$ term on well-posedness. We have discussed this for spherical collapse in Section 6.3, and our results are in agreement with the earlier findings, namely that, for a given α/M^2, large enough values of the coupling constant β render the system hyperbolic. Here, we have focused on a choice of parameters for which black holes are scalarized. This case is more interesting because scalarization is a non-linear process, and one would expect to encounter large gradients, which are prone to causing loss of hyperbolicity. Therefore, examining the effect of the Ricci term in this regime is particularly interesting. These results are displayed in Table 7.1. The table presents the outcomes of different simulations (either loss of hyperbolicity or a scalarized black hole) for various coupling constants α/M^2 and β.

An interesting feature we observe is that, when the equations only change character in a region inside the black hole, then excising this region enlarges the parameter space for which the system is well-posed [437]. We illustrate this fact in Figure 7.2. In this case, the excision surface is allowed to move closer to the horizon, thereby removing the elliptic region from the numerical domain. Hence, the evolution will proceed without impediment due to ill-posedness inside the horizon. This type of excision leaves the physics of the exterior unaffected since the region inside the black hole is causally disconnected from the exterior.

7.3.2 Dynamics of minimum and threshold mass black holes

Next, we explore the dynamical behaviour of the black hole solutions near the minimum and threshold mass through non-linear simulations. To this end, we consider different setups.

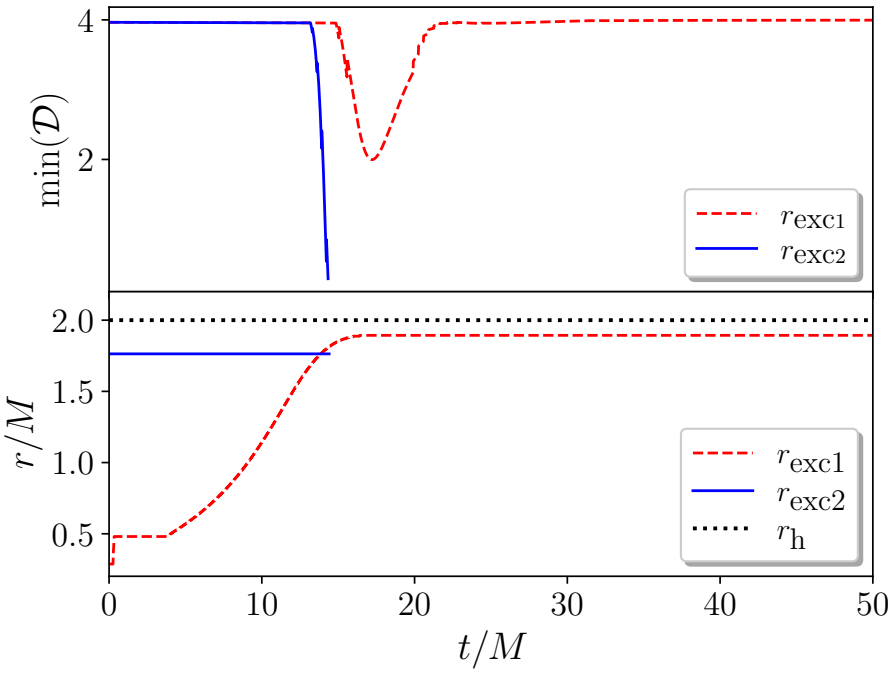

Figure 7.2: The top panel shows the minimum value of the discriminant $\mathcal{D}$ in the radial direction as a function of time for two different excision locations $r_{\rm exc1}$, $r_{\rm exc2}$ such that $r_{\rm exc1}$ is closer to the trapped surface from the interior. In this case, $\alpha/M^2 = 1$, $\beta = 2$ with a scalar pulse of amplitude $a_0 = 2 \times 10^{-3}$. The blue curve corresponds to a fixed location of the excision surface, and this eventually leads to the loss of hyperbolicity. On the other hand, when the excision surface location is allowed to move closer to the trapped surface from the interior, the elliptic region is excised (red dashed curve), and the discriminant remains positive throughout the evolution. The bottom panel illustrates the behaviour of excision surfaces as a function of time. The $r_{\rm exc1}$ changes to keep the elliptic region excised, contrary to the $r_{\rm exc2}$ surface. The horizon radius is indicated by $r_{\rm h}$.

Coupling constants α/M^2	β	Outcome
0.75	0.0	LoH
0.75	0.5	LoH
0.75	2.0	sBH
1.25	0.0	LoH
1.25	2.0	LoH
1.25	3.5	sBH
1.75	0.0	LoH
1.75	3.0	LoH
1.75	4.0	sBH
2.25	0.0	LoH
2.25	5.0	LoH
2.25	5.5	sBH

Table 7.1: The initial scalar pulse has $a_0 = 2\times 10^{-3}$. We denote the initial Misner-Sharp mass by M. The outcome indicates the end state of the evolution. The outcome is either loss of hyperbolicity (LoH) or a scalarized black hole (sBH). It is evident, in accordance with [446], that the addition of the Ricci coupling alleviates the loss of hyperbolicity problem for certain choices of β.

We first consider initial data such that the initial mass M of the system is larger than $M_{\rm th}$. The end state of the evolution is an apparent horizon with a negligible scalar field, consistent with the stationary analysis [318, 332]. This is illustrated in Figure 7.3 where the late time behaviour of the scalar field approaches zero. We then consider a case where the initial mass is below $M_{\rm th}$ and the initial black hole mass is larger than the minimum mass $M_{\rm min}$. As expected, the end state is a black hole with a non-trivial scalar profile. See the top panel of Figure 7.4. We also consider an initial configuration in which the total mass is below $M_{\rm th}$ while the initial black hole mass is smaller than the minimum mass $M_{\rm min}$. In this case, we choose the scalar pulse such that it contributes enough mass to the system to have $M_{\rm min} < M < M_{\rm th}$. Interestingly, the evolution progresses smoothly and the endpoint is again a scalarized black hole, as depicted in the bottom panel of Figure 7.4. As discussed, static scalarized black holes below the minimum do not exist; nevertheless, it is still interesting to understand the dynamics when the initial data mass does not meet this minimum. It was shown in [446] that collapsing a scalar field with an initial mass below the minimum mass was not possible. The scalar field

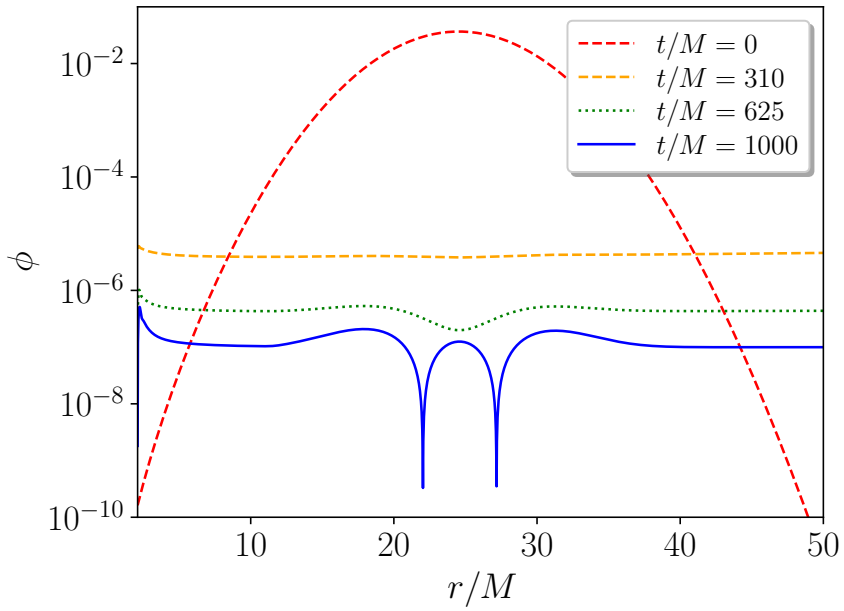

Figure 7.3: Scalar field profile at different times for $\alpha/M^2 = 0.25$, $\beta = 0.5$ with $a_0 = 2\times10^{-3}$. This choice of parameters corresponds to a setup where the initial $M > M_{\rm th}$, *i.e.*, this would be a hairless black hole.

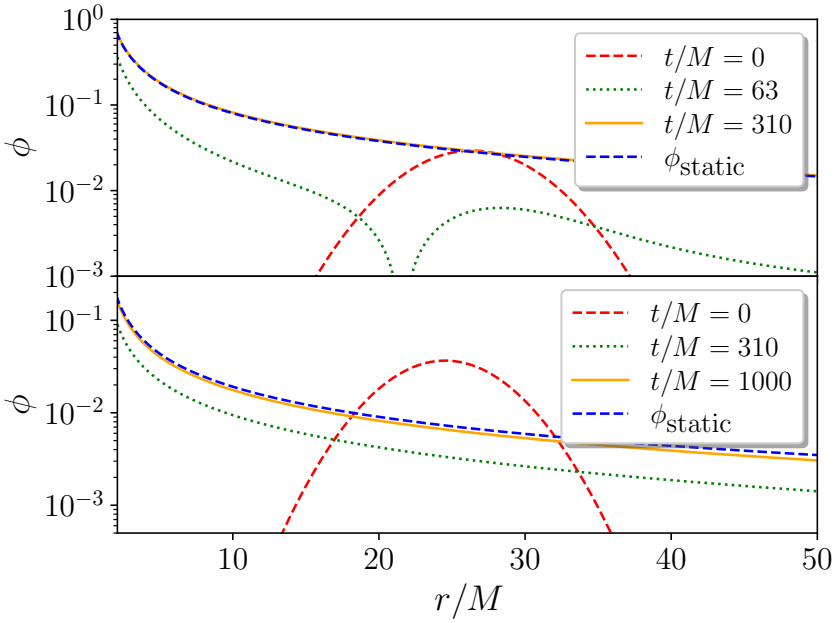

Figure 7.4: Scalar profile for different times. The static solution is indicated by $\phi_{\rm static}$. The top panel is for $\alpha/M^2 = 0.75$, $\beta = 2$, with an initial scalar profile described by $a_0 = 2 \times 10^{-3}$. In the bottom panel we have $\alpha/M^2 = 1$, $\beta = 2$, with $M_{\rm BH} = 0.95$, and initial scalar profile with $a_0 = 1.6 \times 10^{-3}$. The mass of the black hole (only without the scalar field contribution) in this setup is smaller than the minimum mass.

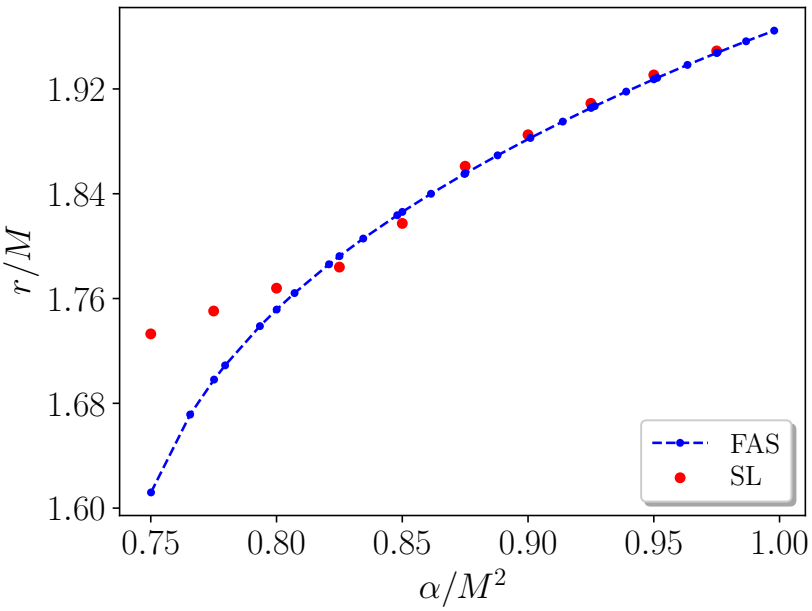

Figure 7.5: A comparison between the finite area singularity (FAS) radius (in dashed blue) extracted from the static solution and the size of the elliptic region (in red dots) formed inside the horizon, which is excised along the sonic line (SL). This is for $\beta = 2$.

dissipates, leaving behind it a flat geometry. Here, we explore the scenario in which the initial data does not meet the minimum mass condition. In the simulations we performed, we always faced a loss of hyperbolicity, *i.e.*, an elliptic region forms outside of the black hole. The observation that hyperbolicity is lost outside the apparent horizon when the minimum mass condition is not satisfied, coupled with the relation between the minimum mass and the finite area singularity, might indicate a connection between the finite area singularity and the lack of hyperbolicity inside the horizon. We examined this possibility by excising the elliptic region along the sonic line and comparing the elliptic region's size with that of the finite area singularity of the static solution, as in Figure 7.5. We have observed a good agreement between both quantities, especially for smaller black holes. The discrepancy in the location of the sonic line and the singularity for larger black holes might be due to the large gradients as the singularity is approached, affecting its localisation.

7.3.3 Quasi-normal modes

Probing the geometry of a black hole using test (scalar, vector, or tensor) fields by utilising linear perturbation theory proved very powerful [447]. Due to the nature of a black hole, where the horizon acts as a dissipation in the system, the behaviour of these fields as a perturbation is described by exponentially decaying oscillations—the so-called quasi-normal modes. The rate of decay and the oscillation frequency are related to the mass and spin of the black hole. In spherical symmetry, there are no tensor propagating degrees of freedom. We can only extract the $\ell = m = 0$ scalar quasi-normal modes of black hole ringing by fitting the extracted value of the scalar field at $r_{\rm ext} = 3r_0$ as

$$\phi(t) = \sum_{n=0}^{\infty} A_n \exp(-\omega_{I,n} t) \sin(\omega_{R,n} t + \varphi_n) \,, \tag{7.3.1}$$

where n denotes the overtone index. The quantities A_n, $\omega_n = \omega_{R,n} - i\omega_{I,n}$, and φ_n are the mode's amplitude, complex frequency, and phase, respectively. To obtain an accurate fit of the decaying oscillatory behaviour, it helps to have as many oscillations as possible before the appearance of the tail. In the cases we considered, we had to adjust the initial data, as given in equations (7.2.14) and (7.2.15), to achieve a few oscillations for an accurate fit. Such fits for different values of α/M^2 are shown in Figure 7.6. The tail behaviour appears very quickly for larger values of α/M^2, which hinders the accurate fitting of the quasi-normal modes. Due to this, we only considered lower values of α/M^2, for which the background solution is given by the Schwarzschild metric [318, 332]. Nonetheless, we observe a deviation from the general relativity quasi-normal modes since the Gauss-Bonnet invariant is non-trivial for the Schwarzschild metric. The results for

$$\delta\omega_R = \left| \frac{\mathrm{Re}(\omega_{\rm GR} - \omega)}{\mathrm{Re}\,\omega_{\rm GR}} \right| , \qquad \delta\omega_I = \left| \frac{\mathrm{Im}(\omega_{\rm GR} - \omega)}{\mathrm{Im}\,\omega_{\rm GR}} \right| , \tag{7.3.2}$$

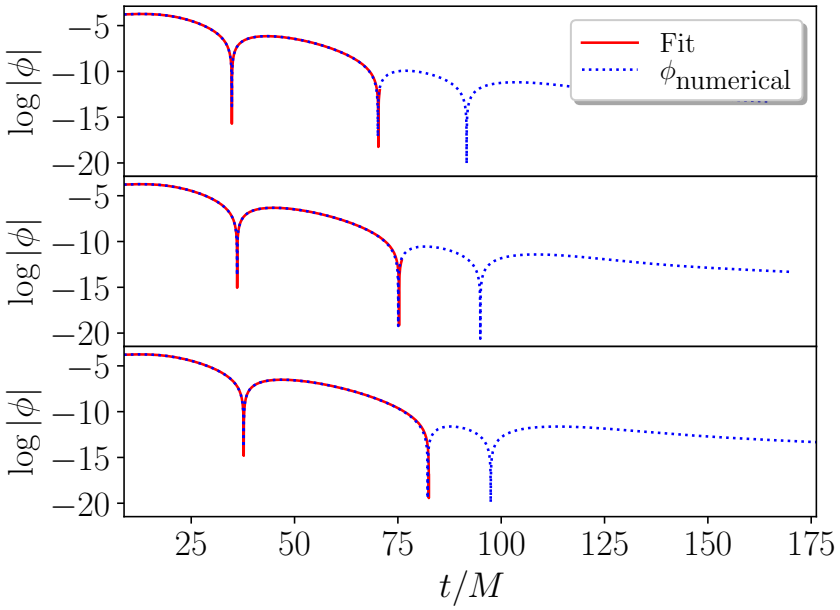

Figure 7.6: The scalar field extracted from the numerical simulation (blue dotted line) and the damped-sinusoid fit (red solid line). Each plot is done for the case $\beta = 2.25$ and, from top to bottom, $\alpha/M^2 = 0.025,\ 0.075,\ 0.125$.

	Re	Im
$\beta = 0,\ \alpha \neq 0$		
c_0	-1.0539×10^{-3}	1.99309×10^{-3}
c_1	2.01256×10^{-1}	8.59663×10^{-1}
c_2	6.9759×10^{-1}	2.52698
$\alpha/M^2 = 0.025,\ \beta \neq 0$		
d_1	1.56327×10^{-4}	4.61635×10^{-4}
d_2	2.47143×10^{-4}	1.40432×10^{-4}
$\alpha/M^2 = 0.075,\ \beta \neq 0$		
d_1	1.00527×10^{-4}	5.0495×10^{-4}
d_2	3.63718×10^{-4}	-3.85884×10^{-5}
$\alpha/M^2 = 0.125,\ \beta \neq 0$		
d_1	2.29461×10^{-4}	4.50753×10^{-4}
d_2	1.15081×10^{-4}	-5.90922×10^{-5}

Table 7.2: The real and imaginary part of the quadratic fit coefficients for quasi-normal modes for different values of the coupling α/M^2. The non-zero values for α/M^2, and β are reported in Table C.1. We extract the scalar quasi-normal modes for $n = 0$.

are summarised in Table C.1 and Figure 7.7. Fitting the deviation in the quasi-normal modes from general relativity for $\beta = 0$, we have

$$\delta\omega_{(\alpha,0)} = \sum_{k=0}^{2} c_k \left(\frac{\alpha}{M^2}\right)^k , \tag{7.3.3}$$

where the coefficients c_k are given in Table 7.2. If we turn on the β term and fit the deviation that it causes to the quasi-normal modes from the Gauss-Bonnet theory, *i.e.*, $\alpha \neq 0,\ \beta = 0$, we obtain

$$\delta\omega_{(\alpha,\beta)} = \delta\omega_{(\alpha,0)} + \sum_{k=1}^{2} d_k(\alpha)\beta^k , \tag{7.3.4}$$

where the coefficients $d_k(\alpha)$ are given in Table 7.2 for the values $\alpha/M^2 = [0.025,\ 0.075,\ 0.125]$.

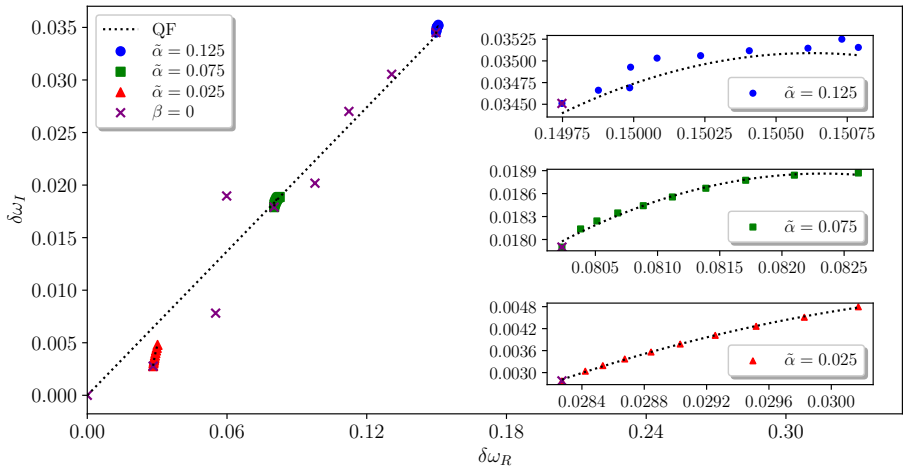

Figure 7.7: Relation between the normalised relative difference of the real and imaginary parts of the quasi-normal modes for different values of $\tilde{\alpha} = \alpha/M^2$ and a quadratic fit (QF) thereof. As the value of $\beta = \{0.5, 0.75, 1, 1.25, 1.5, 1.75, 2, 2.25, 2.5\}$ increases, the deviation in the real and imaginary parts from their general relativity values grows. The purple crosses correspond to different values of α/M^2 as given in Table C.1 with $\beta = 0$.

Coupling constants α/M^2	β	$1/\tau^{\text{fit}}$	$1/\tau^{\text{cf}}$
0.750	2.0	0.00353	0.004305
0.775	2.0	0.00713	0.008509
0.800	2.0	0.0111	0.01254
0.825	2.0	0.0151	0.01643
0.850	2.0	0.0184	0.02019
0.875	2.0	0.0210	0.02383
0.900	2.0	0.0236	0.02737
0.925	2.0	0.0259	0.03082
0.950	2.0	0.0279	0.03418
0.975	2.0	0.0317	0.03746
1.0	2.0	0.0337	0.04067

Table 7.3: The inverse of the tachyonic instability time scale. The first column reports the values extracted with a fit from the numerical solution, while the second column reports the timescales evaluated with a continued fraction method.

7.3.4 Tachyonic instability

Lastly, we examine the timescale of the tachyonic instability responsible for the existence of scalarized black holes; see Section 3.3.2. In simple terms, linear analysis has shown that the tachyonic instability causes the scalar field to grow exponentially [314, 315], see [318] for an analysis specific to the model we consider here and [310] for a review. Nevertheless, the end state of the instability is controlled by the non-linear interactions present in the theory [316–318]. In the simulations, we observe both the linear instability and its non-linear quenching. We are also able to estimate the timescale of the instability. To assess the accuracy of the results, we compare the numerical extraction against an analysis in the static limit, assuming linear perturbations with a continued fraction method. The details are explained in Appendix C.2.

The behaviour of the exponential growth of the scalar field at the horizon (in log scale) is shown in Figure 7.8 with a linear fit from which we extract the time scale (see Table 7.3 for more cases and the results from the linear perturbation analysis). At larger times, the exponential growth stops.

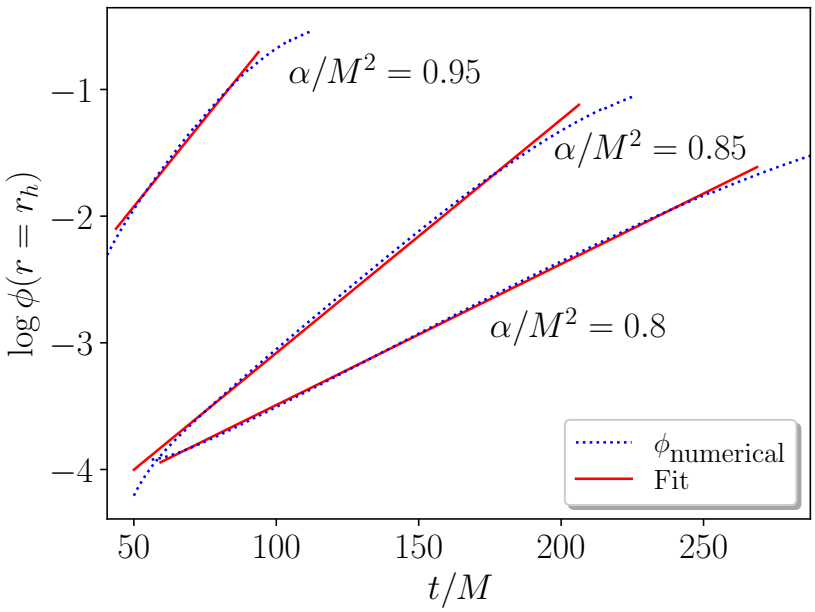

Figure 7.8: The growth of the scalar field at the horizon of a black hole due to the tachyonic instability, which is then quenched. The dashed red line is a linear fit to the exponential growth of the scalar field (in log scale). The slope of the fit is the inverse of the time scale of the instability. This is for $\beta = 2$, and $a_0 = 2 \times 10^{-3}$.

7.4 Discussion

We have explored the dynamics of spherically symmetric black holes in scalar Gauss-Bonnet gravity with an additional Ricci coupling. This additional coupling was shown to help mitigate the ill-posed behaviour of the equations in spherical symmetry [446] (Section 6.3), and there is a positive indication of a similar effect in 3 + 1 simulations [448]. We observe similar behaviour for black hole initial data. We also show that the part of the parameter space where spherical evolution remains well-posed can be enlarged by excising a region inside the horizon in which hyperbolicity is lost. This is accomplished by locating the sonic line (a codimension-one surface separating the elliptic and hyperbolic regions) and performing excision outside of it, thereby removing the elliptic region (and the singularity) from the numerical domain. Since this can be done without affecting the physics of the exterior, it can be seen as an advantage of excision methods in such setups [437].

We have considered initial data that are expected to lead to black holes of different masses. The cases in which the initial mass exceeds the scalarization threshold mass result in a negligible scalar field at late times. This is consistent with the static analysis, as black holes in this mass range are not compact enough to trigger the tachyonic instability necessary to produce a non-trivial scalar configuration. For initial data within the mass range for which scalarization occurs, we have successfully matched the late-time scalar field profile obtained from the simulation with the one obtained by solving the static equations of motion. Therefore, we have captured the role of non-linearities in controlling the instability and dynamically producing scalarized black holes as the endpoint of the instability. Moreover, we have considered initial data for which the initial black hole mass was below the minimum mass threshold. In contrast, the initial scalar pulse contributed enough mass so that the final black hole was expected to be above the minimum mass threshold. We did not encounter any issues in evolving the system and capturing the formation of a scalarized black hole. Finally, when exploring setups for which the total Misner-Sharp mass lies below the minimum mass, we encountered loss of hyperbolicity. This is expected as scalarized black holes do not exist for this mass range.

The presence of a finite-area singularity in the interior of scalarized black holes is poorly understood. Evolving initial data, for a black hole with some initial scalar field, whose total initial mass lies below the minimum mass, has led to the loss of hyperbolicity. The finite-area singularity radius in static black holes gets closer to the horizon as the minimum mass is approached. These two facts motivated us to explore the relationship between the appearance of such a singularity and the loss of hyperbolicity in black hole spacetimes. We generally found a good agreement between the radius of the finite-area singularity and the location of the sonic line. Their locations match better for smaller black holes. Nonetheless, the deviations for larger black holes might be due to insufficient accuracy in locating either the location of the singularity or the sonic line.

Additionally, we have extracted the monopolar scalar quasi-normal modes for a range of couplings. We have restricted our attention to couplings that do not lead to scalarized black holes; otherwise, the tail appeared rather quickly, hindering an accurate extraction of the quasi-normal modes. Nevertheless, in this background, the Gauss-Bonnet invariant is not trivial, and we find a quadratic behaviour for the deviations from general relativity, in the real and imaginary parts of the modes. Finally, we extracted the timescale of the linear tachyonic instability associated with scalarization from our numerical simulations by fitting the linear growth of the scalar field before it is eventually quenched. To check the numerical results for the quasi-normal modes and the time scale of the instability, we produced a continued fraction analysis of linear perturbations in the static limit.

It would be interesting to generalise our study to the case of spinning black holes using 3 + 1 simulations. One would expect that the dynamics of the finite-area singularity would be more intricate in spinning black holes. Hence, a credible relation with the loss of hyperbolicity might be less straightforward and more challenging to establish. Additionally, one could assess numerically the non-linear stability of scalarized black holes by studying more general initial data. In the next chapter, we will discuss whether the loss of hyperbolicity and the positive effect of the Ricci coupling are due to the gauge choice or the propagating physical degrees of freedom by utilising the results of [449].

Chapter VIII

Gauge invariant study for spherical evolution

Contents

This chapter is devoted to investigating the relation between hyperbolicity and the gauge choice in numerical evolution. We do so by using the results of Reall in [449], who introduced a gauge-invariant diagnostic tool for hyperbolicity in scalar-tensor theories. We employ this gauge-invariant approach to investigate hyperbolicity and the loss of well-posedness for spherical evolution in scalar Gauss-Bonnet gravity with an additional Ricci coupling. For convenience, the theory is (for more details, see Section 3.3.3)

$$S = \frac{1}{16\pi}\int \mathrm{d}^4x\sqrt{-g}\left[R + X + f(\phi)\mathcal{G} + h(\phi)R\right] , \tag{8.0.1}$$

and the equations of motion read

$$\begin{aligned} E^{\mu}{}_{\nu} \equiv &- T^{(\phi)\mu}{}_{\nu} + \delta^{\mu\gamma\kappa\lambda}_{\nu\alpha\rho\sigma} R^{\rho\sigma}{}_{\kappa\lambda}\nabla_\gamma\nabla^\alpha f \\ &+ (1+h)G^{\mu}{}_{\nu} + \delta^{\mu}{}_{\nu}\Box h - \nabla^\mu\nabla_\nu h = 0 , \qquad (8.0.2) \\ E \equiv &- \Box\phi - h'(\phi)R - f'(\phi)\mathcal{G} = 0 , \qquad (8.0.3) \end{aligned}$$

with

$$T^{(\phi)}_{\mu\nu} = \frac{1}{2}\nabla^\mu\phi\nabla_\nu\phi - \frac{1}{4}(\nabla\phi)^2 g_{\mu\nu} . \tag{8.0.4}$$

We choose,

$$f(\phi) = \frac{\alpha}{2}\phi^2 , \qquad h(\phi) = -\frac{\beta}{4}\phi^2 . \tag{8.0.5}$$

As we will show, in our setup, the gauge-invariant hyperbolicity reduces to tracking the signature of an "effective metric." We do that in two different gauges and for various coupling constants and initial data. We find that the determinant of the effective metric changes sign when hyperbolicity is lost, consistently with other diagnostic tools (see, *e.g.*, [412, 437, 446]). Our results elucidate the relation between the results of [449] and [424]. They demonstrate that the loss of hyperbolicity during spherical evolution in scalar Gauss-Bonnet gravity is not merely due to an unfortunate gauge choice, but due to the behaviour of physical degrees of freedom that the presence of additional interactions can indeed tame—in our case, the Ricci coupling. Finally, we examine the effect of field redefinitions on hyperbolicity and point

out that this constitutes a limitation of using gauge-invariant criteria for well-posedness.

We discuss some results concerning the principal symbol and the characteristics of second-order scalar-tensor theories. We then focus on scalar Gauss-Bonnet gravity and derive the principal symbol in some detail. We then study the characteristic equations and derive the "effective metric" to be used as a diagnostic tool in numerical simulations. We present our numerical results in Section 8.5. We also consider disformal transformations; first, we present some preliminaries and then inspect the effects of such a transformation on hyperbolicity.

8.1 Principal symbol and characteristics

In this section, we briefly review some of the results in [449] about the principal symbol of a scalar-tensor theory, its symmetries and the characteristics of the partial differential equations. In Section 6.1, we provided a pedagogical introduction to the notions of well-posedness and hyperbolicity, which we hope will be useful to readers less familiar with these concepts.

Consider a general scalar-tensor theory of the form

$$S = \frac{1}{16\pi G}\int \mathrm{d}^4x\sqrt{-g}L(g,\phi)\,, \tag{8.1.1}$$

for the metric $g_{\mu\nu}$, and a scalar ϕ with the equations of motion given by

$$E^{\mu\nu} \equiv -\frac{16\pi G}{\sqrt{|g|}}\frac{\delta S}{\delta g_{\mu\nu}} = 0\,, \tag{8.1.2}$$

$$E \equiv -\frac{16\pi G}{\sqrt{|g|}}\frac{\delta S}{\delta \phi} = 0\,. \tag{8.1.3}$$

We assume the equations of motion to be second order in the metric and scalar field derivatives. Then, for an arbitrary covector ξ_μ the principal sym-

bol, viewed as acting on "polarization" vectors, is defined to be

$$\mathcal{P}(\xi) = \begin{pmatrix} P_{gg}^{\mu\nu\rho\sigma\alpha\beta}\xi_\alpha\xi_\beta & P_{gm}^{\mu\nu\alpha\beta}\xi_\alpha\xi_\beta \\ P_{mg}^{\mu\nu\alpha\beta}\xi_\alpha\xi_\beta & P_{mm}^{\alpha\beta}\xi_\alpha\xi_\beta \end{pmatrix}, \tag{8.1.4}$$

where

$$\begin{aligned} P_{gg}^{\mu\nu\rho\sigma\alpha\beta} &\equiv \frac{\partial E^{\mu\nu}}{\partial(\partial_\alpha\partial_\beta g_{\rho\sigma})}, & P_{gm}^{\mu\nu\alpha\beta} &\equiv \frac{\partial E^{\mu\nu}}{\partial(\partial_\alpha\partial_\beta\phi)}, \\ P_{mg}^{\mu\nu\alpha\beta} &\equiv \frac{\partial E}{\partial(\partial_\alpha\partial_\beta g_{\mu\nu})}, & P_{mm}^{\alpha\beta} &\equiv \frac{\partial E}{\partial(\partial_\alpha\partial_\beta\phi)}. \end{aligned} \tag{8.1.5}$$

A more convenient notation to use is

$$P_{gg}^{\mu\nu\rho\sigma}(\xi) \equiv P_{gg}^{\mu\nu\rho\sigma\alpha\beta}\xi_\alpha\xi_\beta, \tag{8.1.6}$$

$$P_{gm}^{\mu\nu}(\xi) \equiv P_{gm}^{\mu\nu\alpha\beta}\xi_\alpha\xi_\beta, \tag{8.1.7}$$

$$P_{mg}^{\mu\nu}(\xi) \equiv P_{mg}^{\mu\nu\alpha\beta}\xi_\alpha\xi_\beta, \tag{8.1.8}$$

$$P_{mm}(\xi) \equiv P_{mm}^{\alpha\beta}\xi_\alpha\xi_\beta. \tag{8.1.9}$$

8.1.1 Symmetries of the principal symbol

It follows from the definitions (8.1.5), that the components of the principal symbol have the following symmetries

$$P_{gg}^{\mu\nu\rho\sigma\alpha\beta} = P_{gg}^{(\mu\nu)\rho\sigma\alpha\beta} = P_{gg}^{\mu\nu(\rho\sigma)\alpha\beta} = P_{gg}^{\mu\nu\rho\sigma(\alpha\beta)}, \tag{8.1.10}$$

$$P_{gm}^{\mu\nu\alpha\beta} = P_{gm}^{(\mu\nu)\alpha\beta} = P_{gm}^{\mu\nu(\alpha\beta)}, \tag{8.1.11}$$

$$P_{mg}^{\mu\nu\alpha\beta} = P_{mg}^{(\mu\nu)\alpha\beta} = P_{mg}^{\mu\nu(\alpha\beta)}, \tag{8.1.12}$$

$$P_{mm}^{\alpha\beta} = P_{mm}^{(\alpha\beta)}. \tag{8.1.13}$$

Furthermore, in [449], the symmetries of the principal symbol that arise due to the action principle and diffeomorphism invariance were deduced. The first collection of symmetries is a consequence of the action principle, which produces the following relations

$$P_{gg}^{\mu\nu\rho\sigma\alpha\beta} = P_{gg}^{\rho\sigma\mu\nu\alpha\beta}, \qquad P_{gm}^{\mu\nu\alpha\beta} = P_{mg}^{\mu\nu\alpha\beta}, \tag{8.1.14}$$

implying that the principal symbol is symmetric. Moreover, the variation of the action under a compactly supported diffeomorphism generated by an arbitrary vector field yields

$$P_{gg}^{\mu(\nu|\rho\sigma|\alpha\beta)} = 0\,, \qquad P_{gm}^{\mu(\nu\alpha\beta)} = 0\,. \tag{8.1.15}$$

Finally, combining these symmetries enables the writing of the principal symbol components as [449]

$$P_{mg}^{\mu\nu\alpha\beta}\xi_\alpha\xi_\beta = C^{\mu\alpha\nu\beta}\xi_\alpha\xi_\beta\,, \tag{8.1.16}$$

$$P_{gg}^{\mu\nu\rho\sigma\alpha\beta}\xi_\alpha\xi_\beta = C^{\mu(\rho|\alpha\nu|\sigma)\beta}\xi_\alpha\xi_\beta\,, \tag{8.1.17}$$

where $C^{\mu\nu\rho\sigma}$ has the same symmetries as the Riemann tensor

$$C^{\mu\nu\rho\sigma} = C^{[\mu\nu]\rho\sigma} = C^{\mu\nu[\rho\sigma]} = C^{\mu[\nu\rho\sigma]}\,, \tag{8.1.18}$$

additionally, $C^{\alpha_1\alpha_2\alpha_3\beta_1\beta_2\beta_3}$ enjoys

$$\begin{aligned} C^{\alpha_1\alpha_2\alpha_3\beta_1\beta_2\beta_3} &= C^{[\alpha_1\alpha_2\alpha_3]\beta_1\beta_2\beta_3} = C^{\alpha_1\alpha_2\alpha_3[\beta_1\beta_2\beta_3]} \\ &= C^{\beta_1\beta_2\beta_3\alpha_1\alpha_2\alpha_3}\,, \end{aligned} \tag{8.1.19}$$

and

$$C^{\alpha_1\alpha_2[\alpha_3\beta_1\beta_2\beta_3]} = C^{\alpha_1[\alpha_2\alpha_3\beta_1\beta_2\beta_3]}\,, \tag{8.1.20}$$

as its symmetries.

These tensors are functions of $(g_{\mu\nu}, \phi)$ and their first and second derivatives. Furthermore, the symmetries of $C^{\mu_1\mu_2\mu_3\nu_1\nu_2\nu_3}$ imply that we can define a symmetric tensor $C_{\mu\nu}$ by

$$C^{\mu_1\mu_2\mu_3\nu_1\nu_2\nu_3} = -\frac{1}{2}\epsilon^{\mu_1\mu_2\mu_3\rho}\epsilon^{\nu_1\nu_2\nu_3\sigma}C_{\rho\sigma}\,. \tag{8.1.21}$$

8.1.2 Characteristics

A covector ξ_μ is called characteristic if and only if there exists a vector $\Omega = (\omega_{\mu\nu}, \omega)$ such that

$$\mathcal{P}(\xi)\Omega = 0\,, \tag{8.1.22}$$

expanding this equation, we have

$$P^{\mu\nu\rho\sigma}_{gg}(\xi)\omega_{\rho\sigma} + P^{\mu\nu}_{mg}(\xi)\omega = 0\,, \tag{8.1.23}$$
$$P^{\mu\nu}_{mg}(\xi)\omega_{\mu\nu} + P_{mm}(\xi)\omega = 0\,. \tag{8.1.24}$$

Here, $\omega_{\mu\nu}$ is symmetric, *i.e.*, $\omega_{\mu\nu} = \omega_{\nu\mu}$. The definition of ξ_μ to be characteristic, as such, is insufficient in theories with gauge redundancy [450]. In this case, due to diffeomorphism invariance a vector $\Omega = (\xi_{(\mu}X_{\nu)}, 0)$ solves the previous equation for all ξ_μ and X_μ. These unphysical modes can be "removed" by considering only equivalence classes of solutions. Therefore, define the equivalence relation $\omega_{\mu\nu} \sim w_{\mu\nu}$ if $w_{\mu\nu} = \omega_{\mu\nu} + \xi_{(\mu}X_{\nu)}$ for some X_μ. Hence, we can only consider the "physical" space comprised of vectors of the form $\Omega = \Big([\omega_{\mu\nu}], \omega\Big)$, where $[\cdot]$ stands for equivalence class. Hence, we take $\mathcal{P}(\xi)$ to only act on such vectors [449, 450]. With this in mind, equation (8.1.22) yields a degree six polynomial that must vanish for a characteristic ξ_μ. That is,

$$p(\xi) = (C^{-1})^{\mu\nu}\xi_\mu\xi_\nu Q(\xi) = 0\,, \tag{8.1.25}$$

if ξ_μ is characteristic. The quartic polynomial $Q(\xi)$ is given by

$$\begin{aligned} Q(\xi) \equiv \frac{C}{g}(C^{-1})^{\mu\nu}\xi_\mu\xi_\nu P_{mm}(\xi) \\ + \Big(2C_{\mu\rho}C_{\nu\sigma} - C_{\mu\nu}C_{\rho\sigma}\Big)\, P^{\mu\nu}_{mg}(\xi)P^{\rho\sigma}_{mg}(\xi)\,, \end{aligned} \tag{8.1.26}$$

where

$$\begin{aligned}\frac{C}{g} &= \frac{-\sqrt{-g}}{g}\epsilon^{\mu\nu\rho\sigma}C_{0\mu}C_{1\nu}C_{2\rho}C_{3\sigma} \\ &= -\frac{1}{4!}\epsilon^{\mu_1\mu_2\mu_3\mu_4}\epsilon^{\nu_1\nu_2\nu_3\nu_4}C_{\mu_1\nu_1}C_{\mu_2\nu_2}C_{\mu_3\nu_3}C_{\mu_4\nu_4}\,. \end{aligned} \tag{8.1.27}$$

We close this section by reiterating the relation between hyperbolicity and the characteristics of the equations. As discussed in Section 6.1, we can study strong hyperbolicity by finding the characteristic covector and its polarisations. *Therefore, a necessary condition for well-posedness is for the polynomial $p(\xi)$ to have real roots.*

8.2 Case study: scalar Gauss-Bonnet gravity with a Ricci coupling

To compute the components of the principal symbol, we use the definitions (8.1.5). To do so, we note that since only second-order derivatives will contribute to the symbol, we can replace covariant derivatives with partial ones. Therefore, the principal part (P.P.) of covariant derivatives acting on the scalar is trivial. For example,

$$\text{P.P.}\{\nabla^\alpha\nabla_\beta h(\phi)\} = h'\partial^\alpha\partial_\beta\phi\,. \tag{8.2.1}$$

We also need to know the principal part of the Riemann and the Einstein tensor. For the Riemann tensor, we have

$$\begin{aligned}\text{P.P.}\{R_{\alpha_1\alpha_2\beta_1\beta_2}\} = \frac{1}{2}\Big(&\partial_{\alpha_2}\partial_{\beta_1}g_{\alpha_1\beta_2} + \partial_{\alpha_1}\partial_{\beta_2}g_{\alpha_2\beta_1} \\ &-\partial_{\alpha_2}\partial_{\beta_2}g_{\alpha_1\beta_1} - \partial_{\alpha_1}\partial_{\beta_1}g_{\alpha_2\beta_2}\Big)\,,\end{aligned} \tag{8.2.2}$$

while, for the Einstein tensor, recall that it can be written as

$$G^\alpha{}_\beta = -\frac{1}{4}\delta^{\alpha\alpha_1\alpha_2}_{\beta\beta_1\beta_2}R_{\alpha_1\alpha_2}{}^{\beta_1\beta_2}\,. \tag{8.2.3}$$

Now, to compute the symbol (as acting on polarisation vectors), we merely need to perform the replacement

$$\partial_\alpha \partial_\beta g_{\mu\nu} \to \xi_\alpha \xi_\beta \omega_{\mu\nu} \,, \tag{8.2.4}$$

$$\partial_\alpha \partial_\beta \phi \to \xi_\alpha \xi_\beta \omega \,, \tag{8.2.5}$$

and, therefore, we find the principal symbol of the Riemann tensor to be

$$\begin{aligned} \big(P(\xi)\cdot\omega\big)_{\alpha_1\alpha_2}{}^{\beta_1\beta_2} = \frac{1}{2}\Big(&\xi_{\alpha_2}\xi^{\beta_1}\omega_{\alpha_1}^{\beta_2} + \xi_{\alpha_1}\xi^{\beta_2}\omega_{\alpha_2}^{\beta_1} \\ &-\xi_{\alpha_2}\xi^{\beta_2}\omega_{\alpha_1}^{\beta_1} - \xi_{\alpha_1}\xi^{\beta_1}\omega_{\alpha_2}^{\beta_2}\Big) \,, \end{aligned} \tag{8.2.6}$$

while for the Einstein tensor, we have

$$\big(P(\xi)\cdot\omega\big)^\alpha{}_\beta = \frac{1}{2}\delta^{\alpha\alpha_1\alpha_2}_{\beta\beta_1\beta_2}\xi_{\alpha_1}\xi^{\beta_1}\omega_{\alpha_2}^{\beta_2} \,, \tag{8.2.7}$$

and finally for $\nabla^\alpha\nabla_\beta h(\phi)$ we get

$$\big(P(\xi)\cdot\omega\big)^\alpha{}_\beta = h'\xi^\alpha\xi_\beta\omega \,, \tag{8.2.8}$$

thus the result follows immediately, and we have

$$\begin{aligned} \Big(P_{gg}(\xi)\cdot\omega\Big)^\alpha{}_\beta = &\frac{1}{2}(1+h)\delta^{\alpha\gamma_1\gamma_2}_{\beta\delta_1\delta_2}\xi_{\gamma_1}\xi^{\delta_1}\omega_{\gamma_2}^{\delta_2} \\ &- 2\delta^{\alpha\gamma\gamma_1\gamma_2}_{\beta\delta\delta_1\delta_2}\xi_{\gamma_1}\xi^{\delta_1}\omega_{\gamma_2}^{\delta_2}\nabla_\gamma\nabla^\delta f \,, \end{aligned} \tag{8.2.9}$$

$$\begin{aligned} P_{mg}(\xi)^\alpha{}_\beta = P_{gm}(\xi)^\alpha{}_\beta = &\delta^\alpha_\beta h'\xi^2 - h'\xi^\alpha\xi_\beta \\ &+ f'\delta^{\alpha\gamma\gamma_1\gamma_2}_{\beta\delta\delta_1\delta_2}R_{\gamma_1\gamma_2}{}^{\delta_1\delta_2}\xi_\gamma\xi^\delta \,, \end{aligned} \tag{8.2.10}$$

$$P_{mm}(\xi) = -\xi^2 \,. \tag{8.2.11}$$

8.3 Effective metric in spherical symmetry

We will focus on the characteristics of the theory (8.0.1) in spherical symmetry. Hence, there are no spin-2 propagating degrees of freedom, and it is

possible to reduce the characteristic equation (8.1.22) to one equation governing the scalar degree of freedom of the form

$$g_{\text{eff}}^{ab}\xi_a\xi_b\omega = 0\,, \qquad \{a,\ b\} \in \{t, r\}\,. \tag{8.3.1}$$

To that end, we consider the most general spherically symmetric ansatz for the background in polar coordinates

$$\begin{aligned} \mathrm{d}s^2 &= g_{tt}(t,r)\mathrm{d}t^2 + g_{tr}(t,r)\mathrm{d}t\mathrm{d}r \\ &\quad + g_{rr}(t,r)\mathrm{d}r^2 + g_{\theta\theta}(t,r)^2\,\mathrm{d}\Omega^2\,, \end{aligned} \tag{8.3.2}$$

and assume spherical symmetry for the scalar field as well $\phi = \phi(t, r)$.

Since we are working in spherical symmetry we can further assume that the only non-zero components of $\omega_{\mu\nu}$ are $\{\omega_{tt},\ \omega_{tr},\ \omega_{rr},\ \omega_{\theta\theta}\}$, and that $\omega_{\phi\phi} = \sin(\theta)^2\omega_{\theta\theta}$ with $\xi_\mu = (\xi_t,\ \xi_r,\ 0,\ 0)$. Therefore, we can diagonalise the system (8.1.23) – (8.1.24) by solving for the scalar degree of freedom ω. We can achieve that by solving equation (8.1.23) for $\{\omega_{rr},\ \omega_{\theta\theta}\}$, in terms of $\{\omega_{tt},\ \omega_{tr},\ \omega\}$ and substitute back into equation (8.1.24) to end up with an equation governing ω only from which we can read off an effective metric for the scalar degree of freedom. When $h = 0$, our result matches that of [424]. However, the approach presented here straightforwardly generalises to any scalar-tensor theory with second-order equations of motion. It is worth noting that a single equation for the scalar perturbation around time-independent backgrounds was obtained and used to discuss hyperbolicity in [332].

As discussed, a necessary condition for the evolution to be well-posed is for the effective metric to be Lorentzian. Thus, it constitutes a gauge-independent diagnostic tool for hyperbolicity. Therefore, in numerical considerations, we keep track of the determinant of the effective metric.

8.4 Numerical considerations

We perform numerical simulations in two different gauge choices. We use the usual Schwarzschild-like coordinates (see Section 6.3.3) as well as Painleve-Gullstrand coordinates (see Section 7.2.1). Here, we use the effective metric

as a diagnostic tool to track the hyperbolic nature of the partial differential equations throughout the evolution.

We can either evolve the scalar field on flat spacetime or on top of a black hole background with mass $M_{\rm BH}$. For flat initial data, we impose

$$\zeta(0, r = 0) = 0\,, \qquad \alpha(0, r = 0) = 1\,, \tag{8.4.1}$$

and we impose regularity at the centre by requiring $\partial_r \alpha|_{r=0} = 0$. For black hole initial data, we excise a region inside the apparent horizon (see Section 7.2.1). In this case, we fix $M_{\rm BH} = 1$ unless otherwise stated. Finally, we do not explicitly provide the coefficients of the effective metric in these coordinates as they are rather cumbersome.

8.4.1 Evolution equations in the *fixing-the-equation* approach

We also implement the *fixing-the-equation* approach [425–434, 451, 452]. The idea is that, in an effective field theory, there can be spurious degrees of freedom or spurious behaviour of actual degrees of freedom as a result of truncation at a given order in derivatives, and this can be the cause of the loss of hyperbolicity during evolution. Hence, one might be able to maintain well-posedness by "taming" the behaviour of the specific degrees of freedom. In practice, this is achieved by modifying the original system (equations (8.0.2) and (8.0.3)) and supplementing it with a "driver" equation that "steers" the evolution away from ill-posedness and towards the true solution. Note that there is no unique choice for the driver equation. For the system (8.0.2) – (8.0.3) with $h = 0$ we consider the following "fixed" system [428]

$$R_{\mu\nu} - \frac{1}{2} g_{\mu\nu} R = T^{(\phi)}_{\mu\nu} + \Gamma_{\mu\nu}\,, \tag{8.4.2}$$

$$\Box\phi = \Sigma\,, \tag{8.4.3}$$

$$\xi \Box \boldsymbol{u} - (\boldsymbol{u} - \boldsymbol{S}) = 0\,, \tag{8.4.4}$$

where $\Gamma_{\mu\nu}$, and Σ are auxiliary fields arranged in the vector $\boldsymbol{u} = (\Gamma_{\mu\nu}, \Sigma)$, and ξ is a constant timescale that controls how the auxiliary fields approach the original theory, *i.e.*, (8.0.2) and (8.0.3). For more details, we refer the reader to [428]. Note that, to evaluate how the original system would behave, we compute any quantity of interest using the variables evolved in the fixed system.

8.5 Numerical results

We consider initial data that describes an approximately ingoing pulse (equations (6.3.5) and (6.3.6)). We will fix $r_0 = 25$ and $w_0 = 6$ unless otherwise stated.

We start with a small pulse on flat spacetime, with particular values of couplings, $\alpha/M = 0.25$ and $\beta = 0$, which are known to lead to loss of hyperbolicity during this evolution of the data above. We evolve the data using two different coordinate systems and verify that the effective metric does indeed change sign when hyperbolicity is lost. Moreover, as expected, the change of sign happens at the same location for both coordinate systems. As depicted in Figure 8.1, the determinant changes sign at the same radius (within grid spacing) when the system becomes elliptic and when it switches back again (from positive to negative). This demonstrates that the gauge-independent property of the determinant is manifest in numerical simulations. We have performed the same runs with double and quadruple resolutions to check that the sign change occurs at the same radius up to the grid spacing of the two different codes, and we have found consistency in the results. It is worth noting that a small discrepancy in the localisation of the radius might also arise due to the different definitions of the time coordinate in Schwarzschild and Painleve-Gullstrand coordinates. Next, we explore the parameter space of the theory. We track the effective metric to probe the loss of hyperbolicity and inspect its relation to the gauge choice. First, in Schwarzschild coordinates, we re-examine the parameter space already explored in [446]. We find that the effective metric criterion reproduces the results found there, and hence the observed behaviour is not due to the gauge choice. This might indicate that the ill-posedness observed in the literature in various studies of scalar Gauss-

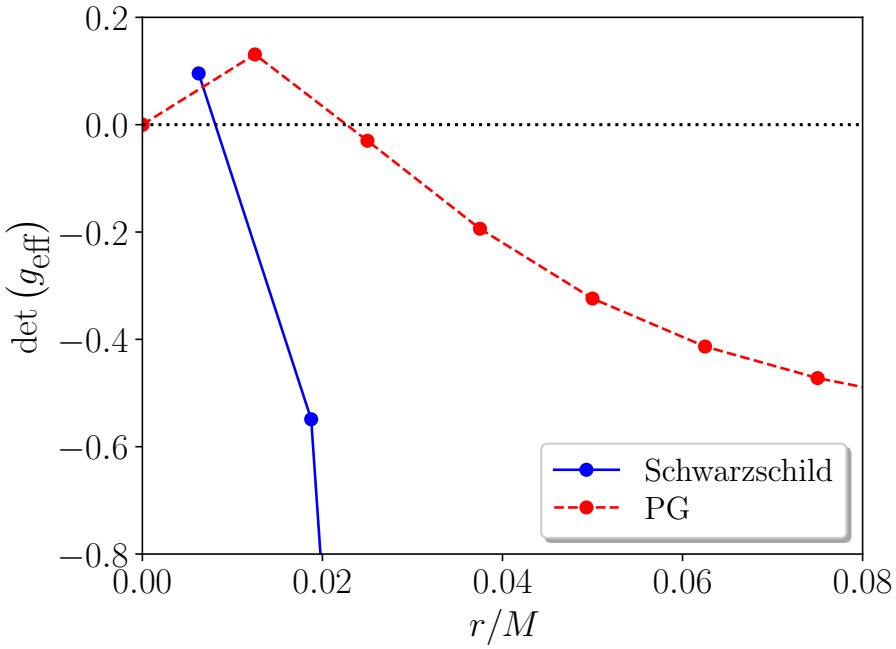

Figure 8.1: The plot shows the determinant of the effective metric at the time slice when hyperbolicity is lost, in different coordinates, for the same initial data, and coupling constants with $\alpha/M = 0.25$, and $\beta = 0$. We observe that the sign of the determinant changes at the same location in both coordinates within a tolerance of grid spacing.

Bonnet gravity [409, 412–414, 421–424, 433, 434, 453] is due to the physical, rather than the gauge modes present in the theory. Furthermore, this provides evidence that additional interactions that would be expected to be present in an effective field theory, such as the Ricci coupling, can be crucial for well-posedness.

In Figure 8.2, we present the characteristic trend of the determinant of the effective metric in Schwarzschild coordinates. Here, we consider $\alpha/M^2 = 0.25$ and different values of $\beta = \{0,\ 0.5,\ 0.525\}$ to illustrate the signature of the effective metric in distinct scenarios. In the top plot, the amplitude of the initial data is $a_0 = 10^{-2}$. When hyperbolicity is lost (with $\beta = 0$), we notice the growth of the determinant and its value crossing zero and becoming positive, *i.e.*, the effective metric of the system is no longer Lorentzian. On the other hand, when $\beta = 0.525$, the effective metric remains Lorentzian, and the final state of the evolution is flat spacetime. In the bottom panel, we consider $a_0 = 1.6 \times 10^{-2}$, which collapses into a black hole with negligible scalar field when $\beta = 0.5$; otherwise ($\beta = 0$), the evolution is ill-posed, as indicated by the effective metric.

To make sure that the behaviour of the effective metric near the loss of hyperbolicity is not affected by the loss of convergence and accumulating errors as the system changes character from hyperbolic to elliptic, we also compute the same determinant in simulations of the same initial data using the fixing-the-equations approach. In this case, the evolution of the "fixed" system remains hyperbolic, but the determinant tracks the hyperbolicity properties of the original system. The behaviour of the effective metric evaluated using the "fixed" system is depicted in Figure 8.2 for different values of the time scale ξ. We observe the same trend produced by the "original" system; hence, the coordinate system or numerical instabilities are not causing the system to change its character. Moreover, in Figure 8.3, we examine the trend of the determinant in the fixed system for which the end state of the evolution is a flat spacetime. We observe that the original system becomes elliptic at some point, as suggested by the effective metric. However, as expected, as the system evolves to flat geometry, the effective metric settles down and becomes Lorentzian again. We also study black hole initial data using Painleve-Gullstrand coordinates. Two examples are given in Figure 8.4, where we have

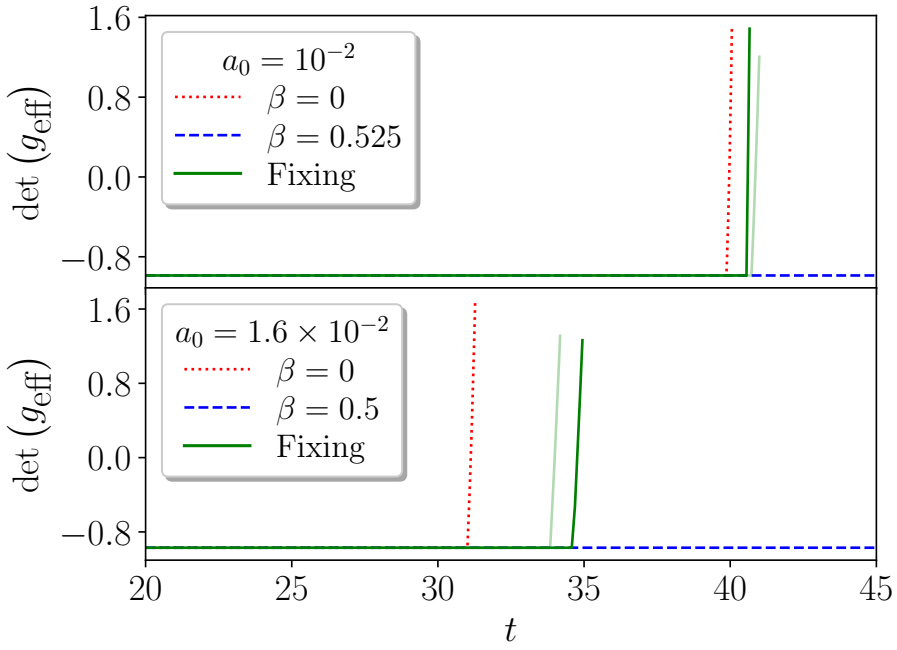

Figure 8.2: The plot shows the maximum of the determinant of the effective metric $\det\left(g^{ab}_{\rm eff}\right)$ in space for different values of β. The evolution was performed in Schwarzschild coordinates. The choice of coupling constant is $\alpha/M^2 = 0.25$. The top panel is for $a_0 = 10^{-2}$ for which the evolution ceases to be well-posed in the $\beta = 0$ case, as the determinant of the effective metric grows and crosses zero. However, the effective metric remains Lorentzian for $\beta = 0.525$, and the evolution remains hyperbolic. We observe similar behaviour in the bottom panel. In this case, the choice of the initial data ($a_0 = 1.6 \times 10^{-2}$) leads to the formation of an apparent horizon with a negligible scalar field. We also show the effective metric in the fixed theory for $\beta = 0$ for two different timescales that increase for darker shades of green.

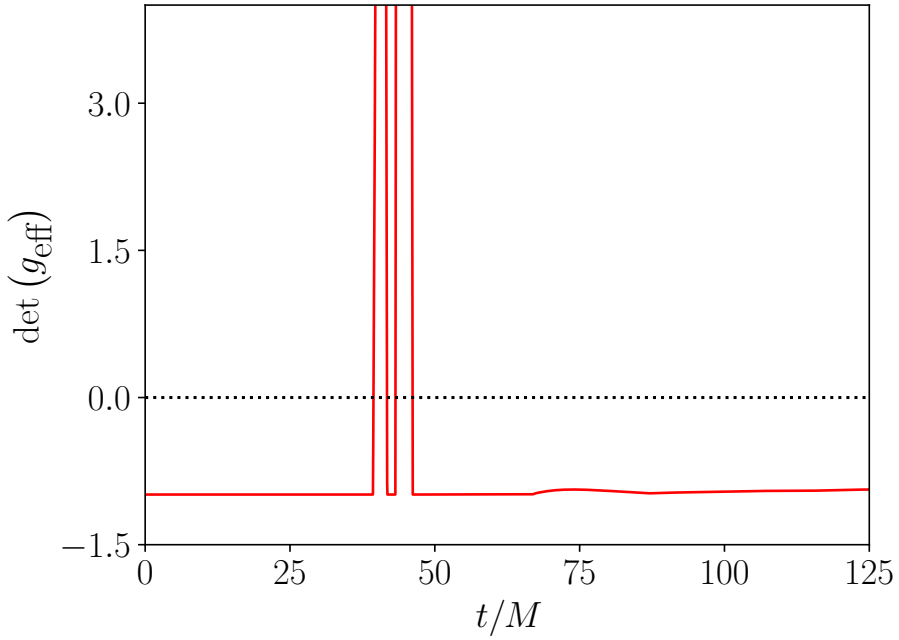

Figure 8.3: We plot the behaviour of the maximum of the determinant of the effective metric reconstructed with the fixed theory for $\alpha/M^2 = 0.25$, $\beta = 0$, and initial data with $a_0 = 9.5 \times 10^{-3}$. We observe that at some point the effective metric flips sign and becomes non-Lorentzian; however, with the fixing procedure, we can evolve the system, resulting in flat spacetime with the effective metric remaining Lorentzian.

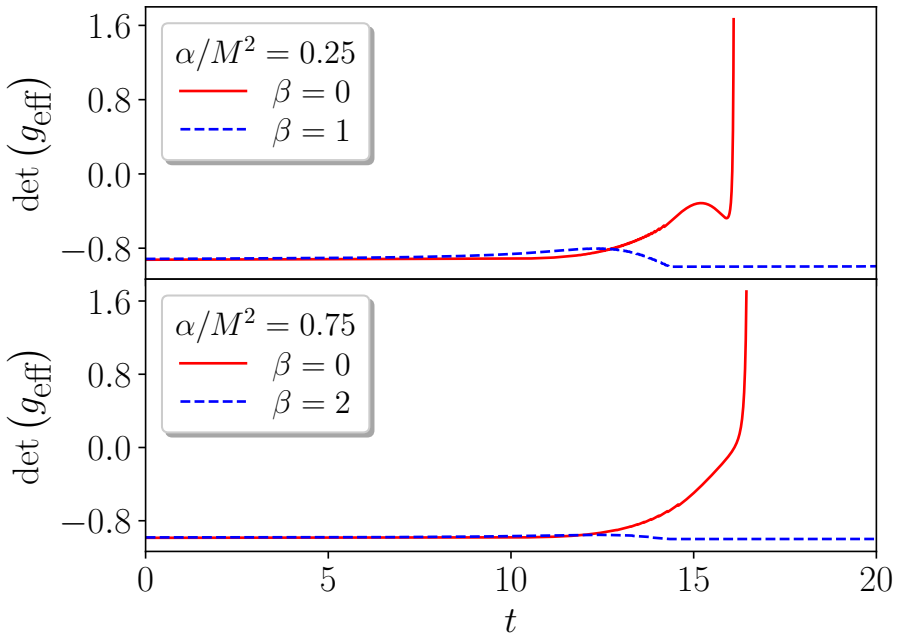

Figure 8.4: Same as Figure 8.2. The evolution was performed in Painleve-Gullstrand coordinates with black hole initial data and a scalar field perturbation. We observe a similar trend to the Schwarzschild case. The system is no longer hyperbolic when the effective metric ceases to be Lorentzian. The top panel depicts initial data with $a_0 = 5 \times 10^{-3}$, $\alpha/M^2 = 0.25$. The final state (when the evolution remains well-posed) is a Schwarzschild black hole. We have the same initial data in the bottom panel, with $\alpha/M^2 = 0.75$, but the final state is a scalarized black hole.

$\alpha/M^2 = 0.25$ (top panel), and $\alpha/M^2 = 0.75$ (bottom panel). The top and bottom panels have $a_0 = 5 \times 10^{-3}$. In both cases, when $\beta = 0$ we observe similar proclivity for the effective metric to become non-Lorentzian, but in the occasions where the evolution is hyperbolic ($\beta > 0$), the end states are either a Schwarzschild (top panel) or a scalarized black hole (bottom panel).

8.6 Disformal transformations

The key advantage of using the determinant of the effective metric, or more generally, the principal symbol analysis of [449], is to assess well-posedness in

a gauge-invariant manner. This makes it a more trustworthy diagnostic than studying the evolution in a particular gauge. Nonetheless, it cannot be seen as a definitive criterion of whether or not a theory is well-posed—after all, well-posedness is a statement about a particular initial value formulation of a theory. One can perform field redefinitions that affect the formulation of the initial value problem and its hyperbolicity.

An invertible linear transformation of the partial differential equations system preserves the hyperbolic nature of the system. If the transformation is derivative-dependent, however, then in general, this is no longer the case. To illustrate this point with an example, we consider the effect of disformal transformations on hyperbolicity.

8.6.1 Preliminaries

Disformal transformations were initially introduced by Bekenstein in [454]. Such transformations are defined through a field redefinition of the form

$$g_{\mu\nu} \to \mathcal{A}(\phi, X)\, g_{\mu\nu} + \mathcal{B}(\phi, X) \nabla_\mu \phi \nabla_\nu \phi =: \tilde{g}_{\mu\nu}\,, \tag{8.6.1}$$

with disformal functions $\mathcal{A}$, and $\mathcal{B}$. In the case of $\mathcal{A} = \mathcal{A}(\phi)$, and $\mathcal{B} = 0$, we retrieve the usual conformal transformations. The disformal functions now depend implicitly on the metric and how the scalar field changes in spacetime through the kinetic term, not only on the field itself.

The disformal field redefinitions should satisfy some "reasonable" conditions to produce a "well-behaved" metric. We impose that the disformal metric is invertible with a non-singular volume element, given by

$$g^{\mu\nu} \to \frac{1}{\mathcal{A}} \left(g^{\mu\nu} - \frac{\mathcal{B}}{\mathcal{A} - 2\mathcal{B}X} \nabla^\mu \phi \nabla^\nu \phi \right)\,, \tag{8.6.2}$$

$$\sqrt{-g} \to \mathcal{A}^2 \left(1 - 2\mathcal{B}X/\mathcal{A}\right)^{1/2} \sqrt{-g}\,, \tag{8.6.3}$$

from which, for positive $\mathcal{A}$ (the case we will consider), we have the condition

$$\mathcal{A} - 2\mathcal{B}X > 0\,. \tag{8.6.4}$$

Two different representations of a Lagrangian related by a disformal trans-

formation will have the same degrees of freedom and physical solutions for invertible transformations [455]. An additional constraint on the functions $\mathcal{A}$, and $\mathcal{B}$ arises as a consequence of invertibility, given by [456]

$$\mathcal{A}\left(\mathcal{A} - X\,\partial_X\mathcal{A} + 2X^2\partial_X\mathcal{B}\right) \neq 0. \tag{8.6.5}$$

Note that if the functions $\mathcal{A}$, and $\mathcal{B}$ are independent of the kinetic term X, then the relation between $g_{\mu\nu}$, and $\tilde{g}_{\mu\nu}$ can be trivially inverted

$$g_{\mu\nu} = \frac{\tilde{g}_{\mu\nu} - \mathcal{B}(\phi)\nabla_\mu\phi\nabla_\nu\phi}{\mathcal{A}(\phi)}\,, \tag{8.6.6}$$

therefore, the transformation is invertible for a non-zero $\mathcal{A}$.

8.6.2 Disformal transformations and hyperbolicity

To examine the effect of field redefinitions on hyperbolicity we consider general relativity minimally coupled to a scalar field (*i.e.*, $f = h = 0$ in the action (8.0.1)), and perform a transformation of the form (8.6.1) such that $\mathcal{A} = a$, and $\mathcal{B} = b$ for some constants a, b. The resultant theory is [457]

$$\begin{aligned} S = \frac{1}{16\pi}\int \mathrm{d}^4x\sqrt{-g}\,[\mathcal{G}_2 + \mathcal{G}_4 R \\ + \partial_X\mathcal{G}_4\left((\Box\phi)^2 - \left(\nabla_\mu\nabla_\nu\phi\right)^2\right)\Big]\,, \end{aligned} \tag{8.6.7}$$

where,

$$\mathcal{G}_2 = \frac{X}{a\mathcal{S}}\,, \tag{8.6.8}$$

$$\mathcal{G}_4 = a\mathcal{S}\,, \qquad \mathcal{S} = \sqrt{1 - \frac{2bX}{a}}\,. \tag{8.6.9}$$

Hence, we end up with a Horndeski theory with a specific choice of the functions $\mathcal{G}_2$ and $\mathcal{G}_4$. For this example, we have chosen the disformal functions to be constants for simplicity. The considered choice is rigid and might lead to some of the conditions we discussed being dynamically violated. Nonethe-

less, in what follows, we will analyse the behaviour of this theory for some initial data at $t = 0$ and ensure that these conditions are fulfilled.

It was shown in [382] that a theory with $\partial_X \mathcal{G}_4 \neq 0$ is not strongly hyperbolic in the generalised harmonic gauge. To understand the effect of field redefinitions in a gauge-independent manner, we proceed as in the case of scalar Gauss-Bonnet and compute the effective metric in this theory. The equations of motion and the principal symbol are given in Appendix D.2.

Now, we can analyse the characteristic equation as we have done in the case of scalar Gauss-Bonnet, and find the determinant of the inverse effective metric (in Schwarzschild-like coordinates (6.3.1)), which yields

$$\begin{aligned}\det\left(g^{ab}_{\text{eff}}\right) = \frac{e^{-2(A+B)}}{(a-2bX)^4}\Big(&-a^2 + a^2b^2X^2 \\ &-2ab^2X^2\mathcal{S} - 4ab^3X^3 + 4b^4X^4\Big)\,,\end{aligned} \tag{8.6.10}$$

and the kinetic term is given by

$$X = \frac{1}{2}\left(e^{-2A}\left(\frac{\partial\phi}{\partial t}\right)^2 - e^{-2B}\left(\frac{\partial\phi}{\partial r}\right)^2\right)\,. \tag{8.6.11}$$

For concreteness, we fix $a = b = 1$, and find the values of X for which the effective metric ceases to be Lorentzian,

$$\det\left(g^{ab}_{\text{eff}}\right) \geq 0 \iff X \lessapprox -0.6573\,. \tag{8.6.12}$$

To study the effect of disformal transformations on hyperbolicity, we evolve general relativity in Schwarzschild coordinates using two types of initial data that lead to condition (8.6.12) being satisfied initially, whilst maintaining the invertibility of the transformation. That is, the physics is left invariant under the disformal change of variables. If we take the initial data for the scalar field to be

- Type-A:

$$\phi(0,r) = a_0 \exp\left[-\left(\frac{r-r_0}{w_0}\right)^4\right]\,, \qquad P(0,r) = 0\,, \tag{8.6.13}$$

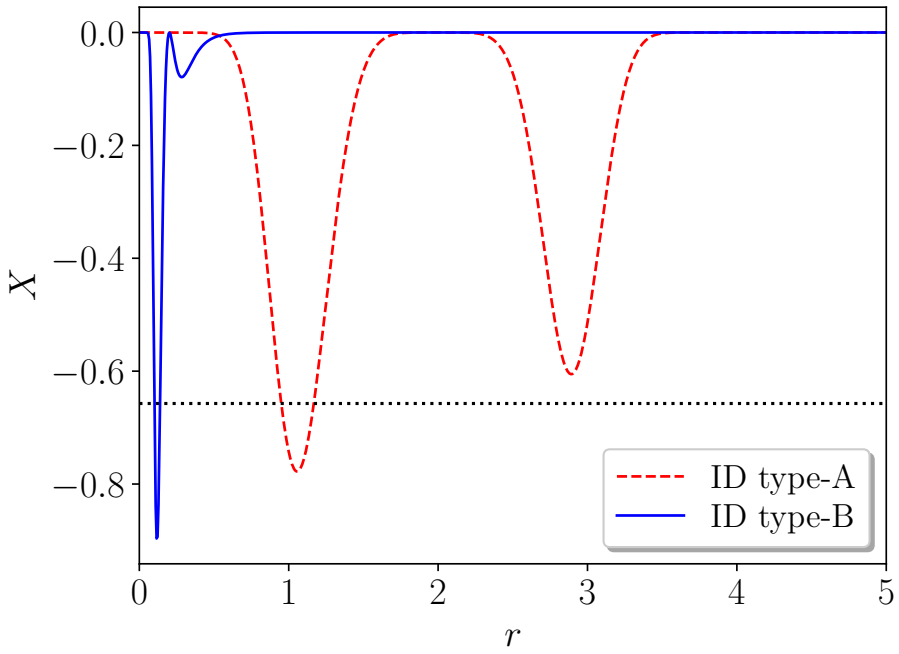

Figure 8.5: The plot shows the kinetic term at $t = 0$. We have type-A initial data with $a_0 = 0.85$, $r_0 = 2$, and $w = 1$. We observe that the effective metric is not Lorentzian, as X is less than the threshold for some r, indicating that the problem is ill-posed after performing the disformal transformation. Nevertheless, the original formulation, *i.e.*, general relativity with a minimal scalar, produces a well-posed evolution. Similar behaviour is observed for a_0 approximately in $[0.78,\ 1.98]$ without being hidden by an apparent horizon. For type-B initial data we have $a_0 = 5{\times}10^{-3}$, $r_0 = 2$, and $w = 1$. For a_0 approximately in $[5 \times 10^{-3},\ 0.7]$, the evolution is akin to the case shown without forming an apparent horizon.

- Type-B:

$$\phi(0, r) = \frac{a_0}{r^5} \left(\exp(1/r) - 1\right)^{-1} , \qquad P(0, r) = 0 . \tag{8.6.14}$$

Then the effective metric will change signature at some $r > 0$, as the value of X is below the threshold, as shown in Figure 8.5. Note that the invertibility condition (8.6.5) is trivially satisfied. Therefore, for such initial data, the problem is ill-posed, while in the original formulation (general relativity with a minimal scalar), the theory is always well-posed.

8.7 Discussion

We have studied the well-posedness of spherical dynamics in scalar Gauss-Bonnet gravity with additional Ricci coupling, using the gauge-invariant method of [449]. In this setup, loss of hyperbolicity can be probed by calculating when an effective metric becomes degenerate.

We have used flat and black hole initial data for various coupling constants and explored the same part of the parameter space as in [445, 446], performing simulations in both of the gauge choices used therein. We find that the determinant of the effective metric changes sign in cases for which loss of hyperbolicity was reported in [445, 446]. At the same time, it remains non-degenerate for sufficiently large values of the Ricci coupling. This indicates that it is the behaviour of the physical degrees of freedom, rather than a gauge choice, that is responsible for dynamically changing the character of the equations from hyperbolic to elliptic. Our results provide further evidence that the Ricci coupling has a positive effect on hyperbolicity in spherical symmetry and that, more broadly, including additional couplings that would be present in an effective field theory can be crucial for having a well-posed initial value problem beyond general relativity.

Although the (sign of the) determinant of the effective metric is a gauge-invariant probe of well-posedness, one could have concerns about accuracy when calculating it numerically in a specific gauge near the loss of hyperbolicity. To address this, we have performed additional simulations utilising the fixing-the-equations approach, where evolution remains hyperbolic, and monitored the evolution of the effective metric of the original system. We found that the determinant changes sign in the same fashion as it did in the original theory. This suggests that our earlier results are reliable and that the growth of the determinant was not due to the accumulation of numerical error near the elliptic region. We have also considered initial data for which one expects the endpoint to be flat space, but for which the original system of equations becomes elliptic during evolution. We have then verified that in the fixed system, evolution proceeds without problems and flat space is indeed the endpoint. We computed the effective metric of the original system using the fixed system and found that it becomes non-Lorentzian when the

system changes character, but then returns to being Lorentzian as the evolution proceeds in the fixed system for longer times.

Additionally, we highlighted a limitation in using the determinant of the effective metric as a probe of hyperbolicity. Although it is gauge invariant, it is not invariant under field redefinitions, which can indeed affect the character of the evolution equations. As an illustrative example, we analysed the effect of disformal transformations on a minimally coupled scalar field in general relativity. This transformation maps general relativity to a certain Horndeski theory, which is not always well-posed. We evolved general relativity for certain choices of the initial data and ensured that the transformation is invertible initially, thereby maintaining the same physics in both theoretical representations. We found that the effective metric of the Horndeski theory indicates that this initial data will lead to elliptic equations, and hence, an ill-posed problem.

It would be fruitful to generalise this analysis to $3 + 1$ dimensions, which will provide a useful diagnostic tool for numerical codes. Nonetheless, the $3 + 1$ case is more complicated and generally it would not be possible to reduce the system to a scalar equation with an effective metric, as the scalar and gravitational degrees of freedom will mix beyond spherical symmetry. Alternatively, one would need to find the roots of the quartic polynomial and check that they are always real.

Chapter IX

Conclusions

In this thesis, we argued that, despite its remarkable successes, general relativity remains an incomplete theory of gravity. Ongoing advances in gravitational wave astronomy may illuminate the nature of gravitational interaction and reveal signatures of new physics emerging well below the Planck scale, for example, in the mergers of binary black holes. Moreover, although cosmological scales were not originally expected to host new physics, we still lack satisfactory explanations for dark matter and dark energy.

To explore extensions of general relativity, we first examined the foundations that render it a robust theoretical framework. We briefly reviewed its geometric structure and the identification of gravity with spacetime curvature. However, historically, articulating these principles proved challenging. Einstein's early formulations were often misunderstood or contested, partly because he was at times confused by his ideas and did not convey them as clearly as possible, leading to objections such as those of Kottler concerning the equivalence principle. Kretschmann's critique of general covariance likewise spurred ongoing debate about what constitutes genuine background independence. While these concerns may appear philosophical, they play a crucial role in the classification and evaluation of gravitational theories (see Section II).

Lovelock's theorem demonstrates that general relativity is unique under

specific assumptions. Departing from these assumptions offers a pathway to generalisation. One natural approach, which we adopt in this thesis, introduces new fundamental fields to encode new physics—particularly scalar fields—as additional degrees of freedom. These fields are simple yet widely studied, relevant to both dark sector phenomenology and high-energy extensions such as quantum gravity. When coupled non-minimally to curvature, scalars can modify the dynamics of compact objects, including black holes and neutron stars. The prototypical example is scalar-tensor theory, originally formulated by Brans and Dicke to embody Mach's principle. Although Brans-Dicke theory and its immediate generalisations are now largely outdated, Horndeski's construction retains relevance by allowing all non-minimal scalar-curvature couplings consistent with second-order field equations. Extending general relativity introduces considerable complexity. The literature contains a vast array of proposals, many of which suffer from pathologies such as ghost modes, gradient instabilities, or ill-posed initial value problems. As emphasised throughout this work, meaningful extensions must be formulated within the effective field theory paradigm. We do not consider these theories fundamental; rather, they provide controlled parametrisations of low-energy deviations from general relativity. This agnostic stance toward the ultraviolet completion of gravity enables us to constrain such deviations empirically, using a finite set of parameters. While effective field theories cannot offer a paradigmatic shift on their own, they serve as essential tools for probing physics across scales, which may ultimately guide us toward a more complete theory.

Additional fields may imprint observable signatures on black holes, potentially detectable in gravitational wave signals. However, many no-hair theorems prohibit black holes from acquiring non-trivial scalar configurations. These theorems apply to a broad class of minimally and non-minimally coupled scalar models. A notable exception arises when a scalar couples to the Gauss-Bonnet invariant. In Section 4.2, we investigated hairy black holes in shift-symmetric scalar-Gauss-Bonnet theories, where the scalar couples linearly to the Gauss-Bonnet term. Shift symmetry leads to a massless scalar and prevents it from acquiring a mass under quantum corrections. This is particularly relevant as current and upcoming experiments will probe horizon-scale

physics and may constrain or detect such light scalar fields. We further discussed the effect of additional interactions and demonstrated that they can qualitatively alter the picture. The regularity condition on the horizon remains, albeit modified, and black holes still possess a minimum mass. Furthermore, the scalar charge per unit mass is affected especially for black holes with masses near the minimum mass. However, in this case, black holes are always dressed with a non-trivial scalar profile, and general relativity black holes are not solutions of this theory.

In most known models, deviations from the Kerr metric appear for solar mass black holes, whilst supermassive black holes are still well described by the Kerr metric. For example, since the tachyonic instability is most strongly controlled by the compactness of the black hole, solar mass black holes are the most susceptible to spontaneous scalarization. Nonetheless, in Section V, we studied a scenario that breaks this picture and analysed it from an effective field theory perspective. We found that the resulting effective field theory does not have the right coupling sign or the right hierarchy of scales. We have also shown that theories with two scalars do not naturally produce scalarization exclusively for supermassive black holes.

We then turned our attention to the dynamics of black holes in such theories. We have investigated the well-posedness of the initial value problem in scalar Gauss-Bonnet gravity with an additional quadratic coupling between the scalar field and the Ricci scalar. Through a combination of spherical collapse simulations, black hole dynamics, and gauge-invariant diagnostics, we have demonstrated that this Ricci coupling significantly improves the hyperbolicity properties of the theory within spherical symmetry. In particular, it can prevent the formation of naked elliptic regions—associated with a breakdown of predictivity—for sufficiently large coupling values that remain consistent with radial black hole stability, cosmological constraints, and bounds on neutron star scalarization. Our results thus highlight the critical role of including additional interactions, beyond those strictly necessary for phenomenology, in constructing well-posed effective field theories of gravity. Moreover, our results show that hyperbolicity loss arises from the behaviour of physical degrees of freedom, confirming the gauge independence of this phenomenon. This also demonstrates that the positive effect of the Ricci

coupling in regulating the dynamics is gauge-independent; however, we have identified a limitation: field redefinitions can alter the character of the evolution equations, complicating the drawing of general conclusions.

Our simulations also reproduced known features of scalarized black hole formation: initial data with mass above the scalarization threshold evolve to bald black holes, while those within the scalarization window dynamically settle into scalarized solutions that match the corresponding static profiles. Below the minimum mass bound, black holes are absent, and the system either dissipates to flat space or develops elliptic behaviour. Notably, the onset of hyperbolicity loss correlates well with the presence of finite-area singularities inside scalarized black holes. This connection warrants further investigation, especially in the context of excision techniques that remove the elliptic region without affecting the exterior solution, thereby extending the range of stable numerical evolution.

A key limitation of this study is the restriction to spherical symmetry. It remains unclear whether the Ricci coupling suffices to improve hyperbolicity in fully dynamical 3+1 simulations. Nonetheless, preliminary studies suggest it may have a stabilising effect [448]. Extending this analysis to more realistic scenarios, such as stellar collapse, would offer a compelling next step and may yield stronger phenomenological relevance than scalar collapse alone. Furthermore, exploring the non-linear stability of scalarized black holes under generic perturbations would provide deeper insight into the long-term dynamics of such solutions within the broader landscape of effective gravitational theories.

Looking ahead, more broadly, upcoming experiments such as LISA, the Einstein Telescope, and other third-generation gravitational wave detectors will significantly enhance our ability to probe the non-perturbative regime of gravity. These advances promise stringent tests of scalar-tensor theories and other extensions of general relativity, offering critical insight into the nature of gravity and the viability of extended theories.

Appendix A: Perturbative coefficients

We present the coefficients in the $\tilde{\alpha}$-expansion of the scalar charge and the ADM mass. To find the perturbative expressions, we solve the perturbed field and scalar equations. To **first order**:

$$(tt): \qquad 0 = (r-2m)B_1' + B_1\,, \tag{A.0.1}$$

$$(rr): \qquad 0 = (2m-r)A_1' + B_1\,, \tag{A.0.2}$$

$$(\phi): \qquad 0 = r^5(2m-r)\phi_1'' + 2r^4(m-r)\phi_1' - 48m^2\,. \tag{A.0.3}$$

To **second order**:

$$\begin{aligned}(tt): \qquad 0 = {} & m^2r^{10}(r-2m)B_2' + m^2r^{10}B_2 + 2304\gamma m^6 - 384\gamma m^3r^3 \\ & - 52m^2r^6 - 8m^3r^5 - 16m^4r^4 + 736m^5r^3 - 2mr^7 \\ & + 12\gamma r^6 - r^8\,,\end{aligned} \tag{A.0.4}$$

$$\begin{aligned}(rr): \qquad 0 = {} & \left(4m^2+2mr+r^2\right)\left[8m^3\left(4\gamma+5r^2\right)\right. \\ & \left. - 16m^2r^3 - 4r^3\gamma + r^5\ \right] + m^2r^9(2m-r)A_2' \\ & + m^2r^9B_2\,,\end{aligned} \tag{A.0.5}$$

$$\begin{aligned}(\phi): \qquad 0 = {} & 40m^2r^4\sigma - 672m^3r^3\sigma - 224m^4r^2\sigma - 2m^2r^{11}\phi_2' \\ & + 2m^3r^{10}\phi_2' - m^2r^{12}\phi_2'' + 2m^3r^{11}\phi_2'' - 512m^5r\sigma \\ & + 3456m^6\sigma + 16mr^5\sigma + 24r^6\sigma\,.\end{aligned} \tag{A.0.6}$$

Higher order equations are very lengthy, but we have calculated them up to $O(\tilde{\alpha}^5)$. We can then solve for the coefficients appearing in the expressions (4.2.30) – (4.2.31) for the charge and mass expansions

$$Q_1 = \frac{2}{m}\,, \tag{A.0.7}$$

$$Q_3 = -\frac{1}{60m^5}\,, \tag{A.0.8}$$

$$Q_4 = -\frac{689\sigma}{36960m^9}\,, \tag{A.0.9}$$

$$Q_5 = \frac{11051\kappa}{720720m^{11}} - \frac{268867\gamma^2}{16336320m^{13}} - \frac{84317\gamma}{180180m^{11}} - \frac{4609603\sigma^2}{130690560m^{13}} - \frac{118549}{158400m^9}\,. \tag{A.0.10}$$

$$M_2 = \frac{49}{40m^3}\,, \tag{A.0.11}$$

$$M_3 = \frac{18107\sigma}{73920m^7}\,, \tag{A.0.12}$$

$$M_4 = \frac{244007\gamma}{360360m^9} - \frac{635421\gamma^2}{10890880m^{11}} + \frac{11838611\sigma^2}{87127040m^{11}} \tag{A.0.13}$$

$$+ \frac{408253}{246400m^7} + \frac{130309\kappa}{1441440m^9}\,, \tag{A.0.14}$$

$$M_5 = \frac{995527207\gamma\sigma}{1241560320m^{13}} - \frac{210006269\gamma^2\sigma}{2595989760m^{15}} + \frac{56711635\kappa\sigma}{496624128m^{13}} + \frac{12276069473\sigma^3}{119189790720m^{15}} + \frac{84509327587\sigma}{50315865600m^{11}}\,. \tag{A.0.15}$$

In equations (4.2.34) – (4.2.35) we presented the general form of the expansions for the scalar field and the Gauss-Bonnet invariant up to third order in $\tilde{\alpha}$, which were used in Figures 4.1, and 4.2. Here we give the analytic expres-

sions for the coefficients appearing in these expansions

$$\phi_0 = 0\,, \tag{A.0.16}$$

$$\phi_1 = \frac{2\alpha\left(3r^2+4m^2+3r\right)}{3mr^3}\,, \tag{A.0.17}$$

$$\phi_2 = \frac{2\sigma\left(-224m^5-84m^4r-24m^3r^2+84m^2r^3+42mr^4+21r^5\right)}{21m^2r^9}\,, \tag{A.0.18}$$

$$\begin{aligned}\phi_3 = \frac{1}{30m^4}\Bigg[&\frac{18432m^9\sigma^2}{r^{15}}+\frac{7680m^8\left(8\gamma^2+3\sigma^2\right)}{7r^{14}}+\frac{15360m^7\left(8\gamma^2-\sigma^2\right)}{13r^{13}}\\&+\frac{240m(2\gamma+\kappa)-952m^3}{5r^5}+\frac{320m^6\left(24\gamma^2+8m^2(7\gamma-\kappa)-33\sigma^2\right)}{r^{12}}\\&+\frac{48m^2\left(-10\gamma^2+58m^4-5m^2(\gamma-\kappa)+15\sigma^2\right)}{r^8}\\&+\frac{96m^4\left(-8\gamma^2+24m^2(3\gamma-\kappa)-5\sigma^2\right)}{r^{10}}+\frac{32m^2\left(15(2\gamma+\kappa)-82m^2\right)}{3r^6}\\&+\frac{160m\left(-6\gamma^2+35m^4+18\kappa m^2+12\sigma^2\right)}{7r^7}+\frac{66m^2}{r^4}+\frac{526m}{3r^3}-\frac{1}{2mr}+\frac{73}{r^2}\\&+\frac{3840m^5\left(4\gamma^2+8m^2(4\gamma-\kappa)-9\sigma^2\right)}{11r^{11}}\\&+\frac{160m^3\left(-72\gamma^2+424m^4-24m^2(2\gamma+\kappa)+99\sigma^2\right)}{9r^9}\Bigg]\,.\end{aligned} \tag{A.0.19}$$

$$\mathcal{G}_1 = \frac{48m^2}{r^6}\,, \tag{A.0.20}$$

$$\begin{aligned}\mathcal{G}_2 = {} & \frac{79872\gamma m^5}{r^{15}} + \frac{14336\gamma m^4}{r^{14}} + \frac{6656\gamma m^3}{r^{13}} - \frac{12288\gamma m^2}{r^{12}} \\ & + \frac{53760m^4}{r^{12}} - \frac{4096m^3}{5r^{11}} - \frac{448m^2}{r^{10}} + \frac{588}{5m^2r^6} - \frac{1408\gamma m}{r^{11}} \\ & + \frac{384\gamma}{mr^9} - \frac{4608m}{r^9} - \frac{64}{mr^7} - \frac{640\gamma}{r^{10}} - \frac{32}{r^8}\,,\end{aligned} \tag{A.0.21}$$

$$\begin{aligned}\mathcal{G}_3 = {} & \frac{106496\gamma m^5\sigma}{r^{19}} - \frac{5603328\gamma m^7\sigma}{r^{21}} - \frac{98304\gamma m^6\sigma}{r^{20}} \\ & + \frac{1892352\gamma m^4\sigma}{r^{18}} + \frac{129024\gamma m^3\sigma}{r^{17}} + \frac{28672\gamma m^2\sigma}{r^{16}} \\ & - \frac{2174976m^6\sigma}{r^{18}} + \frac{3981312m^5\sigma}{11r^{17}} + \frac{841728m^4\sigma}{5r^{16}} \\ & + \frac{507904m^3\sigma}{r^{15}} - \frac{38016m^2\sigma}{r^{14}} + \frac{18107\sigma}{770m^6r^6} \\ & - \frac{181248\gamma m\sigma}{r^{15}} + \frac{4608\gamma\sigma}{m^2r^{12}} - \frac{4096\gamma\sigma}{mr^{13}} \\ & - \frac{122880m\sigma}{7r^{13}} - \frac{12288\gamma\sigma}{r^{14}} - \frac{27648\sigma}{r^{12}}\,.\end{aligned} \tag{A.0.22}$$

Appendix B: Schwarzschild coordinates

Contents

B.1 Characteristic speeds in Schwarzschild coordinates

$$\mathcal{P}_{IJ}(\xi) \coloneqq \mathcal{P}^{\mu}_{IJ}\xi_{\mu} = \frac{\partial V_I}{\partial(\partial_{\mu}u^J)}\xi_{\mu}\,, \tag{B.1.1}$$

for a given covector ξ_{μ}. The covector ξ_{μ} is called characteristic if it satisfies the characteristic equation

$$\det(\mathcal{P}_{IJ}(\xi)) = 0\,. \tag{B.1.2}$$

The system of equations is well-posed if all solutions of the characteristic equation are real. In spherical symmetry, the principal symbol matrix can be written as [413]

$$\mathcal{P}(\xi) = \begin{pmatrix} \mathcal{A}\xi_t + \mathcal{B}\xi_r & \mathcal{Q}\xi_r \\ \mathcal{R}\xi_r & \mathcal{S}\xi_r \end{pmatrix}, \tag{B.1.3}$$

where,

$$\begin{aligned}
\mathcal{A} &\coloneqq \begin{pmatrix} \partial E_Q/\partial\left(\partial_t Q\right) & \partial E_Q/\partial\left(\partial_t P\right) \\ \partial E_P/\partial\left(\partial_t Q\right) & \partial E_P/\partial\left(\partial_t P\right) \end{pmatrix}, \\
\mathcal{B} &\coloneqq \begin{pmatrix} \partial E_Q/\partial\left(\partial_r Q\right) & \partial E_Q/\partial\left(\partial_r P\right) \\ \partial E_P/\partial\left(\partial_r Q\right) & \partial E_P/\partial\left(\partial_r P\right) \end{pmatrix}, \\
\mathcal{Q} &\coloneqq \begin{pmatrix} \partial E_Q/\partial\left(\partial_r A\right) & \partial E_Q/\partial\left(\partial_r B\right) \\ \partial E_P/\partial\left(\partial_r A\right) & \partial E_P/\partial\left(\partial_r B\right) \end{pmatrix}, \\
\mathcal{R} &\coloneqq \begin{pmatrix} \partial C_A/\partial\left(\partial_r Q\right) & \partial C_A/\partial\left(\partial_r P\right) \\ \partial C_B/\partial\left(\partial_r Q\right) & \partial C_B/\partial\left(\partial_r P\right) \end{pmatrix}, \\
\mathcal{S} &\coloneqq \begin{pmatrix} \partial C_A/\partial\left(\partial_r A\right) & \partial C_A/\partial\left(\partial_r B\right) \\ \partial C_B/\partial\left(\partial_r A\right) & \partial C_B/\partial\left(\partial_r B\right) \end{pmatrix}.
\end{aligned} \tag{B.1.4}$$

where $E_Q = 0$, $E_P = 0$ are the evolution equations, and $C_A = 0$, $C_B = 0$ are the constraint equations. The characteristic speed in spherical symmetry is defined as $c \coloneqq -\xi_t/\xi_r$. If ξ_{μ} satisfies the characteristic equation, then the

corresponding values of the characteristic speeds are given by

$$c_{\pm} = \frac{1}{2}\left(\mathrm{Tr}(C) \pm \sqrt{\mathcal{D}}\right) , \tag{B.1.5}$$

where,

$$\mathcal{D} \coloneqq \mathrm{Tr}(C)^2 - 4\mathrm{Det}(C) , \tag{B.1.6}$$

$$C \coloneqq \mathcal{A}^{-1} \cdot \left(\mathcal{B} - \mathcal{Q} \cdot \mathcal{S}^{-1} \cdot \mathcal{R}\right) . \tag{B.1.7}$$

B.2 Code validation

Here, we present the convergence tests to validate the simulations we have performed. We present two cases: one where the end state is a flat background, and another where we observe the formation of an apparent horizon. We use three different resolutions $\{\Delta r_{\mathrm{Low}}, \Delta r_{\mathrm{Mid}}, \Delta r_{\mathrm{High}}\} = \{0.0625, 0.03125, 0.015625\}$. In Figure B.1, we display the convergence behaviour of the Misner-Sharp mass. In both panels, we demonstrate fourth-order convergence up to the formation of the apparent horizon (in the second panel), as expected.

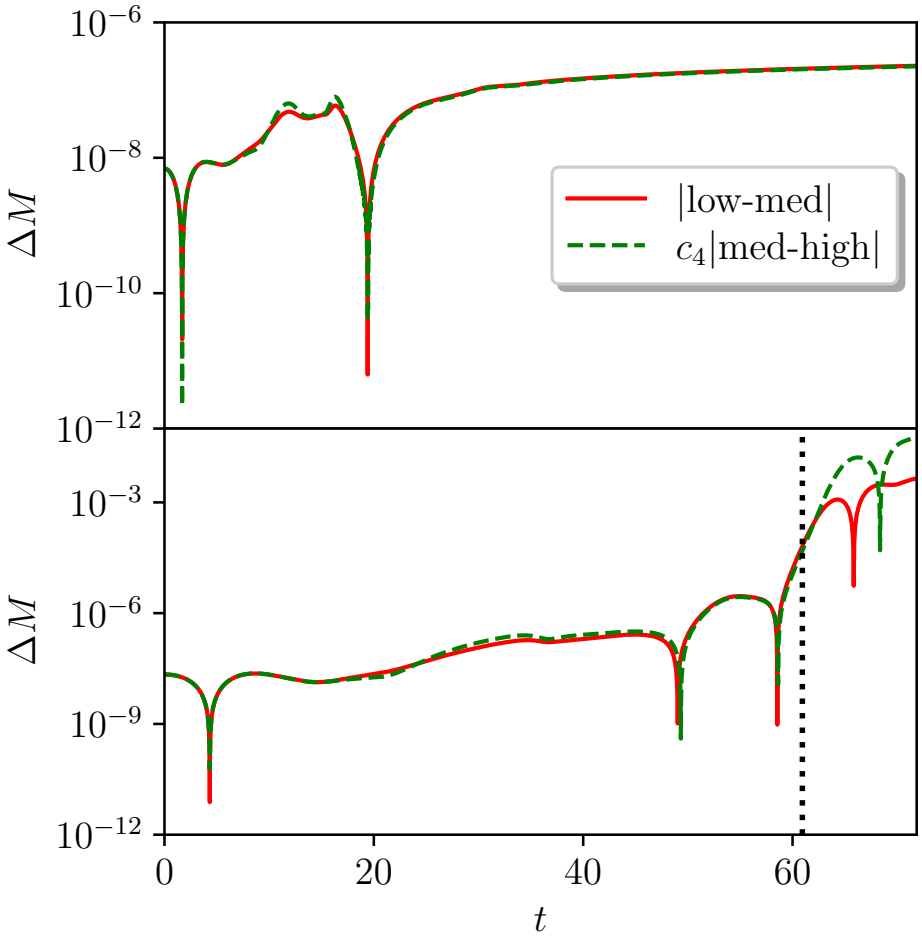

Figure B.1: In both panels, we show the convergence of the Misner-Sharp mass where we plot the absolute difference between the low and medium resolutions, and between the medium and high resolutions for type-I initial data with $r_0 = 25$, $w_0 = 6$. The latter is rescaled by a factor of $c_4 = 16$ for both plots, showing fourth-order convergence. In the top panel, we have $a_0 = 0.3$, and $\alpha/M^2 = 1.25$, $\beta = 0.5$ with the end state being flat spacetime. In the bottom panel, we have $a_0 = 0.4$ and $\alpha/M^2 = 0.025$, $\beta = 0.9$, which forms an apparent horizon indicated by the black dotted line.

B.3 Exploring the parameter space

In Table B.1, we summarise some additional simulations we performed. For each case, we specify the type of initial data used and the amplitude of the pulse a_0. For all cases, we fix $r_0 = 25$ and $w_0 = 6$. We also list the values of the coupling constants α/M^2 and β, the Misner-Sharp mass M at $t = 0$ (used to rescale lengths), and the simulation outcome. Among the outcomes, we distinguish the following cases. We dub *flat* all cases in which the scalar field disperses to infinity. We note *NER* when the discriminant $\mathcal{D}$ becomes negative, signalling the appearance of a naked elliptic region. We mark *BH* and *sBH* when we can trace the formation of an apparent horizon from the condition $\exp(A - B) \to 0$. In the former, the scalar field approaches zero in the late stages of the evolution. In the latter, it is consistent with stationary scalarized black holes.

Finally, we note that in some cases, which encompass large values of α/M^2 and β, we encountered difficulty in imposing the boundary conditions at the centre. A solution to this problem was to increase the order of the Taylor expansion at the centre to select accurate boundary conditions for A and B as shown in equations (6.3.7) – (6.3.9). We also noticed that increasing the strength of the Kreiss-Olliger dissipation and decreasing the order of the stencils of finite differences from fourth to second order mitigated this effect.

Initial data type	a_0	Coupling constants α/M^2	β	M	Outcome
I	0.1	0.0	0.0	0.1693	flat
I	0.1	{0.75, 1.25}	0.0	0.1693	flat
I	0.1	{0.75, 1.25}	0.5	0.1692	flat
I	0.1	{0.75, 1.25}	1.0	0.1694	flat
I	0.1	{0.75, 1.25}	1.5	0.1699	flat
I	0.1	{0.75, 1.25}	2.0	0.1705	flat
I	0.3	0.0	0.0	1.4550	flat
I	0.3	1.25	0.0	1.4550	NER
I	0.3	1.25	0.35	1.4530	flat
I	0.3	1.25	0.5	1.4540	flat
I	0.3	1.75	0.0	1.4550	NER
I	0.3	1.75	0.2	1.4526	NER
I	0.3	1.75	0.35	1.4526	NER
I	0.3	1.75	0.5	1.4542	flat
I	0.3	2.25	0.0	1.4550	NER
I	0.3	2.25	0.2	1.4526	NER
I	0.3	2.25	0.6	1.4561	flat
I	0.4	0.0	0.0	2.4864	BH
I	0.4	0.025	0.0	2.4865	NER
I	0.4	0.025	0.35	2.4795	NER
I	0.4	0.025	0.9	2.4871	BH
II	0.01	0.0	0.0	1.2431	BH
II	0.01	0.75	0.0	1.2431	NER
II	0.01	0.75	0.35	1.2434	NER
II	0.01	0.75	0.5	1.2445	NER
II	0.01	0.75	1.0	1.2518	flat
II	0.015	0.0	0.0	2.6532	BH
II	0.015	0.75	0.0	2.6534	NER
II	0.015	0.75	0.35	2.6553	NER
II	0.015	0.75	1.0	2.7000	BH
II	0.015	0.75	1.5	2.7727	sBH
II	0.015	0.75	2	2.8812	sBH
II	0.016	0.0	0.0	2.9800	NER
II	0.016	0.75	0.0	2.9804	NER
II	0.016	0.75	0.35	2.9829	NER
II	0.016	0.75	1.0	3.0415	BH
II	0.016	0.75	1.5	3.1370	sBH
II	0.016	0.75	2	3.2805	sBH
II	0.02	0.0	0.0	4.3895	BH

Table B.1: We have $r_0 = 25$, and $w_0 = 6$. M is the initial mass. "NER": naked elliptic region. "BH": black hole. "sBH": scalarized black hole.

Appendix C: Painleve-Gullstrand coordinates

Contents

C.1 Code validation

In this section, we present convergence tests to validate the simulations we have performed. We use three different resolutions $\{\Delta x_{\text{Low}}, \Delta x_{\text{Medium}}, \Delta x_{\text{High}}\} = \{0.025,\ 0.0125,\ 0.00625\}$. In Figure C.1, we display second-order convergence of the ζ constraint C_ζ for different times during the evolution.

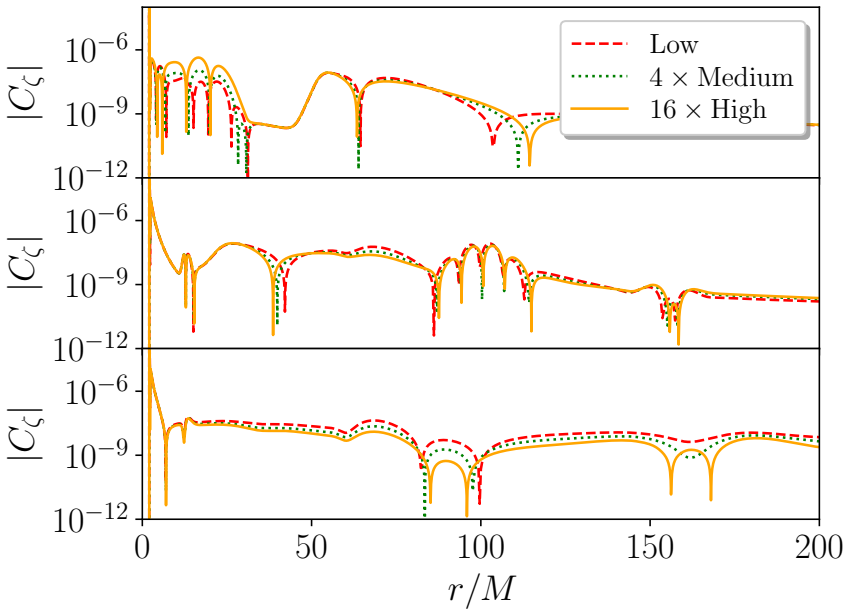

Figure C.1: The convergence behaviour of the ζ constraint C_ζ in space for three resolutions $\Delta x = \{0.025,\ 0.0125,\ 0.00625\}$. Each panel represents an instance in time; the top panel is at $t/M = 30$, the middle panel is at $t/M = 156$, and the bottom panel is at $t/M = 310$. The initial data is $a_0 = 10^{-3}$ with $\alpha/M^2 = 1$, $\beta = 2$. We observe second-order convergence.

C.2 Linear perturbations around Schwarzschild

We want to study small perturbations of equation (3.3.21) around a Schwarzschild background to determine the timescale of the tachyonic instability. We assume a scalar field perturbation of the form

$$\phi = \frac{\delta\phi(r)}{r} Y_{\ell m}(\theta,\varphi) e^{i\omega t}\,, \tag{C.2.1}$$

for which the scalar field equation decouples from the Einstein equations and reads

$$\Box\delta\phi + \alpha f'(0)\mathcal{G}_{\rm Sch}\delta\phi = 0\,, \tag{C.2.2}$$

where the Gauss-Bonnet invariant for the Schwarzschild metric reads $\mathcal{G}_{\rm Sch} = 12/r^6$ (we use units where $M = 1/2$). We use the continued fraction method to compute the growth rates for the scalarized black holes. Let us assume the following ansatz [458]

$$\delta\phi = A^{-i\omega} r^{i\omega-1} e^{i\omega r} \sum_{n=0}^{N} a_n A^n\,, \tag{C.2.3}$$

where $A = g_{tt} = g^{rr} = 1 - 1/r$. With these definitions, equation (C.2.2), after some manipulation, takes the form

$$\sum_{j=-1}^{4} \left(\widetilde{\gamma}_{n,j-1} + \widetilde{\beta}_{n,j} + \widetilde{\alpha}_{n,j+1}\right) a_{n-j} = 0\,. \tag{C.2.4}$$

The coefficients appearing in the relation are given by

$$\widetilde{\alpha}_{n,j} = \binom{0}{j} \alpha^r_{n-j}\,, \tag{C.2.5}$$

$$\widetilde{\beta}_{n,j} = \binom{0}{j} \beta^r_{n-j} + 3\alpha(-1)^j \binom{4}{j}\,, \tag{C.2.6}$$

$$\widetilde{\gamma}_{n,j} = \binom{0}{j} \gamma^r_{n-j}\,. \tag{C.2.7}$$

We notice that, from the definition of the binomial, $\widetilde{\alpha}_{n,j}$ and $\widetilde{\gamma}_{n,j}$ are non-vanishing only for $j = 0$, while $\widetilde{\beta}_{n,j}$ is non-zero for $0 \leq j \leq 4$. The coefficients appearing in the relation are

$$\alpha_n^r = (n+1)\,(n+1-2\mathrm{i}\omega)\,, \tag{C.2.8}$$

$$\beta_n^r = \ell(\ell+1) + (2\omega + \mathrm{i}n)^2 - (n+1-2\mathrm{i}\omega)^2\,, \tag{C.2.9}$$

$$\gamma_n^r = (n-2\mathrm{i}\omega)^2\,. \tag{C.2.10}$$

Notice that (C.2.4) is a five-term relation, but it can be easily brought to a three-term relation through Gaussian elimination (we follow the procedure explained in the appendix of [459]). Then, it takes the generic form

$$\beta_0 a_0 + \alpha_0 a_1 = 0\,, \tag{C.2.11}$$

$$\gamma_n a_{n-1} + \beta_n a_n + \alpha_n R_{n+1} = 0\,, \qquad \text{for } n \geq 1\,. \tag{C.2.12}$$

To invert the relation, we can define the ladder operators which have the following property $a_{n+1} = -\Lambda_n a_n$, with

$$\Lambda_n = \frac{\gamma_{n+1}}{\beta_{n+1} - \alpha_{n+1}\Lambda_{n+1}}\,, \tag{C.2.13}$$

where the coefficients α_n, β_n and γ_n are determined by the Gaussian elimination and are not explicitly reported here. By initializing Λ_N for a very large N with the Nollert procedure [460] the equation one needs to solve to obtain the eigenfrequency ω is

$$\mathcal{L} = \Lambda_1 \alpha_0 - \beta_0 = 0\,. \tag{C.2.14}$$

Coupling constants α/M^2	β	ω_I	ω_I^{cf}	ω_R	ω_R^{cf}
0.0	0.0	0.105304	0.104896	0.106749	0.110455
0.025	0.0	0.105012	0.104279	0.103731	0.106891
0.025	0.5	0.104984		0.103715	
0.025	0.75	0.104968		0.103703	
0.025	1.0	0.104949		0.103688	
0.025	1.25	0.104929		0.10367	
0.025	1.5	0.104906		0.10365	
0.025	1.75	0.104881		0.103626	
0.025	2.0	0.104855		0.103598	
0.025	2.25	0.104829		0.103565	
0.025	2.5	0.104799		0.103528	
0.05	0.0	0.104481	0.103652	0.100866	0.103219
0.0625	0.0	0.103307	0.103334	0.10036	0.101338
0.075	0.0	0.103419	0.103011	0.0981844	0.099425
0.075	0.5	0.103394		0.0981684	
0.075	0.75	0.103383		0.0981544	
0.075	1.0	0.103372		0.0981365	
0.075	1.25	0.103362		0.0981146	
0.075	1.5	0.10335		0.0980896	
0.075	1.75	0.103338		0.0980609	
0.075	2.0	0.103327		0.0980267	
0.075	2.25	0.10332		0.0979849	
0.075	2.5	0.103317		0.097936	
0.0875	0.0	0.103179	0.102683	0.096312	0.097478
0.1	0.0	0.10246	0.102350	0.0947566	0.095494
0.1125	0.0	0.102088	0.102011	0.0927956	0.093471
0.125	0.0	0.10167	0.101664	0.0907635	0.091407
0.125	0.5	0.101654		0.0907499	
0.125	0.75	0.101651		0.0907381	
0.125	1.0	0.101626		0.0907378	
0.125	1.25	0.101615		0.0907279	
0.125	1.5	0.101612		0.0907116	
0.125	1.75	0.101606		0.0906933	
0.125	2.0	0.101603		0.0906713	
0.125	2.25	0.101602		0.0906524	
0.125	2.5	0.101592		0.0906586	

Table C.1: The quasi-normal modes for different values of the couplings α/M^2, and β. The values ω_R^{cf}, and ω_I^{cf} are obtained using the continued fraction method.

Appendix D: Equations of chapter VIII

Contents

D.1 Effective metric coefficients

Here, we provide the coefficient α, β, and γ of the effective metric in Schwarzschild-like coordinates

$$\begin{aligned}\alpha = &\Big[e^{6B}(h+1)r^2\left(12f'h'+r^2\left(3\left(h'\right)^2+h\right)+r^2\right)+384Q\left(f'\right)^3\frac{\partial B}{\partial r}\\&-e^{4B}r\left[f'\left(P^2\left(4rf'+r^3h'\right)-12(h+1)\left(8f'\frac{\partial B}{\partial r}+rh'\left(2r\frac{\partial B}{\partial r}-1\right)\right)\right)\right.\\&\left.+8Qf'\left(12f'h'+r^2\left(3\left(h'\right)^2+h\right)+r^2\right)+Q^2r\left(4f'+r^2h'\right)\left(f'\left(4h''+1\right)-4f''h'\right)\right]\\&+4e^{2B}f'\left[-24f'\frac{\partial B}{\partial r}\left(Q\left(4f'+r^2h'\right)+hr+r\right)+P^2r^2f'\right.\\&\left.+Qr\left(24f'h'+Qr\left(f'\left(4h''+5\right)-4f''h'\right)\right)\right]\Big]\Big/\left(r^2e^{2A+2B}\left(e^{2B}(h+1)r-4Qf'\right)^2\right),\end{aligned} \tag{D.1.1}$$

$$\begin{aligned}\beta = &\frac{4e^{-2(A+B)}\left(4\left(e^{2B}-1\right)f'+e^{2B}r^2h'\right)}{r^2\left(e^{2B}(h+1)r-4Qf'\right)^2}\\&\times\left[PQr^2e^{A+B}\left(f'\left(2h''+1\right)-2f''h'\right)-12f'\frac{\partial B}{\partial t}\left(e^{2B}(h+1)r-4Qf'\right)\right],\end{aligned} \tag{D.1.2}$$

$$\begin{aligned}\gamma = &\left\{-4e^{2B}f'\left[3f'\left[8\frac{\partial A}{\partial r}\left(Q\left(4f'+r^2h'\right)+hr+r\right)+Qr\left(8h'+Qr\right)\right]\right.\right.\\&\left.-P^2r^2\left(f'\left(4h''+1\right)-4f''h'\right)\right]+384Q\left(f'\right)^3\frac{\partial A}{\partial r}\\&-e^{6B}(h+1)r^2\left(12f'h'+r^2\left(3\left(h'\right)^2+h\right)+r^2\right)\\&+e^{4B}r\left[12(h+1)f'\left(8f'\frac{\partial A}{\partial r}+rh'\left(2r\frac{\partial A}{\partial r}+1\right)\right)-Q^2rf'\left(4f'+r^2h'\right)\right.\\&\left.+8Qf'\left(12f'h'+r^2\left(3\left(h'\right)^2+h\right)+r^2\right)\right.\\&\left.\left.-P^2r\left(4f'+r^2h'\right)\left(f'\left(4h''+1\right)-4f''h'\right)\right]\right\}\Big/\left(e^{4B}r^2\left(e^{2B}(h+1)r-4Qf'\right)^2\right).\end{aligned} \tag{D.1.3}$$

D.2 Equations and the principal symbol of theory (8.6.7)

The metric equation of motion is given by [411, 461]

$$
\begin{aligned}
0 = &-\frac{1}{2}\frac{a-bX}{(a-2bX)^2}\mathcal{S}\nabla_\alpha\phi\nabla^\beta\phi - \frac{1}{2}\frac{X}{a\mathcal{S}}\delta^\beta_\alpha \\
&+\frac{1}{2}\left(\frac{-b}{\mathcal{S}} - 2X\frac{b^2}{a\mathcal{S}^3}\right)\delta^{\beta\beta_1\beta_2}_{\alpha\alpha_1\alpha_2}\nabla_{\beta_1}\nabla^{\alpha_1}\phi\nabla_{\beta_2}\nabla^{\alpha_2}\phi \\
&-\frac{1}{2}\frac{b^2}{a\mathcal{S}^3}\delta^{\beta\beta_1\beta_2\beta_3}_{\alpha\alpha_1\alpha_2\alpha_3}\nabla_{\beta_1}\nabla^{\alpha_1}\phi\nabla_{\beta_2}\nabla^{\alpha_2}\phi\nabla^{\alpha_3}\phi\nabla_{\beta_3}\phi \\
&-\frac{1}{4}(a\mathcal{S}+2X\frac{b}{\mathcal{S}})\delta^{\beta\beta_1\beta_2}_{\alpha\alpha_1\alpha_2}R^{\alpha_1\alpha_2}{}_{\beta_1\beta_2} \\
&+\frac{1}{4}\delta^{\beta\beta_1\beta_2\beta_3}_{\alpha\alpha_1\alpha_2\alpha_3}R^{\alpha_1\alpha_2}{}_{\beta_1\beta_2}\nabla^{\alpha_3}\phi\nabla_{\beta_3}\phi\,,
\end{aligned}
\tag{D.2.1}
$$

while the scalar equation is

$$
\begin{aligned}
0 = &-\frac{a-bX}{(a-2bX)^2}\mathcal{S}\Box\phi + \frac{b(2a-bX)}{(a-2bX)^3}\mathcal{S}\nabla_{\alpha_1}\phi\nabla^{\alpha_1}\nabla_{\alpha_2}\phi\nabla^{\alpha_2}\phi \\
&+\frac{1}{6}\left(3\frac{b^2}{a\mathcal{S}^3}+12X\frac{b^3}{a^2\mathcal{S}^5}\right)\delta^{\beta_1\beta_2\beta_3}_{\alpha_1\alpha_2\alpha_3}\nabla^{\alpha_1}\nabla_{\beta_1}\phi\nabla^{\alpha_2}\nabla_{\beta_2}\phi\nabla^{\alpha_3}\nabla_{\beta_3}\phi \\
&+\frac{b^3}{a^2\mathcal{S}^5}\delta^{\beta_1\beta_2\beta_3\beta_4}_{\alpha_1\alpha_2\alpha_3\alpha_4}\nabla^{\alpha_1}\nabla_{\beta_1}\phi\nabla^{\alpha_2}\nabla_{\beta_2}\phi\nabla^{\alpha_3}\nabla_{\beta_3}\phi\nabla^{\alpha_4}\phi\nabla_{\beta_4}\phi \\
&+\frac{1}{2}\left(\frac{b}{\mathcal{S}}+2X\frac{b^2}{a\mathcal{S}^3}\right)\delta^{\beta_1\beta_2\beta_3}_{\alpha_1\alpha_2\alpha_3}\nabla^{\alpha_1}\nabla_{\beta_1}\phi R^{\alpha_2\alpha_3}{}_{\beta_2\beta_3} \\
&+\frac{1}{2}\frac{b^2}{a\mathcal{S}^3}\delta^{\beta_1\beta_2\beta_3\beta_4}_{\alpha_1\alpha_2\alpha_3\alpha_4}\nabla^{\alpha_1}\nabla_{\beta_1}\phi R^{\alpha_2\alpha_3}{}_{\beta_2\beta_3}\nabla^{\alpha_4}\phi\nabla_{\beta_4}\phi\,,
\end{aligned}
\tag{D.2.2}
$$

from which we find the various components of the principal symbol, given by [411, 461]

$$
\begin{aligned}
(P_{gg}(\xi)\cdot\omega)^{\alpha}{}_{\beta} &= \frac{1}{2}\left(a\mathcal{S}+2X\frac{b}{\mathcal{S}}\right)\delta^{\alpha\alpha_1\alpha_2}_{\beta\beta_1\beta_2}\xi_{\alpha_1}\xi^{\beta_1}\omega_{\alpha_2}{}^{\beta_2} \\
&\quad+\frac{1}{2}\frac{b}{\mathcal{S}}\delta^{\alpha\alpha_1\alpha_2\alpha_3}_{\beta\beta_1\beta_2\beta_3}\xi_{\alpha_1}\xi^{\beta_1}\omega_{\alpha_2}{}^{\beta_2}\nabla_{\alpha_3}\phi\nabla^{\beta_3}\phi\,, \qquad \text{(D.2.3)}\\
P_{gm}(\xi)^{\alpha}{}_{\beta} &= \left(\frac{-b}{\mathcal{S}}-2X\frac{b^2}{a\mathcal{S}^3}\right)\delta^{\alpha\alpha_1\alpha_2}_{\beta\beta_1\beta_2}\xi_{\alpha_1}\xi^{\beta_1}\nabla_{\alpha_2}\nabla^{\beta_2}\phi \\
&\quad-\frac{b^2}{a\mathcal{S}^3}\delta^{\alpha\alpha_1\alpha_2\alpha_3}_{\beta\beta_1\beta_2\beta_3}\xi_{\alpha_1}\xi^{\beta_1}\nabla_{\alpha_2}\nabla^{\beta_2}\phi\nabla_{\alpha_3}\phi\nabla^{\beta_3}\phi\,, \qquad \text{(D.2.4)}\\
P_{mm}(\xi) &= -\left(\frac{a-bX}{(a-2bX)^2}\mathcal{S}+2X\frac{b(2a-bX)}{(a-2bX)^3}\mathcal{S}\right)\xi^2 \\
&\quad-\frac{b(2a-bX)}{(a-2bX)^3}\mathcal{S}\delta^{\alpha_1\alpha_2}_{\beta_1\beta_2}\xi_{\alpha_1}\xi^{\beta_1}\nabla_{\alpha_2}\phi\nabla^{\beta_2}\phi \\
&\quad+\frac{1}{2}\left(\frac{b}{\mathcal{S}}+2X\frac{b^2}{a\mathcal{S}^3}\right)\delta^{\alpha_1\alpha_2\alpha_3}_{\beta_1\beta_2\beta_3}\xi_{\alpha_1}\xi^{\beta_1}R_{\alpha_2\alpha_3}{}^{\beta_2\beta_3} \\
&\quad+\frac{1}{2}\frac{b^2}{a\mathcal{S}^3}\delta^{\alpha_1\alpha_2\alpha_3\alpha_4}_{\beta_1\beta_2\beta_3\beta_4}\xi_{\alpha_1}\xi^{\beta_1}\nabla_{\alpha_2}\phi\nabla^{\beta_2}\phi R_{\alpha_3\alpha_4}{}^{\beta_3\beta_4} \\
&\quad+\left(3\frac{b^2}{a\mathcal{S}^3}+2X\frac{3b^3}{a^2\mathcal{S}^5}\right)\delta^{\alpha_1\alpha_2\alpha_3}_{\beta_1\beta_2\beta_3}\xi_{\alpha_1}\xi^{\beta_1}\nabla_{\alpha_2}\nabla^{\beta_2}\phi\nabla_{\alpha_3}\nabla^{\beta_3}\phi \\
&\quad+\frac{3b^3}{a^2\mathcal{S}^5}\delta^{\alpha_1\alpha_2\alpha_3\alpha_4}_{\beta_1\beta_2\beta_3\beta_4}\xi_{\alpha_1}\xi^{\beta_1}\nabla_{\alpha_2}\nabla^{\beta_2}\phi\nabla_{\alpha_3}\nabla^{\beta_3}\phi\nabla_{\alpha_4}\phi\nabla^{\beta_4}\phi\,. \qquad \text{(D.2.5)}
\end{aligned}
$$

Bibliography

[1] A. Einstein, "Zur Allgemeinen Relativitätstheorie", Sitzungsber. Preuss. Akad. Wiss. Berlin (Math. Phys.) **1915**, [Addendum: Sitzungsber.Preuss.Akad.Wiss.Berlin (Math.Phys.) 1915, 799–801 (1915)], 778 (1915).

[2] C. M. Will, "The Confrontation between general relativity and experiment", Living Rev. Rel. **9**, 3 (2006), arXiv:gr-qc/0510072.

[3] C. M. Will, "The Confrontation between General Relativity and Experiment", Living Rev. Rel. **17**, 4 (2014), arXiv:1403.7377 [gr-qc].

[4] C. M. Will, *Theory and Experiment in Gravitational Physics* (Cambridge University Press, Sept. 2018).

[5] S. M. Carroll, *Spacetime and Geometry: An Introduction to General Relativity* (Cambridge University Press, July 2019).

[6] S. Weinberg, *Cosmology* (2008).

[7] D. Baumann, *Cosmology* (Cambridge University Press, July 2022).

[8] A. A. Penzias and R. G. Wilson, "A measurement of excess antenna temperature at 4080-mc/s", The Astrophysical Journal **142**, 419 (1965).

[9] H. P. Robertson, "Kinematics and World-Structure", Astrophys. J. **82**, 284 (1935).

[10] H. P. Robertson, "Kinematics and World-Structure. 2", Astrophys. J. **83**, 187 (1935).

[11] H. P. Robertson, "Kinematics and World-Structure. 3", Astrophys. J. **83**, 257 (1936).

[12] A. G. Walker, "On Milne's Theory of World-Structure", Proc. Lond. Math. Soc. s **2-42**, 90 (1937).

[13] A. Friedman, "On the Curvature of space", Z. Phys. **10**, 377 (1922).

[14] A. Friedman, "Über die krümmung des raumes", Zeitschrift für Physik **10**, 377 (1922).

[15] A. Friedmann, "Über die möglichkeit einer welt mit konstanter negativer krümmung des raumes", Zeitschrift für Physik **21**, 326 (1924).

[16] A. G. Lemaître, "A homogeneous universe of constant mass and increasing radius accounting for the radial velocity of extra-galactic nebulæ", Monthly Notices of the Royal Astronomical Society **91**, 483 (1931), eprint: https://academic.oup.com/mnras/article-pdf/91/5/483/3079971/mnras91-0483.pdf.

[17] A. G. Riess et al. (Supernova Search Team), "Observational evidence from supernovae for an accelerating universe and a cosmological constant", Astron. J. **116**, 1009 (1998), arXiv:astro-ph/9805201.

[18] S. Perlmutter et al. (Supernova Cosmology Project), "Measurements of Ω and Λ from 42 High Redshift Supernovae", Astrophys. J. **517**, 565 (1999), arXiv:astro-ph/9812133.

[19] E. Komatsu et al., "Seven-year Wilkinson Microwave Anisotropy Probe (WMAP) observations: Cosmological interpretation", The Astrophysical Journal Supplement Series **192**, 18 (2011).

[20] P. A. R. Ade et al. (Planck), "Planck 2015 results. XIII. Cosmological parameters", Astron. Astrophys. **594**, A13 (2016), arXiv:1502.01589 [astro-ph.CO].

[21] R. L. Workman et al. (Particle Data Group), "Review of Particle Physics", PTEP **2022**, 083C01 (2022).

[22] M. Cirelli, A. Strumia, and J. Zupan, "Dark Matter", (2024), arXiv:2406.01705 [hep-ph].

[23] G. Bertone and D. Hooper, "History of dark matter", Rev. Mod. Phys. **90**, 045002 (2018), arXiv:1605.04909 [astro-ph.CO].

[24] K. Schwarzschild, "On the gravitational field of a mass point according to Einstein's theory", Sitzungsber. Preuss. Akad. Wiss. Berlin (Math. Phys.) **1916**, 189 (1916), arXiv:physics/9905030.

[25] R. M. Wald, *General Relativity* (Chicago Univ. Pr., Chicago, USA, 1984).

[26] O. Lodge, "Xlvii. on the supposed weight and ultimate fate of radiation", The London, Edinburgh, and Dublin Philosophical Magazine and Journal of Science **41**, 549 (1921).

[27] S. Chandrasekhar, "The maximum mass of ideal white dwarfs", Astrophys. J. **74**, 81 (1931).

[28] K. C. Wali, "Chandrasekhar vs. Eddington—an unanticipated confrontation", Physics Today **35**, 33 (1982), eprint: https://pubs.aip.org/physicstoday/article-pdf/35/10/33/8289868/33_1_online.pdf.

[29] A. Celotti, J. C. Miller, and D. W. Sciama, "Astrophysical evidence for the existence of black holes: Topical review", Class. Quant. Grav. **16**, A3 (1999), arXiv:astro-ph/9912186.

[30] J. R. Oppenheimer and G. M. Volkoff, "On massive neutron cores", Phys. Rev. **55**, 374 (1939).

[31] J. R. Oppenheimer and H. Snyder, "On Continued gravitational contraction", Phys. Rev. **56**, 455 (1939).

[32] R. P. Kerr, "Gravitational field of a spinning mass as an example of algebraically special metrics", Phys. Rev. Lett. **11**, 237 (1963).

[33] B. Carter, "Axisymmetric Black Hole Has Only Two Degrees of Freedom", Phys. Rev. Lett. **26**, 331 (1971).

[34] P. T. Chrusciel, J. Lopes Costa, and M. Heusler, "Stationary Black Holes: Uniqueness and Beyond", Living Rev. Rel. **15**, 7 (2012), arXiv:1205.6112 [gr-qc].

[35] R. Penrose, "Gravitational collapse and space-time singularities", Phys. Rev. Lett. **14**, 57 (1965).

[36] S. W. Hawking, "Black holes in general relativity", Commun. Math. Phys. **25**, 152 (1972).

[37] R. Genzel, A. Eckart, T. Ott, and F. Eisenhauer, "On the nature of the dark mass in the centre of the Milky Way", Monthly Notices of the Royal Astronomical Society **291**, 219 (1997), eprint: https://academic.oup.com/mnras/article-pdf/291/1/219/4082303/291-1-219.pdf.

[38] A. M. Ghez, B. L. Klein, M. Morris, and E. E. Becklin, "High proper-motion stars in the vicinity of sagittarius a*: evidence for a supermassive black hole at the center of our galaxy", The Astrophysical Journal **509**, 678 (1998).

[39] K. Akiyama et al. (Event Horizon Telescope), "First Sagittarius A* Event Horizon Telescope Results. I. The Shadow of the Supermassive Black Hole in the Center of the Milky Way", Astrophys. J. Lett. **930**, L12 (2022), arXiv:2311.08680 [astro-ph.HE].

[40] K. Akiyama et al. (Event Horizon Telescope), "First M87 Event Horizon Telescope Results. I. The Shadow of the Supermassive Black Hole", Astrophys. J. Lett. **875**, L1 (2019), arXiv:1906.11238 [astro-ph.GA].

[41] R. Abbott et al. (KAGRA, VIRGO, LIGO Scientific), "GWTC-3: Compact Binary Coalescences Observed by LIGO and Virgo during the Second Part of the Third Observing Run", Phys. Rev. X **13**, 041039 (2023), arXiv:2111.03606 [gr-qc].

[42] A. Einstein, "Approximative Integration of the Field Equations of Gravitation", Sitzungsber. Preuss. Akad. Wiss. Berlin (Math. Phys.) **1916**, 688 (1916).

[43] A. Einstein and N. Rosen, "On Gravitational waves", J. Franklin Inst. **223**, 43 (1937).

[44] A. S. Blum, "Einstein's second-biggest blunder: The mistake in the 1936 gravitational-wave manuscript of Albert Einstein and Nathan Rosen", Archive for History of Exact Sciences **76**, 623 (2022).

[45] C. M. De Witt, ed., *Proceedings: Conference on the Role of Gravitation in Physics, Chapel Hill, North Carolina, Jan 18-23, 1957* (1957).

[46] H. Bondi, "Plane gravitational waves in general relativity", Nature **179**, 1072 (1957).

[47] J. Weber and J. A. Wheeler, "Reality of the Cylindrical Gravitational Waves of Einstein and Rosen", Rev. Mod. Phys. **29**, 509 (1957).

[48] J. Weber, "Detection and generation of gravitational waves", Phys. Rev. **117**, 306 (1960).

[49] J. Weber, "Observation of the thermal fluctuations of a gravitational-wave detector", Phys. Rev. Lett. **17**, 1228 (1966).

[50] J. Weber, "Evidence for discovery of gravitational radiation", Phys. Rev. Lett. **22**, 1320 (1969).

[51] J. Weber, "Anisotropy and polarization in the gravitational-radiation experiments", Phys. Rev. Lett. **25**, 180 (1970).

[52] S. W. Hawking and W. Israel, eds., *Three Hundred Years of Gravitation* (1987).

[53] R. A. Hulse and J. H. Taylor, "Discovery of a pulsar in a binary system", Astrophys. J. Lett. **195**, L51 (1975).

[54] J. M. Weisberg and J. H. Taylor, "Gravitational Radiation From an Orbiting Pulsar", Gen. Rel. Grav. **13**, 1 (1981).

[55] R. Weiss, "Republication of: Electromagnetically coupled broadband gravitational antenna", Gen. Rel. Grav. **54**, 153 (2022).

[56] B. P. Abbott et al. (LIGO Scientific, Virgo), "Observation of Gravitational Waves from a Binary Black Hole Merger", Phys. Rev. Lett. **116**, 061102 (2016), arXiv:1602.03837 [gr-qc].

[57] R. Abbott et al. (LIGO Scientific, VIRGO, KAGRA), "Tests of General Relativity with GWTC-3", (2021), arXiv:2112.06861 [gr-qc].

[58] E. Berti et al., "Testing General Relativity with Present and Future Astrophysical Observations", Class. Quant. Grav. **32**, 243001 (2015), arXiv:1501.07274 [gr-qc].

[59] N. Yunes, X. Siemens, and K. Yagi, "Gravitational-Wave Tests of General Relativity with Ground-Based Detectors and Pulsar-Timing Arrays", (2024), arXiv:2408.05240 [gr-qc].

[60] M. Colpi et al. (LISA), "LISA Definition Study Report", (2024), arXiv:2402.07571 [astro-ph.CO].

[61] J. R. Gair, M. Vallisneri, S. L. Larson, and J. G. Baker, "Testing General Relativity with Low-Frequency, Space-Based Gravitational-Wave Detectors", Living Rev. Rel. **16**, 7 (2013), arXiv:1212.5575 [gr-qc].

[62] K. Yagi, "Scientific Potential of DECIGO Pathfinder and Testing GR with Space-Borne Gravitational Wave Interferometers", Int. J. Mod. Phys. D **22**, 1341013 (2013), arXiv:1302.2388 [gr-qc].

[63] L. Barack et al., "Black holes, gravitational waves and fundamental physics: a roadmap", Class. Quant. Grav. **36**, 143001 (2019), arXiv:1806.05195 [gr-qc].

[64] B. P. Abbott et al. (LIGO Scientific, Virgo), "GWTC-1: A Gravitational-Wave Transient Catalog of Compact Binary Mergers Observed by LIGO and Virgo during the First and Second Observing Runs", Phys. Rev. X **9**, 031040 (2019), arXiv:1811.12907 [astro-ph.HE].

[65] R. Abbott et al. (LIGO Scientific, Virgo), "GWTC-2: Compact Binary Coalescences Observed by LIGO and Virgo During the First Half of the Third Observing Run", Phys. Rev. X **11**, 021053 (2021), arXiv:2010.14527 [gr-qc].

[66] R. Abbott et al. (LIGO Scientific, VIRGO), "GWTC-2.1: Deep extended catalog of compact binary coalescences observed by LIGO and Virgo during the first half of the third observing run", Phys. Rev. D **109**, 022001 (2024), arXiv:2108.01045 [gr-qc].

[67] M. Punturo et al., "The Einstein Telescope: A third-generation gravitational wave observatory", Class. Quant. Grav. **27**, 194002 (2010).

[68] B. Sathyaprakash et al., "Scientific Objectives of Einstein Telescope", Class. Quant. Grav. **29**, [Erratum: Class.Quant.Grav. 30, 079501 (2013)], 124013 (2012), arXiv:1206.0331 [gr-qc].

[69] E. Barausse et al., "Prospects for Fundamental Physics with LISA", Gen. Rel. Grav. **52**, 81 (2020), arXiv:2001.09793 [gr-qc].

[70] K. G. Arun et al. (LISA), "New horizons for fundamental physics with LISA", Living Rev. Rel. **25**, 4 (2022), arXiv:2205.01597 [gr-qc].

[71] C. Rovelli, "Notes for a brief history of quantum gravity", in 9th Marcel Grossmann Meeting on Recent Developments in Theoretical and Experimental General Relativity, Gravitation and Relativistic Field Theories (MG 9) (June 2000), pp. 742–768, arXiv:gr-qc/0006061.

[72] W. Heisenberg, "Die Grenzen der Anwendbarkeit der bisherigen Quantentheorie", Z. Phys. **110**, 251 (1938).

[73] M. H. Goroff and A. Sagnotti, "Quantum gravity at two loops", Phys. Lett. B **160**, 81 (1985).

[74] G. 't Hooft and M. J. G. Veltman, "One loop divergencies in the theory of gravitation", Ann. Inst. H. Poincare A Phys. Theor. **20**, 69 (1974).

[75] A. E. M. van de Ven, "Two loop quantum gravity", Nucl. Phys. B **378**, 309 (1992).

[76] K. S. Stelle, "Renormalization of Higher Derivative Quantum Gravity", Phys. Rev. D **16**, 953 (1977).

[77] M. Ostrogradsky, "Mémoires sur les équations différentielles, relatives au problème des isopérimètres", Mem. Acad. St. Petersbourg **6**, 385 (1850).

[78] R. P. Woodard, "Ostrogradsky's theorem on Hamiltonian instability", Scholarpedia **10**, 32243 (2015), arXiv:1506.02210 [hep-th].

[79] K. S. Stelle, "Classical Gravity with Higher Derivatives", Gen. Rel. Grav. **9**, 353 (1978).

[80] W. E. East and N. Siemonsen, "Instability and backreaction of massive spin-2 fields around black holes", Phys. Rev. D **108**, 124048 (2023), arXiv:2309.05096 [gr-qc].

[81] A. Held and H. Lim, "Nonlinear evolution of quadratic gravity in 3+1 dimensions", Phys. Rev. D **108**, 104025 (2023), arXiv:2306.04725 [gr-qc].

[82] A. Held and H. Lim, "Black-hole binaries and waveforms in Quadratic Gravity", (2025), arXiv:2503.13428 [gr-qc].

[83] J. F. Donoghue, "General relativity as an effective field theory: The leading quantum corrections", Phys. Rev. D **50**, 3874 (1994), arXiv:gr-qc/9405057.

[84] C. P. Burgess, "Quantum gravity in everyday life: General relativity as an effective field theory", Living Rev. Rel. **7**, 5 (2004), arXiv:gr-qc/0311082.

[85] C. P. Burgess, "Introduction to Effective Field Theory", Ann. Rev. Nucl. Part. Sci. **57**, 329 (2007), arXiv:hep-th/0701053.

[86] J. F. Donoghue, "The effective field theory treatment of quantum gravity", AIP Conf. Proc. **1483**, 73 (2012), arXiv:1209.3511 [gr-qc].

[87] C. J. Isham, "Canonical quantum gravity and the problem of time", NATO Sci. Ser. C **409**, 157 (1993), arXiv:gr-qc/9210011.

[88] S. Carlip, "Quantum gravity: A Progress report", Rept. Prog. Phys. **64**, 885 (2001), arXiv:gr-qc/0108040.

[89] R. P. Woodard, "How Far Are We from the Quantum Theory of Gravity?", Rept. Prog. Phys. **72**, 126002 (2009), arXiv:0907.4238 [gr-qc].

[90] R. Loll, G. Fabiano, D. Frattulillo, and F. Wagner, "Quantum Gravity in 30 Questions", PoS **CORFU2021**, 316 (2022), arXiv:2206.06762 [hep-th].

[91] C. Rovelli, "Time in Quantum Gravity: Physics Beyond the Schrodinger Regime", Phys. Rev. D **43**, 442 (1991).

[92] C. Rovelli, "What Is Observable in Classical and Quantum Gravity?", Class. Quant. Grav. **8**, 297 (1991).

[93] M. B. Green, J. H. Schwarz, and E. Witten, *Superstring Theory. Vol. 1: Introduction*, Cambridge Monographs on Mathematical Physics (Cambridge University Press, July 1988).

[94] J. Polchinski, *String theory. Vol. 2: Superstring theory and beyond*, Cambridge Monographs on Mathematical Physics (Cambridge University Press, Dec. 2007).

[95] J. Polchinski, *String theory. Vol. 1: An introduction to the bosonic string*, Cambridge Monographs on Mathematical Physics (Cambridge University Press, Dec. 2007).

[96] M. Ammon and J. Erdmenger, *Gauge/gravity duality: Foundations and applications* (Cambridge University Press, Cambridge, Apr. 2015).

[97] L. Smolin, in *The structural foundations of quantum gravity* (Oxford University Press, Nov. 2006), arXiv:hep-th/0507235.

[98] M. Krátký, B. Narra, and J. Read, "Is string field theory background independent?", (2025), arXiv:2509.21159 [physics.hist-ph].

[99] C. Rovelli, "Loop quantum gravity", Living Rev. Rel. **1**, 1 (1998), arXiv:gr-qc/9710008.

[100] C. Rovelli, *Quantum gravity*, Cambridge Monographs on Mathematical Physics (Univ. Pr., Cambridge, UK, 2004).

[101] A. Ashtekar and J. Lewandowski, "Background independent quantum gravity: A Status report", Class. Quant. Grav. **21**, R53 (2004), arXiv:gr-qc/0404018.

[102] T. Thiemann, *Modern Canonical Quantum General Relativity*, Cambridge Monographs on Mathematical Physics (Cambridge University Press, 2007).

[103] S. Weinberg, "Ultraviolet divergences in quantum theories of gravitation", in *General Relativity: An Einstein Centenary Survey* (1980), pp. 790–831.

[104] M. Reuter and F. Saueressig, *Quantum Gravity and the Functional Renormalization Group: The Road towards Asymptotic Safety* (Cambridge University Press, Jan. 2019).

[105] M. Niedermaier and M. Reuter, "The Asymptotic Safety Scenario in Quantum Gravity", Living Rev. Rel. **9**, 5 (2006).

[106] R. Percacci, *An Introduction to Covariant Quantum Gravity and Asymptotic Safety*, Vol. 3, 100 Years of General Relativity (World Scientific, 2017).

[107] M. Niedermaier, "The Asymptotic safety scenario in quantum gravity: An Introduction", Class. Quant. Grav. **24**, R171 (2007), arXiv:gr-qc/0610018.

[108] M. Reuter, "Nonperturbative evolution equation for quantum gravity", Phys. Rev. D **57**, 971 (1998), arXiv:hep-th/9605030.

[109] M. Reuter and F. Saueressig, "Renormalization group flow of quantum gravity in the Einstein-Hilbert truncation", Phys. Rev. D **65**, 065016 (2002), arXiv:hep-th/0110054.

[110] J. Ambjorn and R. Loll, "Nonperturbative Lorentzian quantum gravity, causality and topology change", Nucl. Phys. B **536**, 407 (1998), arXiv:hep-th/9805108.

[111] J. Ambjorn, J. Jurkiewicz, and R. Loll, "A Nonperturbative Lorentzian path integral for gravity", Phys. Rev. Lett. **85**, 924 (2000), arXiv:hep-th/0002050.

[112] J. Ambjorn, A. Goerlich, J. Jurkiewicz, and R. Loll, "Nonperturbative Quantum Gravity", Phys. Rept. **519**, 127 (2012), arXiv:1203.3591 [hep-th].

[113] S. W. Hawking and G. F. R. Ellis, *The Large Scale Structure of Space-Time*, Cambridge Monographs on Mathematical Physics (Cambridge University Press, Feb. 2023).

[114] J. M. M. Senovilla and D. Garfinkle, "The 1965 Penrose singularity theorem", Class. Quant. Grav. **32**, 124008 (2015), arXiv:1410.5226 [gr-qc].

[115] R. Penrose, "Gravitational collapse: The role of general relativity", Riv. Nuovo Cim. **1**, 252 (1969).

[116] M. Dafermos, "The mathematical analysis of black holes in general relativity", (2014), eprint: https://api.semanticscholar.org/CorpusID:44229194.

[117] J. Sbierski, "On the Existence of a Maximal Cauchy Development for the Einstein Equations: a Dezornification", Annales Henri Poincare **17**, 301 (2016), arXiv:1309.7591 [gr-qc].

[118] Y. Choquet-Bruhat and R. P. Geroch, "Global aspects of the Cauchy problem in general relativity", Commun. Math. Phys. **14**, 329 (1969).

[119] R. M. Wald, "Gravitational collapse and cosmic censorship", in *Black holes, gravitational radiation and the universe: essays in honor of C.V. Vishveshwara*, edited by B. R. Iyer and B. Bhawal (Springer Netherlands, Dordrecht, 1999), pp. 69–86, arXiv:gr-qc/9710068.

[120] J. Isenberg, "On strong cosmic censorship", Surveys Diff. Geom. **20**, 17 (2015), arXiv:1505.06390 [gr-qc].

[121] M. Van de Moortel, "The Strong Cosmic Censorship Conjecture", (2025), arXiv:2501.13180 [gr-qc].

[122] M. Abdul Karim et al. (DESI), "DESI DR2 Results II: Measurements of Baryon Acoustic Oscillations and Cosmological Constraints", (2025), arXiv:2503.14738 [astro-ph.CO].

[123] K. Lodha et al. (DESI), "Extended Dark Energy analysis using DESI DR2 BAO measurements", (2025), arXiv:2503.14743 [astro-ph.CO].

[124] E. Hubble and M. L. Humason, "The Velocity-Distance Relation among Extra-Galactic Nebulae", Astrophys. J. **74**, 43 (1931).

[125] V. C. Rubin and W. K. Ford Jr., "Rotation of the Andromeda Nebula from a Spectroscopic Survey of Emission Regions", Astrophys. J. **159**, 379 (1970).

[126] V. C. Rubin, N. Thonnard, and W. K. Ford Jr., "Rotational properties of 21 SC galaxies with a large range of luminosities and radii, from NGC 4605 (R = 4kpc) to UGC 2885 (R = 122 kpc)", Astrophys. J. **238**, 471 (1980).

[127] D. N. Spergel et al. (WMAP), "First year Wilkinson Microwave Anisotropy Probe (WMAP) observations: Determination of cosmological parameters", Astrophys. J. Suppl. **148**, 175 (2003), arXiv:astro-ph/0302209.

[128] G. Bertone, D. Hooper, and J. Silk, "Particle dark matter: Evidence, candidates and constraints", Phys. Rept. **405**, 279 (2005), arXiv:hep-ph/0404175.

[129] B. Carr and F. Kuhnel, "Primordial Black Holes as Dark Matter: Recent Developments", Ann. Rev. Nucl. Part. Sci. **70**, 355 (2020), arXiv:2006.02838 [astro-ph.CO].

[130] G. Jungman, M. Kamionkowski, and K. Griest, "Supersymmetric dark matter", Phys. Rept. **267**, 195 (1996), arXiv:hep-ph/9506380.

[131] B. Dasgupta and J. Kopp, "Sterile Neutrinos", Phys. Rept. **928**, 1 (2021), arXiv:2106.05913 [hep-ph].

[132] A. Ringwald, "Axions and Axion-Like Particles", in 49th Rencontres de Moriond on Electroweak Interactions and Unified Theories (2014), pp. 223–230, arXiv:1407.0546 [hep-ph].

[133] D. J. E. Marsh, "Axion Cosmology", Phys. Rept. **643**, 1 (2016), arXiv:1510.07633 [astro-ph.CO].

[134] G. F. Chapline, "Cosmological effects of primordial black holes", Nature **253**, 251 (1975).

[135] P. Meszaros, "Primeval black holes and galaxy formation", Astron. Astrophys. **38**, 5 (1975).

[136] B. J. Carr, "The Primordial black hole mass spectrum", Astrophys. J. **201**, 1 (1975).

[137] S. Clesse and J. García-Bellido, "Massive Primordial Black Holes from Hybrid Inflation as Dark Matter and the seeds of Galaxies", Phys. Rev. D **92**, 023524 (2015), arXiv:1501.07565 [astro-ph.CO].

[138] M. Sasaki, T. Suyama, T. Tanaka, and S. Yokoyama, "Primordial black holes—perspectives in gravitational wave astronomy", Class. Quant. Grav. **35**, 063001 (2018), arXiv:1801.05235 [astro-ph.CO].

[139] A. M. Green and B. J. Kavanagh, "Primordial Black Holes as a dark matter candidate", J. Phys. G **48**, 043001 (2021), arXiv:2007.10722 [astro-ph.CO].

[140] B. Carr, K. Kohri, Y. Sendouda, and J. Yokoyama, "Constraints on primordial black holes", Rept. Prog. Phys. **84**, 116902 (2021), arXiv:2002.12778 [astro-ph.CO].

[141] Y. B. Zel'dovich and I. D. Novikov, "The Hypothesis of Cores Retarded during Expansion and the Hot Cosmological Model", Sov. Astron. **10**, 602 (1967).

[142] S. Hawking, "Gravitationally collapsed objects of very low mass", Mon. Not. Roy. Astron. Soc. **152**, 75 (1971).

[143] B. J. Carr and S. W. Hawking, "Black holes in the early Universe", Mon. Not. Roy. Astron. Soc. **168**, 399 (1974).

[144] P. Meszaros, "The behaviour of point masses in an expanding cosmological substratum", Astron. Astrophys. **37**, 225 (1974).

[145] M. Y. Khlopov, B. A. Malomed, I. B. Zeldovich, and Y. B. Zeldovich, "Gravitational instability of scalar fields and formation of primordial black holes", Mon. Not. Roy. Astron. Soc. **215**, 575 (1985).

[146] H. I. Kim, C. H. Lee, and J. H. MacGibbon, "Diffuse gamma-ray background and primordial black hole constraints on the spectral index of density fluctuations", Phys. Rev. D **59**, 063004 (1999), arXiv:astro-ph/9901030.

[147] J. Yokoyama, "Cosmological constraints on primordial black holes produced in the near critical gravitational collapse", Phys. Rev. D **58**, 107502 (1998), arXiv:gr-qc/9804041.

[148] S. S. Gershtein and Y. B. Zeldovich, "Rest Mass of Muonic Neutrino and Cosmology", JETP Lett. **4**, 120 (1966).

[149] R. Cowsik and J. McClelland, "An Upper Limit on the Neutrino Rest Mass", Phys. Rev. Lett. **29**, 669 (1972).

[150] A. S. Szalay and G. Marx, "Neutrino rest mass from cosmology", Astron. Astrophys. **49**, 437 (1976).

[151] P. Hut, "Limits on Masses and Number of Neutral Weakly Interacting Particles", Phys. Lett. B **69**, 85 (1977).

[152] K. Sato and M. Kobayashi, "Cosmological Constraints on the Mass and the Number of Heavy Lepton Neutrinos", Prog. Theor. Phys. **58**, 1775 (1977).

[153] B. W. Lee and S. Weinberg, "Cosmological Lower Bound on Heavy Neutrino Masses", Phys. Rev. Lett. **39**, 165 (1977).

[154] D. A. Dicus, E. W. Kolb, and V. L. Teplitz, "Cosmological Upper Bound on Heavy Neutrino Lifetimes", Phys. Rev. Lett. **39**, [Erratum: Phys.Rev.Lett. 39, 973 (1977)], 168 (1977).

[155] M. I. Vysotsky, A. D. Dolgov, and Y. B. Zeldovich, "Cosmological Restriction on Neutral Lepton Masses", JETP Lett. **26**, 188 (1977).

[156] J. E. Gunn, B. W. Lee, I. Lerche, D. N. Schramm, and G. Steigman, "Some astrophysical consequences of the existence of a heavy stable neutral lepton", The Astrophysical Journal **223**, 1015 (1978).

[157] A. G. Doroshkevich, Y. B. Zeldovich, R. A. Sunyaev, and M. Khlopov, "Astrophysical implications of the neutrino rest mass. II. The density-perturbation spectrum and small-scale fluctuations in the microwave background", Sov. Astron. Lett. **6**, 252 (1980).

[158] A. G. Doroshkevich, Y. B. Zeldovich, R. A. Sunyaev, and M. Khlopov, "Astrophysical implications of the neutrino rest mass. III. Nonlinear growth of perturbations and the missing mass", Sov. Astron. Lett. **6**, 257 (1980).

[159] Y. B. Zeldovich, A. A. Klypin, M. Y. Khlopov, and V. M. Chechetkin, "Astrophysical constraints on the mass of heavy stable neutral leptons", Sov. J. Nucl. Phys. **31**, 664 (1980).

[160] P. J. E. Peebles, "Primeval adiabatic perturbations - effect of massive neutrinos", The Astrophysical Journal **258**, 415 (1982).

[161] D. N. Schramm and G. Steigman, "Relic Neutrinos and the Density of the Universe", Astrophys. J. **243**, 1 (1981).

[162] S. D. M. White, C. S. Frenk, and M. Davis, "Clustering in a Neutrino Dominated Universe", Astrophys. J. Lett. **274**, L1 (1983).

[163] S. Dodelson and L. M. Widrow, "Sterile-neutrinos as dark matter", Phys. Rev. Lett. **72**, 17 (1994), arXiv:hep-ph/9303287.

[164] K. Abazajian, G. M. Fuller, and M. Patel, "Sterile neutrino hot, warm, and cold dark matter", Phys. Rev. D **64**, 023501 (2001), arXiv:astro-ph/0101524.

[165] G. Steigman and M. S. Turner, "Cosmological Constraints on the Properties of Weakly Interacting Massive Particles", Nucl. Phys. B **253**, 375 (1985).

[166] P. Gondolo and G. Gelmini, "Cosmic abundances of stable particles: Improved analysis", Nucl. Phys. B **360**, 145 (1991).

[167] M. Srednicki, R. Watkins, and K. A. Olive, "Calculations of Relic Densities in the Early Universe", Nucl. Phys. B **310**, 693 (1988).

[168] K. Griest and D. Seckel, "Three exceptions in the calculation of relic abundances", Phys. Rev. D **43**, 3191 (1991).

[169] G. Bertone, "The moment of truth for WIMP Dark Matter", Nature **468**, 389 (2010), arXiv:1011.3532 [astro-ph.CO].

[170] L. Roszkowski, E. M. Sessolo, and S. Trojanowski, "WIMP dark matter candidates and searches—current status and future prospects", Rept. Prog. Phys. **81**, 066201 (2018), arXiv:1707.06277 [hep-ph].

[171] S. Weinberg, *The quantum theory of fields: volume 3, supersymmetry* (Cambridge University Press, 2005).

[172] J.-L. Gervais and B. Sakita, "Field Theory Interpretation of Supergauges in Dual Models", Nucl. Phys. B **34**, 632 (1971).

[173] Y. A. Golfand and E. P. Likhtman, "Extension of the Algebra of Poincare Group Generators and Violation of p Invariance", JETP Lett. **13**, 323 (1971).

[174] D. V. Volkov and V. P. Akulov, "Possible universal neutrino interaction", JETP Lett. **16**, 438 (1972).

[175] J. Wess and B. Zumino, "Supergauge Transformations in Four-Dimensions", Nucl. Phys. B **70**, 39 (1974).

[176] H. Pagels and J. R. Primack, "Supersymmetry, Cosmology and New TeV Physics", Phys. Rev. Lett. **48**, 223 (1982).

[177] S. Dimopoulos and H. Georgi, "Softly Broken Supersymmetry and SU(5)", Nucl. Phys. B **193**, 150 (1981).

[178] R. D. Peccei and H. R. Quinn, "Constraints Imposed by CP Conservation in the Presence of Instantons", Phys. Rev. D **16**, 1791 (1977).

[179] R. D. Peccei and H. R. Quinn, "CP Conservation in the Presence of Instantons", Phys. Rev. Lett. **38**, 1440 (1977).

[180] F. Wilczek, "Problem of Strong P and T Invariance in the Presence of Instantons", Phys. Rev. Lett. **40**, 279 (1978).

[181] S. Weinberg, "A New Light Boson?", Phys. Rev. Lett. **40**, 223 (1978).

[182] M. Dine, W. Fischler, and M. Srednicki, "A Simple Solution to the Strong CP Problem with a Harmless Axion", Phys. Lett. B **104**, 199 (1981).

[183] J. E. Kim, "Weak Interaction Singlet and Strong CP Invariance", Phys. Rev. Lett. **43**, 103 (1979).

[184] M. A. Shifman, A. I. Vainshtein, and V. I. Zakharov, "Can Confinement Ensure Natural CP Invariance of Strong Interactions?", Nucl. Phys. B **166**, 493 (1980).

[185] M. Milgrom, "A modification of the newtonian dynamics as a possible alternative to the hidden mass hypothesis", The Astrophysical Journal **270**, 365 (1983).

[186] M. Milgrom, "MOND theory", Can. J. Phys. **93**, 107 (2015), arXiv:1404.7661 [astro-ph.CO].

[187] J. D. Bekenstein, "Relativistic gravitation theory for the MOND paradigm", Phys. Rev. D **70**, [Erratum: Phys.Rev.D 71, 069901 (2005)], 083509 (2004), arXiv:astro-ph/0403694.

[188] K. G. Begeman, A. H. Broeils, and R. H. Sanders, "Extended rotation curves of spiral galaxies: Dark haloes and modified dynamics", Mon. Not. Roy. Astron. Soc. **249**, 523 (1991).

[189] M. Milgrom and R. H. Sanders, "MOND predictions of halo phenomenology in disc galaxies", Mon. Not. Roy. Astron. Soc. **357**, 45 (2005), arXiv:astro-ph/0406487.

[190] M. Milgrom and R. H. Sanders, "MOND rotation curves of very low mass spiral galaxies", Astrophys. J. Lett. **658**, L17 (2007), arXiv:astro-ph/0611494.

[191] R. H. Sanders, "The published extended rotation curves of spiral galaxies: confrontation with modified dynamics", Astrophys. J. **473**, 117 (1996), arXiv:astro-ph/9606089.

[192] S. Dodelson and M. Liguori, "Can Cosmic Structure form without Dark Matter?", Phys. Rev. Lett. **97**, 231301 (2006), arXiv:astro-ph/0608602.

[193] C. Skordis, D. F. Mota, P. G. Ferreira, and C. Boehm, "Large Scale Structure in Bekenstein's theory of relativistic Modified Newtonian Dynamics", Phys. Rev. Lett. **96**, 011301 (2006), arXiv:astro-ph/0505519.

[194] C. Skordis, "Generalizing tensor-vector-scalar cosmology", Phys. Rev. D **77**, 123502 (2008), arXiv:0801.1985 [astro-ph].

[195] C. Skordis, "The tensor-vector-scalar theory and its cosmology", Classical and Quantum Gravity **26**, 143001 (2009).

[196] B. Famaey and S. McGaugh, "Modified Newtonian Dynamics (MOND): Observational Phenomenology and Relativistic Extensions", Living Rev. Rel. **15**, 10 (2012), arXiv:1112.3960 [astro-ph.CO].

[197] B. P. Schmidt et al. (Supernova Search Team), "The High Z supernova search: Measuring cosmic deceleration and global curvature of the universe using type Ia supernovae", Astrophys. J. **507**, 46 (1998), arXiv:astro-ph/9805200.

[198] P. M. Garnavich et al. (Supernova Search Team), "Supernova limits on the cosmic equation of state", Astrophys. J. **509**, 74 (1998), arXiv:astro-ph/9806396.

[199] W. L. Freedman et al. (HST), "Final results from the Hubble Space Telescope key project to measure the Hubble constant", Astrophys. J. **553**, 47 (2001), arXiv:astro-ph/0012376.

[200] A. G. Riess et al. (Supernova Search Team), "Type Ia supernova discoveries at z > 1 from the Hubble Space Telescope: Evidence for past deceleration and constraints on dark energy evolution", Astrophys. J. **607**, 665 (2004), arXiv:astro-ph/0402512.

[201] P. Astier et al. (SNLS), "The Supernova Legacy Survey: Measurement of Ω_M, Ω_Λ and w from the first year data set", Astron. Astrophys. **447**, 31 (2006), arXiv:astro-ph/0510447.

[202] M. Kowalski et al. (Supernova Cosmology Project), "Improved Cosmological Constraints from New, Old and Combined Supernova Datasets", Astrophys. J. **686**, 749 (2008), arXiv:0804.4142 [astro-ph].

[203] R. Kessler et al., "First-year Sloan Digital Sky Survey-II Supernova results: Hubble diagram and cosmological parameters", The Astrophysical Journal Supplement Series **185**, 32 (2009).

[204] R. Amanullah et al., "Spectra and Hubble space telescope light curves of six type ia supernovae at 0.511 < z < 1.12 and the union2 compilation", The Astrophysical Journal **716**, 712 (2010).

[205] N. Suzuki et al., "The hubble space telescope cluster supernova survey. v. improving the dark-energy constraints above z > 1 and building an early-type-hosted supernova sample", The Astrophysical Journal **746** (2011).

[206] M. Sako et al. (SDSS), "The Data Release of the Sloan Digital Sky Survey-II Supernova Survey", Publ. Astron. Soc. Pac. **130**, 064002 (2018), arXiv:1401.3317 [astro-ph.CO].

[207] P. de Bernardis et al. (Boomerang), "A Flat universe from high resolution maps of the cosmic microwave background radiation", Nature **404**, 955 (2000), arXiv:astro-ph/0004404.

[208] A. E. Lange et al. (Boomerang), "Cosmological parameters from the first results of BOOMERANG", Phys. Rev. D **63**, 042001 (2001), arXiv:astro-ph/0005004.

[209] A. Balbi et al., "Constraints on cosmological parameters from MAXIMA-1", Astrophys. J. Lett. **545**, [Erratum: Astrophys.J.Lett. 558, L145–L146 (2001), Erratum: Astrophys.J. 558, L145–L146 (2001)], L1 (2000), arXiv:astro-ph/0005124.

[210] C. Pryke, N. W. Halverson, E. M. Leitch, J. Kovac, J. E. Carlstrom, W. L. Holzapfel, and M. Dragovan, "Cosmological parameter extraction from the first season of observations with DASI", Astrophys. J. **568**, 46 (2002), arXiv:astro-ph/0104490.

[211] G. F. Hinshaw et al., "Nine-year Wilkinson Microwave Anisotropy Probe (WMAP) observations: Cosmological parameter results", The Astrophysical Journal Supplement Series **208** (2012).

[212] Z. Hou et al., "Constraints on cosmology from the cosmic microwave background power spectrum of the 2500 deg2 spt-sz survey", The Astrophysical Journal **782** (2012).

[213] P. Ade et al., "Planck 2013 results. xvi. cosmological parameters", Astronomy and Astrophysics **571** (2013).

[214] K. T. Story et al., "A measurement of the cosmic microwave background damping tail from the 2500-square-degree spt-sz survey", The Astrophysical Journal **779** (2012).

[215] J. L. Sievers et al. (Atacama Cosmology Telescope), "The Atacama Cosmology Telescope: Cosmological parameters from three seasons of data", JCAP **10**, 060 (2013), arXiv:1301.0824 [astro-ph.CO].

[216] M. Tegmark et al. (SDSS), "Cosmological parameters from SDSS and WMAP", Phys. Rev. D **69**, 103501 (2004), arXiv:astro-ph/0310723.

[217] U. Seljak et al. (SDSS), "Cosmological parameter analysis including SDSS Ly-alpha forest and galaxy bias: Constraints on the primordial spectrum of fluctuations, neutrino mass, and dark energy", Phys. Rev. D **71**, 103515 (2005), arXiv:astro-ph/0407372.

[218] D. J. Eisenstein et al. (SDSS), "Detection of the Baryon Acoustic Peak in the Large-Scale Correlation Function of SDSS Luminous Red Galaxies", Astrophys. J. **633**, 560 (2005), arXiv:astro-ph/0501171.

[219] C. Blake et al., "The wigglez dark energy survey: mapping the distance-redshift relation with baryon acoustic oscillations", Monthly Notices of the Royal Astronomical Society **418**, 1707 (2011).

[220] F. Beutler et al., "The 6df galaxy survey: baryon acoustic oscillations and the local hubble constant", Monthly Notices of the Royal Astronomical Society **416**, 3017 (2011).

[221] K. S. Dawson et al., "The baryon oscillation spectroscopic survey of sdss-iii", The Astronomical Journal **145** (2012).

[222] L. Anderson et al., "The clustering of galaxies in the sdss-iii baryon oscillation spectroscopic survey: baryon acoustic oscillations in the data release 9 spectroscopic galaxy sample", in (2012).

[223] L. Samushia et al., "The clustering of galaxies in the sdss-iii dr9 baryon oscillation spectroscopic survey: testing deviations from Λ and general relativity using anisotropic clustering of galaxies", Monthly Notices of the Royal Astronomical Society **429**, 1514 (2012).

[224] S. Weinberg, "The Cosmological Constant Problem", Rev. Mod. Phys. **61**, 1 (1989).

[225] J. Polchinski, "The Cosmological Constant and the String Landscape", in 23rd Solvay Conference in Physics: The Quantum Structure of Space and Time (Mar. 2006), pp. 216–236, arXiv:hep-th/0603249.

[226] C. P. Burgess, "The Cosmological Constant Problem: Why it's hard to get Dark Energy from Micro-physics", in 100e Ecole d'Ete de Physique: Post-Planck Cosmology (2015), pp. 149–197, arXiv:1309.4133 [hep-th].

[227] J. Martin, "Everything You Always Wanted To Know About The Cosmological Constant Problem (But Were Afraid To Ask)", Comptes Rendus Physique **13**, 566 (2012), arXiv:1205.3365 [astro-ph.CO].

[228] S. Nobbenhuis, "Categorizing different approaches to the cosmological constant problem", Found. Phys. **36**, 613 (2006), arXiv:gr-qc/0411093.

[229] S. M. Carroll, "The Cosmological constant", Living Rev. Rel. **4**, 1 (2001), arXiv:astro-ph/0004075.

[230] A. Padilla, "Lectures on the Cosmological Constant Problem", (2015), arXiv:1502.05296 [hep-th].

[231] V. Sahni and A. A. Starobinsky, "The Case for a positive cosmological Lambda term", Int. J. Mod. Phys. D **9**, 373 (2000), arXiv:astro-ph/9904398.

[232] P. J. E. Peebles and B. Ratra, "The Cosmological Constant and Dark Energy", Rev. Mod. Phys. **75**, 559 (2003), arXiv:astro-ph/0207347.

[233] T. Padmanabhan, "Cosmological constant: The Weight of the vacuum", Phys. Rept. **380**, 235 (2003), arXiv:hep-th/0212290.

[234] E. J. Copeland, M. Sami, and S. Tsujikawa, "Dynamics of dark energy", Int. J. Mod. Phys. D **15**, 1753 (2006), arXiv:hep-th/0603057.

[235] E. V. Linder, "The Dynamics of Quintessence, The Quintessence of Dynamics", Gen. Rel. Grav. **40**, 329 (2008), arXiv:0704.2064 [astro-ph].

[236] J. Frieman, M. Turner, and D. Huterer, "Dark Energy and the Accelerating Universe", Ann. Rev. Astron. Astrophys. **46**, 385 (2008), arXiv:0803.0982 [astro-ph].

[237] M. Li, X.-D. Li, S. Wang, and Y. Wang, "Dark Energy", Commun. Theor. Phys. **56**, 525 (2011), arXiv:1103.5870 [astro-ph.CO].

[238] S. Tsujikawa, "Quintessence: A Review", Class. Quant. Grav. **30**, 214003 (2013), arXiv:1304.1961 [gr-qc].

[239] Y. Fujii, "Origin of the Gravitational Constant and Particle Masses in Scale Invariant Scalar - Tensor Theory", Phys. Rev. D **26**, 2580 (1982).

[240] L. H. Ford, "Cosmological-constant damping by unstable scalar fields", Phys. Rev. D **35**, 2339 (1987).

[241] C. Wetterich, "Cosmology and the Fate of Dilatation Symmetry", Nucl. Phys. B **302**, 668 (1988), arXiv:1711.03844 [hep-th].

[242] P. J. E. Peebles and B. Ratra, "Cosmology with a Time Variable Cosmological Constant", Astrophys. J. Lett. **325**, L17 (1988).

[243] B. Ratra and P. J. E. Peebles, "Cosmological Consequences of a Rolling Homogeneous Scalar Field", Phys. Rev. D **37**, 3406 (1988).

[244] R. R. Caldwell, R. Dave, and P. J. Steinhardt, "Cosmological imprint of an energy component with general equation of state", Phys. Rev. Lett. **80**, 1582 (1998), arXiv:astro-ph/9708069.

[245] C. F. Kolda and D. H. Lyth, "Quintessential difficulties", Phys. Lett. B **458**, 197 (1999), arXiv:hep-ph/9811375.

[246] L.-M. Wang, R. R. Caldwell, J. P. Ostriker, and P. J. Steinhardt, "Cosmic concordance and quintessence", Astrophys. J. **530**, 17 (2000), arXiv:astro-ph/9901388.

[247] T. Chiba, T. Okabe, and M. Yamaguchi, "Kinetically driven quintessence", Phys. Rev. D **62**, 023511 (2000), arXiv:astro-ph/9912463.

[248] C. Armendariz-Picon, V. F. Mukhanov, and P. J. Steinhardt, "A Dynamical solution to the problem of a small cosmological constant and late time cosmic acceleration", Phys. Rev. Lett. **85**, 4438 (2000), arXiv:astro-ph/0004134.

[249] H. Bernardo, B. Bose, G. Franzmann, S. Hagstotz, Y. He, A. Litsa, and F. Niedermann (Foundational Aspects of Dark Energy (FADE)), "Modified Gravity Approaches to the Cosmological Constant Problem", Universe **9**, 63 (2023), arXiv:2210.06810 [gr-qc].

[250] J. Khoury, J. Sakstein, and A. R. Solomon, "Superfluids and the Cosmological Constant Problem", JCAP **08**, 024 (2018), arXiv:1805.05937 [hep-th].

[251] N. Arkani-Hamed, S. Dimopoulos, G. Dvali, and G. Gabadadze, "Nonlocal modification of gravity and the cosmological constant problem", (2002), arXiv:hep-th/0209227.

[252] F. Niedermann and A. Padilla, "Gravitational Mechanisms to Self-Tune the Cosmological Constant: Obstructions and Ways Forward", Phys. Rev. Lett. **119**, 251306 (2017), arXiv:1706.04778 [hep-th].

[253] A. Joyce, B. Jain, J. Khoury, and M. Trodden, "Beyond the Cosmological Standard Model", Phys. Rept. **568**, 1 (2015), arXiv:1407.0059 [astro-ph.CO].

[254] J. Khoury, "Les Houches Lectures on Physics Beyond the Standard Model of Cosmology", (2013), arXiv:1312 . 2006 [astro-ph.CO].

[255] A. Einstein, "The foundation of the general theory of relativity.", Annalen Phys. **49**, 769 (1916).

[256] H. Bondi, "Negative Mass in General Relativity", Rev. Mod. Phys. **29**, 423 (1957).

[257] J. Norton, "What was Einstein's principle of equivalence?", Studies in History and Philosophy of Science Part A **16**, 203 (1985).

[258] D. Lehmkuhl, in *The Routledge Companion to Philosophy of Physics*, edited by E. Knox and A. Wilson (Routledge, 2022).

[259] H. C. Ohanian, "What is the principle of equivalence", American Journal of Physics **45**, 903 (1977).

[260] E. Di Casola, S. Liberati, and S. Sonego, "Nonequivalence of equivalence principles", Am. J. Phys. **83**, 39 (2015), arXiv:1310.7426 [gr-qc].

[261] R. V. Eotvos, D. Pekar, and E. Fekete, "CONTRIBUTIONS TO THE LAW OF PROPORTIONALITY OF INERTIA AND GRAVITY", Annalen Phys. **68**, 11 (1922).

[262] R. Dicke, *Gravitation and the universe*, American Philosophical Society: Memoirs of the American Philosophical Society (American Philosophical Society, 1970).

[263] V. B. Braginskii and V. I. Panov, "Verification of equivalence of inertial and gravitational masses", Zh. Eksp. Teor. Fiz. **61**, 873 (1971).

[264] E. G. Adelberger, "New tests of Einstein's equivalence principle and Newton's inverse-square law", Classical and Quantum Gravity **18**, 2397 (2001).

[265] S. Schlamminger, K. .-. Choi, T. A. Wagner, J. H. Gundlach, and E. G. Adelberger, "Test of the equivalence principle using a rotating torsion balance", Phys. Rev. Lett. **100**, 041101 (2008), arXiv:0712.0607 [gr-qc].

[266] T. A. Wagner, S. Schlamminger, J. H. Gundlach, and E. G. Adelberger, "Torsion-balance tests of the weak equivalence principle", Class. Quant. Grav. **29**, 184002 (2012), arXiv:1207 . 2442 [gr-qc].

[267] P. Touboul et al. (MICROSCOPE), "MICROSCOPE Mission: Final Results of the Test of the Equivalence Principle", Phys. Rev. Lett. **129**, 121102 (2022), arXiv:2209.15487 [gr-qc].

[268] C. C. Speake and C. M. Will, "Tests of the weak equivalence principle", Classical and Quantum Gravity **29**, 180301 (2012).

[269] F. Kottler, "Über Einsteins Äquivalenzhypothese und die Gravitation", Annalen der Physik **355**, 955 (1916).

[270] J. Synge, *Relativity: the general theory*, North-Holland series in physics v. 1 (North-Holland Publishing Company, 1960).

[271] R. Dicke, *The theoretical significance of experimental relativity*, Documents on modern physics (Gordon and Breach, 1965).

[272] T. Clifton, P. G. Ferreira, A. Padilla, and C. Skordis, "Modified Gravity and Cosmology", Phys. Rept. **513**, 1 (2012), arXiv:1106.2476 [astro-ph.CO].

[273] K. S. Thorne, D. L. Lee, and A. P. Lightman, "Foundations for a Theory of Gravitation Theories", Phys. Rev. D **7**, 3563 (1973).

[274] J. D. Norton, "General covariance and the foundations of general relativity: eight decades of dispute", Reports of Progress in Physics **56**, 791 (1993).

[275] E. Kretschmann, "Über den physikalischen sinn der relativitätspostulate", Annalen Der Physik **53**, 575 (1917).

[276] C. W. Misner, K. S. Thorne, and J. A. Wheeler, *Gravitation* (W. H. Freeman, San Francisco, 1973).

[277] P. G. Bergmann, "Topics in the theory of general relativity. In Lectures in Theoretical Physics, Brandeis University Summer Institute in Theoretical Physics", (1957).

[278] J. Anderson, *Principles of relativity physics* (Academic Press, 1967).

[279] J. L. Anderson, "Covariance, invariance, and equivalence: a viewpoint", General Relativity and Gravitation **2**, 161 (1971).

[280] D. Giulini, "Some remarks on the notions of general covariance and background independence", Lect. Notes Phys. **721**, 105 (2007), arXiv:gr-qc/0603087.

[281] L. I. Schiff, "On Experimental Tests of the General Theory of Relativity", American Journal of Physics **28**, 340 (1960).

[282] R. H. Dicke, "Eötvös Experiment and the Gravitational Red Shift", American Journal of Physics **28**, 344 (1960).

[283] K. S. Thorne and C. M. Will, "Theoretical Frameworks for Testing Relativistic Gravity. I. Foundations", Astrophys. J. **163**, 595 (1971).

[284] K. Nordtvedt, "Equivalence Principle for Massive Bodies. 1. Phenomenology", Phys. Rev. **169**, 1014 (1968).

[285] C. M. Will and K. Nordtvedt Jr., "Conservation Laws and Preferred Frames in Relativistic Gravity. I. Preferred-Frame Theories and an Extended PPN Formalism", Astrophys. J. **177**, 757 (1972).

[286] C. M. Will, "Relativistic Gravity tn the Solar System. 111. Experimental Disproof of a Class of Linear Theories of Gravitation", Astrophys. J. **185**, 31 (1973).

[287] C. Brans and R. H. Dicke, "Mach's principle and a relativistic theory of gravitation", Phys. Rev. **124**, 925 (1961).

[288] R. H. Dicke, "Mach's principle and invariance under transformation of units", Phys. Rev. **125**, 2163 (1962).

[289] T. P. Sotiriou, V. Faraoni, and S. Liberati, "Theory of gravitation theories: A No-progress report", Int. J. Mod. Phys. D **17**, 399 (2008), arXiv:0707.2748 [gr-qc].

[290] E. Poisson, *A Relativist's Toolkit: The Mathematics of Black-Hole Mechanics* (Cambridge University Press, Dec. 2009).

[291] J. W. York Jr., "Role of conformal three geometry in the dynamics of gravitation", Phys. Rev. Lett. **28**, 1082 (1972).

[292] G. W. Gibbons and S. W. Hawking, "Action Integrals and Partition Functions in Quantum Gravity", Phys. Rev. D **15**, 2752 (1977).

[293] L. Lehner, R. C. Myers, E. Poisson, and R. D. Sorkin, "Gravitational action with null boundaries", Phys. Rev. D **94**, 084046 (2016), arXiv:1609.00207 [hep-th].

[294] D. Lovelock, "The Einstein tensor and its generalizations", J. Math. Phys. **12**, 498 (1971).

[295] D. Lovelock, "The four-dimensionality of space and the einstein tensor", J. Math. Phys. **13**, 874 (1972).

[296] T. Kaluza, "Zum Unitätsproblem der Physik", Sitzungsber. Preuss. Akad. Wiss. Berlin (Math. Phys.) **1921**, 966 (1921), arXiv:1803.08616 [physics.hist-ph].

[297] H. Ruegg and M. Ruiz-Altaba, "The Stueckelberg field", Int. J. Mod. Phys. A **19**, 3265 (2004), arXiv:hep-th/0304245.

[298] S. Capozziello and M. De Laurentis, "Extended Theories of Gravity", Phys. Rept. **509**, 167 (2011), arXiv:1108.6266 [gr-qc].

[299] E. E. Flanagan, "The conformal frame freedom in theories of gravitation", Class. Quant. Grav. **21**, 3817 (2004), arXiv:gr - qc / 0403063.

[300] V. Faraoni and S. Nadeau, "The (pseudo)issue of the conformal frame revisited", Phys. Rev. D **75**, 023501 (2007), arXiv:gr-qc/0612075.

[301] G. W. Horndeski, "Second-order scalar-tensor field equations in a four-dimensional space", Int. J. Theor. Phys. **10**, 363 (1974).

[302] C. Deffayet, S. Deser, and G. Esposito-Farese, "Generalized Galileons: All scalar models whose curved background extensions maintain second-order field equations and stress-tensors", Phys. Rev. D **80**, 064015 (2009), arXiv:0906.1967 [gr-qc].

[303] S. Weinberg, "Effective Field Theory for Inflation", Phys. Rev. D **77**, 123541 (2008), arXiv:0804.4291 [hep-th].

[304] T. Kobayashi, M. Yamaguchi, and J. Yokoyama, "Generalized G-inflation: Inflation with the most general second-order field equations", Prog. Theor. Phys. **126**, 511 (2011), arXiv:1105.5723 [hep-th].

[305] M. Saravani and T. P. Sotiriou, "Classification of shift-symmetric Horndeski theories and hairy black holes", Phys. Rev. D **99**, 124004 (2019), arXiv:1903.02055 [gr-qc].

[306] T. P. Sotiriou and S.-Y. Zhou, "Black hole hair in generalized scalar-tensor gravity", Phys. Rev. Lett. **112**, 251102 (2014), arXiv:1312.3622 [gr-qc].

[307] T. P. Sotiriou and S.-Y. Zhou, "Black hole hair in generalized scalar-tensor gravity: An explicit example", Phys. Rev. D **90**, 124063 (2014), arXiv:1408.1698 [gr-qc].

[308] F. Thaalba, G. Antoniou, and T. P. Sotiriou, "Black hole minimum size and scalar charge in shift-symmetric theories", Class. Quant. Grav. **40**, 155002 (2023), arXiv:2211.05099 [gr-qc].

[309] T. Damour and G. Esposito-Farese, "Nonperturbative strong field effects in tensor - scalar theories of gravitation", Phys. Rev. Lett. **70**, 2220 (1993).

[310] D. D. Doneva, F. M. Ramazanoğlu, H. O. Silva, T. P. Sotiriou, and S. S. Yazadjiev, "Spontaneous scalarization", Rev. Mod. Phys. **96**, 015004 (2024), arXiv:2211.01766 [gr-qc].

[311] N. Andreou, N. Franchini, G. Ventagli, and T. P. Sotiriou, "Spontaneous scalarization in generalised scalar-tensor theory", Phys. Rev. D **99**, [Erratum: Phys.Rev.D 101, 109903 (2020)], 124022 (2019), arXiv:1904.06365 [gr-qc].

[312] S. W. Hawking, "Black holes in the Brans-Dicke theory of gravitation", Commun. Math. Phys. **25**, 167 (1972).

[313] T. P. Sotiriou and V. Faraoni, "Black holes in scalar-tensor gravity", Phys. Rev. Lett. **108**, 081103 (2012), arXiv:1109.6324 [gr-qc].

[314] H. O. Silva, J. Sakstein, L. Gualtieri, T. P. Sotiriou, and E. Berti, "Spontaneous scalarization of black holes and compact stars from a Gauss-Bonnet coupling", Phys. Rev. Lett. **120**, 131104 (2018), arXiv:1711.02080 [gr-qc].

[315] D. D. Doneva and S. S. Yazadjiev, "New Gauss-Bonnet Black Holes with Curvature-Induced Scalarization in Extended Scalar-Tensor Theories", Phys. Rev. Lett. **120**, 131103 (2018), arXiv:1711.01187 [gr-qc].

[316] H. O. Silva, C. F. B. Macedo, T. P. Sotiriou, L. Gualtieri, J. Sakstein, and E. Berti, "Stability of scalarized black hole solutions in scalar-Gauss-Bonnet gravity", Phys. Rev. D **99**, 064011 (2019), arXiv:1812.05590 [gr-qc].

[317] C. F. B. Macedo, J. Sakstein, E. Berti, L. Gualtieri, H. O. Silva, and T. P. Sotiriou, "Self-interactions and Spontaneous Black Hole Scalarization", Phys. Rev. D **99**, 104041 (2019), arXiv:1903.06784 [gr-qc].

[318] G. Antoniou, A. Lehébel, G. Ventagli, and T. P. Sotiriou, "Black hole scalarization with Gauss-Bonnet and Ricci scalar couplings", Phys. Rev. D **104**, 044002 (2021), arXiv:2105.04479 [gr-qc].

[319] K. V. Staykov, D. D. Doneva, P. G. S. Fernandes, and S. S. Yazadjiev, *Rotating scalarized black holes: the role of the coupling*, Mar. 2025, arXiv:2503.15206 [gr-qc].

[320] A. Eichhorn and P. G. S. Fernandes, "Purely metric Horndeski theories and spontaneous curvaturization of black holes", Phys. Rev. D **111**, 104007 (2025), arXiv:2502.14717 [gr-qc].

[321] A. Dima, E. Barausse, N. Franchini, and T. P. Sotiriou, "Spin-induced black hole spontaneous scalarization", Phys. Rev. Lett. **125**, 231101 (2020), arXiv:2006.03095 [gr-qc].

[322] C. A. R. Herdeiro, E. Radu, H. O. Silva, T. P. Sotiriou, and N. Yunes, "Spin-induced scalarized black holes", Phys. Rev. Lett. **126**, 011103 (2021), arXiv:2009.03904 [gr-qc].

[323] E. Berti, L. G. Collodel, B. Kleihaus, and J. Kunz, "Spin-induced black-hole scalarization in Einstein-scalar-Gauss-Bonnet theory", Phys. Rev. Lett. **126**, 011104 (2021), arXiv:2009 . 03905 [gr-qc].

[324] D. F. Carneiro, E. A. Freiras, B. Goncalves, A. G. de Lima, and I. L. Shapiro, "On useful conformal tranformations in general relativity", Grav. Cosmol. **10**, 305 (2004), arXiv:gr-qc/0412113.

[325] M. P. Dabrowski, J. Garecki, and D. B. Blaschke, "Conformal transformations and conformal invariance in gravitation", Annalen Phys. **18**, 13 (2009), arXiv:0806.2683 [gr-qc].

[326] T. Damour and K. Nordtvedt, "General relativity as a cosmological attractor of tensor scalar theories", Phys. Rev. Lett. **70**, 2217 (1993).

[327] D. Anderson, N. Yunes, and E. Barausse, "Effect of cosmological evolution on Solar System constraints and on the scalarization of neutron stars in massless scalar-tensor theories", Phys. Rev. D **94**, 104064 (2016), arXiv:1607.08888 [gr-qc].

[328] T. Anson, E. Babichev, C. Charmousis, and S. Ramazanov, "Cosmological instability of scalar-Gauss-Bonnet theories exhibiting scalarization", JCAP **06**, 023 (2019), arXiv:1903.02399 [gr-qc].

[329] N. Franchini and T. P. Sotiriou, "Cosmology with subdominant Horndeski scalar field", Phys. Rev. D **101**, 064068 (2020), arXiv:1903.05427 [gr-qc].

[330] G. Antoniou, L. Bordin, and T. P. Sotiriou, "Compact object scalarization with general relativity as a cosmic attractor", Phys. Rev. D **103**, 024012 (2021), arXiv:2004.14985 [gr-qc].

[331] G. Ventagli, G. Antoniou, A. Lehébel, and T. P. Sotiriou, "Neutron star scalarization with Gauss-Bonnet and Ricci scalar couplings", Phys. Rev. D **104**, 124078 (2021), arXiv:2111.03644 [gr-qc].

[332] G. Antoniou, C. F. B. Macedo, R. McManus, and T. P. Sotiriou, "Stable spontaneously-scalarized black holes in generalized scalar-tensor theories", Phys. Rev. D **106**, 024029 (2022), arXiv:2204.01684 [gr-qc].

[333] H. Georgi, "Effective field theory", Ann. Rev. Nucl. Part. Sci. **43**, 209 (1993).

[334] J. D. Wells, *Effective Theories in Physics : From Planetary Orbits to Elementary Particle Masses*, Springer Briefs in physics (Oxford University Press, 2012).

[335] W. D. Goldberger, "Les Houches lectures on effective field theories and gravitational radiation", in Les Houches Summer School - Session 86: Particle Physics and Cosmology: The Fabric of Spacetime (Jan. 2007), arXiv:hep-ph/0701129.

[336] J. E. Chase, "Event horizons in static scalar-vacuum space-times", Commun. Math. Phys. **19**, 276 (1970).

[337] J. D. Bekenstein, "Novel "no-scalar-hair" theorem for black holes", Phys. Rev. D **51**, R6608 (1995).

[338] J. B. Hartle, "Long-range neutrino forces exerted by Kerr black holes", Phys. Rev. D **3**, 2938 (1971).

[339] C. Teitelboim, "Nonmeasurability of the lepton number of a black hole", Lett. Nuovo Cim. **3S2**, 397 (1972).

[340] J. D. Bekenstein, "Nonexistence of baryon number for static black holes", Phys. Rev. D **5**, 1239 (1972).

[341] J. D. Bekenstein, "Nonexistence of baryon number for black holes. ii", Phys. Rev. D **5**, 2403 (1972).

[342] T. P. Sotiriou, "Black Holes and Scalar Fields", Class. Quant. Grav. **32**, 214002 (2015), arXiv:1505.00248 [gr-qc].

[343] C. A. R. Herdeiro, "Black Holes: On the Universality of the Kerr Hypothesis", Lect. Notes Phys. **1017**, 315 (2023), arXiv:2204.05640 [gr-qc].

[344] T. Damour and A. M. Polyakov, "The String dilaton and a least coupling principle", Nucl. Phys. B **423**, 532 (1994), arXiv:hep-th/9401069.

[345] A. Arvanitaki, S. Dimopoulos, S. Dubovsky, N. Kaloper, and J. March-Russell, "String Axiverse", Phys. Rev. D **81**, 123530 (2010), arXiv:0905.4720 [hep-th].

[346] R. Essig et al., "Working Group Report: New Light Weakly Coupled Particles", in Snowmass 2013: Snowmass on the Mississippi (Oct. 2013), arXiv:1311.0029 [hep-ph].

[347] L. Hui, J. P. Ostriker, S. Tremaine, and E. Witten, "Ultralight scalars as cosmological dark matter", Phys. Rev. D **95**, 043541 (2017), arXiv:1610.08297 [astro-ph.CO].

[348] P. Kanti, N. E. Mavromatos, J. Rizos, K. Tamvakis, and E. Winstanley, "Dilatonic black holes in higher curvature string gravity", Phys. Rev. D **54**, 5049 (1996), arXiv:hep-th/9511071.

[349] N. Yunes and L. C. Stein, "Non-Spinning Black Holes in Alternative Theories of Gravity", Phys. Rev. D **83**, 104002 (2011), arXiv:1101.2921 [gr-qc].

[350] P. G. S. Fernandes, C. Burrage, A. Eichhorn, and T. P. Sotiriou, "Shadows and properties of spin-induced scalarized black holes with and without a Ricci coupling", Phys. Rev. D **109**, 104033 (2024), arXiv:2403.14596 [gr-qc].

[351] L. Hui and A. Nicolis, "No-Hair Theorem for the Galileon", Phys. Rev. Lett. **110**, 241104 (2013), arXiv:1202.1296 [hep-th].

[352] S. Mignemi and N. R. Stewart, "Dilaton axion hair for slowly rotating Kerr black holes", Phys. Lett. B **298**, 299 (1993), arXiv:hep-th/9206018.

[353] P. G. S. Fernandes, D. J. Mulryne, and J. F. M. Delgado, "Exploring the small mass limit of stationary black holes in theories with Gauss–Bonnet terms", Class. Quant. Grav. **39**, 235015 (2022), arXiv:2207.10692 [gr-qc].

[354] Z. Lyu, N. Jiang, and K. Yagi, "Constraints on Einstein-dilation-Gauss-Bonnet gravity from black hole-neutron star gravitational wave events", Phys. Rev. D **105**, [Erratum: Phys.Rev.D 106, 069901 (2022), Erratum: Phys.Rev.D 106, 069901 (2022)], 064001 (2022), arXiv:2201.02543 [gr-qc].

[355] S. E. Perkins, R. Nair, H. O. Silva, and N. Yunes, "Improved gravitational-wave constraints on higher-order curvature theories of gravity", Phys. Rev. D **104**, 024060 (2021), arXiv:2104.11189 [gr-qc].

[356] A. Maselli, N. Franchini, L. Gualtieri, and T. P. Sotiriou, "Detecting scalar fields with Extreme Mass Ratio Inspirals", Phys. Rev. Lett. **125**, 141101 (2020), arXiv:2004.11895 [gr-qc].

[357] A. Maselli, N. Franchini, L. Gualtieri, T. P. Sotiriou, S. Barsanti, and P. Pani, "Detecting fundamental fields with LISA observations of gravitational waves from extreme mass-ratio inspirals", Nature Astron. **6**, 464 (2022), arXiv:2106.11325 [gr-qc].

[358] H. Witek, L. Gualtieri, P. Pani, and T. P. Sotiriou, "Black holes and binary mergers in scalar Gauss-Bonnet gravity: scalar field dynamics", Phys. Rev. D **99**, 064035 (2019), arXiv:1810.05177 [gr-qc].

[359] L. Hui, A. Podo, L. Santoni, and E. Trincherini, "Effective Field Theory for the perturbations of a slowly rotating black hole", JHEP **12**, 183 (2021), arXiv:2111.02072 [hep-th].

[360] M. Minamitsuji and K. Maeda, "Black hole thermodynamics in Horndeski theories", Phys. Rev. D **108**, 084061 (2023), arXiv:2308.01082 [gr-qc].

[361] E. Babichev, C. Charmousis, and A. Lehébel, "Asymptotically flat black holes in Horndeski theory and beyond", JCAP **04**, 027 (2017), arXiv:1702.01938 [gr-qc].

[362] P. Creminelli, N. Loayza, F. Serra, E. Trincherini, and L. G. Trombetta, "Hairy Black-holes in Shift-symmetric Theories", JHEP **08**, 045 (2020), arXiv:2004.02893 [hep-th].

[363] G. Antoniou, A. Bakopoulos, and P. Kanti, "Evasion of No-Hair Theorems and Novel Black-Hole Solutions in Gauss-Bonnet Theories", Phys. Rev. Lett. **120**, 131102 (2018), arXiv:1711.03390 [hep-th].

[364] B. P. Abbott et al. (LIGO Scientific, Virgo), "GW170817: Observation of Gravitational Waves from a Binary Neutron Star Inspiral", Phys. Rev. Lett. **119**, 161101 (2017), arXiv:1710.05832 [gr-qc].

[365] T. Damour and G. Esposito-Farese, "Tensor - scalar gravity and binary pulsar experiments", Phys. Rev. D **54**, 1474 (1996), arXiv:gr-qc/9602056.

[366] N. Yunes and X. Siemens, "Gravitational-Wave Tests of General Relativity with Ground-Based Detectors and Pulsar Timing-Arrays", Living Rev. Rel. **16**, 9 (2013), arXiv:1304 . 3473 [gr-qc].

[367] B. C. Seymour and K. Yagi, "Testing General Relativity with Black Hole-Pulsar Binaries", Phys. Rev. D **98**, 124007 (2018), arXiv:1808.00080 [gr-qc].

[368] S. Barsanti, A. Maselli, T. P. Sotiriou, and L. Gualtieri, "Detecting Massive Scalar Fields with Extreme Mass-Ratio Inspirals", Phys. Rev. Lett. **131**, 051401 (2023), arXiv:2212.03888 [gr-qc].

[369] L. Speri, S. Barsanti, A. Maselli, T. P. Sotiriou, N. Warburton, M. van de Meent, A. J. K. Chua, O. Burke, and J. Gair, "Probing fundamental physics with Extreme Mass Ratio Inspirals: a full Bayesian inference for scalar charge", (2024), arXiv:2406.07607 [gr-qc].

[370] G. D'Addario, A. Padilla, P. M. Saffin, T. P. Sotiriou, and A. Spiers, "Ringdowns for black holes with scalar hair: The large mass case", Phys. Rev. D **109**, 084046 (2024), arXiv:2311.17666 [gr-qc].

[371] A. Eichhorn, P. G. S. Fernandes, A. Held, and H. O. Silva, "Breaking black-hole uniqueness at supermassive scales", Class. Quant. Grav. **42**, 105006 (2025), arXiv:2312.11430 [gr-qc].

[372] T. Anson, E. Babichev, and S. Ramazanov, "Reconciling spontaneous scalarization with cosmology", Phys. Rev. D **100**, 104051 (2019), arXiv:1905.10393 [gr-qc].

[373] S. Liu, Y. Liu, Y. Peng, and C.-Y. Zhang, *Rotating black holes in a class of scalar-Gauss-Bonnet gravity*, Mar. 2025, arXiv:2503.13267 [gr-qc].

[374] C. Smarra, L. Capuano, and A. Kuntz, *Probing supermassive black hole scalarization with Pulsar Timing Arrays*, May 2025, arXiv:2505.20402 [gr-qc].

[375] D. C. Rodrigues, F. de O. Salles, I. L. Shapiro, and A. A. Starobinsky, "Auxiliary fields representation for modified gravity models", Phys. Rev. D **83**, 084028 (2011), arXiv:1101.5028 [gr-qc].

[376] A. De Felice and T. Tanaka, "Inevitable ghost and the degrees of freedom in f(R,G) gravity", Prog. Theor. Phys. **124**, 503 (2010), arXiv:1006.4399 [astro-ph.CO].

[377] A. De Felice, T. Suyama, and T. Tanaka, "Stability of Schwarzschild-like solutions in f(R,G) gravity models", Phys. Rev. D **83**, 104035 (2011), arXiv:1102.1521 [gr-qc].

[378] P. G. S. Fernandes and D. J. Mulryne, "A new approach and code for spinning black holes in modified gravity", Class. Quant. Grav. **40**, 165001 (2023), arXiv:2212.07293 [gr-qc].

[379] J. Hadamard, "Sur les problemes aux derivees partielles et leur signification physique", Princeton university bulletin, 49 (1902).

[380] H.-O. Kreiss and J. Lorenz, *Initial-boundary value problems and the navier-stokes equations* (Society for Industrial and Applied Mathematics, 2004), eprint: https://epubs.siam.org/doi/book/10.1137/1.9780898719130.

[381] O. Sarbach and M. Tiglio, "Continuum and Discrete Initial-Boundary-Value Problems and Einstein's Field Equations", Living Rev. Rel. **15**, 9 (2012), arXiv:1203.6443 [gr-qc].

[382] G. Papallo and H. S. Reall, "On the local well-posedness of Lovelock and Horndeski theories", Phys. Rev. D **96**, 044019 (2017), arXiv:1705.04370 [gr-qc].

[383] M. E. Taylor, "Paradifferential operators", Pseudodifferential Operators and Nonlinear PDE, 67 (1991).

[384] R. L. Arnowitt, S. Deser, and C. W. Misner, "Dynamical Structure and Definition of Energy in General Relativity", Phys. Rev. **116**, 1322 (1959).

[385] Y. Foures-Bruhat, "Theoreme d'existence pour certains systemes derivees partielles non lineaires", Acta Mat. **88**, 141 (1952).

[386] F. Pretorius, "Evolution of binary black hole spacetimes", Phys. Rev. Lett. **95**, 121101 (2005), arXiv:gr-qc/0507014.

[387] M. Campanelli, C. O. Lousto, P. Marronetti, and Y. Zlochower, "Accurate evolutions of orbiting black-hole binaries without excision", Phys. Rev. Lett. **96**, 111101 (2006), arXiv:gr-qc/0511048.

[388] J. G. Baker, J. Centrella, D.-I. Choi, M. Koppitz, and J. van Meter, "Gravitational wave extraction from an inspiraling configuration of merging black holes", Phys. Rev. Lett. **96**, 111102 (2006), arXiv:gr-qc/0511103.

[389] T. Nakamura, K. Oohara, and Y. Kojima, "General Relativistic Collapse to Black Holes and Gravitational Waves from Black Holes", Prog. Theor. Phys. Suppl. **90**, 1 (1987).

[390] K. C. B. New, D.-I. Choi, J. M. Centrella, P. MacNeice, M. F. Huq, and K. Olson, "Three-dimensional adaptive evolution of gravitational waves in numerical relativity", Phys. Rev. D **62**, 084039 (2000), arXiv:gr-qc/0007045.

[391] T. W. Baumgarte and S. L. Shapiro, "On the numerical integration of Einstein's field equations", Phys. Rev. D **59**, 024007 (1998), arXiv:gr-qc/9810065.

[392] D. Alic, C. Bona-Casas, C. Bona, L. Rezzolla, and C. Palenzuela, "Conformal and covariant formulation of the Z4 system with constraint-violation damping", Phys. Rev. D **85**, 064040 (2012), arXiv:1106.2254 [gr-qc].

[393] P. Romatschke, "New Developments in Relativistic Viscous Hydrodynamics", Int. J. Mod. Phys. E **19**, 1 (2010), arXiv:0902.3663 [hep-ph].

[394] W. Israel and J. M. Stewart, "Transient relativistic thermodynamics and kinetic theory", Annals Phys. **118**, 341 (1979).

[395] P. Kovtun, "First-order relativistic hydrodynamics is stable", JHEP **10**, 034 (2019), arXiv:1907.08191 [hep-th].

[396] F. S. Bemfica, M. M. Disconzi, and J. Noronha, "Causality and existence of solutions of relativistic viscous fluid dynamics with gravity", Phys. Rev. D **98**, 104064 (2018), arXiv:1708.06255 [gr-qc].

[397] C. A. R. Herdeiro and E. Radu, "Asymptotically flat black holes with scalar hair: a review", Int. J. Mod. Phys. D **24**, 1542014 (2015), arXiv:1504.08209 [gr-qc].

[398] S. Mignemi and N. R. Stewart, "Charged black holes in effective string theory", Phys. Rev. D **47**, 5259 (1993), arXiv:hep-th/9212146.

[399] G. Antoniou, A. Bakopoulos, and P. Kanti, "Black-Hole Solutions with Scalar Hair in Einstein-Scalar-Gauss-Bonnet Theories", Phys. Rev. D **97**, 084037 (2018), arXiv:1711.07431 [hep-th].

[400] R. Benkel, T. P. Sotiriou, and H. Witek, "Black hole hair formation in shift-symmetric generalised scalar-tensor gravity", Class. Quant. Grav. **34**, 064001 (2017), arXiv:1610.09168 [gr-qc].

[401] R. Benkel, T. P. Sotiriou, and H. Witek, "Dynamical scalar hair formation around a Schwarzschild black hole", Phys. Rev. D **94**, 121503 (2016), arXiv:1612.08184 [gr-qc].

[402] M. Okounkova, L. C. Stein, M. A. Scheel, and D. A. Hemberger, "Numerical binary black hole mergers in dynamical Chern-Simons gravity: Scalar field", Phys. Rev. D **96**, 044020 (2017), arXiv:1705.07924 [gr-qc].

[403] M. Okounkova, M. A. Scheel, and S. A. Teukolsky, "Numerical black hole initial data and shadows in dynamical Chern–Simons gravity", Class. Quant. Grav. **36**, 054001 (2019), arXiv:1810.05306 [gr-qc].

[404] M. Okounkova, L. C. Stein, M. A. Scheel, and S. A. Teukolsky, "Numerical binary black hole collisions in dynamical Chern-Simons gravity", Phys. Rev. D **100**, 104026 (2019), arXiv:1906.08789 [gr-qc].

[405] H. O. Silva, H. Witek, M. Elley, and N. Yunes, "Dynamical Descalarization in Binary Black Hole Mergers", Phys. Rev. Lett. **127**, 031101 (2021), arXiv:2012.10436 [gr-qc].

[406] M. Elley, H. O. Silva, H. Witek, and N. Yunes, "Spin-induced dynamical scalarization, descalarization, and stealthness in scalar-Gauss-Bonnet gravity during a black hole coalescence", Phys. Rev. D **106**, 044018 (2022), arXiv:2205.06240 [gr-qc].

[407] J. T. Gálvez Ghersi and L. C. Stein, "Numerical renormalization-group-based approach to secular perturbation theory", Phys. Rev. E **104**, 034219 (2021), arXiv:2106.08410 [hep-th].

[408] C. Palenzuela, E. Barausse, M. Ponce, and L. Lehner, "Dynamical scalarization of neutron stars in scalar-tensor gravity theories", Phys. Rev. D **89**, 044024 (2014), arXiv:1310.4481 [gr-qc].

[409] W. E. East and J. L. Ripley, "Dynamics of Spontaneous Black Hole Scalarization and Mergers in Einstein-Scalar-Gauss-Bonnet Gravity", Phys. Rev. Lett. **127**, 101102 (2021), arXiv:2105.08571 [gr-qc].

[410] D. D. Doneva, A. Vañó-Viñuales, and S. S. Yazadjiev, "Dynamical descalarization with a jump during a black hole merger", Phys. Rev. D **106**, L061502 (2022), arXiv:2204.05333 [gr-qc].

[411] G. Papallo, "On the hyperbolicity of the most general Horndeski theory", Phys. Rev. D **96**, 124036 (2017), arXiv:1710.10155 [gr-qc].

[412] J. L. Ripley and F. Pretorius, "Hyperbolicity in Spherical Gravitational Collapse in a Horndeski Theory", Phys. Rev. D **99**, 084014 (2019), arXiv:1902.01468 [gr-qc].

[413] J. L. Ripley and F. Pretorius, "Gravitational collapse in Einstein dilaton-Gauss–Bonnet gravity", Class. Quant. Grav. **36**, 134001 (2019), arXiv:1903.07543 [gr-qc].

[414] J. L. Ripley and F. Pretorius, "Dynamics of a $\mathbb{Z}_2$ symmetric EdGB gravity in spherical symmetry", Class. Quant. Grav. **37**, 155003 (2020), arXiv:2005.05417 [gr-qc].

[415] M. Bezares, M. Crisostomi, C. Palenzuela, and E. Barausse, "K-dynamics: well-posed 1+1 evolutions in K-essence", JCAP **03**, 072 (2021), arXiv:2008.07546 [gr-qc].

[416] P. Figueras and T. França, "Gravitational Collapse in Cubic Horndeski Theories", Class. Quant. Grav. **37**, 225009 (2020), arXiv:2006.09414 [gr-qc].

[417] P. Figueras and T. França, "Black hole binaries in cubic Horndeski theories", Phys. Rev. D **105**, 124004 (2022), arXiv:2112.15529 [gr-qc].

[418] L. Bernard, L. Lehner, and R. Luna, "Challenges to global solutions in Horndeski's theory", Phys. Rev. D **100**, 024011 (2019), arXiv:1904.12866 [gr-qc].

[419] Á. D. Kovács and H. S. Reall, "Well-posed formulation of Lovelock and Horndeski theories", Phys. Rev. D **101**, 124003 (2020), arXiv:2003.08398 [gr-qc].

[420] Y. Liu, C.-Y. Zhang, Q. Chen, Z. Cao, Y. Tian, and B. Wang, "Critical scalarization and descalarization of black holes in a generalized scalar-tensor theory", Sci. China Phys. Mech. Astron. **66**, 100412 (2023), arXiv:2208.07548 [gr-qc].

[421] W. E. East and J. L. Ripley, "Evolution of Einstein-scalar-Gauss-Bonnet gravity using a modified harmonic formulation", Phys. Rev. D **103**, 044040 (2021), arXiv:2011.03547 [gr-qc].

[422] M. Corman, J. L. Ripley, and W. E. East, "Nonlinear studies of binary black hole mergers in Einstein-scalar-Gauss-Bonnet gravity", Phys. Rev. D **107**, 024014 (2023), arXiv:2210.09235 [gr-qc].

[423] L. Aresté Saló, K. Clough, and P. Figueras, "Well-Posedness of the Four-Derivative Scalar-Tensor Theory of Gravity in Singularity Avoiding Coordinates", Phys. Rev. Lett. **129**, 261104 (2022), arXiv:2208.14470 [gr-qc].

[424] A. H. K. R, J. L. Ripley, and N. Yunes, "Where and why does Einstein-scalar-Gauss-Bonnet theory break down?", Phys. Rev. D **107**, 044044 (2023), arXiv:2211.08477 [gr-qc].

[425] J. Cayuso, N. Ortiz, and L. Lehner, "Fixing extensions to general relativity in the nonlinear regime", Phys. Rev. D **96**, 084043 (2017), arXiv:1706.07421 [gr-qc].

[426] G. Allwright and L. Lehner, "Towards the nonlinear regime in extensions to GR: assessing possible options", Class. Quant. Grav. **36**, 084001 (2019), arXiv:1808.07897 [gr-qc].

[427] R. Cayuso and L. Lehner, "Nonlinear, noniterative treatment of EFT-motivated gravity", Phys. Rev. D **102**, 084008 (2020), arXiv:2005.13720 [gr-qc].

[428] N. Franchini, M. Bezares, E. Barausse, and L. Lehner, "Fixing the dynamical evolution in scalar-Gauss-Bonnet gravity", Phys. Rev. D **106**, 064061 (2022), arXiv:2206.00014 [gr-qc].

[429] R. Cayuso, P. Figueras, T. França, and L. Lehner, "Modelling self-consistently beyond General Relativity", Phys. Rev. Lett. **131**, 111403 (2023), arXiv:2303.07246 [gr-qc].

[430] G. Lara, M. Bezares, and E. Barausse, "UV completions, fixing the equations, and nonlinearities in k-essence", Phys. Rev. D **105**, 064058 (2022), arXiv:2112.09186 [gr-qc].

[431] M. Bezares, L. ter Haar, M. Crisostomi, E. Barausse, and C. Palenzuela, "Kinetic screening in nonlinear stellar oscillations and gravitational collapse", Phys. Rev. D **104**, 044022 (2021), arXiv:2105.13992 [gr-qc].

[432] M. Gerhardinger, J. T. Giblin Jr., A. J. Tolley, and M. Trodden, "Well-posed UV completion for simulating scalar Galileons", Phys. Rev. D **106**, 043522 (2022), arXiv:2205.05697 [hep-th].

[433] G. Lara, H. P. Pfeiffer, N. A. Wittek, N. L. Vu, K. C. Nelli, A. Carpenter, G. Lovelace, M. A. Scheel, and W. Throwe, "Scalarization of isolated black holes in scalar Gauss-Bonnet theory in the fixing-the-equations approach", Phys. Rev. D **110**, 024033 (2024), arXiv:2403.08705 [gr-qc].

[434] M. Corman, L. Lehner, W. E. East, and G. Dideron, "Nonlinear studies of modifications to general relativity: Comparing different approaches", Phys. Rev. D **110**, 084048 (2024), arXiv:2405.15581 [gr-qc].

[435] G. Calabrese, L. Lehner, O. Reula, O. Sarbach, and M. Tiglio, "Summation by parts and dissipation for domains with excised regions", Class. Quant. Grav. **21**, 5735 (2004), arXiv:gr-qc/0308007.

[436] C. W. Misner and D. H. Sharp, "Relativistic equations for adiabatic, spherically symmetric gravitational collapse", Phys. Rev. **136**, B571 (1964).

[437] J. L. Ripley and F. Pretorius, "Scalarized Black Hole dynamics in Einstein dilaton Gauss-Bonnet Gravity", Phys. Rev. D **101**, 044015 (2020), arXiv:1911.11027 [gr-qc].

[438] B. Kleihaus, J. Kunz, T. Utermöhlen, and E. Berti, "Quadrupole instability of static scalarized black holes", Phys. Rev. D **107**, L081501 (2023), arXiv:2303.04107 [gr-qc].

[439] M. Minamitsuji and S. Mukohyama, "Instability of scalarized compact objects in Einstein-scalar-Gauss-Bonnet theories", (2023), arXiv:2305.05185 [gr-qc].

[440] J. Ziprick and G. Kunstatter, "Numerical study of black-hole formation in painlevé-gullstrand coordinates", Phys. Rev. D **79**, 101503 (2009).

[441] Y. Kanai, M. Siino, and A. Hosoya, "Gravitational collapse in Painleve-Gullstrand coordinates", Prog. Theor. Phys. **125**, 1053 (2011), arXiv:1008.0470 [gr-qc].

[442] J. G. Baker, M. Campanelli, and C. O. Lousto, "The Lazarus project: A Pragmatic approach to binary black hole evolutions", Phys. Rev. D **65**, 044001 (2002), arXiv:gr-qc/0104063.

[443] M. Alcubierre, B. Bruegmann, P. Diener, M. Koppitz, D. Pollney, E. Seidel, and R. Takahashi, "Gauge conditions for long term numerical black hole evolutions without excision", Phys. Rev. D **67**, 084023 (2003), arXiv:gr-qc/0206072.

[444] F. Corelli, M. De Amicis, T. Ikeda, and P. Pani, "Nonperturbative gedanken experiments in Einstein-dilaton-Gauss-Bonnet gravity: Nonlinear transitions and tests of the cosmic censorship beyond general relativity", Phys. Rev. D **107**, 044061 (2023), arXiv:2205.13007 [gr-qc].

[445] F. Thaalba, N. Franchini, M. Bezares, and T. P. Sotiriou, "The dynamics of spherically symmetric black holes in scalar-Gauss-Bonnet gravity with a Ricci coupling", (2024), arXiv:2409.11398 [gr-qc].

[446] F. Thaalba, M. Bezares, N. Franchini, and T. P. Sotiriou, "Spherical collapse in scalar-Gauss-Bonnet gravity: Taming ill-posedness with a Ricci coupling", Phys. Rev. D **109**, L041503 (2024), arXiv:2306.01695 [gr-qc].

[447] K. D. Kokkotas and B. G. Schmidt, "Quasinormal modes of stars and black holes", Living Rev. Rel. **2**, 2 (1999), arXiv:gr-qc/9909058.

[448] D. D. Doneva, L. Aresté Saló, and S. S. Yazadjiev, "3+1 nonlinear evolution of Ricci-coupled scalar-Gauss-Bonnet gravity", Phys. Rev. D **110**, 024040 (2024), arXiv:2404.15526 [gr-qc].

[449] H. S. Reall, "Causality in gravitational theories with second order equations of motion", Phys. Rev. D **103**, 084027 (2021), arXiv:2101.11623 [gr-qc].

[450] D. Christodoulou, *Mathematical problems of general relativity i*, Vol. 1 (European Mathematical Society, 2008).

[451] A. Coates and F. M. Ramazanoğlu, "Treatments and placebos for the pathologies of effective field theories", Phys. Rev. D **108**, L101501 (2023), arXiv:2307.07743 [gr-qc].

[452] M. E. Rubio, G. Lara, M. Bezares, M. Crisostomi, and E. Barausse, "Fixing the dynamical evolution of self-interacting vector fields", Phys. Rev. D **110**, 063015 (2024), arXiv:2407.08774 [gr-qc].

[453] M. Corman and W. E. East, "Black hole-neutron star mergers in Einstein-scalar-Gauss-Bonnet gravity", Phys. Rev. D **110**, 084065 (2024), arXiv:2405.18496 [gr-qc].

[454] J. D. Bekenstein, "The Relation between physical and gravitational geometry", Phys. Rev. D **48**, 3641 (1993), arXiv:gr-qc/9211017.

[455] K. Takahashi, H. Motohashi, T. Suyama, and T. Kobayashi, "General invertible transformation and physical degrees of freedom", Phys. Rev. D **95**, 084053 (2017), arXiv:1702.01849 [gr-qc].

[456] M. Zumalacárregui and J. García-Bellido, "Transforming gravity: from derivative couplings to matter to second-order scalar-tensor theories beyond the Horndeski Lagrangian", Phys. Rev. D **89**, 064046 (2014), arXiv:1308.4685 [gr-qc].

[457] D. Bettoni and S. Liberati, "Disformal invariance of second order scalar-tensor theories: Framing the Horndeski action", Phys. Rev. D **88**, 084020 (2013), arXiv:1306.6724 [gr-qc].

[458] E. W. Leaver, "An Analytic representation for the quasi normal modes of Kerr black holes", Proc. Roy. Soc. Lond. A **402**, 285 (1985).

[459] S. H. Völkel, N. Franchini, and E. Barausse, "Theory-agnostic reconstruction of potential and couplings from quasinormal modes", Phys. Rev. D **105**, 084046 (2022), arXiv:2202.08655 [gr-qc].

[460] H.-P. Nollert, "Quasinormal modes of Schwarzschild black holes: The determination of quasinormal frequencies with very large imaginary parts", Phys. Rev. D **47**, 5253 (1993).

[461] N. Tanahashi and S. Ohashi, "Wave propagation and shock formation in the most general scalar–tensor theories", Class. Quant. Grav. **34**, 215003 (2017), arXiv:1704.02757 [hep-th].